Springer Climate

Leila Maria Véspoli de Carvalho
Charles Jones *Editors*

The Monsoons and Climate Change

Observations and Modeling

Springer

Springer Climate

Series editor

John Dodson, Menai, Australia

Springer Climate is an interdisciplinary book series dedicated on all climate research. This includes climatology, climate change impacts, climate change management, climate change policy, regional climate, climate monitoring and modeling, palaeoclimatology etc. The series hosts high quality research monographs and edited volumes on Climate, and is crucial reading material for Researchers and students in the field, but also policy makers, and industries dealing with climatic issues. Springer Climate books are all peer-reviewed by specialists (see Editorial Advisory board). If you wish to submit a book project to this series, please contact your Publisher (elodie.tronche@springer.com).

More information about this series at http://www.springer.com/series/11741

Leila Maria Véspoli de Carvalho
Charles Jones
Editors

The Monsoons and Climate Change

Observations and Modeling

Springer

Editors
Leila Maria Véspoli de Carvalho
Department of Geography and Earth Research Institute
University of California
Santa Barbara, CA
USA

Charles Jones
Earth Research Institute
University of California
Santa Barbara, CA
USA

ISSN 2352-0698 ISSN 2352-0701 (electronic)
Springer Climate
ISBN 978-3-319-21649-2 ISBN 978-3-319-21650-8 (eBook)
DOI 10.1007/978-3-319-21650-8

Library of Congress Control Number: 2015951391

Springer Cham Heidelberg New York Dordrecht London
© Springer International Publishing Switzerland 2016
Chapter 2 has been written by an employee of the US Government.
Chapter 9 was created within the capacity of an US governmental employment. US copy-right protection does not apply.
This work is subject to copyright. All rights are reserved by the Publisher, whether the whole or part of the material is concerned, specifically the rights of translation, reprinting, reuse of illustrations, recitation, broadcasting, reproduction on microfilms or in any other physical way, and transmission or information storage and retrieval, electronic adaptation, computer software, or by similar or dissimilar methodology now known or hereafter developed.
The use of general descriptive names, registered names, trademarks, service marks, etc. in this publication does not imply, even in the absence of a specific statement, that such names are exempt from the relevant protective laws and regulations and therefore free for general use.
The publisher, the authors and the editors are safe to assume that the advice and information in this book are believed to be true and accurate at the date of publication. Neither the publisher nor the authors or the editors give a warranty, express or implied, with respect to the material contained herein or for any errors or omissions that may have been made.

Printed on acid-free paper

Springer International Publishing AG Switzerland is part of Springer Science+Business Media (www.springer.com)

Preface

Monsoon systems are unique features of the climate of the Earth. While monsoons were historically defined as a "reversal in the surface winds accompanied by changes in precipitation" over the Bay of Bengal and Arabian Sea, modern studies in fact show that, except for the Polar Regions, monsoons occur in Africa, Asia, Indonesia, Australia, and the Americas. Driven primarily by the thermal contrast between large land masses and surrounding oceans, the monsoons exhibit a phenomenal range of spatial and temporal variability. The annual onset of the rainy season and its demise, for instance, show considerable changes from year to year in each monsoon system. Similarly, the intensity of the monsoons varies on subseasonal, inter-annual, decadal, and centennial time scales. It is, therefore, widely recognized that the monsoons play a vital role for humans and the environment. Often the occurrence of extreme events, such as heavy precipitation or droughts, can have significant impacts on millions of people who live in monsoon regions and rely on water for human consumption, agriculture, energy, and transportation.

Observational and theoretical evidence points to the undeniable fact that the Earth's climate is changing rapidly, and anthropogenic activities have been an important component of this change. Climate variability and change pose significant challenges for humans to develop adaptation strategies that can minimize negative impacts. This is the case in particular when important uncertainties in projections of regional climate change exist. While the monsoons have been investigated for many decades and the understanding of the physical mechanisms associated with them has progressed steadily over the years, there are many unresolved questions of how the continual warming of the planet will affect the monsoons.

This book originated from the conference session entitled "The Global Monsoons and Climate Change: Observations, Models and Projections" held at the fall meeting of the American Geophysical Union (AGU) in 2012 in San Francisco, California. A significant portion of the material presented here includes results from the Coupled Model Intercomparison Project Phase 5 (CMIP5) model simulations, which contributed to the Fifth Assessment of the Intergovernmental Panel on

Climate Change (IPCC) finalized in 2013. Thus, the main goal of this book is to provide a concise and timely assessment of the monsoons and climate change.

The book has 11 chapters. Chapter 1 introduces the main intent of the book. A global view of the monsoons and its change are presented in Chap. 2. Chapters 3 and 4 discuss the Asian Monsoon variability and the projected changes in the twenty-first century. Chapter 5 covers the Australian summer monsoon and potential changes in upcoming decades, and the monsoon systems in South America and North America are discussed in Chaps. 6 and 7, respectively. Chapter 8 explores the seasonal variation of the Indo-Pacific monsoon circulation and interactions with the climate of East Africa. Connections between the North American and South American Monsoon systems are covered in Chap. 9. Since all monsoon systems exhibit significant variability on intra-seasonal time scales, Chap. 10 discusses future changes in the Madden-Julian Oscillation (MJO). Lastly, Chap. 11 analyzes the importance of the monsoon systems on glaciers in the central Andes and Himalayas.

The completion of this book was possible with the contributions of several authors who are experts in the research of monsoons and climate change. Their efforts and dedication are greatly appreciated, and we also thank Forest Cannon, Abheera Hazra, and Jesse Norris for their kind help in proofreading several sections of the book. Finally, we express our sincere appreciation for the support and professionalism of the editorial staff of Springer International Publishing.

Santa Barbara, CA, USA

Leila Maria Véspoli de Carvalho
Charles Jones

Contents

Contributors

H. Annamalai International Pacific Research Center, University of Hawaii, Honolulu, HI, USA

Paola A. Arias Grupo de Ingeniería y Gestión Ambiental (GIGA), Escuela Ambiental, Universidad de Antioquia, Medellín, Colombia; Departamento de Geofísica, Universidad de Chile, Santiago, Chile

Mathew Barlow Department of Environmental, Earth and Atmospheric Sciences, University of Massachusetts, Lowell, MA, USA

Bodo Bookhagen Institute of Earth and Environmental Science, University of Potsdam, Potsdam-Golm, Germany

Iracema F.A. Cavalcanti Climate Prediction and Weather Forecast Center, National Institute of Space Research (CPTEC/INPE), Cachoeira Paulista, Brazil

Leila Maria Véspoli de Carvalho Department of Geography, University of California, Santa Barbara, CA, USA; Earth Research Institute, University of California, Santa Barbara, CA, USA

Hirokazu Endo Climate Research Department, Meteorological Research Institute, Tsukuba, Ibaraki, Japan

Rong Fu Jackson School of Geosciences, University of Texas at Austin, Austin, TX, USA

Chris Funk Santa Barbara Climate Hazards Group, Department of Geography, University of California, Santa Barbara, CA, USA; Earth Resources Observation Systems Data Center, U.S. Geological Survey, Reston, USA

Andrew Hoell Santa Barbara Climate Hazards Group, Department of Geography, University of California, Santa Barbara, CA, USA

Pang-Chi Hsu International Laboratory on Climate and Environment Change and College of Atmospheric Science, Nanjing University of Information Science and Technology, Nanjing, China; International Pacific Research Center, University of Hawaii, Honolulu, HI, USA

Greg Husak Santa Barbara Climate Hazards Group, University of California, Santa Barbara, CA, USA

Charles Jones Department of Geography, University of California Santa Barbara, Santa Barbara, CA, USA; Earth Research Institute, University of California Santa Barbara, Santa Barbara, CA, USA

Akio Kitoh University of Tsukuba, Tsukuba, Ibaraki, Japan

Joel Michaelsen Santa Barbara Climate Hazards Group, University of California, Santa Barbara, CA, USA

Aurel Moise Bureau of Meteorology Research and Development, Melbourne, VIC, Australia

Shraddhanand Shukla Santa Barbara Climate Hazards Group, Department of Geography, University of California, Santa Barbara, CA, USA; University Corporation of Atmospheric Research, Boulder, CO, USA

K.R. Sperber Program for Climate Model Diagnosis and Intercomparison, Lawrence Livermore National Laboratory, Livermore, CA, USA

Hui Wang NOAA/NWS/NCEP/Climate Prediction Center, College Park, MD, USA; Innovim, Greenbelt, MD, USA

Huqiang Zhang Bureau of Meteorology Research and Development, Melbourne, VIC, Australia

Chapter 1
The Monsoons and Climate Change

Leila Maria Véspoli de Carvalho

Abstract Monsoon systems are unique features of the climate of the Earth and the reality of global warming has important implications for the environment and human society. This chapter provides a brief overview of this important topic.

Keywords Monsoons · Climate change · Population · IPCC · CMIP5

Monsoon systems are among the most extraordinary and intriguing phenomena on our planet. The word "monsoon" comes from the Arabic word "*mawsim,*" meaning "season." Historically, the term monsoon" describes the seasonal variation in surface winds that played significant roles in navigation and maritime trades, particularly with India (Tripati and Raut 2006). Today, this term is used in a much broader context. Monsoons are considered planetary manifestations of pronounced thermal contrasts between large land masses and ocean basins enhanced by the existence of high elevations and plateaus, such as the Tibetan Plateau in Asia and the Andes in South America. These efficient engines pump moisture from large ocean basins across great distances in meandering flows that reach tropical lands during summer to drive the most powerful precipitating systems on Earth.

Monsoon regions are globally distributed over all tropical continents and in tropical oceans in the eastern and western North Pacific, and in the southern Indian Ocean. Figure 1.1 represents the geographical distribution of these monsoon regions by the relative contribution of summer precipitation to the total annual precipitation. Six monsoon systems have been recognized: the African, South Asian, East Asian, Australian, North American, and South American Monsoons. Although the American monsoon system has not been clearly identified with wind reversals (Webster et al. 1998), when the long-term mean is removed, an evident seasonal reversal in circulation emerges (Vera et al. 2006; Zhou and Lau 1998). These magnificent systems regulate the hydrological cycle in large portions of the

L.M.V. de Carvalho (✉)
Department of Geography, University of California, Santa Barbara, CA, USA
e-mail: leila@eri.ucsb.edu

L.M.V. de Carvalho
Earth Research Institute, University of California, Santa Barbara, CA, USA

© Springer International Publishing Switzerland 2016

L.M.V. de Carvalho and C. Jones (eds.), *The Monsoons and Climate Change*,
Springer Climate, DOI 10.1007/978-3-319-21650-8_1

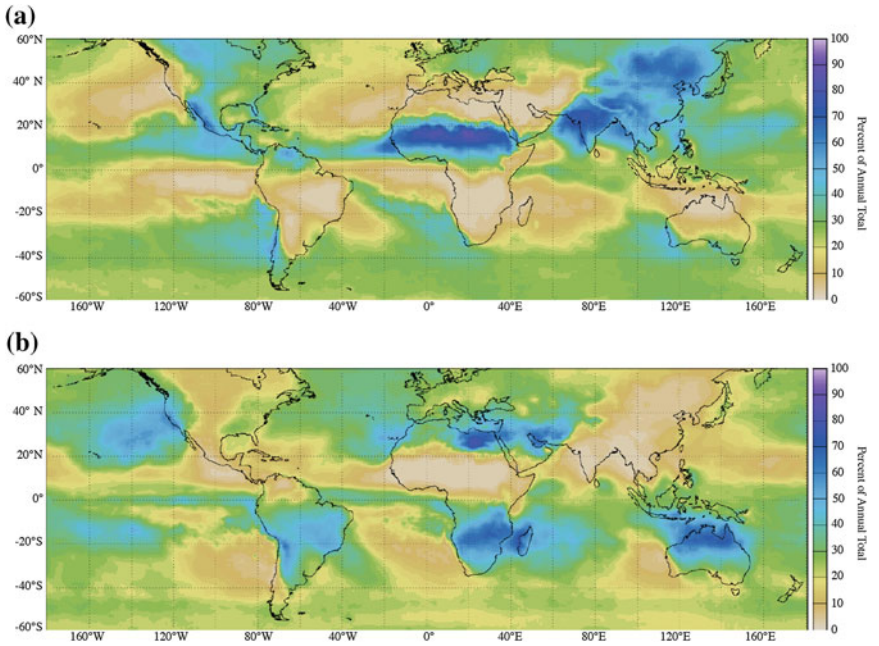

Fig. 1.1 Percent of annual precipitation during the summer peak in the northern hemisphere (June, July, August) and southern hemisphere summer (December, January, February). Precipitation data is from the Tropical Rainfall Measurement Mission (TRMM) at 25° resolution. **a** Percent of annual precipitation during June, July and August. **b** Percent of annual precipitation during December, January and February

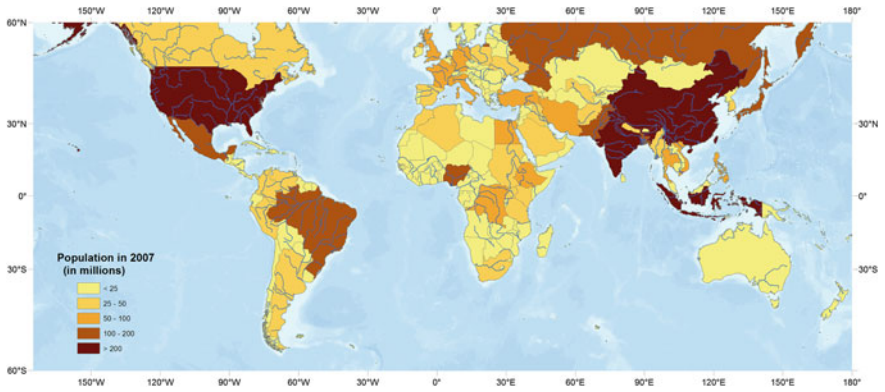

Fig. 1.2 World's population (in millions of inhabitants) as of 2007, and major river systems. *Data source* Environmental Systems Research Institute (ESRI)

tropics and are essential for creating the Earth's most diverse ecosystems and allowing the development of agriculture and human settlements throughout time.

Figure 1.2 shows the geographic distribution of the world's population and evidences the remarkable importance of monsoon systems for the subsistence of billions of people. The Earth's population in 2013 was estimated to be 7,162 billion people, with about 43 % of this population living in four countries largely affected by monsoonal regimes: China (first in the rank), India (second), Indonesia (third), and Brazil (fourth). According to projections of the United Nations (2013), the world's population is estimated to reach over 10 billion by the end of the twenty-first century, with India leading the rank and the most populated countries exhibiting territory partially or totally influenced by monsoon systems. Therefore, more than 50 % the Earth's population will be directly or indirectly influenced by monsoon systems and will be mostly susceptible to the effects of global warming and climate change in these regions. With the growth in population, the demand for food is expected to increase proportionally. Rice is among the most important crops that feeds the world (Seck et al. 2012), and countries influenced by the South Asia and East Asia monsoons lead rice production (http://www.geohive.com/). Climate change in monsoon regions increases the risks of infectious diseases that are usually exacerbated in developing countries due to inadequate sanitary conditions, malnutrition, and insufficient access to health services, clean water, and other basic necessities (Jones et al. 2008; Patz et al. 2005). Thus, variations and changes in intensity, frequency, and regularity of monsoonal precipitation are and will continue to be crucial for food and health security.

The abundant rainfall produced by summer convective systems over land controls soil moisture and the extent of wetlands and river flows, creates feedback (Douville et al. 2001; Eltahir 1998; Small 2001) and regulate carbon cycles (Richey et al. 2002). The dry period during the winter months following the wet season reinvigorates crop cycles, which are relevant for carbon sequestration (Carvalho et al. 2009). The dry season is also the period of intense biomass burning, particularly from rainforests and pasture, a practice that is very common in all monsoon regions (Crutzen and Andreae 1990; Fearnside 2000; Hao and Liu 1994; Haywood et al. 2008; Lestari et al. 2014). Hobbs et al. (1997) estimate that about 80 % of all biomass burning occurs in the tropics. Biomass burning from anthropogenic or natural origin releases large quantities of CO, CO_2, acetonitrile, methyl chloride, hydrocarbons, NO, O_3, and aerosols in the atmosphere, which are transported through long distances affecting air quality across the globe and causing complex feedback in the climate system that have yet to be identified and properly quantified (Andreae et al. 1988; Andreae et al. 2001; Freitas et al. 2005). Global warming may cause regional variations in monsoonal circulation and modify the length of the wet and dry seasons, resulting in variations in the distribution of precipitation and cloudiness that can accelerate climate change by modifying carbon cycles (Luo 2007; White et al. 1999) and radiation budgets, among other processes. The anthropogenic component of these changes is difficult to evaluate as society evolves and exerts significant pressure on the environment by intensifying land-use-land-cover-change and releasing greenhouse gases and aerosols in the atmosphere (Karl and Trenberth 2003; Trenberth 2011).

The increase in surface temperatures also has important implications for the hydrological cycle in regions where the water supply depends on the melting of snow and ice, such as the Andes and the Himalayas. There is evidence that the South American Monsoon and the Indian Monsoon are essential for supplying moisture and precipitation to high elevations (Barnett et al. 2005; Bird et al. 2011), and possibly controlling surface temperatures through cloud radiative transfer processes. In addition, changes in precipitation affect the volume and timing of runoff with dramatic impacts for populations living downslope of these mountains (Bookhagen and Burbank 2010; Bookhagen and Strecker 2012).

Understanding and assessing the anthropogenic influence on the monsoons is especially challenging for several reasons: vast areas covered by rain forests and complex terrain with limited access to instrumentation; intermittent and scarce observations, particularly for periods extending before the satellite era; and monsoon regions dominated by developing and least developing countries (according to the United Nations) that provide limited support for installing and maintaining meteorological stations. Although monitoring climate variations in monsoon regions has considerably improved since the advent of satellites, long-term trends and regional to local climate change signals are virtually unknown in large areas under the influence of monsoon systems.

The compelling evidence of warming of the climate system since the twentieth century and the anthropogenic interference in this process motivated the United Nations to create the Intergovernmental Panel on Climate Change (IPCC). The IPCC is a scientific intergovernmental body that was established in 1988 by the World Meteorological Organization (WMO) and the United Nations Environment Programme (UNE), with the goal of producing reports that support the United Nations Framework Convention on Climate Change, which is considered the main international treaty on climate change. The IPCC reports "cover the scientific, technical and socio-economic information relevant to understanding the scientific basis of the risk of human-induced climate change, its potential impacts and options for adaptation and mitigation" (www.ipcc.ch). The completion of the Fifth Assessment Report of (AR5) the Intergovernmental Panel on Climate Change (IPCC 2013) provided the most updated scientific understanding of climate change and its implications.

The main purpose of this book is to provide a concise and timely assessment of monsoons and climate change based on the AR5 and other recent scientific contributions; its 11 chapters cover the monsoons from a global perspective as well as each individual monsoon system. A global view of the monsoons and their changes are presented in Chap. 2. Chapters 3 and 4 discuss the Asian Monsoon variability and the projected changes in the twenty-first century, while Chap. 5 covers the Australian summer monsoon and potential changes in the coming decades. The monsoon systems in South America and North America are discussed in Chaps. 6 and 7, respectively. Chapter 8 explores the seasonal variation of the Indo-Pacific monsoon circulation and interactions with the climate of East Africa. Connections between the North American and South American Monsoon systems are discussed in Chap. 9. Since all monsoon systems exhibit significant variability on

intra-seasonal time scales, Chap. 10 discusses future changes in the Madden-Julian Oscillation (MJO). Finally, Chap. 11 analyzes the importance of the monsoon for glacier systems.

Acknowledgments Leila Maria Véspoli de Carvalho acknowledges the support of the Climate and Large-scale Dynamics Program of the National Science Foundation (AGS-1053294 and AGS 1116105), the NOAA Climate Program Office (NA10OAR4310170), the CGIAR Research Program on Climate Change, Agriculture and Food Security (CCAFS), and the International Potato Center in Lima, Peru (SB120184). The author is grateful to Forest Cannon and Yingjie Hu for producing Figs. 1.1 and 1.2 in this chapter.

References

Andreae MO et al (1988) Biomass-burning emissions and associated haze layers over Amazonia. J Geophys Res Atmos 93:1509–1527

Andreae MO et al (2001) Transport of biomass burning smoke to the upper troposphere by deep convection in the equatorial region. Geophys Res Lett 28:951–954

Barnett TP, Adam JC, Lettenmaier DP (2005) Potential impacts of a warming climate on water availability in snow-dominated regions. Nature 438:303–309

Bird BW, Abbott MB, Vuille M, Rodbell DT, Stansell ND, Rosenmeier MF (2011) A 2300-year-long annually resolved record of the South American summer monsoon from the Peruvian Andes. Proc Natl Acad Sci 108:8583–8588

Bookhagen B, Burbank DW (2010) Toward a complete Himalayan hydrological budget: spatiotemporal distribution of snowmelt and rainfall and their impact on river discharge. J Geophy Res Earth Surf 115:F03019

Bookhagen B, Strecker MR (2012) Spatiotemporal trends in erosion rates across a pronounced rainfall gradient: Examples from the southern Central Andes. Earth Planet Sci Lett 327–328: 97–110

Carvalho JLN, Cerri CEP, Feigl BJ, Píccolo MC, Godinho VP, Cerri CC (2009) Carbon sequestration in agricultural soils in the Cerrado region of the Brazilian Amazon. Soil and Tillage Res 103:342–349

Crutzen PJ, Andreae MO (1990) Biomass burning in the tropics: impact on atmospheric chemistry and biogeochemical cycles. Science 250:1669–1678

Douville H, Chauvin F, Broqua H (2001) Influence of soil moisture on the Asian and African monsoons. part i: mean monsoon and daily precipitation. J Clim 14:2381–2403

Eltahir EAB (1998) A soil moisture-rainfall feedback mechanism: theory and observations. Water Resour Res 34:765–776

Fearnside P (2000) Global warming and tropical land-use change: greenhouse gas emissions from biomass burning, decomposition and soils in forest conversion, shifting cultivation and secondary vegetation. Clim Change 46:115–158

Freitas S et al (2005) Monitoring the transport of biomass burning emissions in South America. Environ Fluid Mech 5:135–167

Hao WM, Liu M-H (1994) Spatial and temporal distribution of tropical biomass burning. Glob Biogeochem Cycles 8:495–503

Haywood JM et al (2008) Overview of the dust and biomass-burning experiment and african monsoon multidisciplinary analysis special observing period-0. J Geophys Res: Atmos 113: D00C17

Hobbs PV, Reid JS, Kotchenruther RA, Ferek RJ, Weiss R (1997) Direct radiative forcing by smoke from biomass burning. Science 275:1777–1778

IPCC (2013) The physical sience basis. Contributions of working group i to the fifth assessment report of the intergovernmental panel on climate change. In: Stocker TF, Qin D, Plattner G-K, Tignor M, Allen SK, Boschung J, Nauels A, Xia Y, Bex V, Midgley PM (eds). Cambridge University Press, Cambridge, UK and New York, USA, pp 1535

Jones KE, Patel NG, Levy MA, Storeygard A, Balk D, Gittleman JL, Daszak P (2008) Global trends in emerging infectious diseases. Nature 451:990–993

Karl TR, Trenberth KE (2003) Modern global climate change. Science 302:1719–1723

Lestari RK, Watanabe M, Imada Y, Shiogama H, Field RD, Takemura T, Kimoto M (2014) Increasing potential of biomass burning over Sumatra, Indonesia induced by anthropogenic tropical warming. Environ Res Lett 9:104010

Luo Y (2007) Terrestrial carbon-cycle feedback to climate warming. Annu Rev Ecol Evol Syst 38:683–712

Patz JA, Campbell-Lendrum D, Holloway T, Foley JA (2005) Impact of regional climate change on human health. Nature 438:310–317

Richey JE, Melack JM, Aufdenkampe AK, Ballester VM, Hess LL (2002) Outgassing from Amazonian rivers and wetlands as a large tropical source of atmospheric CO2. Nature 416:617–620

Seck P, Diagne A, Mohanty S, Wopereis MS (2012) Crops that feed the world 7: rice. Food Sec 4:7–24

Small EE (2001) The influence of soil moisture anomalies on variability of the North American monsoon system. Geophys Res Lett 28:139–142

Trenberth KE (2011) Attribution of climate variations and trends to human influences and natural variability. Wiley Interdisc Rev Clim Change 2:925–930

Tripati S, Raut LN (2006) Monsoon wind and maritime trade: a case study of historical evidence from Orissa, India. Curr Sci 90:864–871

United Nations, D. o. E. a. S. A., Population Division (2013) World population prospects: The 2012 revision, vol II, Demographic profiles (ST/ESA/SER.A/345), I

Vera C et al (2006) Toward a unified view of the American monsoon systems. J Clim 19: 4977–5000

Webster PJ, Magaña VO, Palmer TN, Shukla J, Tomas RA, Yanai M, Yasunari T (1998) Monsoons: Processes, predictability, and the prospects for prediction. J Geophys Res Oceans 103:14451–14510

White MA, Running SW, Thornton PE (1999) The impact of growing-season length variability on carbon assimilation and evapotranspiration over 88 years in the eastern US deciduous forest. Int J Biometeorol 42:139–145

Zhou JY, Lau KM (1998) Does a monsoon climate exist over South America? J Clim 11: 1020–1040

Chapter 2
Global Monsoon in a Changing Climate

Pang-Chi Hsu

Abstract Monsoons, the most energetic tropical climate system, exert a great social and economic impact upon billions of people around the world. This chapter reviews recent progress in our understanding of the global monsoon (GM) system and its associated precipitation changes in the present and future warming climates. The GM can be viewed as an integrated system of all regional monsoons over the globe that are driven by solar forcing and bounded by the planetary-scale overturning circulation. The GM precipitation (GMP), defined as the total summer monsoon precipitation amount within the GM area (GMA), experienced multi-decadal variability in the twentieth century. The observed GMP over land shows a slightly increasing trend from 1900 throughout the 1940s, and then a downward trend from the 1950s until the end of the 1970s; there was no clear trend after 1980. The GMP over the ocean has had more uncertainty over the past three decades, and trends are inconsistent among different global rainfall datasets. In the twenty-first century, the GMP is expected to increase robustly, based on the projections by the state-of-the-art coupled models that participated in Phases 3 and 5 of the Coupled Model Intercomparison Project (CMIP3 and CMIP5). The change in GMP under global warming is primarily due to changes to the hydrological cycle induced by warmer temperatures. The increase in water vapor contributes positively to moisture convergence and surface evaporation over the GMA, but is partly offset by the weakening of the monsoon circulation.

Keywords Global monsoon · Monsoon precipitation variability · Global warming · CMIP3 · CMIP5

P.-C. Hsu (✉)
International Laboratory on Climate and Environment Change and College of Atmospheric Science, Nanjing University of Information Science and Technology, Nanjing, China
e-mail: pangchi@hawaii.edu

P.-C. Hsu
International Pacific Research Center, University of Hawaii, Honolulu, HI, USA

© Springer International Publishing Switzerland 2016

L.M.V. de Carvalho and C. Jones (eds.), *The Monsoons and Climate Change*,
Springer Climate, DOI 10.1007/978-3-319-21650-8_2

2.1 Introduction

"Monsoon" is conventionally defined as the seasonal reversal in lower-tropospheric winds (Ramage 1971), and its associated precipitation is characterized by a contrast between wet summers and dry winters (Webster 1987). The contrast is induced by the annual cycle of solar heating and seasonal changes in large-scale continent-ocean thermal contrast. Monsoons occur around the globe: in Asia, Australia, Africa, and throughout the Americas (Webster et al. 1998). From a regional perspective, an individual monsoon system evolves according to the local land-sea configuration, orography, and feedback with the distinct elements of the climate system. The features and variations of each regional monsoon have been extensively studied over the past three decades (e.g., Davidson et al. 1983; McBride 1987; Tao and Chen 1987; Webster 1987; Ding 1994; Higgins et al. 1997; Webster et al. 1998; Sultan and Janicot 2003; Goswami 2005; Vera et al. 2006).

More recently, an emerging concept of the global monsoon (GM) has been proposed to describe the combined variability of monsoon systems around the world. Considering that all regional monsoons are associated with the annual cycle of solar heating and that the global-scale circulation is necessitated by mass conservation, Trenberth et al. (2000) depicted the GM system as a persistent global-scale overturning of the tropical atmosphere that varies with seasons. In a dynamic sense, the rainfall distributions reflect the tropospheric heat sources that drive the circulation in the tropics; thus, the planetary-scale overturning circulation is closely associated with the seasonal variation of precipitation. Wang and Ding (2008) documented that in the climatological context, the GM system is the dominant mode of annual precipitation and 850 hPa winds in the tropics. Applying a multi-variable empirical orthogonal function (EOF) analysis to climatological monthly precipitation and low-level wind fields, two leading modes—accounting for 84 % of the annual variance—were obtained. The first mode, called the solstitial mode, represents the atmospheric response to the meridional differential of annual solar forcing. The second mode, the equinoctial asymmetry mode, reflects the asymmetric patterns between spring and autumn. Both modes characterize the seasonality of tropical climate (Wang and Ding 2008).

In short, the GM is a response of the coupled climate system to the annual cycle of solar forcing. From this global perspective, the precipitation over each monsoon region combines to form the GM system, which is associated with a planetary-scale overturning circulation throughout the tropics (Trenberth et al. 2000, 2006).

2.2 Delineations of Global Monsoon Precipitation, Area, and Intensity

The monsoon climate features the seasonal variations in both wind and precipitation. Earlier studies used the reversal in wind direction and speed to identify a monsoon domain (Ramage 1971). Such monsoon domains are found mainly over

the Eastern Hemisphere because the seasonal wind reversal is less significant over the Americas. Besides the wind field, precipitation is another fundamental variable used to delineate the monsoon climate. Monsoon precipitation is characterized by a concentration of yearly rainfall in the local summer and a dry period in the local winter (Webster 1987). Using a simple parameter based on precipitation, Wang and Ding (2006) defined the global monsoon area (GMA) as the regions in which the annual range (AR—the local summer-minus-winter rainfall) of rainfall exceeds 180 mm and the summer-to-annual rainfall ratio is greater than 35 %. In the Northern Hemisphere (NH), the summer is defined as June to August (JJA) and the winter is defined as December to February (DJF). In the Southern Hemisphere (SH), the definitions are reversed. Figure 2.1 shows the derived GMA based on the climatological monthly rainfall averaged from the Global Precipitation Climatology Project (GPCP; Adler et al. 2003) and the CPC Merged Analysis of Precipitation (CMAP; Xie and Arkin 1997) datasets. The known monsoon systems around the world, including the Asian, Australian, northern and southern African, and North and South American Monsoons, are well identified.

Following the approach of Wang and Ding (2006), other studies modified the lengths of summer and winter seasons and the criteria of rainfall indices. For example, Liu et al. (2009) used a longer length of local summer (May to September (MJJAS) for the NH) and winter (November to March (NDJFM) for the NH) months. The two criteria for GMA were modified as the AR (MJJAS and NDJFM difference) exceeding 2 mm day^{-1} and the ratio of summer-to-annual rainfall exceeding 55 %. The defined GMA (Fig. 2 in Liu et al. 2009) is almost identical to that shown in Fig. 2.1. The GMA presented in Wang et al. (2011) was based on alternative criteria—AR (JJA and DJF difference) exceeding 2 mm day^{-1} and 70 % of the annual mean, and it also agrees with the results shown in Fig. 2.1 and other similar studies (Wang and Ding 2008; Liu et al. 2009). Therefore, the defined GMA is not very sensitive to the two criteria with some modifications.

Total rainfall amount during a local summer (JJA for the NH, and DJF for the SH) is the major factor determining the amplitude of AR. Generally, a larger AR (wet-dry season contrast) reflects a more active monsoon. Therefore, the total GM

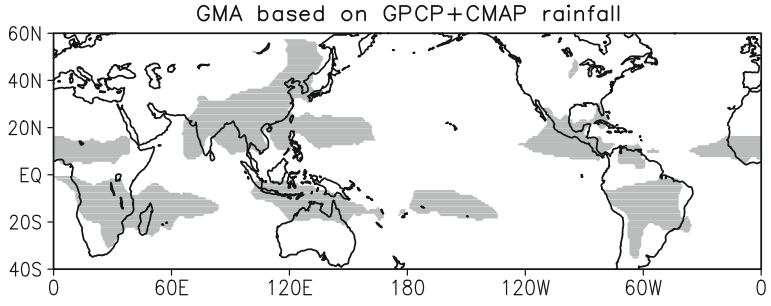

Fig. 2.1 Observed global monsoon area (*shaded area*) derived from the average of GPCP and CMAP climatological rainfall for 1979–2008

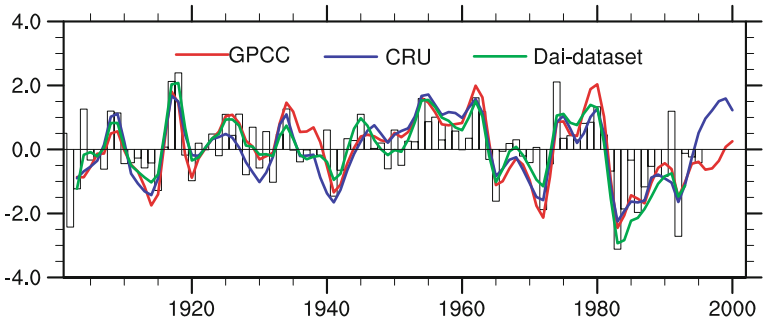

Fig. 2.2 Time series of normalized global land monsoon precipitation anomalies. The bars denote the GMP over land based on the data compiled by Dai (*Dai-dataset*). The anomalies are calculated relative to the mean of 1951–1979, using the precipitation datasets developed by the Global Precipitation Climatology Centre (*GPCC*) and by the Climate Research Unit (*CRU*), and the Dai-dataset. The *red*, *blue*, and *green curves* are 5-year running means of GPCC, CRU and Dai-dataset, respectively. According to Zhang and Zhou (2011)

precipitation (GMP)—the sum of summer rainfall within the GMA—is proposed to describe the monsoon strength (Wang and Ding 2006, 2008; Liu et al. 2009). Given that the global circulation and the land-sea surface-temperature contrast may experience significant changes from one climate condition to another, induced by sea-surface-temperature (SST) anomalies or anthropogenic forcing, the GMA may be subject to some temporal/spatial variability. To describe the GMP change associated with a varying GMA, the global monsoon intensity (GMI) index, which measures the GMP amount per unit area, was introduced (Zhou et al. 2008a; Hsu et al. 2011; Wang et al. 2011). Because the area in each grid box varies with latitude, an area-conserving metric is applied when calculating the GMA and GMP. The long-term variability of GMA, GMP, and GMI over the past decades and their projected changes under certain global warming scenarios, are reviewed in the following two sections, respectively.

2.3 Observed Changes in Global Monsoon Activity

2.3.1 Trends in GM Precipitation in the Twentieth Century

After the concept of the GM was proposed, a number of researchers began to investigate the variability of GMP over continental monsoon areas inhabited by billions of people. Chase et al. (2003) analyzed the variation of land precipitation along with surface pressure and upper-level divergence in the Asian, Australian, and African monsoon regions between 1950 and 1998. Consistent reductions in land rainfall and monsoonal circulations have been detected over the monsoon

regions globally since 1950. However, this decreasing trend has leveled off since 1979, when the strongest global warming has been reported in terms of averaged surface temperature. Using four sets of rain gauge observations for the 1948–2003 period, Wang and Ding (2006) also pointed out an overall downward trend in rainfall over land within global monsoon domains, particularly before 1980. The weakening of GMP over land was mainly attributed to the decreased summer monsoon rainfall in the NH because the monsoon rainfall in the SH showed no significant trend over the same period (Wang and Ding 2006). Zhou et al. (2008a) further pointed out that not only the monsoon precipitation intensity, but also the total monsoon area, contributed to this weakening trend in global land monsoon rainfall from 1949 to 2002.

Using a century-long observational rainfall dataset, Zhang and Zhou (2011) found that the global land monsoon precipitation exhibited a significant multi-decadal variability during the twentieth century (Fig. 2.2). A significant upward trend in the global land monsoon precipitation was shown in the first half of the century (1901–1955), followed by a downward trend in the latter half (1955–2001), as documented in other studies (Chase et al. 2003; Wang and Ding 2006; Zhou et al. 2008a). Because of this multi-decadal change, the overall trend for the twentieth century (1901–2001) was not statistically significant at the 95 % confidence level.

As discussed above, the results based on rain-gauge observations show no significant trend in rainfall over the global land monsoon areas since 1979. Was this the same for the precipitation change over the oceanic monsoon regions? Wang and Ding (2006) used the GPCP dataset to examine the GMP over oceans and found a significant increasing trend from 1979 to 2003. This change in oceanic monsoon rainfall, however, is not robust and depends on data sources (Zhou et al. 2008b; Hsu et al. 2011). In contrast to the GPCP data, the CMAP data indicate a weak declining monsoon rainfall over the global oceanic monsoon regions for the period of 1979–2008. The inconsistency of rainfall variability over the oceans between the GPCP and CMAP datasets was attributed to different algorithms used to retrieve the precipitation from the satellite data (Gruber et al. 2000).

The trends in global oceanic monsoon rainfall have dominated the trends in total GMP over the past three decades (Wang and Ding 2006; Zhou et al. 2008b; Hsu et al. 2011). The GMP showed an increasing trend from 1979 to 2008 based on the GPCP rainfall data, while it revealed a downward tendency over the same period using the CMAP dataset (Fig. 2.3). Zhou et al. (2008b) found that the oceanic monsoon rainfall derived from the GPCP dataset was highly correlated with that of the Special Sensor Microwave Imager (SSM/I), which might be the best available precipitation estimates over the ocean. This suggests that the trend in GMP obtained from the GPCP data is probably more reliable than that from the CMAP data. With a focus on the monsoon change at the hemispheric scale, Wang et al. (2013) found consistent enhancements of NH monsoon rainfall and of the Walker and Hadley circulations from 1979 to 2011.

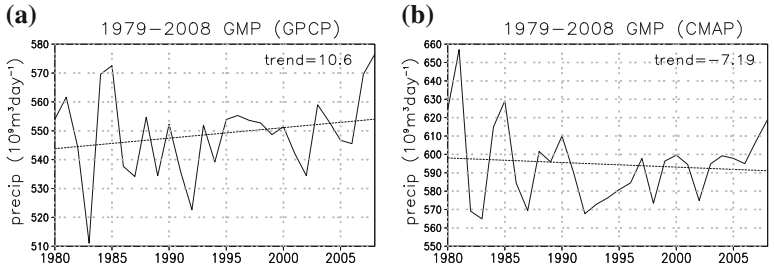

Fig. 2.3 **a** Time series of global monsoon precipitation (GMP; units: 10^{9} m^{3} day^{-1}) calculated from (s) the GPCP and **b** the CMAP datasets for 1979–2008. The linear trend of each time series is indicated by a *dotted line*, with the linear trend [units: 10^{9} m^{3} day^{-1}(29 year)$^{-1}$] noted on each panel. (Adapted from Hsu et al. 2011)

2.3.2 *Factors Controlling the GMP Change*

Variations in GMP can be attributed to tropical atmospheric responses to varying forcing fields, such as SST, shortwave forcing resulting from the effect of aerosols, and longwave forcing induced by growing greenhouse gas emissions. Wang et al. (2012) discussed the mechanisms regulating the NH summer monsoon rainfall over land and adjacent ocean areas. They suggested that the zonal contrast of eastern and western Pacific SST plays an important role in causing the enhanced NH monsoon precipitation. The recent trend of eastern Pacific cooling and western Pacific warming favors the high (low) pressure anomaly in the eastern (western) Pacific and the trades that transport moisture into the Asian and African monsoon regions (Wang et al. 2013). Moreover, the intensification of NH monsoon rainfall is consistent with the increased inter-hemispheric thermal contrast. The pattern associated with a warmer NH and a cooler SH over the past three decades would induce strengthened cross-equatorial flows driven by meridional pressure gradients. As a result, more moisture is transported from the SH into the NH, favoring the monsoon rainfall in the NH (Wang et al. 2012).

Long-term simulations under different forcing fields may help to clarify the factors controlling the observed GMP changes. Zhou et al. (2008b) showed that the observed weakening trend in global land monsoon precipitation over the second half of the twentieth century was successfully reproduced by the NCAR Community Atmosphere Model version 2 (CAM2) driven by observed SSTs between 1950 and 2000. The results indicated that the changes in GMP over land may have arisen from oceanic forcing. In the second half of the twentieth century (1950–2000), significant warming trends were observed over the central-eastern Pacific Ocean and the tropical Indian Ocean. Zhou et al. (2008b) further argued that the recent warming over the central-eastern Pacific Ocean and the tropical Indian Ocean contributed to the reduction of global land monsoon precipitation during the period of 1950–2000 reported by Wang and Ding (2006).

In addition to the SST influence, aerosols have been reported to have significant impacts on regional rainfall in several ways (e.g., Turner and Annamalai 2012).

Focusing on the effect of volcanic aerosols, Kim et al. (2008) analyzed the GMP changes in the twentieth-century simulations for the period of 1951–1999 from the models participating in the third phase of the Coupled Model Intercomparison Project (CMIP3). They found that among 21 CMIP3 models, those with volcanic aerosols simulated the decreasing trends of NH land monsoon rainfall since 1950, suggesting that the natural volcanic forcing could be an important contributor to the reduction of global land monsoon precipitation. The results of Kim et al. (2008) were similar to the findings of Lambert et al. (2004), who argued that variation in land precipitation was controlled more by the natural shortwave forcing of volcanic aerosols than by the longwave forcing of greenhouse gases. External forcing associated with volcanic aerosols plays a crucial role in multi-decadal variability of torrential precipitation in both observations and model simulations (Broccoli et al. 2003; Gillett et al. 2004).

2.4 Future Projections of Global Monsoon

The rise in the average temperature of the Earth's atmosphere and oceans—namely, global warming—has been observed since the late twentieth century and is projected with very high probability to continue in the coming century (e.g., IPCC 2007, 2013). Estimates of GM change under a warmer future climate primarily rely on projections from climate models. Thanks to great advances in computing power and numerical model developments, state-of-the-art atmospheric general circulation models (AGCMs) and ocean-atmosphere, coupled general circulation models (CGCMs) driven by various global-warming forcings, may help to provide consistent projected signals and enhance our confidence in these future GM changes. A number of robust signals related to GM change were identified from the recent modeling studies based on various multi-model ensemble (MME) approaches (Hsu et al. 2012, 2013; Chen and Sun 2013; Kitoh et al. 2013; Lee and Wang 2014). In this section, future changes in GM domain, total amount of monsoon precipitation, extreme monsoon precipitation events, timing of monsoon onset and retreat, and inter-annual variability of GM are reviewed and discussed.

2.4.1 Changes in GM Domain

Based on simulations of three high-resolution (20–50 km) AGCMs forced by various future SST warming patterns during the twenty-first century, Hsu et al. (2012) indicated a consistent increase of GMA under global warming. The GMA increased around 7–9 % from the end of the twentieth century to the end of the twenty-first century in these simulations. Marked expansions occurred over the oceans, which accounted for 80–90 % of the total contribution to the GMA change in these simulations.

The expansions of GM domain were also projected in the MMEs of CMIP3 and CMIP5 models, although the spread of individual models is large (Hsu et al. 2012, 2013; Kitoh et al. 2013; Lee and Wang 2014). As shown in Fig. 2.4, the GMA projections show a 3–6 % increase from the late twentieth century (1979–2003) to the end of the twenty-first century (2075–2099) based on many ensemble members (~20 or more) of CMIP5 models under the Representative Concentration Pathways 4.5 (RCP4.5) scenario and of CMIP3 models under the Special Report on Emissions Scenarios (SRES) A1B scenario (Chen and Sun 2013; Hsu et al. 2013; Kitoh et al. 2013). The averaged expansion of GMA was larger (~9 %) when the models were forced with the higher greenhouse gas emissions under the RCP8.5 scenario (Kitoh et al. 2013). Even so, Hsu et al. (2013) indicated that the expansion rate of GMA is not significantly correlated with the increase in global mean surface air temperature.

Rather than analyzing MMEs based on all CMIP3 or all CMIP5 models, Lee and Wang (2014) conducted an MME analysis based on the four models among 20 CMIP5 models that most accurately simulated monsoon precipitation characteristics during the period of 1980–2005. Similar to the results of all models' MME, the four best models' MME (B4MME) projects an increased GMA with a change rate of 4.6 % (2.6 % for land and 6.3 % for ocean) from the end of the twentieth century (1980–2005) to the end of the twenty-first century (2070–2095) under the RCP4.5 scenario. However, this change does not exceed the uncertainty measured by a standard deviation of inter-model spread.

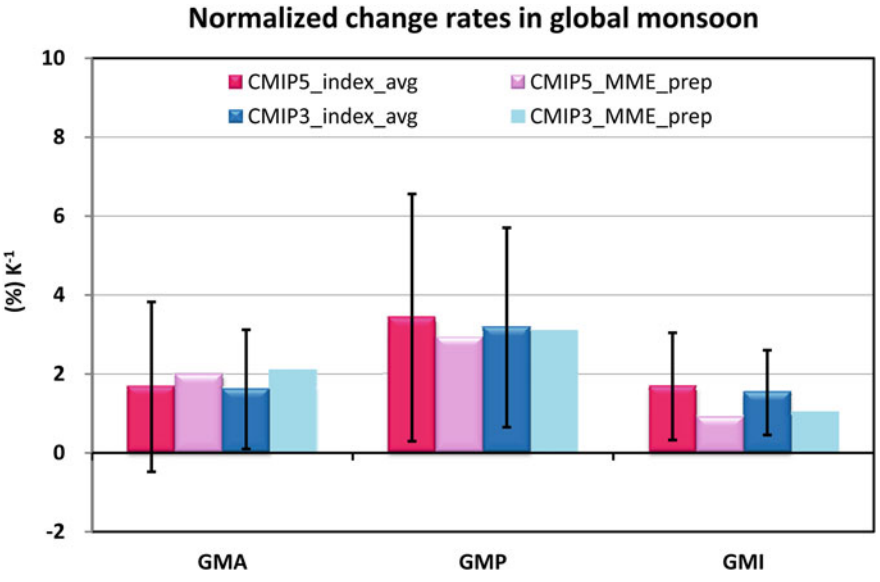

Fig. 2.4 Averages and inter-model standard deviations [*red* (*blue*) bars with whiskers] of GMA, GMP and GMI change rates between RCP4.5 (A1B) from 2075 until 2099, and historical (20C3 M) from 1979 to 2003 in 19 CMIP5 (24 CMIP3) simulations. *Pink* (*light blue*) bars show the change rates calculated from the CMIP5 (CMIP3) multi-model ensemble mean precipitation. (Adapted from Hsu et al. 2013)

According to the CMIP5 MME results, under the RCP4.5, the increased GMA will be distributed along the edges of the present-day GMA, especially for the global oceanic monsoon regions (Hsu et al. 2013). This is consistent with the B4MME results of Lee and Wang (2014), which suggested that the monsoon domain will tend to increase over oceanic monsoon regions while it will apparently not change over land except for a westward movement of Asian continental monsoon areas. Based on the RCP8.5 simulations, Kitoh et al. (2013) identified GMA expansions mainly over the central-to-eastern tropical Pacific, the southern Indian Ocean, and eastern Asia.

The future expansion of GMA may be attributed to both an increased annual range of precipitation under global warming (Chou and Lan 2012) and a stronger summer-to-annual rainfall ratio (Hsu et al. 2012; Lee and Wang 2014). Hsu et al. (2013) analyzed the absolute change of monthly rainfall within the GMA and found a prominent increase in local summer monsoon rainfall over the globe. Projected winter rainfall within the GMA, however, shows less significant change, with a small increase (decrease) in the NH (SH). These results indicate that global warming may induce a wetter summer over the GM regions, and enhance the contrast between rainy and dry seasons (especially in the SH).

2.4.2 *Changes in GM Precipitation and Intensity*

The expansion of the GMA may cause changes in GMP, as a larger monsoon domain would receive more rainfall. As shown in Fig. 2.4, the MME indicates a 6–9 % increase in GMP under the SRES A1B and RCP4.5 scenarios (Hsu et al. 2013), and much more ($\sim$16.6 %) in the RCP8.5 scenarios from the end of the twentieth century to the end of the twenty-first century (Kitoh et al. 2013). Due to a greater rate of increase of GMP than of GMA, the GM intensity, which is defined as the monsoon precipitation amount per unit area, will tend to strengthen in future warmer climate. The increase of GMI from the end of the twentieth century until the end of the twenty-first century ranges from 2 to 4 % in the CMIP3 and CMIP5 MME results, respectively (Fig. 2.4).

Precipitation extremes occurring in all regional monsoons are projected to increase at a much greater rate than the GMP (Kitoh et al. 2013). For example, GMP will increase by −6.5 to 12.9 % by the end of the twenty-first century, according to the RCP8.5 simulations, while the simple daily precipitation intensity index, defined as total precipitation divided by the number of rainy days (≥1 mm), shows—0.7 to 14.7 % increase. The index of seasonal maximum precipitation total over five consecutive days within the global monsoon areas shows an even greater increase (6.2–22.1 %) under the RCP8.5 scenario. As well as the increase in extreme precipitation events, indices of extreme dry events (such as maximum number of consecutive no-rain days) within the GMA are projected to increase (Lu and Fu 2010; Turner and Annamalai 2012). This suggests that although the frequency of precipitation events would decrease in a future warmer climate, the precipitation intensity of individual events could be greater (Kitoh et al. 2013).

Lee and Wang (2014) illustrated the spatial distribution of GMP change based on the B4MME (Fig. 2.5). The CMIP5 models projected a remarkable enhancement (reduction) of monsoon rainfall over Asia (northern America). Monsoon rainfall over Australia and Africa also show positive contributions to the increased GMP, but with less significance and robustness. The relative contributions from regional monsoons to the GMP projected by the B4MME generally agree with those derived from the CMIP5 models' MME (Kitoh et al. 2013); in other words, the Eastern-hemisphere monsoons will produce more precipitation than the Western-hemisphere monsoons, and the NH monsoons will produce more precipitation than the SH monsoons. This means that future changes in GMP can be characterized by a prominent east–west contrast and a north–south asymmetry. As with the summer mean monsoon rainfall projections, the extreme precipitation events are also projected to increase most significantly in the Asian monsoon domain, suggesting that the Asian monsoon is particularly sensitive to global warming (Kitoh et al. 2013).

To better understand the physical processes that cause the increase in GMP projected by the CMIP5 models, Hsu et al. (2013) examined a column-integrated moisture budget within the GMA in present-day and future-climate simulations, respectively.

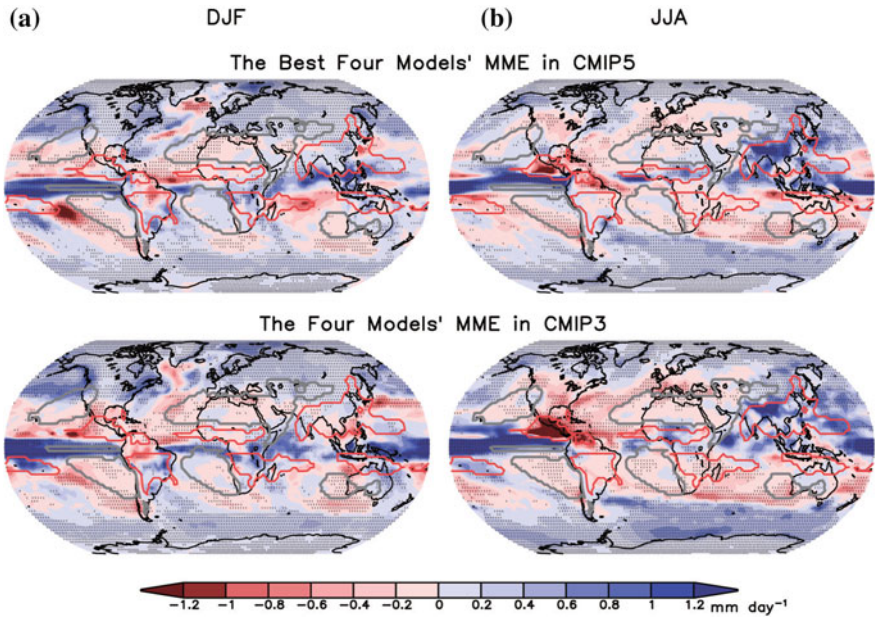

Fig. 2.5 Changes in **a** annual mean precipitation, and **b** annual range of precipitation. The annual range is defined as absolute value of JJAS mean minus DJFM mean precipitation rate. Changes are given for the RCP4.5 (A1B) simulation for 2070–2095 relative to the historical simulation for 1980–2005, in CMIP5 (CMIP3) in the *upper* (*bottom*) panels. *Red* contours delineate the GMA. (Adapted from Lee and Wang 2014)

The column-integrated moisture tendency equation is

$$\frac{\partial w}{\partial t} + <;\nabla \cdot (q\mathbf{V}) >; = E - P \tag{2.1}$$

where w is precipitable water (total column water vapor), t is time, $< >$ indicates a vertical integration from 1,000 to 100 hPa, ∇ is the horizontal gradient operator, q is specific humidity, $\mathbf{V}$ is the horizontal vector wind, E is evaporation, and P is precipitation. This equation assumes that the condensates immediately fall to the surface as precipitation after they form. Although w and q differ between the present-day state and the future-climate state, they are assumed to be in a state of equilibrium in both periods. Thus, for each period, the tendency term ($\partial w/\partial t$) vanishes. The diagnostic equation of GMP change is then derived based on the difference of the remaining terms between the present-day and future-climate states. The change in GMP may be attributed to changes in horizontal moisture advection, moisture convergence associated with mass convergence (or vertical motion), and surface evaporation, as shown in the following equation:

$$\Delta\mathrm{GMP} = -\Delta < V \cdot \nabla q > \; - \Delta < q\nabla \cdot V > \; + \Delta E. \tag{2.2}$$

The operator Δ represents the difference between future-climate and present-day simulations (future minus present-day).

The diagnostic results of CMIP5 models show that increases in both moisture convergence and surface evaporation will contribute to increased GMP, whereas moisture advection will contribute insignificantly to GMP change (Fig. 2.6a). Because the changes in atmospheric moisture and circulation affect both moisture convergence and surface evaporation, it is necessary to examine their relative contributions. The changes in moisture convergence and surface evaporation may be decomposed into three terms, as shown below:

$$-\Delta < q \times D > \; = - < q_{\mathrm{pd}} \times \Delta D > \; - < \Delta q \times D_{\mathrm{pd}} > \; - < \Delta q \times \Delta D >, \tag{2.3}$$

$$\begin{aligned} \Delta \mathrm{E} &= \Delta[\alpha|\mathbf{V}|(q_s - q_a)] \\ &= \alpha[\Delta|\mathbf{V}| \times (q_s - q_a)_{\mathrm{pd}} + |\mathbf{V}|_{\mathrm{pd}} \times \Delta(q_s - q_a) + \Delta|\mathbf{V}| \times \Delta(q_s - q_a)], \end{aligned} \tag{2.4}$$

where D denotes divergence, $\alpha = L\rho C_E$, L is latent heat, ρ is the air density at sea level, C_E is the exchange coefficient, $|\mathbf{V}|$ is surface wind speed, q_s and q_a are the specific humidity at sea surface and at 10 m, respectively, and the subscript 'pd' denotes the present-day simulation. The first term on the right-hand sides of Eqs. (2.3) and (2.4) is associated with circulation change, which may be regarded as a dynamic contributor. The second term involves the change of water-vapor content; thus, it reflects the thermodynamic effect on the GMP. The third term is a nonlinear term including the effects of both moisture and circulation changes.

A robust feature simulated by the CMIP5 models is that the thermodynamic effect due to increased water-vapor content plays an important role in enhancing

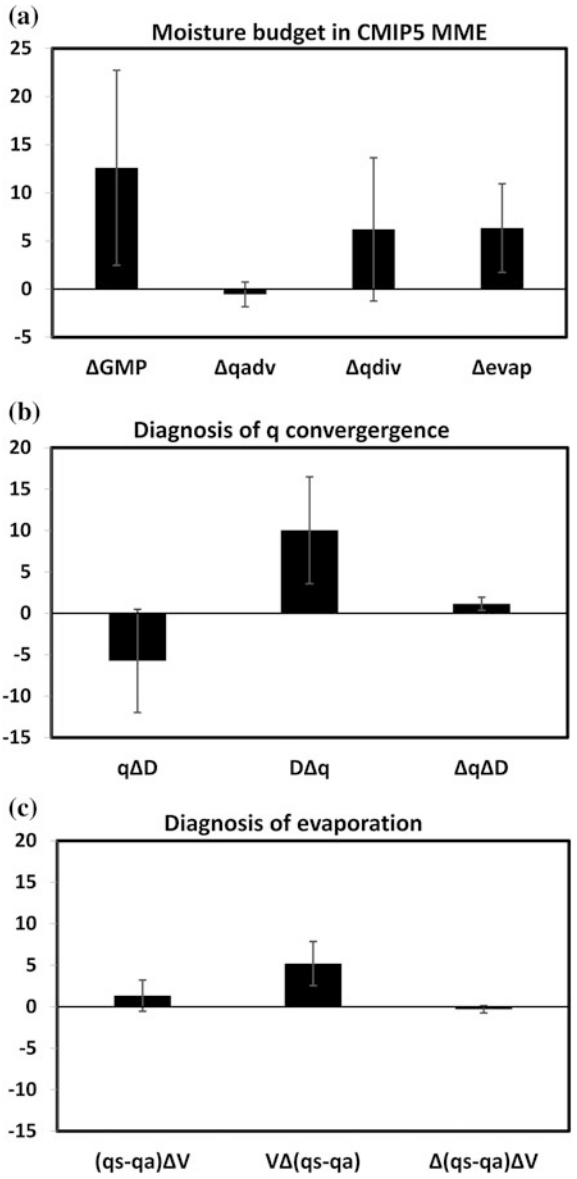

Fig. 2.6 **a** Moisture processes responsible for the GMP change based on 19 CMIP5 MME. *Left* to *right* changes in GMP, horizontal moisture advection, moisture convergence, and surface evaporation within the GMA (Units: 10^{14} W). Whiskers indicate inter-model standard deviations of the 19 models **b** and **c** are the same as (**a**), except for the diagnoses of moisture convergence change and evaporation change, respectively. *Left* to *right* contributions of dynamic effect associated with circulation change, thermodynamic component associated with water vapor change, and the nonlinear product of the two changes. (Adapted from Hsu et al. 2013)

both moisture convergence (Fig. 2.6b) and evaporation (Fig. 2.6c). However, the dynamic effect is less robust and shows different contributions to moisture convergence and evaporation between different models. The CMIP5 models suggest that a weaker monsoon convergence flow under global warming will have a tendency to decrease monsoon rainfall (Fig. 2.6b). Although this dynamic component offsets the thermodynamic component to a large extent, the thermodynamic

component still dominates the increased GMP (Fig. 2.6a). As for evaporation, the dynamic effect related to the increased surface wind speed reveals positive, but minor, contributions to GMP in the averaged result of CMIP5 models (Fig. 2.6c). These diagnostic results from Hsu et al. (2013) confirm the findings in Cherchi et al. (2011), Hsu et al. (2012), and Kitoh et al. (2013), which emphasized the role of enhanced moisture convergence and evaporation in the increase of GMP.

2.4.3 Changes in Monsoon Onset and Retreat

Aside from the total amount of monsoon precipitation (GMP), the temporal distribution of rainfall throughout the rainy season is another important issue. Changes in the timing of monsoon onset and retreat, and the durations of monsoon rainy periods, will strongly affect agricultural and socio-economic policies. The onset (retreat) of the monsoon rainy season is generally concurrent with an abrupt increase (decrease) in precipitation. Wang and LinHo (2002) defined the timing of monsoon onset (retreat) as the date when the relative climatological mean precipitation (i.e., the difference between the climatological daily precipitation and dry month) first exceeds (drops below) 5 mm day^{-1}. Using this definition, Kitoh et al. (2013) examined the changes in monsoon onset and retreat in each land monsoon domain around the globe. The CMIP5 models project significant changes in the timing of monsoon onset and retreat over land in Asia and Australia. The onset date of the Asian-Australian monsoon tends to advance, while the monsoon retreat is delayed, indicating a lengthening of the monsoon rainy season. Similar projected results were identified from the B4MME of CMIP5 models (Lee and Wang 2014) and from the CMIP3 models (Kumar et al. 2011). The CMIP5 MME projections of monsoon onset and retreat changes in the American and African monsoon regions were less significant and had a larger spread (Kitoh et al. 2013).

2.4.4 Changes in Inter-annual Variability of GMP

The El Niño/Southern Oscillation (ENSO) has been a crucial factor in modulating the year-to-year GMP variations in recent decades (e.g., Zhou et al. 2008b; Wang et al. 2012). According to the observations, the GMP has experienced a great inter-annual variation and has been significantly negatively correlated with the central-eastern Pacific SST averaged over the monsoon year defined from May to the following April (Yasunari 1991). The negative correlation coefficient between the ENSO and GMP was found consistently in the CMIP5 pre-industry control simulations (Hsu et al. 2013), confirming that the inter-annual variability of the GMP was largely due to internal processes of the atmosphere (Wang et al. 2012).

The change in ENSO amplitude in a warmer climate shows a large diversity among the CMIP5 model projections. In terms of the Niño 3 or Niño 3.4 index in

future simulations, some models projected increasing ENSO variability, some showed less variability, and some exhibited no change (Guilyardi et al. 2012; Kim and Yu 2012; Stevenson et al. 2012). The mean of CMIP5 projections indicates a stable or slightly weaker ENSO in the RCP4.5 simulations relative to the present-day simulations (Kim and Yu 2012; Hsu et al. 2013). Although the change in ENSO intensity is uncertain in these future projections, the general ENSO-GMP relationship remains significant and even becomes stronger under global warming. Hsu et al. (2013) found that the negative correlation coefficient between the Niño 3.4 index and GMP may increase from the present day to the end of the twenty-first century. Moreover, the year-to-year standard deviation of GMP is intensified in the RCP 4.5 simulations. This suggests that more extreme monsoon years might occur in the future (Turner and Annamalai 2012). A large portion of the change in the year-to-year GMP comes from the land monsoon rather than the oceanic monsoon (Hsu et al. 2013).

2.5 Conclusions

Monsoon is a response of the climate system to the annual variation in solar forcing. It is characterized by seasonal wind reversals and a wet-dry season contrast (Ramage 1971; Webster et al. 1987). From a global perspective, the annual variation of insolation is the essential driver for all of the regional monsoons around the world, although different land-sea configurations control the variability of individual monsoon systems. Thus, the monsoon rainfall features over the globe can be viewed as parts of an integrated GM system, which is associated with a persistent global-scale overturning of the atmosphere, varying with the time of year (Trenberth et al. 2000, 2006).

The GM precipitation has profound impacts on billions of people living in the GM regions. Its variability and possible changes in future warmer climates have attracted growing interest in recent years. Wang and Ding (2006) used the characteristics of monsoon precipitation to delineate the GMA, which includes the annual range of rainfall exceeding 2 mm day^{-1} and the ratio of summer-to-annual rainfall being larger than 35 %. The GMP is then defined as the local summer rainfall within the GMA, and the GMI measures the total GMP amount per unit area (Zhou et al. 2008a; Hsu et al. 2011). Similar definitions of GM indices using different months or different rainfall ratios have been proposed, but the resultant GMA and the change in GM intensity are not sensitive to the fine details of these criteria (Liu et al. 2009; Hsu et al. 2011; Wang et al. 2012).

The long-term variation of GMP over land has been analyzed based on various rain-gauge observations (Wang and Ding 2006; Zhang and Zhou 2011). A significant phase transition of global land monsoon precipitation was identified around the 1950s. The GMP over land showed an overall increasing trend from the beginning of the twentieth century to the 1950s (Zhang and Zhou 2011); it then experienced a downward trend from 1950 to 1980, followed by an insignificant

trend until the present (Wang and Ding 2006). Because the decreasing trend of GMP over land was well reproduced by an AGCM driven by observed SSTs over the past five decades, Zhou et al. (2008b) suggested that the variability of global land monsoon rainfall would arise mainly from oceanic forcing. Besides the SST effect, the external forcing from volcanic aerosols also played an important role in the reduction of global land monsoon precipitation. The CMIP3 models with volcanic aerosols simulated a more robust and significant downward trend in land GMP than those without volcanic aerosols (Kim et al. 2008).

Although no significant change in land GMP has been detected from the rain-gauge data since 1979 (Chase et al. 2003; Wang and Ding 2006), an increasing trend in the overall GMP (sum of land and oceanic monsoon rainfall) over the past three decades is shown in the GPCP global rainfall dataset. This increased GMP results primarily from the upward trend in global oceanic monsoon precipitation (Wang et al. 2012). In contrast to the GPCP result, a decreased GMP over the ocean is shown in the CMAP global rainfall dataset (Hsu et al. 2011), reflecting the uncertainty of global oceanic monsoon rainfall among different precipitation datasets (Zhou et al. 2008b; Hsu et al. 2011). Wang et al. (2013) calculated the trends in the GMP using the average of the GPCP and CMAP rainfall datasets, along with the variation of tropical circulations to assess the NH monsoon change. Their results indicated that all the summer monsoon rainfall in the NH, as well as the Hadley and Walker circulations, have been enhanced since 1979. This intensification of NH monsoon activity is related to the recent trend of SST cooling in the eastern Pacific and warming in the western Pacific (Wang et al. 2013), enhancing the trades that transport moisture into the Asian and African monsoon regions.

By the end of the twenty-first century, the GMP is projected to increase by 6–9 % ($\sim$16 %) relative to the end of the twentieth century, based on the CMIP5 RCP4.5 (8.5) simulations (Kitoh et al. 2013; Hsu et al. 2013). The enhanced GMP can be attributed to the expansion of GMA and the enhancement of GMI. The findings of overall increases in the GM area, precipitation, and intensity in the CMIP5 projections, are consistent with the CMIP3 model projections (Hsu et al. 2013), although some differences of regional monsoon characteristics have been found between the two generations of CMIP models (Lee and Wang 2014). On the regional scale, a large spread of GM variability was detected among model projections, indicating much more uncertainty in the projected regional monsoon changes (Giorgi et al. 2001; Kitoh et al. 2005; Cook and Vizy 2006; Li et al. 2006; Lu and Fu 2010; Hsu and Li 2012; Moise et al. 2012; Turner and Annamalai 2012; Sperber et al. 2013).

Future projections of increased GMP are mainly based on changes to the hydrological cycle, induced by warmer temperatures. An examination of column-integrated moisture budget in the GMA suggests that increases in moisture convergence and surface evaporation are both responsible for increases in GMP, while the effect of moisture advection is insignificant (Hsu et al. 2012, 2013; Kitoh et al. 2013). Further analysis has indicated that the thermodynamic effect associated with increased water vapor contributes positively to moisture convergence, but this

contribution is partly offset by the dynamic effect related to the weakening of the monsoon overturning (divergent) circulation. This partial cancellation between the thermodynamic and dynamic components of moisture convergence was also found in the modulation of regional monsoon precipitation (Cherchi et al. 2011; Moise et al. 2012). Regarding the future enhancement of evaporation within the GMA, moisture analysis suggests that the increase in specific humidity over the ocean due to increasing SSTs will play a major role. However, the future change related to surface wind speed shows different results between the high-resolution AGCMs (Hsu et al. 2012) and CMIP5 models (Hsu et al. 2013).

In summary, from the global perspective, the GM system is likely to show enhanced activity in a warmer climate. The increased area, precipitation, and intensity of the future GM are consistently projected by GCMs with different physics and various forcing scenarios. However, the models also show discrepancies in terms of individual monsoon regions, which reduce our confidence in future regional monsoon changes (IPCC 2007, 2013). Unlike the GM change that is largely controlled by planetary-scale forcings, effects on regional monsoon variation are much more complicated (IPCC 2007; Turner and Annamalai 2012). How individual monsoons may respond to a warming climate will be discussed in the following chapters.

Acknowledgments This work was supported by the NSFC grant (41375100), Research Project of the Chinese Ministry of Education (213014A), Natural Science Foundation of Jiangsu Province, China (BK20140046), and by the International Pacific Research Center (IPRC) at University of Hawaii.

References

Adler RF et al (2003) The version 2 global precipitation climatology project (gpcp) monthly precipitation analysis (1979–present). J Hydrometeorol 4:1147–1167. doi:10.1175/1525-7541(2003)004<1147:TVGPCP>2.0.CO;2

Broccoli AJ, Dixon KW, Delworth TL, Knutson TR, Stouffer RJ, Zeng F (2003) Twentieth-century temperature and precipitation trends in ensemble climate simulations including natural and anthropogenic forcing. J Geophys Res 108:4798. doi:10.1029/2003JD003812

Chase TN, Knaff JA, Pielke RA Sr, Kalnay E (2003) Changes in global monsoon circulations since 1950. Nat Hazards 29:229–254

Chen H-P, Sun J-Q (2013) How large precipitation changes over global monsoon regions by CMIP5 models? Atmos Oceanic Sci Lett 6:306–311. doi:10.3878/j.issn.1674-2834.13.0002

Cherchi A, Alessandri A, Masina S, Navarra A (2011) Effects of increased CO_2 levels on monsoons. Clim Dyn 37:83–101. doi:10.1007/s00382-010-0801-7

Chou C, Lan C-W (2012) Changes in the annual range of precipitation under global warming. J. Climate 25:222–235. doi:10.1175/JCLID-11-00097.1

Cook KH, Vizy EK (2006) Coupled model simulations of the West African monsoon system: twentieth- and twenty-first-century simulations. J Climate 19:3681–3703. doi:10.1175/JCLI3814.1

Davidson N, McBride J, McAvaney B (1983) The onset of the Australian monsoon during winter MONEX: synoptic aspects. Mon Wea Rev 111:496–516

Ding YH (1994) Monsoons over China. Springer, Heidelberg, p 419
Gillett NP, Weaver AJ, Zwiers FW, Wehner MF (2004) Detection of volcanic influence on global precipitation. Geophys Res Lett 31:L12217. doi:10.1029/2004GL020044
Giorgi F, Whetton PH, Jones RG, Christensen JH, Mearns LO, Hewitson B, vonStorch H, Francisco R, Jack C (2001) Emerging patterns of simulated regional climatic changes for the 21st century due to anthropogenic forcings. Geophys Res Lett 28:3317–3320. doi:10.1029/2001GL013150
Goswami BN (2005) The Asian monsoon: interdecadal variability. In: Wang B (ed) The Asian monsoon. Praxis, Springer, Berlin Heidelberg, pp 295–327
Guilyardi E, Bellenger H, Collins M, Ferrett S, Cai W, Wittenberg A (2012) A first look at ENSO in CMIP5. CLIVAR Exchanges 58:29–32
Gruber A, Su X, Kanamitsu M, Schemm J (2000) The comparison of two merged rain gauge-satellite precipitation datasets. Bull Amer Meteor Soc 81:2631–2644
Higgins RW, Yao Y, Wang XL (1997) Influence of the North American monsoon system on the U.S. summer precipitation regime. J Climate 10:2600–2622
Hsu P, Li T, Wang B (2011) Trends in global monsoon area and precipitation over the past 30 years. Geophys Res Lett 38:L08701. doi:10.1029/2011GL046893
Hsu P, Li T (2012) Is "rich-get-richer" valid for Indian Ocean and Atlantic ITCZ? Geophys Res Lett 39:L13705. doi:10.1029/2012GL052399
Hsu P, Li T, Luo J-J, Murakami H, Kitoh A, Zhao M (2012) Increase of global monsoon area and precipitation under global warming: a robust signal? Geophys Res Lett 39:L06701. doi:10.1029/2012GL051037
Hsu P-C, Li T, Murakami H, Kitoh A (2013) Future change of the global monsoon revealed from 19 CMIP5 models. J Geophys Res Atmos 118:1247–1260. doi:10.1002/jgrd.50145
Intergovernmental Panel on Climate Change (IPCC) (2007) Climate change 2007. In: Solomon S et al (eds) The physical science basis. Contribution of working group i to the fourth assessment report of the IPCC. Cambridge University Press, Cambridge, UK
IPCC (2013) Climate change 2013: the physical science basis. In: Contribution of working group i to the fifth assessment report of the IPCC, intergovernmental panel on climate change, Geneva, Switzerland
Kim H-J, Wang B, Ding Q (2008) The global monsoon variability simulated by CMIP3 coupled climate models. J Clim 21:5271–5294
Kim ST, Yu J-Y (2012) The two types of ENSO in CMIP5 models. Geophys Res Lett 39:L11704. doi:10.1029/2012GL052006
Kitoh A, Hosaka M, Adachi Y, Kamiguchi K (2005) Future projections of precipitation characteristics in East Asia simulated by the MRI CGCM2. Adv Atmos Sci 22:467–478
Kitoh A, Endo H, Krishna Kumar K, Cavalcanti IFA, Goswami P, Zhou T (2013) Monsoons in a changing world: a regional perspective in a global context. J Geophys Res Atmos 118:3053–3065. doi:10.1002/jgrd.50258
Kumar KK et al (2011) The once and future pulse of Indian monsoonal climate. Clim Dyn 36:2159–2170
Lambert FH, Stott PA, Allen MR, Palmer MA (2004) Detection and attribution of changes in 20th century land precipitation. Geophys Res Lett 31:L10203. doi:10.1029/2004GL019545
Lee J-Y, Wang B (2014) Future change of global monsoon in the CMIP5. Clim Dyn 42:101–119. doi:10.1007/s00382-012-1564-0
Li W, Fu R, Dickinson RE (2006) Rainfall and its seasonality over the Amazon in the 21st century as assessed by the coupled models for the IPCC AR4. J Geophys Res Atmos 111:D02111. doi:10.1029/2005JD006355
Liu J, Wang B, Ding Q, Kuang X, Soon W, Zorita E (2009) Centennial variations of the global monsoon precipitation in the last millennium: Results from ECHO-G model. Clim 22:2356–2371. doi:10.1175/2008JCLI2353.1
Lu R, Fu Y (2009) Intensification of East Asian summer rainfall interannual variability in the twenty-first century simulated by 12 CMIP3 coupled models. J Clim 23:3316–3331. doi:10.1175/2009JCLI3130.1

McBride JL (1987) The Australian summer monsoon. In: Chang CP, Krishnamurti TN (eds) Monsoon meteorology. Oxford University Press, New York, pp 203–231

Moise AF, Colman RA, Brown JR (2012) Behind uncertainties in projections of Australian tropical climate: analysis of 19 CMIP3 models. J Geophys Res Atmos 117:D10103. doi:10.1029/2011JD017365

Ramage CS (1971) Monsoon meteorology. Academic Press, London, p 296

Sperber KR, Annamalai H, Kang I-S, Kitoh A, Moise A, Turner AG, Wang B, Zhou T (2013) The Asian summer monsoon: an intercomparison of CMIP5 vs. CMIP3 simulations of the late 20th century. Clim Dyn 41:2711–2744. doi:10.1007/s00382-012-1607-6

Stevenson S, Fox-Kemper B, Jochum M, Neale R, Deser C, Meehl G (2012) Will there be a significant change to El Nino in the 21st century? J Clim 25:2129–2145, cCSM4 special issue. doi:10.1175/JCLI-D-11-00252.1

Sultan B, Janicot S (2003) The West African monsoon dynamics. Part II: the "preonset" and "Onset" of the summer monsoon. J Clim 16:3407–3427

Tao S, Chen L (1987) A review of recent research on the East Asian summer monsoon in China. In: Chang C-P, Krishnamurti TN (eds) Monsoon meteorology, Oxford University Press, pp 60–92

Trenberth KE, Stepaniak DP, Caron JM (2000) The global monsoon as seen through the divergent atmospheric circulation. J Clim 13:3969–3993

Trenberth KE, Hurrell JW, Stepaniak DP (2006) The Asian monsoon: global perspectives. In: Wang B (ed) The Asian monsoon, Praxis Publishing Ltd., Chichester, 781 pp

Turner AG, Annamalai A (2012) Climate change and the South Asian summer monsoon. Nat Clim Change 2 doi:10.1038/NCLIMATE1495

Vera C et al (2006) Toward a unified view of the American monsoon systems. J Clim 19:4977–5000. doi:10.1175/JCLI3896.1

Wang B, Lin Ho (2002) Rainy season of the Asian-Pacific summer monsoon. J Clim 15:386–398

Wang B, Ding Q (2006) Changes in global monsoon precipitation over the past 56 years. Geophys Res Lett 33:L06711

Wang B, Ding Q (2008) Global monsoon: dominant mode of annual variation in the tropics. Dyn Atmos Oceans 44:165–183

Wang B, Ding Q, Liu J (2011) Concept of the global monsoon. In: Chang C-P, Wang B, Lau GN-C (eds) The global monsoon system: research and forecast, 2nd edn. World Scientific Publication Company, 608 pp

Wang B, Liu Y, Kim H-J, Webster PJ, Yim S-Y (2012) Recent change of the global monsoon precipitation (1979–2008). Clim Dyn 39:1123–1135. doi:10.1007/s00382-011-1266-z

Wang B, Liu J, Kim H-J, Webster PJ, Yim S-Y, Xiang B (2013) Northern hemisphere summer monsoon intensified by mega-El Niño/southern oscillation and atlantic multidecadal oscillation. PNAS 110:5347–5352. doi:10.1073/pnas.1219405110

Webster PJ (1987) The elementary monsoon. In: Fein JS, Stephens PL (eds) Monsoons. Wiley-Interscience, New York

Webster PJ et al (1998) Monsoons: processes, predictability, and the prospects for prediction. J Geophys Res Atmos 103:14451–14510

Xie PP, Arkin PA (1997) Global precipitation: a 17-year monthly analysis based on gauge observations, satellite estimates, and numerical model outputs. Bull Am Meteorol Soc 78:2539–2558. doi:10.1175/1520-0477(1997)078<2539:GPAYMA>2.0.CO;2

Yasunari T (1991) The monsoon year–a new concept of the climatic year in the tropics. Bull Amer Meteor Soc 72:1331–1338. doi:http://dx.doi.org/10.1175/1520-0477(1991)072<1331:TMYNCO>2.0.CO;2

Zhang L, Zhou T (2011) An assessment of monsoon precipitation changes during 1901–2001. Clim Dyn 37:279–296

Zhou T, Yu R, Li H, Wang B (2008a) Changes in global land monsoon area and total rainfall accumulation over the last half century. Geophys Res Lett 35:L16707

Zhou T, Zhang L, Li H (2008b) Ocean forcing to changes in global monsoon precipitation over recent half-century. J Clim 21:3833–3852

Chapter 3
South Asian Summer Monsoon Variability in a Changing Climate

H. Annamalai and K.R. Sperber

Abstract This chapter provides a succinct review of the current understanding of the South Asian summer monsoon and the ability of present-day climate models to represent its variability in a changing climate. Beginning with a processes-based review of the large- and regional-scale aspects of the monsoon precipitation climatology, the systematic model errors in precipitation and monsoonal diabatic heating are also highlighted. Certain necessary conditions for the representation of synoptic systems, boreal summer intra-seasonal variability, and the El Niño Southern Oscillation (ENSO)-monsoon teleconnection in climate models are presented, followed by discussion of the improved (or not improved) performance of climate models in simulating natural modes of variability. Lastly, we evaluate the ability of models to simulate the observed long-term declining trend in the seasonal mean monsoon rainfall, including possible mechanisms for this trend. Despite dedicated efforts, there is a lack of substantial improvement in monsoon modeling, which in our view is due to the lack of high-quality observations (atmosphere and ocean) over the monsoon-influenced regions to constrain the model physics. Our conclusion is that without such an observational effort, improving the physical processes in numerical models will be severely limited.

Keywords South Asian monsoon · ENSO · CMIP3 · CMIP5

H. Annamalai (✉)
International Pacific Research Center, University of Hawaii, Honolulu, HI, USA
e-mail: hanna@hawaii.edi

K.R. Sperber
Program for Climate Model Diagnosis and Intercomparison,
Lawrence Livermore National Laboratory, Livermore, CA, USA
e-mail: sperber1@llnl.gov

© Springer International Publishing Switzerland 2016

L.M.V. de Carvalho and C. Jones (eds.), *The Monsoons and Climate Change*,
Springer Climate, DOI 10.1007/978-3-319-21650-8_3

3.1 Introduction

Over the past six decades, sustained research from observations, models, and theory have led to the consensus that monsoons arise due to complex interactions among the ocean, atmosphere and land components of the climate system. The annual variation in solar radiative forcing provides the necessary thermodynamic conditions for the development of regional monsoons. For instance, in the annual cycle, the Asian-Australian monsoon (AAM) system can be regarded as the seasonal displacement of the large-scale Intertropical Convergence Zone (ITCZ) that is anchored by the north-south migration of the Indo-Pacific Warm Pool (regions where sea surface temperature is >28 °C). Despite measurable progress in our overall understanding of the monsoons (e.g., Webster et al. 1998), and exponential growth in "computing facilities," modeling the seasonal displacement of the warm pool (Annamalai et al. 2015a, b) and the associated rainfall patterns have met with limited progress (Sperber et al. 2013). Systematic model errors in the climatological basic states cascade into the simulation of subseasonal (Sperber and Annamalai 2008), inter-annual (Turner et al. 2005; Annamalai et al. 2007), and long-term variations of the monsoons (e.g., Annamalai et al. 2013). Additionally, it is recognized that the monsoon phenomenon is intrinsically complex, and that any error in one component of the simulated climate system cascades into the other components. Thus, future projections of mean monsoon and its spectrum of variability by the state-of-the-art climate models exhibit large uncertainties (Turner and Annamalai 2012).

Compared to six decades ago, present-day climate scientists have access to observations from multiple platforms (in situ, satellite, reanalysis, dedicated field experiments, etc.) and powerful computers for analyzing this data. This has led to innumerable scientific publications pertaining to various aspects of the AAM. However, the lack of significant progress in monsoon modeling raises questions: (1) Is our understanding adequate enough to model the monsoons? (2) Is the current level of observations adequate enough to constrain the models? and (3) Have we reached the upper limit of understanding and modeling of monsoons? This chapter provides a concise review of the current understanding of the South Asian monsoon and the ability of present-day climate models to represent its variability in a changing climate.

We begin with a brief review of the processes that may be important for the development and maintenance of the mean monsoon precipitation (Sect. 3.2). In Sect. 3.3, we discuss the subseasonal variations (synoptic and intra-seasonal variations), while Sect. 3.4 is devoted to inter-annual variations with a particular emphasis on the ENSO-monsoon association. The long-term declining tendency in regional monsoon rainfall is discussed in Sect. 3.5. In each section, after reviewing observational aspects, we will present and discuss their representation in climate models, and close with cautionary notes on both observational and climate model uncertainties. Finally, in Sect. 3.6 we provide our perspective of future directions in monsoon research.

3.2 Mean Monsoon

3.2.1 Large-Scale Aspects

In the annual cycle, based on thermodynamic principles, intense solar heating during boreal spring and early summer requires the occurrence of deep convection poleward of the Equator. Figure 3.1a shows the satellite-based observed precipitation and SST climatology during boreal summer. Figure 3.1b shows sea-level pressure (shaded) and 850 hPa wind climatologies constructed from ERA-interim reanalysis. The intense solar heating in late spring and early summer anchors the north-northwest migration of the warm pool. This, in conjunction with land-surface heating, leads to the formation of a diagonally oriented low-pressure area that extends from the Arabian peninsula to the tropical western Pacific (TWP; Fig. 3.1b). Figure 3.1a shows that ocean points in the region 10°–20°N; 70°–160°E experience high-mean SST (>28 °C) and intense rainfall (>9 mm/day), supporting the thermodynamic view that the tropical SST distribution determines the low-level moist static energy (MSE) that in turn anchors moist convection (Neelin and Held 1987; Raymond 1995). At the low level, the Mascarene High in the Southern Hemisphere and the low-pressure region in the Northern Hemisphere, called the "monsoon trough," are connected by the cross-equatorial flow (Fig. 3.1b) that feeds moisture to monsoon convection. More discussions on the large-scale features of mean monsoon can be found in Turner and Annamalai (2012) and Sperber et al. (2013).

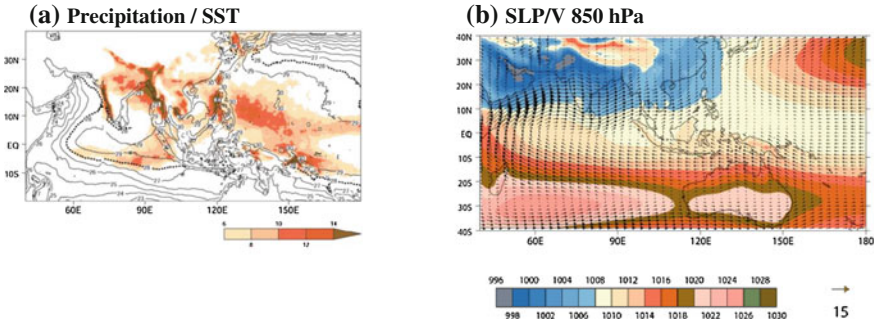

Fig. 3.1 Seasonal mean (JJAS) climatology of: **a** precipitation (mm/day; *shaded*) and SST (°C, contour), and **b** 850 hPa wind (m/s) and sea level pressure (hPa; *shaded*). Unit vector is also shown. Precipitation is taken from TRMM and SST is from TRMM Microwave Imager (TMI) for 1998–2012; SLP and wind are taken from ERA-Interim for the period 1989–2012

3.2.2 Regional-Scale Aspects

At regional scales, the poleward migration of the warm pool (28 °C isotherm reaches as far as 28°N; Fig. 3.1a) has specific dynamic and thermodynamic implications for the monsoon over the TWP that include: (1) the northeastward extension of the subtropical high (Fig. 3.1b; Wu and Wang 2001); (2) the eastward extension of the monsoon trough and low-level westerlies (Fig. 3.1b); and (3) enhanced surface fluxes and boundary layer entropy (Raymond 1995). Despite the fact that the SST-convection relationship is nonlinear and complex over the warm pool region (Lau et al. 1997), a necessary condition is that coupled models need to realistically simulate the zonal and meridional extent of the warm pool over the TWP to anchor in situ convection (Annamalai et al. 2015a, b).

Over southern Asia, convection-Rossby-wave interactions (Rodwell and Hoskins 1996), in conjunction with warmer SST over the Bay of Bengal and cooler SST over the Arabian Sea (Shenoi et al. 2000), help set up an east-west asymmetry of precipitation (Fig. 3.1a). Prior to monsoon development, the northern Indian Ocean is the warmest of all tropical oceans (Schott and McCreary 2001). During the monsoon season, the SST drops to about 23–24 °C along the Somali coast (Fig. 3.1a), primarily due to the upwelling of cold water by the cross-equatorial low-level jet (Fig. 3.1b). Subsequent horizontal advection by ocean currents, in conjunction with evaporative cooling, results in colder SST over the central Arabian Sea (McCreary et al. 1993). In the absence of such ocean-atmosphere processes, SST over the Bay of Bengal remains very high. Given the theoretical evidence that the intensity of the low-level jet along the Somali coast depends on an accurate representation of the East African Highlands (Hoskins and Rodwell 1995), horizontal and vertical resolutions used in the atmospheric model component will have an impact on the intensity of upwelling and SST cooling off Somalia. Thus, we recognize that the cross-equatorial jet and monsoon convection are intrinsically tied to each other. From a vorticity perspective, regions south of the axis of the low-level jet experience anticyclonic flow (Fig. 3.1b) and descent (not shown). As a consequence, the equatorial western Indian Ocean (0°–10°N; 60°E–70°E) experiences minimum rainfall despite the presence of high mean SST, implying dynamical rather than thermodynamical control.

Both high SST and steep orography along the ocean-land boundaries play a critical role in the rainfall distribution (Fig. 3.1a). These determine the locations of maximum rainfall in the vicinity of the Western Ghats, the northern bay adjoining the Arakan Range in Burma, and the South China Sea adjoining the northern mountain chain of the Philippines. Note that orographic-only forced rainfall along the foothills of the Himalayas and Tibetan Plateau is modest. The concentrated rainfall (>18 mm/day) over the central-northern Bay of Bengal may be attributed to dynamics (monsoon trough), thermodynamics (high mean SST and associated MSE), and orographic forcings (Annamalai et al. 2015a, b).

3.2.3 Mean Monsoon in CMIP3/5 Models

In climate models, the mean state of the monsoon, particularly the large-scale circulation features, are better represented than regional-scale precipitation (Sperber et al. 2013). For instance, the Asian summer monsoon is comprised of multiple rainfall maximum zones (Fig. 3.1a) that represent (1) the Indian monsoon (70°E–100°E, 10°N–25°N); (2) the tropical western Pacific (110°E–150°E, 10°N–20°N); and (3) the eastern equatorial Indian Ocean (10°S–0°, 90°E–110°E). Because these centers do not respond in unison to any internal or external forcing (Annamalai and Sperber 2005; Annamalai et al. 2007; Annamalai 2010), and influence each other at all time-scales, a realistic representation of these regional centers is a pre-requisite if the models are to adequately capture the monsoon variability in a changing climate.

As seen in Fig. 3.2 for summertime precipitation, the multi-model mean (MMM) error relative to GPCP observations has shown little improvement in CMIP5 as compared to CMIP3 (Sperber et al. 2013). For the Asian summer monsoon, the MMM monsoon rainfall is underestimated over South Asia and the central-eastern equatorial Indian Ocean, and overestimated over the western equatorial Indian Ocean and tropical west Pacific. The indication is that systematic model errors persist over the regional rainfall zones in subsequent generations of climate models. On a positive note, the increased model resolutions in CMIP5 improve the representation of orographic-induced rainfall (Sperber et al. 2013). For the austral summer monsoon, the rainfall is excessive over most of the Maritime Continent, and deficient over northern Australia (not shown). One implication from our analysis is that uncertainties in future projections (e.g., IPCC 2013) of AAM mean rainfall may not have been reduced from CMIP3 to CMIP5, given the persistence of present-day mean-state errors.

The positive rainfall errors over the western Indian Ocean as well as over the Maritime Continent persist throughout the annual cycle (Annamalai et al. 2015b). An initial investigation has revealed the extent of the monsoon errors and their manifestation in the various model components. The errors in precipitation induce errors in wind-stress that subsequently impact ocean currents and thermocline depths (Nagura et al. 2013), and they impact the simulated SST (Annamalai et al. 2015a, b).

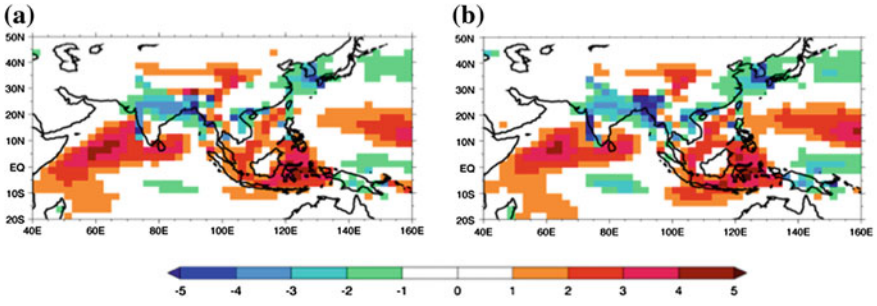

Fig. 3.2 Boreal summer mean precipitation climatology difference (mm/day) between the present-day CMIP/55 multi-model-mean (MMM) and GPCP observations. According to Fig. 3.1 of Sperber et al. 2013. **a** CMIP5 MMM *minus* Obs. **b** CMIP3 MMM *minus* Obs

Another constraint to model improvement is "observational uncertainty." For example, an initial examination of the differences in boreal summer rainfall climatologies between two frequently used rainfall products (GPCP and CMAP) for model validation (not shown; see Fig. 3.1f of Sperber et al. 2013) indicates errors that are similar to the CMIP5/3 MMM precipitation differences seen in Fig. 3.2a, b.

As mentioned above, the regional distribution of mean monsoon precipitation is *likely* to arise due to complex interactions among dynamical, thermodynamical, and orographic forcings. Given that the interaction between large-scale motions and convection is inherent for the AAM system, a collective measure of all forcings that make up the monsoon rainfall can be inferred by the models' ability to represent the vertical profile of diabatic heating. Figure 3.3 shows the vertical profile of diabatic heating (Q), area-averaged over the South Asian monsoon region (5°–25°N, 60°–100°E) during boreal summer, from CMIP5 models. Q is computed as a residual of the thermodynamic energy equation, following the approach used by Hoskins et al. (1989) and Nigam et al. (2000). The vertical structure of Q dictates the efficacy of the divergent circulation that either exports or imports MSE. Among the models, large diversity exists both in terms of vertically integrated Q amplitude as well as its vertical structure, which is expected to influence the three-dimensional circulation (Hoskins and Wang 2006). In the reanalysis, as expected over deep convective

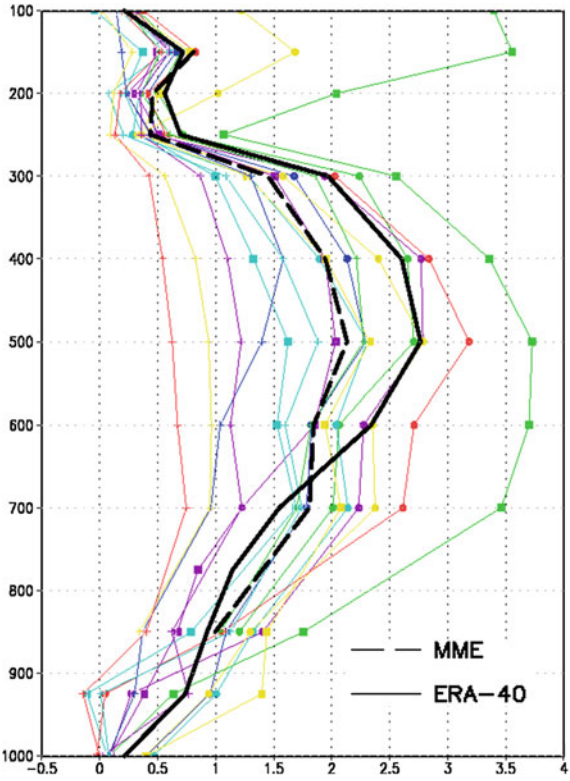

Fig. 3.3 Vertical distribution of Q estimated from CMIP5 and ERA reanalysis (*solid line*). The multi-model-mean composite (*dashed line*) is also shown (from Cherchi et al. 2014)

regions, Q peaks around the mid-troposphere (500–400 hPa). Many models, on the other hand, tend to have maxima at the mid-troposphere, but their simulated amplitude is overestimated in the lower troposphere (900–700 hPa) and underestimated in the 700–300 hPa layer, a feature readily apparent in the multi-model mean composite (black long-dashed line). Some outliers, such as CSIRO-Mk3-6-0 and ACCESS1-3, do not show any appreciable vertical structure since the simulated monsoon over South Asia is virtually absent in those models (Sperber et al. 2013). TRMM observations indicate that over the monsoon region, the stratiform rainfall contribution to Q intensity is about 40 % (Schumacher et al. 2004). In contrast, most of the CMIP3 models produce too much convective (95 % of the total) and too little stratiform precipitation (Dai 2006). Given the persistence of systematic errors (Fig. 3.2), we speculate that errors in the partitioning of total rainfall into convective-stratiform may still persist in CMIP5. Furthermore, in CMIP5 models, higher Q intensity at lower tropospheric levels may be attributed to misrepresentations in shallow convection.

To understand the models' ability to simulate the annual cycle of precipitation, cumulative and fractional accumulation methods are applied (Sperber and Annamalai 2014) using pentad precipitation. This approach provides an advantage over using threshold-based techniques to analyze monsoon rainfall, since many models have dry biases, and thus fail to attain absolute rainfall amounts adequate for defining monsoons. In the fractional accumulation approach, all of the models are interpreted within the context of their own annual cycle—irrespective of absolute biases in amount. Figure 3.4a shows the All-India rainfall accumulations, indicating that there is large dispersion in the ability of the CMIP5 models to simulate the absolute rainfall amounts. The fractional accumulations, as seen in Fig. 3.4b, reveal a systematic bias, with the monsoon onset being delayed in most models.

Over the Australian region (not shown; see Sperber and Annamalai 2014), nearly half of the models suggest an early onset while others suggest a delayed onset. Additionally, models that have realistic fractional accumulation over India (e.g., MIROC-ESM) can fail to capture the annual cycle over Australia, and vice versa

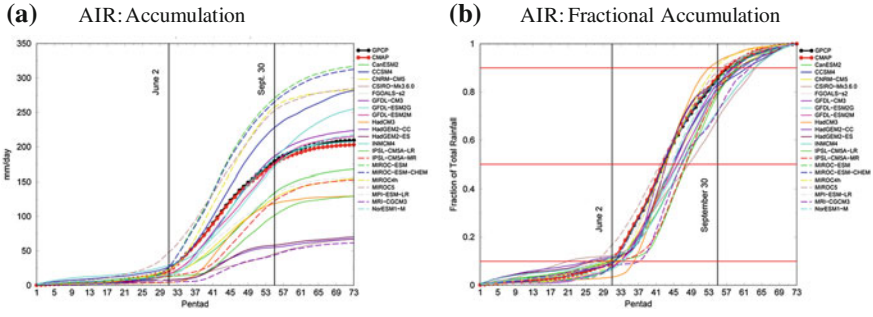

Fig. 3.4 **a** Cumulative rainfall over India, and **b** fractional accumulated rainfall over India (from Sperber and Annamalai 2014)

(e.g., MRI-CGCM3). In summary, a complete north-south migration of the ITCZ that heralds the AAM system may be absent in many models, or it may be too weak. Additionally, the rate at which precipitation accumulates during the peak monsoon season can vary substantially across the suite of models (Sperber and Annamalai 2014). This suggests that the space-time characteristics of rainfall are not well simulated. To conclude, model systematic errors in simulating the annual cycle of the South Asian monsoon persist despite dedicated modeling efforts.

3.3 Subseasonal Variability of the South Asian Summer Monsoon

3.3.1 Intra-seasonal (30 to 50-Day) Variability

The space-time evolution of the boreal summer intra-seasonal variability (BSISV) is more complex than its boreal winter counterpart, the MJO. While the MJO is dominated by eastward propagation (Madden and Julian 1994), in the BSISV the equatorial component interacts with the mean monsoon flow, resulting in north and northwestward propagating components over the northern Indian Ocean and tropical west Pacific, manifested as monsoon active-break phases (Lau and Chan 1986; Annamalai and Sperber 2005). With regard to BSISV, diagnostics on CMIP3 models suggest that one of the necessary conditions is that the models capture the equatorial component with sufficient amplitude for the generation of Rossby waves. The poleward migration of BSISV depends on the poleward extension of mean easterly shear and the three-dimensional distribution of moisture (Wang and Xie 1997). An idealized coupled model study suggests the role of anomalous horizontal moisture advection by the mean winds as one possible thermodynamic factor for the poleward migration (Ajayamohan et al. 2011). Modeling and theoretical studies suggest that "mean conditions" act as necessary, if not sufficient, conditions for the existence of BSISV.

From the CMIP3 database, Sperber and Annamalai (2008) noted that only 2 of 17 models represented BSISV, but this was an improvement compared to the previous generation of models (Waliser et al. 2004). Compared to CMIP3, the multi-model-mean composite evolution of the BSISV in CMIP5 captures salient features (Sperber et al. 2013), an encouraging model improvement. Figure 3.5 shows the space-time evolution of BSISV as simulated by the MIROC5 coupled model, where day 0 corresponds to maximum convective anomalies over the eastern equatorial Indian Ocean. Initial enhanced convective anomalies are noted along equatorial Africa at day−15, extending into the western equatorial Indian Ocean by day−10, and further eastward extension amplification occurs during day −5 and day 0. The combined Rossby-Kelvin pattern in enhanced convective anomalies is noticeable at day 5 with signatures of poleward migration over Indian longitudes and eastward extension into the Maritime Continent, with weak signatures of northwest propagation over tropical west Pacific from day 10 to day 20.

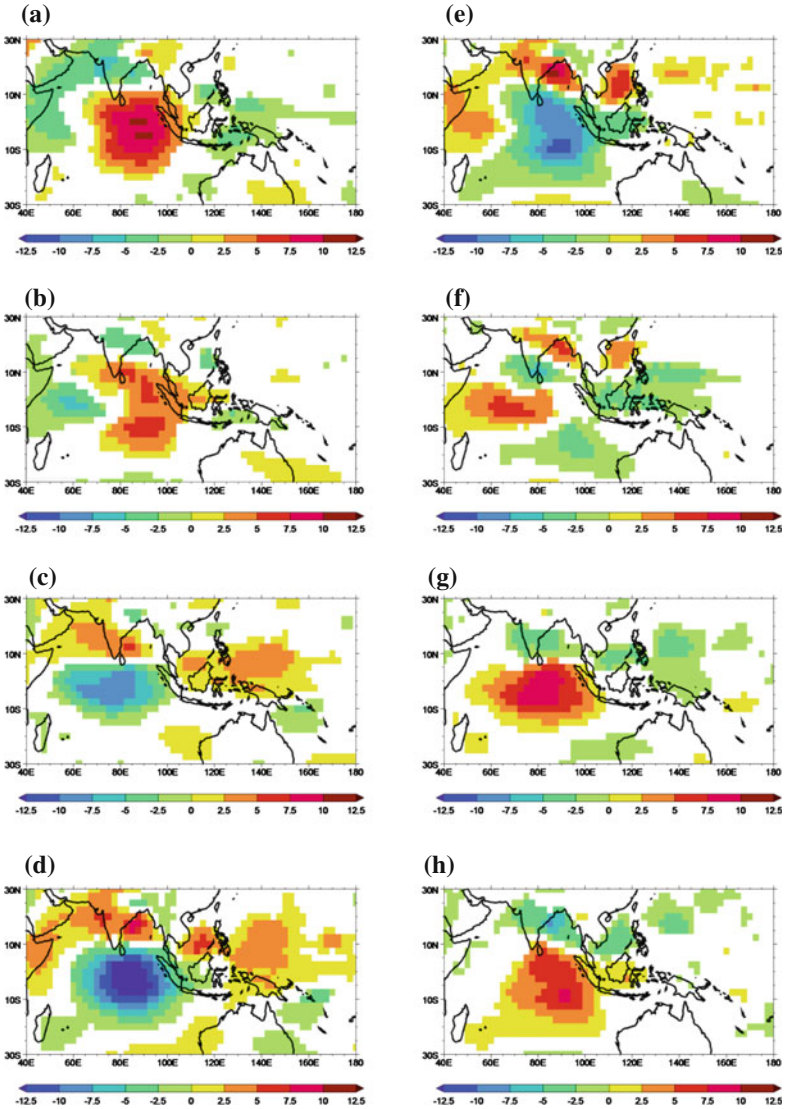

Fig. 3.5 Lag regression of 20- to 100 day bandpass filtered OLR from MIROC5. The lag regressions have been scaled by one standard deviation to give units of W m^{-2}. Data are plotted where the regressions are statistically significant at the 5 % level, assuming each pentad is independent. **a** Day −15 **b** Day −10 **c** Day −5 **d** Day 0 **e** Day 5 **f** Day 10 **g** Day 15 **h** Day 20

At day−15 and day−10, one can note the migration of suppressed convective anomalies over the Indian longitudes and into the Maritime Continent, and the cycle is repeated. The space-time pattern clearly indicates that this mode is associated with northward propagation over Indian longitudes and northwestward migration of

convection over the tropical west Pacific. In Fig. 3.5, the northward propagation occurs in conjunction with equatorial eastward propagation from the Indian Ocean to the west Pacific. One can easily delineate the coexistence of the three propagating components, and as such the intra-seasonal modes are more complex during northern summer compared to northern winter. Yet the fact that coupled models, even if only a very few of them, capture BSISV representation is encouraging and needs to be considered to be a "boost" for model developers.

While active and break conditions are inherent to monsoon dynamics, prolonged dryness or extended breaks (lasting 7 days or more) during the peak rainy season often result in droughts (e.g., Ramamurty 1969). Similarly, prolonged active monsoon conditions anchor local flooding. In observations, a break event is considered if for three consecutive days rainfall anomalies averaged over central India (21°–27°N, 72°–85°E) are below one standard deviation. Figure 3.6 shows the observed yearly statistics of monsoon breaks during boreal summer. While extended breaks occur in years of normal monsoon (e.g., 2000) and in neutral ENSO conditions (e.g., 1979), they tend to occur more frequently during years of warmer SST conditions over the equatorial Pacific and equatorial Indian Ocean. While the phase of BSISV leads to break conditions, the existence of "extended breaks" is anchored by seasonally persisting boundary forcing. Idealized numerical experiments performed with an AGCM support the role of boundary forcing (Prasanna and Annamalai 2012), in which the frequency of occurrences of extended monsoon

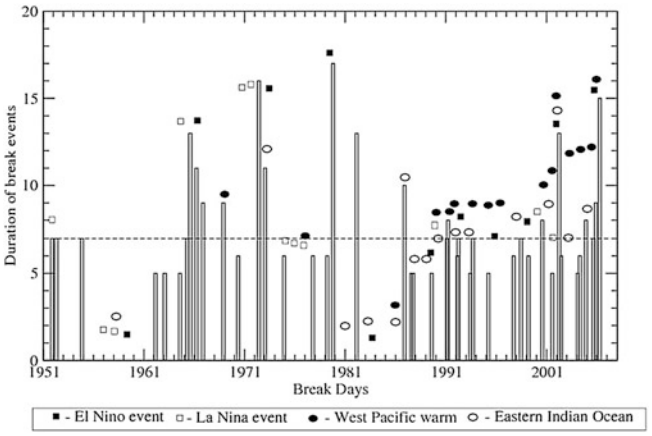

Fig. 3.6 Yearly statistics of break days observed over central India. Years of anomalous sea surface temperature conditions over Niño 3.4 region (*filled squares* for El Niño and *open squares* for La Niña), equatorial West Pacific (*filled circles*) and eastern equatorial Indian Ocean (90°E–110°E, 10°S–0; *open circles*) are highlighted. The *filled squares* and *open squares* indicate JJAS Niño 3.4 SST anomalies above and below one standard deviation, respectively. Similarly *filled circles* and *open circles* indicate JJAS SST anomalies above one standard deviation over the equatorial western Pacific and eastern equatorial Indian Ocean, respectively. The *horizontal dotted line* represents break days corresponding to 7 days (from Prasanna and Annamalai 2012)

breaks over South Asia is significantly enhanced in response to El Niño forcing. Do climate models capture extended breaks?

To examine whether a coupled model that displays realistic simulation of mean monsoon precipitation and aspects of subseasonal variability also captures extended breaks, we diagnosed all of the five-member ensemble simulations of the Geophysical Fluid Dynamics Laboratory (GFDL) Climate Model version 2.1 (CM2.1) coupled model. The criterion for a break event is similar to observations, except that the averaging domain is considered over the whole of India (8–28°N, 63–97°E). For the models, the reason for choosing a different region is due to limitations in simulating the rainfall basic state and intra-seasonal variability over central India (Sperber and Annamalai 2008). Figure 3.7 summarizes the occurrences of breaks lasting for 3–7 days and longer. Both in observations and model simulations, the occurrences of short breaks (lasting for 3 days) and extended breaks (lasting for 7 days or more) are higher, and it is encouraging that each model ensemble member captures this distribution.

In summary, understanding and modeling the daily rainfall characteristics over central India involves: (1) understanding its statistical distribution (Fig. 3.6); (2) identifying the processes from quality observations (dynamical and thermodynamical, and their interactions); and (3) constraining model physics with field observations. Perhaps it is not the lack of representation of a particular process, but the partitioning that results from weaknesses in the various parameterization schemes that hinder skillful simulations of BSISV. A major stumbling block, in our opinion, is the lack of quality three-dimensional moisture and radiation observations over South Asia. At present, the research community depends solely on reanalysis products to elucidate these processes, and in data-sparse regions, model biases are severe in global reanalysis.

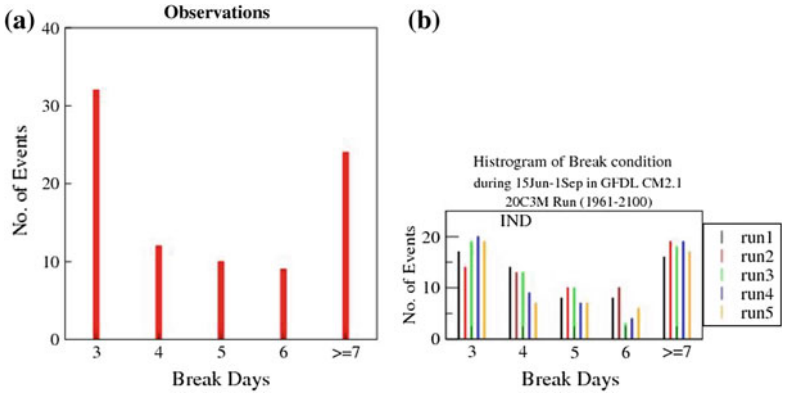

Fig. 3.7 **a** Histogram of break days estimated from observed rainfall averaged over central India (21°–27°N, 72°–85°E); **b** as in (**a**) but from five-member CM2.1 integrations (1961–2000) and rainfall averaged over India (8°–28°N, 63°–97°E)

3.3.2 Synoptic Systems

Boreal summer monsoon depressions, having a horizontal scale of about 2,000–3,000 km, form over the quasi-stationary monsoon trough. They are the most important components of the monsoon circulation. During the peak monsoon season (July–August), most of them form over the warm waters of the northern Bay of Bengal, and move in a west-northwesterly direction with 4–6 systems forming each year (Sikka 2006). Over central India, the rainfall associated with the depressions contributes about 50 % of the seasonal mean, and almost all extreme rainfall events there are associated with depressions (Sikka 2006). Therefore, to assess the future changes in the expected number of flood days, it is important to examine climate model projections of the depression strengths.

Observational and theoretical studies show that realistic mean conditions are a necessary, but not sufficient, condition for the formation and growth of monsoon depressions. Central-northern Bay of Bengal depressions develop in a region where the meridional gradient of potential vorticity (PV) vanishes (Shukla 1978). This PV behavior is one of the necessary conditions for the zonal jet instability mechanism of Charney and Stern (1962). Additionally, observational studies highlight the role of scale interactions since the BSISV modulates the formation of monsoon synoptic systems (e.g., Krishnamurthy and Ajayamohan 2010). Therefore, both the mean monsoon and space-time evolution of BSISV appear to be necessary conditions for the genesis and development of monsoon synoptic systems.

Only a few studies have evaluated the representation of monsoon depressions in climate models, partly due to resolution constraints and/or due to model systematic errors. Over the ASM region, in both NCEP-NCAR and ERA-15 reanalyses, Annamalai et al. (1999) noted that relevant statistics, such as the growth/decay rate and the genesis/lysis locations, are in good agreement between the two reanalyses, although the intensity is higher in ERA-15, which was performed at a higher spatial resolution (T106).

In our earlier study, we examined the ability of select CMIP3 models to represent monsoon depressions (Stowasser et al. 2009), with the estimated number density for the period (1981–2000) summarized in Fig. 3.8. The following criteria must be satisfied for a system that we identify and track: (1) a local vorticity maximum at 850 hPa exceeds 5×10^{-5} s^{-1} (Annamalai et al. 1999), and (2) a local pressure minimum exists within a radius of 250 km of the vorticity maximum; this minimum pressure defines the center of the storm system. To be considered as a model storm trajectory, a storm must last at least 2 days (see Stowasser et al. (2009) for details). The reanalysis confirms that most of the systems form north of 15°N in the Bay of Bengal and move inland in a westward to west-northwestward direction (Fig. 3.8a). Over the Arabian Sea, our analysis also captures the relatively less frequent mid-tropospheric cyclones whose signatures are seen at lower troposphere levels.

Although all three models represent the local maximum density over the Bay of Bengal, the west-northwestward movement into the land regions is best captured by

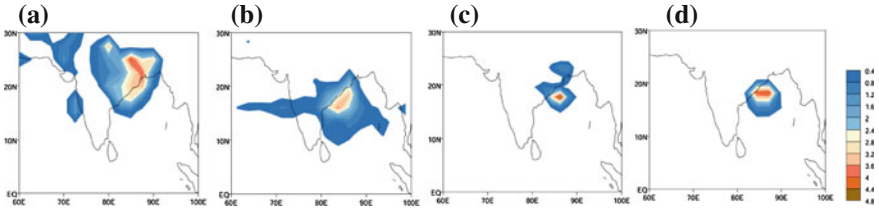

Fig. 3.8 Occurrence of synoptic systems from: **a** ERA-40 data (1981–2000), the suite of twentieth century integrations of coupled models; **b** GFDL CM_2.1; **c** MPI; and **d** MRI. The last 20 years of the 20c3 m, simulations (1981–2000) are used for the calculation. The units are numbers per 2.5° square box per 4 months (JJAS) period (from Stowasser et al. 2009)

GFDL_CM2.1 (Fig. 3.8b). Compared to reanalysis, the genesis locations in the GFDL_CM2.1 are shifted southwestward, and the model fails to capture the systems along the southern slope of the Himalayas. Despite its reasonable success in simulating the statistics of synoptic systems in the current climate, the GFDL_CM2.1 did not reveal any changes in the characteristics of monsoon depressions in a warmer climate (Stowasser et al. 2009). Bengtsson et al. (2006) found that the simulated depressions' intensity in the ECHAM5 model is stronger than those in ERA-40 reanalysis, while the track is closer to observations. Extending their analysis with ECHAM5 coupled model simulations, they note an increase in the depressions' intensity in the twenty-first century compared to twentieth century integrations. However, our analysis suggests that in the ECHAM5 coupled model studied by Bengsston et al. (2006), systems making landfall were not represented (Fig. 3.8c).

A striking result from observations is a steady decline in the formation of monsoon depressions since the 1970s (Sikka 2006). Additionally, there is no change in the formation of the total number of synoptic lows over South Asia, but their intensification into depression strength has declined. Our ongoing analysis with CMIP5 solutions is focused on identifying the possible processes for the declining tendency in monsoon depressions. Any future projections of the intensity of monsoon synoptic systems require that climate models capture not only their statistics but also the effect of any long-term forcing.

3.4 Inter-annual Variability

For the Asian monsoon, a successful prediction of the seasonal mean (June through September) rainfall anomalies helps in the planning of agriculture and hydroelectric and fresh water resources. With two-thirds of the south/southeast Asian workforce being agro-related and a large portion of the cultivable land rain-fed, seasonal forecasts of monsoon rainfall anomalies are increasingly scrutinized. Before models are used for operational predictions, a question that needs to be systematically examined is "Do the present-day coupled models accurately represent the necessary

ingredients to account for the inter-annual variations of the monsoon, particularly exceptionally strong and weak monsoons?"

Charney and Shukla (1981) hypothesized that the seasonal mean rainfall and circulation anomalies of the *large-scale* monsoon are governed by slowly varying boundary conditions, such as SST, snow cover, soil moisture, etc., a hypothesis supported by many observational and modeling studies (e.g., Walker and Bliss 1932; Rasmusson and Carpenter 1983; Soman and Slingo 1997; Annamalai and Liu 2005; Lau and Nath 2000). For example, within available observations, all exceptionally weak monsoon years (15 % below normal) over India co-occurred with El Niño (Pillai and Annamalai 2012). Of the boundary forcing elements, ENSO dominates monsoon inter-annual variations, although the specific mechanism(s) through which ENSO influences the monsoon, remains an open question.

Sensitivity experiments (Turner et al. 2005) and diagnosis of a suite of models that participated in CMIP3 (Annamalai et al. 2007) suggest that realistic representation of the basic states in the tropical Pacific and rainfall over South Asia, as well as the timing and location of the diabatic heating anomalies associated with ENSO, are necessary conditions for simulation of the monsoon-ENSO teleconnection. Additionally, at inter-annual time scales, the SST-rainfall relationship over the warm pool is complex (Wu and Kirtman 2005). Therefore, the realistic simulation of regional SST variations is another necessary condition; even if these conditions are met, examining the association in one realization (Annamalai et al. 2007) and/or a select period within one realization (Sperber et al. 2013) may not yield robust results, since the variance of ENSO itself waxes and wanes on decadal-to-centennial time scales (Wittenberg 2009).

Annamalai et al. (2007) examined the ENSO-monsoon association in CMIP3 models. To check if the models represent the timing of the teleconnection correctly, lead/lag correlations between Niño 3.4 (5°S–5°N, 120°–170°W) SST anomalies and All-India rainfall (AIR) anomalies were computed. For each of the four models, this correlation is calculated separately for each realization, and then an ensemble-mean pattern is computed.

In observations, negative correlations (Fig. 3.9a, black line) occur only after April. The observed maximum correlation after the monsoon season has led to suggestions that variations in the intensity of the monsoon can potentially influence the surface wind stress in the equatorial Pacific and thereby modify the statistical properties of ENSO (e.g., Kirtman and Shukla 2000). In the twentieth century (20c3 m) simulations, all of the models capture the inverse relationship during boreal summer, but the maximum negative correlation occurs too early in the GFDL_CM_2.0, MRI, and MPI_ECHAM5 simulations. While three of the models reasonably represent the spring predictability barrier, seen as the near-zero correlations during the preceding winter/spring, the MPI_ECHAM5 simulations (purple line, Fig. 3.9a) are incorrect in this respect, with the presence of pronounced negative correlations from the preceding winter. Of the four models, GFDL_CM_2.1 best captures the timing of the relationship. The ability to resolve the timing is possibly related to the ability to simulate the space-time evolution of SST and the associated diabatic heating anomalies during El Niño events. In the

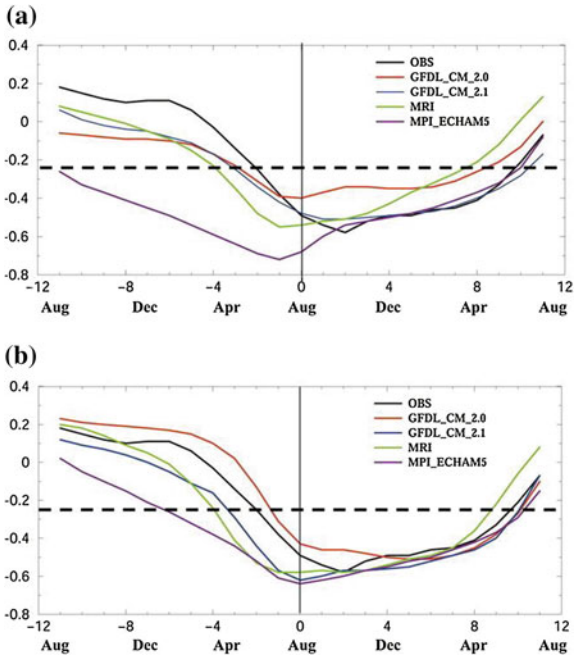

Fig. 3.9 Lag-lead correlation between AIR anomalies and Niño 3.4 SST anomalies: **a** 20c3 m and **b** 1pctto2x simulations. In **a** and **b**, the results from observations are also shown. *Horizontal dotted lines* represent the 5 % significance level. Lag-12 corresponds to Niño 3.4 SST anomalies 1 year before the monsoon season

1pctto2x integrations (Fig. 3.9b), the tendency is for the spring predictability barrier to be more apparent, and in the case of GFDL_CM_2.0 and MRI, there is a tendency for the negative correlations to persist for about 3–6 months after the monsoon season. Overall, the results presented so far indicate that the ENSO-monsoon relationship remains strong and stable in a warmer climate.

In these four CMIP3 models that depicted realistic mean monsoon precipitation and ENSO characteristics, the future projection of South Asian monsoon inter-annual variability (Fig. 3.10; Turner and Annamalai 2012) is examined. The PDF is based on the pre-industrial control run (solid), and in the simulation where a 1 % per year increase in the concentration of CO_2 was imposed (dashed). The standard deviation in the control simulations is also given for each of the models.

While all four models suggest a reduction in the occurrences of normal monsoon years over South Asia, a statistically significant shift in the tail of the PDF is noted only for the MRI model (Fig. 3.10d), i.e., the response is very great in the model that has low monsoon variability (low standard deviation) in the control simulation. In summary, while it is encouraging that ENSOENSO-monsoon association remains intact in a warmer planet, the uncertainties in the future projection of ENSO itself cause uncertainty in the future behavior of exceptionally weak or strong monsoons over South Asia.

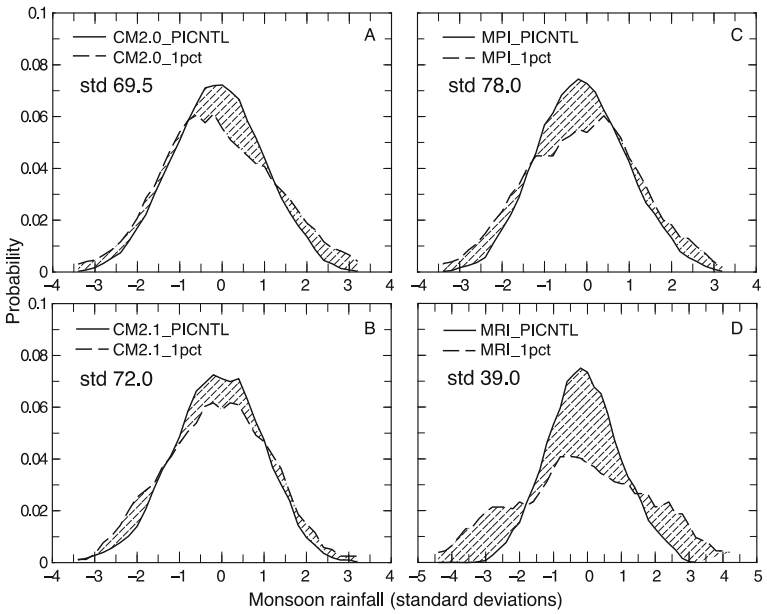

Fig. 3.10 Probability density functions of inter-annual variability in monsoon rainfall in control and future climate scenarios. Shown are normalized probabilities of occurrences in four CMIP3 models. Pre-industrial control (*solid*) and 1 % per year increase in CO_2 concentrations (*dashed*) are shown. The future variations are scaled by preindustrial control inter-annual standard deviations. The differences in the shape of the PDFs have been tested for significance based on K-S test (according to Turner and Annamalai 2012)

3.5 Long-Term Variability

During the last six decades (1950–2010), seasonal mean rainfall observations over India suggest a declining trend (e.g., Ramanathan et al. 2005). While the drying trend may be due to factors other than increased GHG concentration, such as aerosols (Ramanathan et al. 2005), Annamalai et al. (2013) showed that anthropogenic forcing through SST warming over the tropical western Pacific likely caused an east-west shift in monsoon rainfall, with a drying tendency over South Asia. Unlike in future projections due to anthropogenic forcing, where rainfall increases over both South Asia and tropical western Pacific (e.g., Turner and Annamalai 2012), in the last six decades, atmospheric response to SST warming over the tropical Indian Ocean has not yet occurred (see Annamalai et al. 2013 for more details).

To ascertain the spatial extent of drying over South Asia, the linear trend was estimated in gridded observational rainfall and analyzed circulation fields. In land-based rainfall products (e.g., Fig. 3.11a), the declining pattern over the plains of central India and Indo-China is consistent with other studies (e.g., Ramanathan et al. 2005). The spatial extent of drying is captured in other rainfall observations

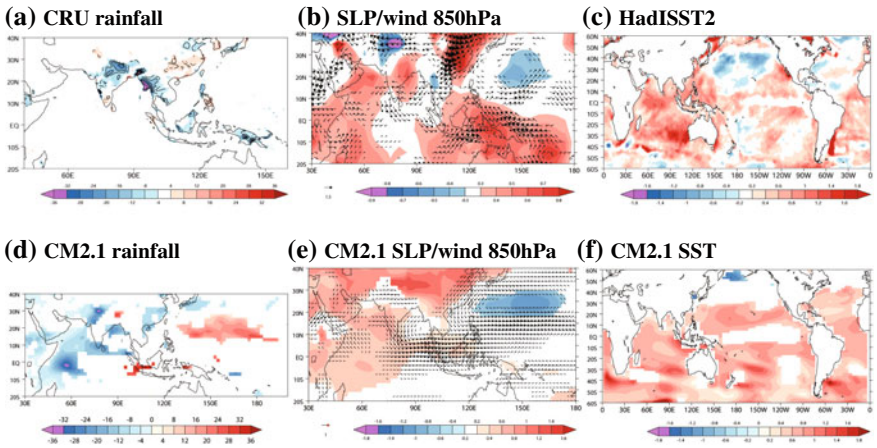

Fig. 3.11 **a** Linear trend in observed rainfall (mm month^{-1} (52 yr)$^{-1}$) during boreal summer (JJAS) from the CRU gridded dataset for 1949–2000. **b** As in (**a**), but for sea level pressure (hPa (52 yr)$^{-1}$) from Hadley Centre data and 850 hPa wind (m s^{-1} (52 yr) $^{-1}$) from the NCEP-NCAR reanalysis. **c** As in (**a**), but for SST data from HadISST2 (8C (52 yr)$^{-1}$). **d** as in (**a**), but from CM2.1. **e** as in (**b**), but from CM2.1 and **f** as in (**c**), but from CM2.1. In each of the panels, negative trend values are shown in blue and purple while positive values are in *red*. At each grid, only trend values greater than local inter-annual standard deviations are shown (adapted from Annamalai et al. 2013)

(not shown here; see Bollasina et al. 2011), but the estimated intensity is higher in CRU (Fig. 3.11a). From the results presented here and elsewhere, one robust feature is the declining tendency in monsoon rainfall over Central India, but because of observational uncertainties and different algorithms used in re-gridding station rainfall observations, the magnitude of this decline varies among the products.

In seeking attribution for this declining tendency, Annamalai et al. (2013) estimated trends in SST and circulation fields. From 1949 to 2000, it is clear from Fig. 3.11c that SST increased in both the tropical Indian Ocean and the western tropical Pacific (a region extending over 10°S–30°N, 60°–150°E)—in the former region by 0.75 °C, and in the latter by 0.5 °C. Yet, despite the SST rise, SLP has increased over the western Indian Ocean, and climatological southwesterly monsoon winds have weakened (Fig. 3.11b).

In the tropical western Pacific (10°–30°N, 130°–170°E), in contrast, SLP has dropped and the cross-equatorial flow emanating from the Australian high, the low-level westerlies, and anomalous cyclonic circulation have strengthened (Fig. 3.11b). Direct rainfall observations are unavailable; nevertheless, the decrease in sea-surface salinity from 1955 to 2003 (Delcroix et al. 2007), the increased atmospheric water vapor content from 1988 to 2006 (Santer et al. 2007), and the drop in SLP (Copsey et al. 2006) all suggest that this region has had more rainfall in recent decades. Thus, observations point to a change in the monsoon circulation that has resulted in less rainfall over South Asia and more over the tropical western Pacific.

Is there support from a coupled model simulation for this observed east-west shift in monsoon rainfall? Between 1949 and 2000, barring regional details, CM2.1 simulated the observed drying over South Asia (Fig. 3.11d), the increased SLP, and the reduced monsoon circulation over the northern Indian Ocean (Fig. 3.11e), the increased SST in the Indo-Pacific Warm Pool, and the insignificant warming along the equatorial eastern Pacific (Fig. 3.11f). In the tropical western Pacific, increased rainfall (Fig. 3.11d) is dynamically consistent with stronger low-level cyclonic circulation and lower SLP (Fig. 3.11e). While the coupled model captures the broad features noted in observations and reanalysis (Fig. 3.11a–c), there are certain limitations, including lack of simulation of positive rainfall trend over southern China and negative rainfall trend over the plains of Indo-China (Fig. 3.11d).

Turner and Annamalai (2012) examined the spatial pattern of the monsoon rainfall response to anthropogenic warming for the time-mean equilibrium response to increasing greenhouse-gas concentrations in only the 1pctto2x experiment for 20 CMIP3 models. The multimodel mean (see Fig. 3.3 in Turner and Annamalai 2012) results suggest enhanced rainfall over parts of South Asia, and the same mean change computed for the four "reasonable" models (models considered in Fig. 3.10) shows a similar result, providing more confidence in such a projection. The strengthened monsoon rainfall is generally attributed to increasing atmospheric moisture content over the warmer Indian Ocean, resulting in increased vertically integrated moisture fluxes towards India; such thermodynamic forcing has been consistently shown to lead to precipitation increases for South Asia.

In summary, climate models need to capture the "observed" east-west shifts in monsoon rainfall in the current climate to warrant confidence in their future projections. A cursory examination with CMIP5 models (not shown) suggests that most models fail to capture the drying tendency over South Asia between 1950 and 2005 in their historical simulations.

3.6 Conclusions

It is now recognized that any future projections of long-term changes in climate can only be made by complex climate models that depend on supercomputers. The world modeling summit held in May, 2008, argued that "climate models will, as in the past, play an important, and perhaps central role in guiding the trillion-dollar decisions that the peoples, governments, and industries of the world will be making to cope with the consequences of changing climate" (Shukla et al. 2009). Can the ultra-super computers alone solve the monsoon-modeling issue?

It is fair to mention that in climate science, there is no bigger problem than modeling the monsoons. Despite the availability of supercomputers, there are numerous other factors that will limit our ability to model the monsoons due to the inherent complexity of the monsoon itself. For example, while the importance of large-scale orographic and boundary forcings, such as SST, are fairly well understood (Hoskins and Rodwell 1995; Charney and Shukla 1981), the specific role of

thermodynamic processes as well as oceanic process in shaping the mean monsoon precipitation and its spectrum of variability are just beginning to unfold.

Furthermore, observational, theoretical, and modeling studies confirm that the mean monsoon precipitation and circulation influence monsoon variability on all time scales. Moreover, it has been suggested that scale interactions with ENSO impact the frequency of occurrence of extreme (drought and flood) monsoon conditions (>15 % of the climatological normal; Pillai and Annamalai 2012), with extended active (break) monsoon conditions giving rise to flood (drought) years (Prasanna and Annamalai 2012). During flood years, the frequency of occurrence of heavy rainfall events associated with synoptic systems is higher (Stowasser et al. 2009). Almost all heavy rainfall events (>50 mm/day) are associated with synoptic systems that are largely punctuated by the phase of intra-seasonal variability (Krishnamurthy and Ajayamohan 2010). Thus, the statistics of monsoon extremes are—to a certain degree—modulated by the phases of natural modes of variability. In summary, the processes involved in the "scale interactions" present in the monsoon system have not yet been understood, nor has their realistic representation in climate models been assessed.

We posed a few questions in the introduction—all suggesting limitations in monsoon modeling. It is our contention that despite many books and numerous scientific publications on monsoons, our knowledge of monsoon behavior is still limited. A classic example is the monsoon season of 2014, in which break-like conditions prevailed for more than five consecutive weeks, and the June 2014 monthly rainfall anomaly was about 44 % below normal over continental India (*source* India Meteorological Department. http://www.imdpune.gov.in/mons_monitor/mm_index.html)—and we do not yet know the reasons for this peculiar behavior. While the moderate strength developing El Niño in the equatorial Pacific in 2014 was expected to exert an impact on the South Asian monsoon, the prolonged persistence of dry spells in the month of June was rather unique.

As mentioned in the introduction, we believe that high-quality, three-dimensional observations of the atmosphere (thermodynamic variables) and ocean (temperature, salinity, etc.) over the monsoon- influenced regions are essential for better understanding, modeling, and predicting monsoon behavior. *Our conclusion is that without such a comprehensive observational effort, improving the physical processes in numerical models is severely limited.* As a result, this poses severe constraints in improving skills in monsoon prediction with weather and climate models.

Acknowledgments H. Annamalai's research was supported by the Office of Science (BER), U.S. Department of Energy, Grant DEFG02-07ER6445. K.R. Sperber's was supported by the Office of Science (BER), U.S. Department of Energy, through a Lawrence Livermore National Laboratory contract DE-AC52-07NA27344. We acknowledge the World Climate Research Programme's Working Group on Coupled Modelling, which is responsible for CMIP, and we thank the climate modeling groups for producing and making their model output available. For CMIP, the U.S. Department of Energy's Program for Climate Model Diagnosis and Intercomparison provided coordinating support and led the development of software infrastructure in partnership with the Global Organization for Earth System Science Portals.

References

Ajayamohan RS, Annamalai H, Luo J-J, Hafner J, Yamagata T (2011) Poleward propagation of boreal summer intraseasonal oscillations in a coupled model: role of internal processes. Clim Dyn 37:851–867

Annamalai H (2010) Moist dynamical linkage between the equatorial Indian Ocean and the South Asian monsoon trough. J Atmos Sci 67:589–610

Annamalai H, Liu P (2005) Response of the Asian summer monsoon to changes in ENSO properties. Quart J R Meteor Soc 131:805–831

Annamalai H, Sperber KR (2005) Regional heat sources and the active and break phases of boreal summer intraseasonal (30–50 day) variability. J Atmos Sci 62:2726–2748

Annamalai H, Hamilton K, Sperber KR (2007) South Asian summer monsoon and its relationship with ENSO in the IPCC AR4 simulations. J Clim 20:1071–1092

Annamalai H, Mehari M, Sperber KR (2015a) A recipe for diagnosing ENSO-monsoon relationship in CMIP5 models (submitted)

Annamalai H, Taguchi B, Sperber KR, McCreary JP, Ravichandran M, Cherchi A, Martin G, Moise A (2015b) Persistence of Systematic errors in the Asian-Australian monsoon precipitation in climate models: a way forward. CLIVAR Exchanges, Special Issue on Monsoon. (No. 66 Vol. 19 No. 1)

Annamalai H, Slingo JM, Sperber KR, Hodges K (1999) The Mean evolution and variability of the Asian summer monsoon: comparison of ECMWF and NCEP/NCAR reanalyses. Mon Wea Rev 127:1157–1186

Annamalai H, Hafner J, Sooraj KP, Pillai P (2013) Global warming shifts monsoon circulation, drying South Asia. J Clim 26(9):2701–2718

Bengtsson L, Hodges K, Roecker R (2006) Storm tracks and climate change. J Clim 19:3518–3543

Bollasina MA, Ming Y, Ramaswamy V (2011) Anthropo- genic aerosols and the weakening of the South Asian summer monsoon. Science 334:502–505

Charney JG, Shukla J (1981) Monsoon predictability. In: Lighthill J, Pearce RP (eds) Monsoon dynamics. Cambridge Press, London, pp 99–109

Charney JG, Stern ME (1962) On the stability of internal baroclinic jet in a rotating atmosphere. J Atmos Sci 19:159–172

Cherchi A, Annamalai H, Masina S, Navarra A (2014) South Asian monsoon and eastern mediterranean climate: the monsoon-desert mechanism in CMIP5 models. J Clim (in press)

Copsey D, Sutton R, Knight JR (2006) Recent trends in sea level pressure in the Indian Ocean region. Geophys Res Lett 33:L19712. doi:10.1029/2006GL027175

Dai A (2006) Precipitation characteristics in eighteen coupled climate models. J Climate 19:4605–4630. doi:10.1175/JCLI3884.1

Delcroix T, Cravatte S, McPhaden MJ (2007) Decadal variations and trends in tropical Pacific sea surface salinity since 1970. J Geophys Res 112:C03012. doi:10.1029/C003801

Hoskins B, Hsu H, James I, Masutani M, Sardeshmukh P, White G (1989) Diagnostics of the global atmospheric circulation based on ECMWF analysis 1979–1989. WCRP-27, WMO/TD-326, p 217

Hoskins BJ, Rodwell MJ (1995) A model of the Asian summer monsoon. Part I: the global scale. J Atmos Sci 52:1329–1340

Hoskins B, Wang B (2006) Large-scale atmospheric dynamics. In: Wang B (ed) The Asian monsoon. Springer, New York, pp 357–415

IPCC Climate Change (2013) The physical science basis. Cambridge University Press, New York

Kirtman BP, Shukla J (2000) Influence of the Indian summer monsoon on ENSO. Quart J R Meteor Soc 126:213–239

Krishnamurthy V, Ajayamohan RS (2010) The composite structure of monsoon low pressure systems and its relation to Indian Rainfall. J Clim 23:4285–4305

Lau KM, Chan PH (1986) Aspects of the 40–50 day oscillation during the northern summer as inferred from out-going longwave radiation. Mon Weather Rev 114:1354–1367
Lau KM, Wu HT, Bony S (1997) The role of large-scale atmospheric circulation in the relationship between tropical convection and sea surface temperature. J Clim 10:381–392
Lau NC, Nath MJ (2000) Impact of ENSO on the variability of the Asian-Australian monsoon as simulated in GCM experiments. J Clim 13:4287–4309
Madden RA, Julian PR (1994) Detection of a 40–50 day oscillation in the zonal wind in the tropical Pacific. Mon Weather Rev 122:813–837
McCreary JP, Kundu PK, Molinari R (1993) A numerical investigation of dynamics, thermodynamics and mixed-layer processes in the Indian Ocean. Prog Oceanogr 31:181–244
Nagura M, Sasaki W, Tozuka T, Luo J-J, Behera SK, Yamagata T (2013) Longitudinal biases in the Seychelles Dome simulated by 35 ocean-atmosphere coupled general circulation models. J Geophys Res Oceans 118. doi:10.1029/2012JC008352
Neelin JD, Held IM (1987) Modeling tropical convergence based on the moist static energy budget. Mon Wea Rev 115:3–12
Nigam S, Chung C, DeWeaver E (2000) ENSO diabatic heating in ECMWF and NCEP–NCAR reanalyses and NCAR CCM3 simulation. J Climate 13:3152–3171
Pillai PA, Annamalai H (2012) Moist dynamics of severe monsoons over South Asia: role of the tropical SST. J Atmos Sci 69:97–115
Prasanna V, Annamalai H (2012) Moist dynamics of extended monsoon breaks over South Asia. J Clim 25(11):3810–3827
Ramamurthy R (1969) Monsoons of India: some aspects of the break in the southwest monsoon during July–August. Forcasting manual, Part IV No. 18.3, India Meteorological Department, 13 pp
Ramanathan V et al (2005) Atmospheric brown clouds: impacts on South Asian climate and hydrological cycle. Proc Natl Acad Sci USA 102:5326–5333
Rasmusson EM, Carpenter TH (1983) The relationship between eastern equatorial Pacific sea surface temperature and surface wind fields associated with the Southern Oscillation/El Niño. Mon Weather Rev 111:517–528
Raymond DJ (1995) Regulation of moist convection over the West Pacific warm pool. J Atmos Sci 52:3945–3959
Rodwell M, Hoskins B (1996) Monsoons and the dynamics of deserts. Quart J R Meteor Soc 122:1385–1404
Santer BD et al (2007) Identification of human-induced changes in atmospheric moisture content. Proc Natl Acad Sci USA 104:15 248–15 253
Schott F, McCreary JP (2001) The monsoon circulation of the Indian Ocean. Prog Oceanogr 51:1–123
Schumacher C, Houze RA, Kraucunas I (2004) Tropical dynamical response to latent heating estimates derived from the TRMM precipitation radar. J Atmos Sci 61:1341–1358
Sikka DR (2006) A study on the monsoon low-pressure systems over the Indian region and their relationship with drought and excess monsoon seasonal rainfall. COLA Rep. 217, 145 pp
Shenoi SS, Shankar D, Shetye S (2000) Differences in heat budget of the near-surface Arabian Sea and Bay of Bengal: implications for the summer monsoon. J Geophys Res Ocean 107:3052
Shukla J (1978) CISK–barotropic–baroclinic instability and the growth of monsoon depressions. J Atmos Sci 35:495–508
Shukla J et al (2009) Revolution in climate prediction is both necessary and possible. Bull Am Meteorol Soc 16–19
Soman MK, Slingo JM (1997) Sensitivity of the Asian summer monsoon to aspects of sea surface temperature anomalies in the tropical Pacific Ocean. Quart J R Meteor Soc 123:309–336
Sperber KR, Annamalai H (2008) Coupled model simulations of boreal summer intraseasonal (30–50 day) variability, Part I: systematic errors and caution on use of metrics. Clim Dyn 31:345–372

Sperber KR, Annamalai H (2014) The use of fractional accumulated precipitation for the evaluation of the annual cycle of monsoons. Clim Dyn. doi:10.1007/s00382-014-2099-3 (in press)
Sperber KR, Annamalai H, Kang I-S, Kitoh A, Moise A, Turner A, Wang B, Zhou T (2013) The Asian summer monsoon: an intercomparison of CMIP5 versus CMIP3 simulations of the late 20th century. Clim Dyn 41(9):2711–2744
Stowasser M, Annamalai H, Hafner J (2009) Response of the South Asian summer monsoon to global warming: mean and synoptic systems. J Clim 22(4):1014
Turner AG, Inness PM, Slingo JM (2005) The role of the basic state in the ENSO-monsoon relationship and implications for predictability. Quart J Roy Meteor Soc 131:781–804
Turner A, Annamalai H (2012) Climate change and the South Asian monsoon. Nat Clim Chang 2:587–595
Waliser et al (2004) AGCM simulations of intraseasonal variability associated with the Asian summer monsoon. Clim Dyn 21:423–446
Walker GT, Bliss EW (1932) World weather. V Mem R Meteor Soc 4:53–84
Wang B, Xie X (1997) A model for the boreal summer intraseasonal oscillation. J Atmos Sci 54:72–86
Webster PJ, Magana VO, Palmer TN, Shukla J, Thomas RA, Yani M, Yasunari T (1998) The monsoon: processes, predictability and prediction. J Geophys Res 103:14451–14510
Wittenberg AT (2009) Are historical records sufficient to constrain ENSO simulations? Geophys Res Lett 36:L12702
Wu R, Wang B (2001) Multi-stage onset of summer monsoon over the western North Pacific. Clim Dyn 17:277–289
Wu RG, Kirtman BP (2005) Roles of Indian and Pacific Ocean air-sea coupling in tropical atmospheric variability. Clim Dyn 25:155–170

Chapter 4
Projecting Changes of the Asian Summer Monsoon Through the Twenty-First Century

Hirokazu Endo and Akio Kitoh

Abstract This chapter provides an updated review of our current understanding of future changes in the Asian summer monsoon. It is based on recent studies that include analysis of the state-of-the-art CMIP5 model simulations together with projections of extremes and regional-scale climate from higher-resolution models. It is projected that both the amount and intensity of Asian summer monsoon rainfall are likely to increase under global warming, and that the rate of increase will be higher than that in other monsoon regions, which suggests a substantial increase in the risk of extreme rainfall events.

Keywords Asian monsoon · CMIP5 · Precipitation · Global warming · High-resolution model

4.1 Introduction

The Asian monsoon region is one of the most water-rich areas of the world, and billions of people depend on this water to sustain both their daily lives and industries. However, the region has often suffered from floods caused by unusually intense rainfall, as well as droughts caused by long periods of reduced rainfall, particularly in the more vulnerable countries. The monsoon region receives most of its annual rainfall during the summer season. Therefore, reliable projections of future summer monsoon rainfall are required, not only of average and extreme rainfall, but also of seasonality. Such projections are especially important for impact, vulnerability, and adaptation studies in relation to climate change in the Asian monsoon.

H. Endo (✉)
Climate Research Department, Meteorological Research Institute,
1-1 Nagamine, Tsukuba, Ibaraki 305-0052, Japan
e-mail: hendo@mri-jma.go.jp

A. Kitoh
University of Tsukuba, 1-1-1 Tennodai, Tsukuba, Ibaraki 305-8572, Japan

© Springer International Publishing Switzerland 2016

L.M.V. de Carvalho and C. Jones (eds.), *The Monsoons and Climate Change*,
Springer Climate, DOI 10.1007/978-3-319-21650-8_4

Monsoons are driven by the annual cycle of solar insolation and the differential heating of the land and ocean, which lead to the seasonal reversal of surface winds as well as the contrast between wet summers and dry winters (Wang and Ding 2008). Spatial patterns of projected changes in surface temperature are robust among climate models, with greater warming over land than ocean, and at northern high latitudes (Meehl et al. 2007). Therefore, the land-sea temperature contrast is expected to become larger in summer, and this will be accompanied by ample moisture availability in a warmer climate, leading to a more intense monsoon. However, despite their common basic mechanisms, monsoons over different regions are subject to various factors; consequently, the responses of regional monsoons to global warming are complex and uncertain (Meehl et al. 2007; Turner and Annamalai 2012).

Recently, many climate modeling groups worldwide have participated in the Coupled Model Intercomparison Project Phase 5 (CMIP5). Under CMIP5, a series of experiments was performed, including twentieth century historical simulations and twenty-first century climate projections, which applied four different representative concentration pathway (RCP) scenarios (Taylor et al. 2012). The results have been analyzed from various perspectives by many researchers, and were assessed in the Intergovernmental Panel on Climate Change (IPCC) Fifth Assessment Report (AR5) (IPCC 2013).

With respect to future changes in the Asian monsoon climate under global warming, Kitoh (2011) provided a review based on studies of the Coupled Model Intercomparison Project Phase 3 (CMIP3) model simulations and other model experiments. In this chapter, we offer an updated review of our current understanding of likely future changes in the Asian summer monsoon, based on recent studies that include analysis of the state-of-the-art CMIP5 model simulations, together with projections of extremes and regional-scale climate from higher-resolution models.

4.2 Present-Day Simulation by CMIP3 and CMIP5 Models

4.2.1 Comparison of CMIP3 with CMIP5

For simulating the present-day Asian summer monsoon system, the CMIP5 models show a general improvement over the CMIP3 models. Sperber et al. (2013) showed that the CMIP5 multi-model mean outperforms the CMIP3 multi-model mean for all of the diagnostics calculated over the Asian monsoon region, including the seasonally averaged climatology of precipitation and 850 hPa wind (Fig. 4.1), the annual cycle climatology, inter-annual variability, and intra-seasonal variability. Wang et al. (2014) also reported that the CMIP5 models are significantly better than the CMIP3 models in terms of Asian–Australian monsoon metrics for precipitation climatology and variability. However, there are systematic errors that are consistent between the CMIP3 and CMIP5 models, although the magnitude of the errors is

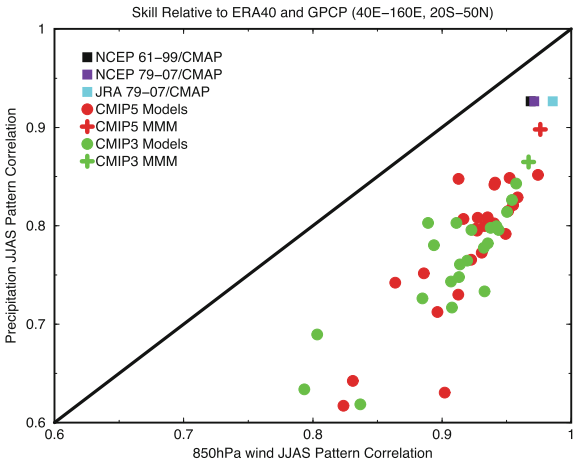

Fig. 4.1 Scatterplot of the pattern correlation with observations of simulated 850 hPa wind climatology versus the pattern correlation with observations of simulated precipitation climatology from June to September. The scores are relative to ERA40 and GPCP over the 40°E–160°E, 20°S–50°N region. *Circles* denote scores for individual models for the CMIP3 and CMIP5, and plus marks indicate scores of the multi-model mean fields. (Modified from Sperber et al. 2013)

generally smaller for CMIP5. For example, in the CMIP5 models, Indian summer monsoon rainfall is lower and the monsoon onset over India is later than in reality (Levine et al. 2013; Sperber et al. 2013), while the western North Pacific summer monsoon rainfall is higher, with a cyclonic circulation bias in the lower troposphere (Sperber et al. 2013). Levine et al. (2013) attributed the deficit in Indian summer monsoon rainfall to cold biases over the northern Arabian Sea, which develop in winter and persist until summer, reducing evaporation over the ocean and weakening the moisture flux towards India.

The East Asian summer monsoon (EASM), which affects eastern China, Korea and southern Japan, is a subsystem of the Asian summer monsoon system, but has features that are distinct from the South Asian summer monsoon (SASM) affecting the Indian subcontinent and the Indochina Peninsula. One of the prominent features of the EASM is the rainfall concentration in a northeast-southwest-elongated rain belt (Wang et al. 2008), referred to as the Meiyu/Baiu rain-band, which extends from eastern China to southern Japan in early summer (May–July). The Meiyu/Baiu rainband forms on the northern boundary of a warm and moist air mass in the subtropics, with moisture supply from low-level southerly winds. These southerlies blow between a heat low over the Asian continent and the North Pacific subtropical high in association with extratropical disturbances propagating along the East Asian Jet (Sampe and Xie 2010).

Seo et al. (2013) assessed the skill of the CMIP3 and CMIP5 ensembles in reproducing EASM rainfall for the present, and showed that the CMIP5 models are much better than the CMIP3 models at representing the spatial pattern of climatology and inter-annual variability (Fig. 4.2). Sperber et al. (2013) also showed that

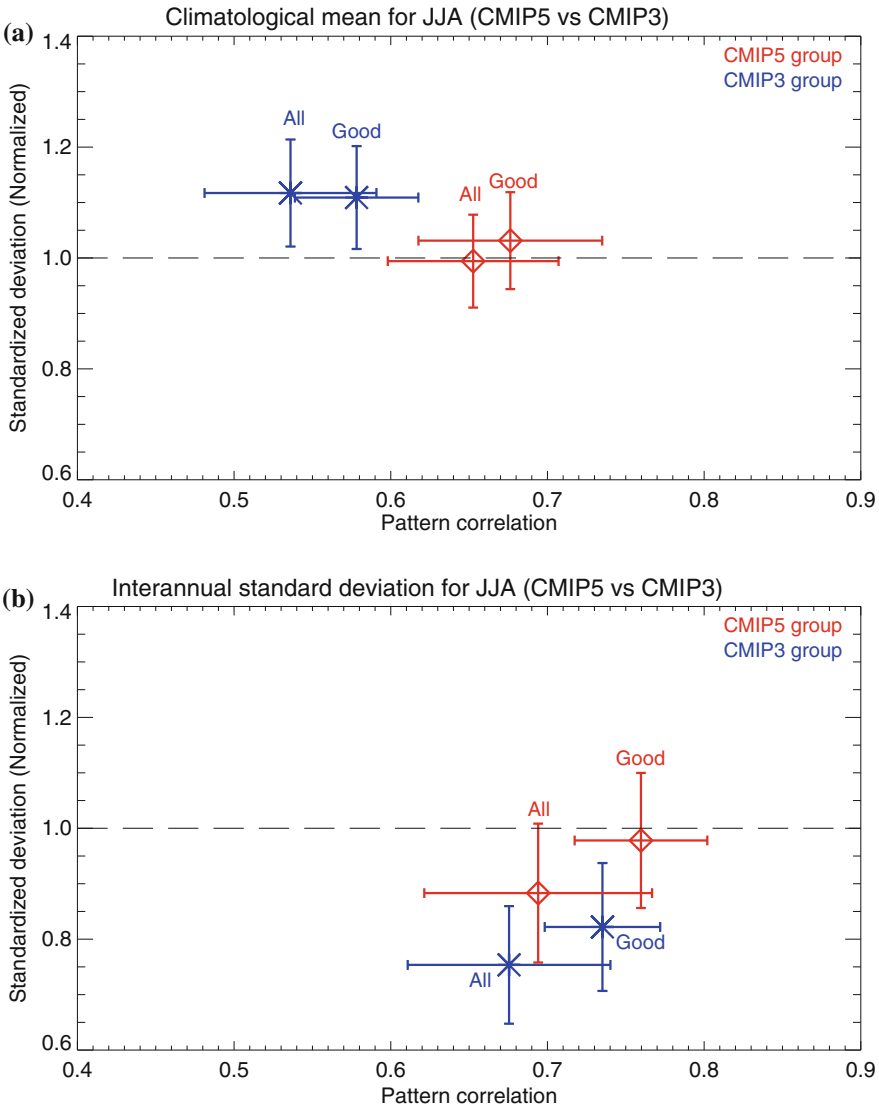

Fig. 4.2 Pattern correlation (*horizontal axis*) and spatial standardized deviation ratio (*vertical axis*) between observation and CMIP3 (*blue*) and CMIP5 (*red*) for all-model and good-model ensembles for: **a** the climatology, and **b** the inter-annual standard deviation fields in precipitation. The scores are calculated from June to August over the 100°E–180°E, 25°N–50°N region. Inter-model standard deviations are shown for the model ensembles. 15 (14) models out of all 23 (22) models for CMIP5 (CMIP3) are selected as the good model ensemble (Seo et al. 2013)

the CMIP5 models are superior to the CMIP3 ones in simulating inter-annual rainfall variability of north-south dipole anomalies associated with the EASM. A similar improvement was also found for Atmospheric Model Intercomparison Project (AMIP)-type simulations using atmospheric general circulation models (AGCMs) for CMIP5 over CMIP3 models (Song and Zhou 2014). On the other hand, EASM rainfall is commonly underestimated by the CMIP3 and CMIP5 models (Chen and Sun 2013; Seo et al. 2013; Sperber et al. 2013). Thus, the dry bias in the EASM is a common problem even in most contemporary climate models. It is believed that the use of models with a resolution high enough to realistically represent the Meiyu/Baiu rainband, and with improved physics schemes, will be necessary to overcome this weakness.

4.2.2 Twentieth-Century Climate Realization

Observational studies show that global monsoon precipitation over land followed a slight increasing trend during the first half of the twentieth century, and a generally decreasing trend from the 1950s to the 1980s, and then a recovering trend until the present (e.g., Wang and Ding 2006; Hsu et al. 2011; Zhang and Zhou 2011; Wang et al. 2012; Kitoh et al. 2013). The CMIP5 model ensemble, driven by observed historical forcing, can reproduce a gradual decline from the early twentieth century until the 1980s and a subsequent recovery, while it is unable to reproduce the mid-twentieth century maximum over the land monsoon region (Fig. 4.3a).

The Asian monsoon region has also experienced multi-decadal variability in summer monsoon rainfall. Observed SASM rainfall has declined since the mid-twentieth century (Fig. 4.4a; Zhang and Zhou 2011; Turner and Annamalai 2012; Ramesh and Goswami 2014), while EASM rainfall has followed a decreasing trend from the 1950s to the 1980s and a subsequent recovering trend (Fig. 4.4b; Zhang and Zhou 2011), although there are some discrepancies in the variations among datasets. The CMIP5 model ensemble shows a gradual decrease in EASM rainfall from the mid-twentieth century until the 1980s, which vaguely resembles the observed temporal variation (Fig. 4.4b), suggesting that the observed multi-decadal variations are partly forced by external factors, including greenhouse gases, anthropogenic aerosols, volcanic eruptions, and solar variability. Song et al. (2014) examined the responses of EASM circulation to natural and anthropogenic forcing during the second half of the twentieth century, using the attribution simulations (historical, historicalGHG, and historicalNat) performed by the 17 CMIP5 models. They found that anthropogenic aerosol forcing played a role in the observed weakening of the EASM circulation by reducing the land-sea thermal contrast, although the authors noted that the internal variability mode of the Pacific Decadal Oscillation (PDO) may also have contributed to the monsoon weakening.

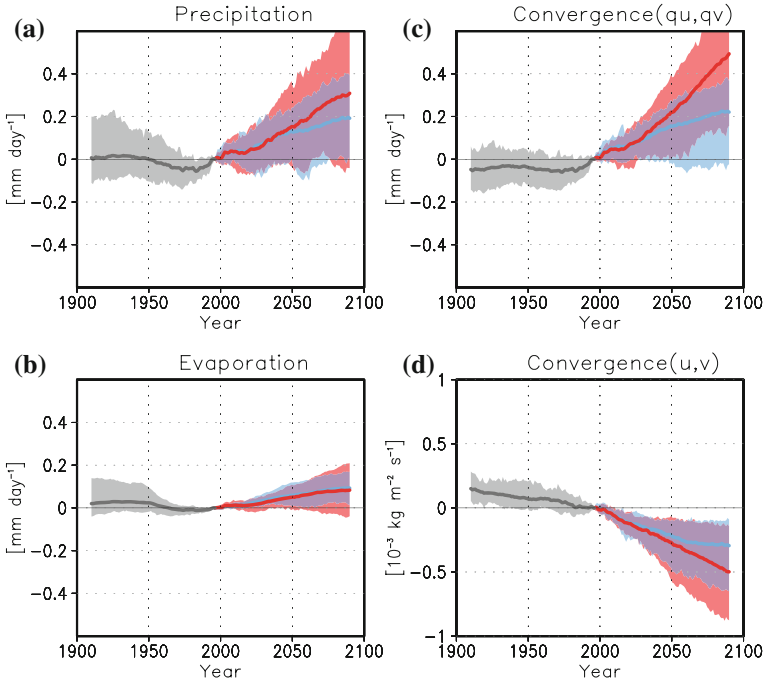

Fig. 4.3 Time series of simulated anomalies in the summer season (May–September in the Northern Hemisphere; November–March in the Southern Hemisphere), smoothed with **a** 20 year running mean over the global land monsoon domain for **a** precipitation (mm day^{-1}); **b** evaporation (mm day^{-1}); **c** water vapor flux convergence in the lower (below 500 hPa) troposphere (mm day^{-1}); and **d** wind convergence in the lower troposphere (10^{-3} kg m^{-2} s^{-1}), relative to the present (1986–2005), based on the monthly output of CMIP5 models. Historical (*gray*—29 models), RCP4.5 (*light blue*—24 models), and RCP8.5 (*red*—24 models) simulations are shown in all-model averages (*thick lines*), together with the 10th and 90th percentiles (*shading*)

The role of anthropogenic aerosols in the SASM has been extensively examined, via observational and modeling studies, alongside efforts to increase the complexity of climate models. Recent studies using a single climate model showed that anthropogenic aerosols were probably responsible for the observed decrease in SAMS rainfall during the late twentieth century (Meehl et al. 2008; Bollasina et al. 2011, 2014; Cowan and Cai 2011; Ganguly 2012a, b), although the CMIP5 multi-model mean has difficulty in reproducing the observed decadal-scale variations in SASM rainfall (Fig. 4.4a; Ramesh and Goswami 2014). For instance, using the Geophysical Fluid Dynamics Laboratory CM3 model (GFDL-CM3), which represents both direct and indirect aerosol effects, Bollasina et al. (2011) found that aerosol-induced differential cooling of the source and non-source regions reduces the large-scale meridional atmospheric temperature contrast, which weakens the

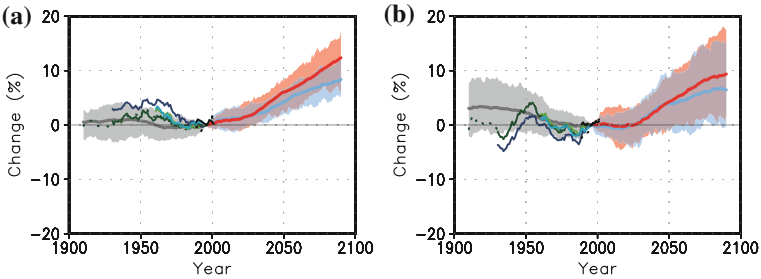

Fig. 4.4 Time series of observed and model-simulated precipitation anomalies (%) relative to the present-day average during the summer season (May-September) over: **a** the SASM region, and **b** the EASM region (land only), based on CMIP5 multi-models. All time series are smoothed with a 20 year running mean. For the time series of simulations, historical (*gray*—40 models), RCP4.5 (*light blue*—34 models), and RCP8.5 (*red*—32 models) simulations are shown in all-model averages (*thick lines*), together with the 10th and 90th percentile (*shading*). For the time series of observations, Climate Research Unit (CRU) TS3.2 (update from Mitchell and Jones 2005—*dark blue*), Global Precipitation Climatology Centre (GPCC) v6 (Becker et al. 2013—*dark green*), GPCC Variability Analysis of Surface Climate Observations (VASClimO; Beck et al. 2005—*light green*), Highly Resolved Observational Data Integration Towards the Evaluation of Water Resources (APHRODITE) v1101 (Yatagai et al. 2012—*light blue*), Global Precipitation Climatology Project (GPCP) v2.2 (updated from Huffman et al. 2009—*black*), and Climate Prediction Center (NOAA) Merged Analysis of Precipitation (CMAP) v1201 (updated from Xie and Arkin 1997—*black with dots*) are shown. GPCC v6 (*dotted line*) GPCC VASClimO, GPCP v2.2 and CMAP v1201 were calculated using all grids for the periods 1901–2010, 1951–2000, 1979–2010, and 1979–2010, respectively. CRU TS3.2, GPCC v6 (*solid line*), and APHRODITE v1101, were calculated using only grid boxes (2.5° in longitude/latitude) where at least one observation site existed for more than 80 % of the periods 1921–2005, 1921–2005, and 1951–2005, respectively. See Kitoh et al. (2013) for details of the definition of the regional land monsoon domains

local Hadley circulation, leading to suppressed SASM rainfall. In addition, there are emerging indications that anthropogenic aerosols affect monsoon seasonality. Observational data have revealed that the onset of the SASM advanced during the late twentieth century (Lau and Kim 2006, 2010; Kajikawa et al. 2012). Corresponding to this trend, many modeling studies have concluded that forcing by anthropogenic absorbing aerosols, such as black carbon and dust, causes a significant increase in SASM rainfall during the pre-monsoon season (May–June) (Lau et al. 2006; Meehl et al. 2008; Wang et al. 2009; Bollasina et al. 2013). Lau et al. (2006) proposed the elevated heat pump (EHP) mechanism, which posits that the accumulation of black carbon and dust over the Indo-Gangetic Plain and over the foothills of the Himalayas may induce enhanced warming in the middle and upper troposphere, leading to increased rainfall over northern India in late spring and early summer. However, the response of the SASM to aerosol forcing very much depends on climate models, and a definitive explanation of the physical mechanism remains elusive.

4.3 Projected Changes in the CMIP3 and CMIP5 Models

4.3.1 Global Perspectives

There is consensus among the CMIP3 and CMIP5 ensembles that global-mean rainfall increases at a rate of about 1–3 % per Kelvin, which is much less than the increase rate of water vapor (around 7 % per Kelvin) expected from the Clausius-Clapeyron equation (Vecchi and Soden 2007; Chadwick et al. 2013). This is because the changes in global-mean rainfall are constrained by changes in the net radiative cooling rate in the troposphere, which are limited by increased CO_2 forcing (Sugi and Yoshimura 2004). At the same time, the lower rate of increase in rainfall than water vapor requires a general weakening of convective mass flux, implying a weakening of the atmospheric overturning circulation, especially for the Walker circulation (Held and Soden 2006; Vecchi and Soden 2007).

With regard to the spatial distribution of the tropical-rainfall response to a warmer climate, two fundamental views have been presented: (1) the currently observed rainfall pattern will be enhanced, which is based on the hypothesis that increased moisture content enhances atmospheric moisture transport and its convergence/divergence under the assumption that there are no atmospheric circulation changes (i.e., the wet-get-wetter (WeGW) mechanism; Held and Soden 2006; Chou et al. 2009); and (2) rainfall will increase over the areas where sea surface temperature (SST) is warmer than the tropical mean, which is based on the hypothesis that local change in convective instability strongly depends on the relative SST, accompanied by atmospheric circulation changes (i.e., the warmer-get-wetter (WaGW) mechanism; Xie et al. 2010; Ma and Xie 2013). Analyzing the CMIP5 projections, Huang et al. (2013) revealed that the changes in tropical rainfall are largely explained by a combination of the WeGW and WaGW effects, in that the former enhances rainfall in the wet season, while the latter displaces the inter-tropical convergence zone (ITCZ) toward the Equator. They suggested that—given large uncertainties in the SST warming pattern—projections of tropical seasonal mean rainfall, such as summer monsoon rainfall, are more reliable than the annual mean.

From a global point of view, monsoon rainfall characteristics over Asia-Australia, the Americas, and Africa can be viewed as an integrated global monsoon system, associated with a global-scale persistent atmospheric overturning circulation that changes with season (Trenberth et al. 2000). Wang and Ding (2008) have demonstrated that the global monsoon represents the dominant mode of annual variation of tropical rainfall and circulation, characterizing the seasonality of tropical climate. The global summer monsoon rainfall is projected to likely be strengthened in the twenty-first century, with increases in its area and intensity by the CMIP3 and CMIP5 multi-model ensembles (Hsu et al. 2012, 2013; Kitoh et al. 2013; Lee and Wang 2014). Kitoh et al. (2013) showed that the increase in global monsoon area (GMA) by the end of the twenty-first century—compared with the present—is projected to be −0.7, 5.4, and 9.4 % (0.4, 9.4, and 17.4 %) for RCP4.5 (RCP8.5) at the 10th, 50th, and 90th percentiles, respectively, among the CMIP5

models, and the increase in global monsoon intensity (GMI) is projected to be −0.5, 3.6, and 4.9 % (−0.2, 5.5, and 8.5 %). Besides, rainfall extremes related to the monsoon are expected to increase at a much higher rate than the mean rainfall (Kitoh et al. 2013).

Figure 4.3 shows the time series of precipitation, evaporation, lower-tropospheric water-vapor flux convergence, and lower-tropospheric wind convergence, averaged over the global land monsoon domain (Kitoh et al. 2013). The increase in monsoon rainfall can be attributed to enhanced moisture flux convergence, resulting from increased atmospheric moisture (i.e., the thermodynamic effect), and also to increased surface evaporation due to a warmer SST. However, the intensity of the monsoon circulation is projected to become weaker as the climate warms (i.e., the dynamic effect), which is counter-intuitive, given the projected increase in the land-sea temperature difference (Ueda et al. 2006; Meehl et al. 2007). This dynamic effect may therefore partly offset the positive thermodynamic effect on rainfall changes (Cherchi et al. 2011; Chadwick et al. 2013; Kitoh et al. 2013).

On the regional scale, reliable projections of monsoon rainfall have been challenging; this is because simulation of regional monsoon response to global warming is subject to various uncertainties, including land-sea thermal contrast, the spatial pattern of SST change, model physics such as cumulus parameterization, and land processes such as soil moisture and surface albedo (Endo et al. 2012; Rowell 2012; Ma and Xie 2013; Ma and Yu 2014; Mizuta et al. 2014). Kitoh et al. (2013) investigated future rainfall changes in the seven regional land monsoons around the world, using the CMIP5 model ensemble, and found that rainfall should increase in most monsoon regions, but that the rates of increase may be significantly different between different regions. Following their results, Endo and Kitoh (2014) examined the relative importance of the thermodynamic and dynamic effects on regional monsoon rainfall using the CMIP5 model ensemble, and revealed that the thermodynamic effect is largely compensated by the dynamic effect in most regional monsoons. However, in the Asian monsoon regions, including the SASM and EASM regions, the dynamic effect is smaller and surface evaporation increases at a higher rate than in other monsoon regions, resulting in a much larger increase in rainfall (Fig. 4.5).

4.3.2 South Asian Summer Monsoon

Figure 4.6 (left and center) shows projected changes in rainfall and 850 hPa wind over south Asia during the summer (June–September) in the CMIP3 and CMIP5 multi-model ensembles. Both projections indicate an overall increase in South Asian summer rainfall, in agreement with earlier studies (e.g., Kitoh et al. 1997; Douville et al. 2000; Meehl and Arblaster 2003; May 2004; Ashrit et al. 2005). On the other hand, the lower-tropospheric monsoon westerly is projected to weaken over the northern Indian Ocean (Equator to 10°N), but with a slight strengthening

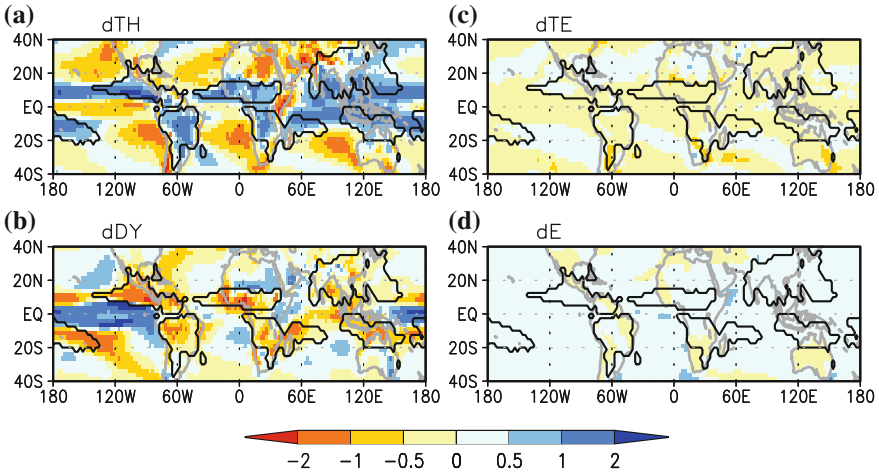

Fig. 4.5 Projected changes in the moisture budget based on 20 CMIP5 models between the present (1986–2005) and future (2080–2099) under the RCP8.5 scenario for the summer season (May–September in the Northern Hemisphere; November–March in the Southern Hemisphere). Shown are **a** thermodynamic term (δTH); **b** dynamic term (δDY); **c** transient eddy term (δTE); and **d** evaporation term (δE). Units are mm day^{-1}. The monsoon domains are indicated by *thick contours*. See Endo and Kitoh (2014) for details of their definition

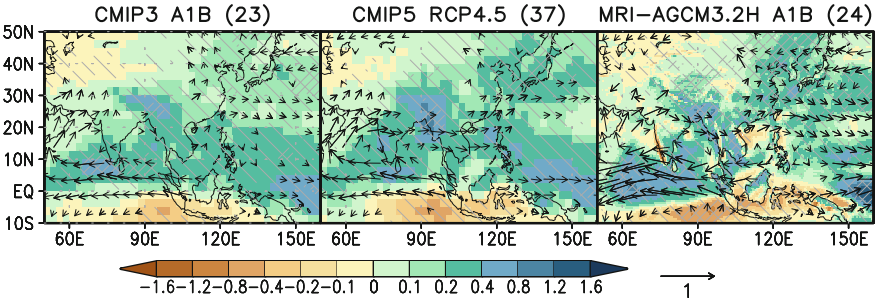

Fig. 4.6 Projected changes in precipitation (*shading*) and 850 hPa wind (*vectors*) relative to the present from June to September from: (*left*) SRES A1B scenario with 23 CMIP3 models; (*center*) RCP4.5 scenario with 37 CMIP5 models; and (*right*) SRES A1B scenario with the 60 km MRI-AGCM time slice experiments with 24 members (combination of three different cumulus schemes, four different SST anomalies, and two different initial conditions). The periods for the present-day climate (the future climate) are 1980–1999, 1986–2005, and 1979–2003 (2080–2099, 2080–2099, and 2075–2099) for CMIP3, CMIP5, and MRI-AGCM3.2, respectively. The projected changes are normalized by the global annual mean SAT changes in each scenario. *Light* (*dense*) *hatching* denotes the areas where more than 66 % (90 %) of models or members have the same sign in the precipitation changes. Only vectors with more than 66 % of models or members having the same sign for the changes in the 850 hPa zonal or meridional winds are shown

around 20°N, suggesting a northward shift of lower-tropospheric circulation systems (e.g., Kitoh et al. 1997; Sandeep and Ajayamohan 2014). This enhancement of the monsoon westerly in the subtropical region is found in most CMIP5 models (Fig. 4.6 (center); Ogata et al. 2014). Based on seven selected CMIP5 models, Wang et al. (2014) indicated that lower-tropospheric circulation intensity associated with the Indian summer monsoon will decrease in the future. This weakening of the monsoon circulation is over-compensated by an increase in atmospheric moisture content, leading to increased SASM rainfall (Ueda et al. 2006; Christensen et al. 2013).

Figure 4.7a shows projected changes in the indices of mean and extreme precipitation, as well as in seasonal evolution associated with the SASM, based on the CMIP5 projections. The CMIP5 models project an increase in mean summer precipitation (Pav) and its inter-annual variability (Psd), as well as in heavy precipitation events (simple precipitation daily intensity index (SDII) and seasonal maximum 5 day precipitation total (R5d)), but they disagree on the sign of the changes in seasonal maximum consecutive dry days (CDD). In particular, Psd and R5d are projected to increase remarkably by more than 20 % (on the median) under the RCP8.5 scenario. This is probably because changes in extreme precipitation are influenced more by atmospheric moisture build-up due to warming, compared to the changes of mean precipitation. Regarding monsoon seasonality in South Asia, the CMIP5 models project an earlier onset, later retreat, and resultant longer duration, with robust inter-model agreement (Kitoh et al. 2013).

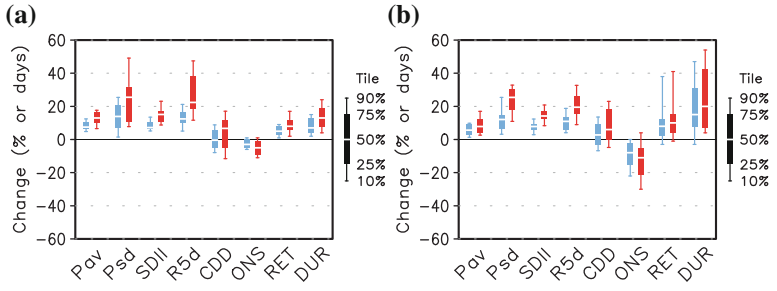

Fig. 4.7 Projected changes in averaged precipitation (Pav), standard deviation of inter-annual variability in seasonal average precipitation (Psd), simple precipitation daily intensity index (SDII), seasonal maximum 5 day precipitation total (R5d), seasonal maximum consecutive dry days (CDD), monsoon onset date (ONS), retreat date (RET), and duration (DUR), under the RCP4.5 (*light blue*; 24 models) and RCP8.5 scenarios (*red*—26 models), during the summer season (May–September) for the future (2080–2099) relative to the present (1979–2003) over **a** the SASM region, and **b** the EASM region (land only), based on CMIP5 multi-models. Units are % for Pav, Psd, SDII, R5d, and CDD; and days for ONS, RET, and DUR. The indices Pav, Psd, SDII, R5d and CDD were calculated for each model's original grid, and then averaged over the land monsoon domains determined by each model in the present day. The indices ONS, RET and DUR were calculated based on the criteria proposed by Wang and LinHo (2002), using regionally averaged climatological cycles of precipitation. See Kitoh et al. (2013) for details of the definition of the regional land monsoon domains

4.3.3 East Asian Summer Monsoon

Based on the CMIP3 and CMIP5 models, precipitation associated with the EASM is projected to increase overall in its amount and intensity with global warming (Figs. 4.4b , 4.6 (left and center), and 4.7b; Kitoh and Uchiyama 2006; Kusunoki and Arakawa 2012; Chen and Sun 2013; Kitoh et al. 2013; Seo and Ok 2013; Seo et al. 2013; Wang et al. 2014). The rate of increase of precipitation based on the CMIP5 multi-model mean, scaled by the global-mean surface air temperature (SAT) changes, is somewhat higher than that from the CMIP3 (Fig. 4.6). The EASM-related low-level circulation is also somewhat intensified for the CMIP5 models, although there are large differences among the projections, in contrast to the projected weakening of the SASM-related circulation (Wang et al. 2014; Christensen et al. 2013). Inter-annual variability of EASM rainfall is projected to increase at a much higher rate than that of mean precipitation: for the RCP4.5 (RCP8.5) scenario, the median increase in Psd is 12.1 % (25.4 %), while the median increase in Pav is 5.7 % (7.8 %) (Fig. 4.7b). The inadequate skill of the CMIP5 models in simulating EASM features such as the Meiyu/Baiu rain band, as described in Sect. 4.2.1, limits confidence in more detailed aspects of their projections, including precipitation extremes and monsoon seasonality (Christensen et al. 2013).

4.4 Projected Changes in High-Resolution Models

4.4.1 South Asian Summer Monsoon

Future projections by high-resolution models have been performed to realistically represent weather extremes and to provide as much regional detail as possible, based on time-slice AGCM and regional climate model (RCM) experiments. Figure 4.6 (right) shows time-slice projections from the 60 km mesh Meteorological Research Institute (MRI)-AGCM ensemble, based on a multi-physics and multi-SST framework (Endo et al. 2012). The result shows an overall increase in rainfall over South Asia, but with a significant reduction in rainfall along the west coast of India where much topography-influenced rainfall occurs in the current climate. However, such a reduction in orographic rainfall was not projected by either the CMIP3 or CMIP5 model ensembles, which may be due to insufficient horizontal resolution to resolve the steep topography. This significant reduction in orographic rainfall in a warmer climate was first predicted by Rajendran and Kitoh (2008), based on a projection using a 20 km mesh MRI-AGCM (Mizuta et al. 2006). A similar decreasing trend was observed in the late twentieth century (Rajendran et al. 2012; Krishnan et al. 2013). It is argued that either a weakening of the lower-tropospheric monsoon westerly associated with a slowdown of Hadley-type overturning circulation (Rajendran et al. 2012; Krishnan et al. 2013), or a northward shift of the monsoon westerly associated with enhanced land-sea

thermal contrast (Sandeep and Ajayamohan 2014), are responsible for the decreased rainfall along the western coast of India.

There have been several attempts to project the South Asian climate using RCMs driven by lateral and surface boundary conditions derived from global models. Using the 50 km mesh RCM PRECIS (Providing Regional Climates for Impact Studies), Kumar et al. (2011) obtained general increases in summer rainfall amounts and intensity over India, but slight decreases in rainfall amounts in some areas of India. In contrast, using the 20/50 km mesh RegCM3 (Centre for Theoretical Physics Regional Climate Model), Ashfaq et al. (2009) projected the overall suppression of South Asian summer rainfall, together with prolonged monsoon break periods, caused by a weakening of the large-scale monsoon flow and reduction in the contribution from the active phase of intra-seasonal variability. Using the non-hydrostatic RCM COSMO-CLM (Climate Limited-Area Modeling Community of Consortium for Small-Scale Modeling) with a 0.44 degree grid interval, Dobler and Ahrens (2011) found an increasing trend in rainfall intensity over large parts of India in contrast to an overall decreasing trend in rainfall amount over India. Thus, the results of projections of the SASM by RCMs are diverse.

4.4.2 East Asian Summer Monsoon

Models with a higher horizontal resolution are necessary to better reproduce extreme rainfall associated with tropical cyclones and the Meiyu/Baiu rain band (e.g., Kitoh and Kusunoki 2008). A series of global warming projections using 20 km mesh MRI-AGCMs (Mizuta et al. 2006, 2012) has been performed, showing increases in both mean precipitation and extreme precipitation associated with the Meiyu/Baiu rain band (Kamiguchi et al. 2006; Kusunoki et al. 2006; Kusunoki and Mizuta 2008; Kusunoki et al. 2011; Endo et al. 2012). To quantify uncertainty in the future projections, ensemble projections with 60 km mesh MRI-AGCMs have also been performed under multi-physics and multi-SST frameworks, showing consistent results with the 20 km MRI-AGCMs over East Asia, and with good agreement among members (Fig. 4.6 (right); Kusunoki et al. 2011; Endo et al. 2012; Kusunoki and Mizuta 2013). Regarding the seasonality of the rainy season, the 20/60 km MRI-AGCMs consistently project a delay in the termination of the rainy season (Baiu season) in early summer over Japan (Kusunoki et al. 2006; Kusunoki and Mizuta 2008; Kusunoki et al. 2011), which is also suggested by the CMIP3 models (Kitoh and Uchiyama 2006; Hirahara et al. 2012). A similar trend was observed between 1901 and 2009 on the Sea of Japan side of eastern and western Japan (Endo 2011). The intensification of the Meiyu/Baiu rain band is attributed to enhanced moisture flux convergence, owing to increased atmospheric moisture content, and an intensified southwesterly wind associated with the EASM (Kimoto 2005; Kitoh and Uchiyama 2006; Kusunoki et al. 2006; Kusunoki et al. 2011).

Further dynamical downscaling using a 5 km non-hydrostatic regional climate model (NHM-5 km), which can resolve meso-scale rainfall systems, has been

performed by MRI to project changes in heavy rainfall during the summer season in the vicinity of Japan under the SRES A1B scenario. Kitoh et al. (2009) found that the heaviest hourly precipitation (the 99.9th percentile) is projected to increase by 7 % in the near future (2015–2039), and by 21 % at the end of the twenty-first century (2075–2099) over Japan. Kanada et al. (2010) projected a remarkable increase in intense daily rainfall on the Pacific side of Japan in July, caused by intensified convective instability resulting from enhancement of atmospheric moisture supply from the Pacific in the lower troposphere and a dry air intrusion from the Asian continent in the mid-troposphere. In addition, Kanada et al. (2012) projected a significant increase in intense rainfall over western Japan in early July (the late Baiu season), when the proportion of intense rainfall (above 100 mm/day) within the total amount increases from 9 % at present to 15 % by the end of the twenty-first century (Fig. 4.8). They suggested that increased water-vapor supply from the south of the

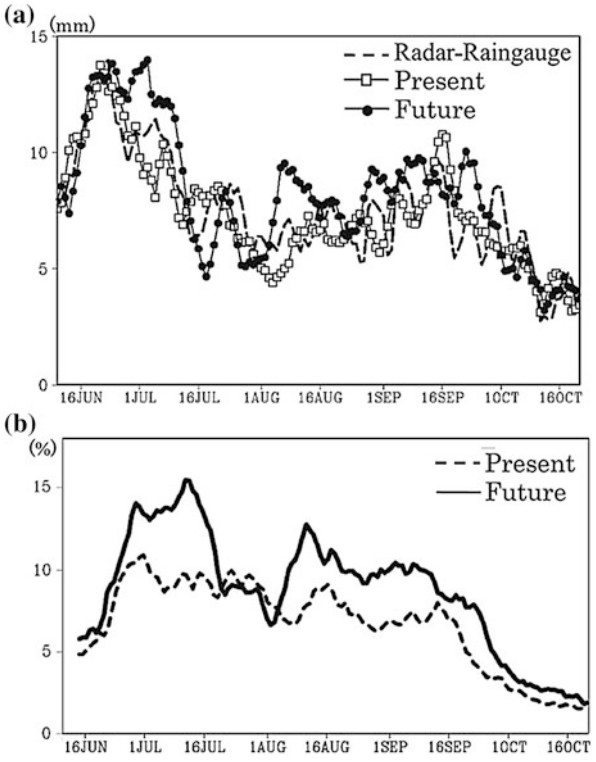

Fig. 4.8 **a** Seasonal variations of 25 year mean daily precipitation amounts (mm) averaged within the 127°E–137°E and 30°N–35°N domain, as observed by radar-rain gauge analyzed precipitation (1996–2009, *dashed line*), and simulated for the present (1979–2003, *open squares*) and the future (2075–2099, *black circles*) by NHM-5 km. **b** Seasonal variations in the proportion of intense precipitation (above 100 mm day^{-1}) within the total amounts, averaged within the same domain, as simulated for the present-day (*dashed line*) and the future (*thick solid line*) by NHM-5 km. All data represent 5 day moving averages (Kanada et al. 2012)

Baiu front and an intensified frontal zone with intense mean updrafts would contribute to the projected increase in intense rainfall.

4.5 Conclusions

State-of-the-art climate models project that both the amount and intensity of Asian summer monsoon rainfall are likely to increase under global warming, and that the rates of increase will be higher than those in other monsoon regions. Overall climate change projections obtained from the CMIP5 models are similar to those of the CMIP3 models. Considering the improvements in CMIP5 compared to CMIP3 in simulating present-day characteristics, we now have more confidence in future projections. The strongest effect of climate change on the monsoons is the increase in atmospheric moisture with warming of the atmosphere, which results in an increase in total monsoon rainfall even if the strength of the monsoon circulation weakens or does not change (Christensen et al. 2013). Besides, rainfall extremes are projected to increase at a higher rate than total rainfall, suggesting a substantial increase in the risk of extreme rainfall events (e.g., Kusunoki and Mizuta 2013).

At present, atmospheric aerosol loading influences the Asian monsoon climate in various ways, such as black carbon-induced enhancement and sulfate-induced suppression of precipitation (Turner and Annamalai 2012), which may have obscured changes in the Asian monsoon that would otherwise have been brought about by the increase in greenhouse gases. As we advance into the twenty-first century, the relative effect of aerosols could be overwhelmed by the effect of increasing greenhouse gases, but we cannot quantify the effects on rainfall. This remains one of the uncertainties that prevents us from assessing the future change of the Asian monsoon more precisely.

Acknowledgments We would like to acknowledge the modeling groups, the Program for Climate Model Diagnosis and Intercomparison (PCMDI), and the WCRP's Working Group on Coupled Modelling (WGCM) for making the WCRP CMIP3 and CMIP5 multi-model datasets available to us. This study was supported by the Environment Research and Technology Development Fund (2A-1201 and 2-1503) of the Ministry of the Environment and the SOUSEI Program of the Ministry of Education, Culture, Sports, Science, and Technology of Japan. We would also like to thank Osamu Arakawa of the University of Tsukuba for data management.

References

Ashfaq M, Shi Y, Tung W-w, Trapp RJ, Gao X, Pal JS, Diffenbaugh NS (2009) Suppression of south Asian summer monsoon precipitation in the twenty-first century. Geophys Res Lett 36. doi:10.1029/2008gl036500

Ashrit RG, Kitoh A, Yukimoto S (2005) Transient response of ENSO-monsoon teleconnection in MRI-CGCM2.2 climate change simulations. J Meteor Soc Jpn 83:273–291

Beck C, Grieser J, Rudolf BA (2005) New monthly precipitation climatology for the global land areas for the period 1951 to 2000. DWD Klimastatusbericht 2004:181–190

Becker A, Finger P, Meyer-Christoffer A, Rudolf B, Schamm K, Schneider U, Ziese M (2013) A description of the global land-surface precipitation data products of the Global Precipitation Climatology Centre with sample applications including centennial (trend) analysis from 1901–present. Earth Syst Sci Data 5:71–99

Bollasina MA, Ming Y, Ramaswamy V (2011) Anthropogenic aerosols and the weakening of the South Asian summer monsoon. Science 334(6055):502–505. doi:10.1126/science.1204994

Bollasina MA, Ming Y, Ramaswamy V (2013) Earlier onset of the Indian monsoon in the late twentieth century: the role of anthropogenic aerosols. Geophys Res Lett 40:3715–3720. doi:10.1002/grl.50719

Bollasina MA, Ming Y, Ramaswamy V, Schwarzkopf, MD, Naik, V (2014) Contribution of local and remote anthropogenic aerosols to the twentieth century weakening of the South Asian monsoon. Geophys Res Lett 41. doi:10.1002/2013GL058183

Chadwick R, Boutle I, Martin G (2013) Spatial patterns of precipitation change in CMIP5: why the rich do not get richer in the tropics. J Clim 26:3803–3822. doi:10.1175/jcli-d-12-00543.1

Chen H, Sun J (2013) Projected change in East Asian summer monsoon precipitation under RCP scenario. Meteorol Atmos Phys 121:55–77. doi:10.1007/s00703-013-0257-5

Cherchi A, Alessandri A, Masina S, Navarra A (2011) Effects of increased CO_2 levels on monsoons. Clim Dyn 37:83–101. doi:10.1007/s00382-010-0801-7

Chou C, Neelin JD, Chen C-A, Tu J-Y (2009) Evaluating the "rich-get-richer" mechanism in tropical precipitation change under global warming. J Clim 22:1982–2005. doi:10.1175/2008jcli2471.1

Cowan T, Cai W (2011) The impact of Asian and non-Asian anthropogenic aerosols on twentieth century Asian summer monsoon. Geophys Res Lett 38:L11703. doi:10.1029/2011gl047268

Christensen JH, Krishna Kumar K, Aldrian E, An S-I, Cavalcanti IFA, de Castro M, Dong W, Goswami P, Hall A, Kanyanga JK, Kitoh A, Kossin J, Lau N-C, Renwick J, Stephenson D, Xie S-P, Zhou T (2013) Climate phenomena and their relevance for future regional climate change. In: Stocker TF, Qin D, Plattner G-K, Tignor M, Allen SK, Boschung J, Nauels A, Xia Y, Bex V, Midgley PM (eds) Climate change 2013: the physical science basis. Contribution of working group I to the fifth assessment report of the intergovernmental panel on climate change. Cambridge University Press, Cambridge, United Kingdom, pp 1217–1308

Dobler A, Ahrens B (2011) Four climate change scenarios for the Indian summer monsoon by the regional climate model COSMO-CLM. J Geophys Res 116. doi:10.1029/2011jd016329

Douville H, Royer J-F, Polcher J, Cox P, Gedney N, Stephenson DB, Valdes PJ (2000) Impact of CO_2 doubling on the Asian summer monsoon: Robust versus model-dependent responses. J Meteorol Soc Jpn 78:421–439

Endo H (2011) Long-term changes of seasonal progress in Baiu rainfall using 109 years (1901–2009) daily station data. SOLA 7:5–8. doi:10.2151/sola.2011-002

Endo H, Kitoh A, Ose T, Mizuta R, Kusunoki S (2012) Future changes and uncertainties in Asian precipitation simulated by multiphysics and multi–sea surface temperature ensemble experiments with high-resolution Meteorological Research Institute atmospheric general circulation models (MRI-AGCMs). J Geophys Res Atmos 117:D16118. doi:10.1029/2012jd017874

Endo H, Kitoh A (2014) Thermodynamic and dynamic effects on regional monsoon rainfall changes in a warmer climate. Geophys Res Lett 41. doi:10.1002/2013GL059158

Ganguly D, Rasch PJ, Wang H, Yoon J-H (2012a) Climate response of the South Asian monsoon system to anthropogenic aerosols. J Geophys Res 117:D13209. doi:10.1029/2012JD017508

Ganguly D, Rasch PJ, Wang H, Yoon J (2012b) Fast and slow responses of the South Asian monsoon system to anthropogenic aerosols. Geophys Res Lett 39:L18804. doi:10.1029/2012GL053043

Held IM, Soden BJ (2006) Robust responses of the hydrological cycle to global warming. J Clim 19:5686–5699. doi:10.1175/jcli3990.1

Hirahara S, Ohno H, Oikawa Y, Maeda S (2012) Southward shift of the jet stream and lingering of Baiu season under global warming. J Meteor Soc Japan

Hsu P-c, Li T, Wang B (2011) Trends in global monsoon area and precipitation over the past 30 years, Geophys Res Lett 38. doi:10.1029/2011gl046893

Hsu P-C, Li T, Luo J-J, Murakami H, Kitoh A, Zhao M (2012) Increase of global monsoon area and precipitation under global warming: A robust signal? Geophys Res Lett 39:L06701. doi:10.1029/2012gl051037

Hsu P-C, Li T, Murakami H, Kitoh A (2013) Future change of the global monsoon revealed from 19 CMIP5 models. J Geophys Res 118:1247–1260. doi:10.1002/jgrd.50145

Huang P, Xie S-P, Hu K, Huang G, Huang R (2013) Patterns of the seasonal response of tropical rainfall to global warming. Nat Geosci 6:357–361

Huffman GJ, Adler RF, Bolvin DT, Gu G (2009) Improving the global precipitation record: GPCP Version 2.1. Geophys Res Lett 36:L17808. doi:10.1029/2009gl040000

IPCC, 2013: Climate Change 2013: The physical science basis. Contribution of Working Group I to the Fifth Assessment Report of the Intergovernmental Panel on Climate Change [Stocker, T. F., D. Qin, G.-K. Plattner, M. Tignor, S.K. Allen, J. Boschung, A. Nauels, Y. Xia, V. Bex and P.M. Midgley (eds.)]. Cambridge University Press, Cambridge, United Kingdom and New York, NY, USA, 1535 pp

Kajikawa Y, Yasunari T, Yoshida S, Fujinami H (2012) Advanced Asian summer monsoon onset in recent decades. Geophys Res Lett 39:L03803. doi:10.1029/2011GL050540

Kamiguchi K, Kitoh A, Uchiyama T, Mizuta R, Noda A (2006) Changes in precipitation-based extremes indices due to global warming projected by a global 20 km-mesh atmospheric model. SOLA 2:64–67. doi:10.2151/sola.2006-017

Kanada S, Nakano M, Kato T (2010) Changes in mean atmospheric structures around Japan during July due to global warming in regional climate experiments using a cloud-system resolving model. Hydrol Res Lett 4:11–14. doi:10.3178/hrl.4.11

Kanada S, Nakano M, Kato T (2012) Projections of future changes in precipitation and the vertical structure of the frontal zone during the Baiu season in the vicinity of Japan using a 5 km-mesh regional climate model. J Meteor Soc Jpn 90A:65–86. doi:10.2151/jmsj.2012-A03

Kimoto M (2005) Simulated change of the east Asian circulation under global warming scenario. Geophys Res Lett 32:L16701. doi:10.1029/2005GL023383

Kitoh A (2011) Impact of climate change on Asian monsoon characteristics. In: Chang C-P et al (eds) Chap. 32. World Scientific, Singapore, pp 557–568

Kitoh A, Uchiyama T (2006) Changes in onset and withdrawal of the East Asian summer rainy season by multi-model global warming experiments. J Meteor Soc Jpn 84:247–258

Kitoh A, Kusunoki S (2008) East Asian summer monsoon simulation by a 20 km mesh AGCM. Clim Dyn 31:389–401. doi:10.1007/s00382-007-0285-2

Kitoh A, Yukimoto S, Noda A, Motoi T (1997) Simulated changes in the Asian summer monsoon at times of increased atmospheric CO_2. J Meteorol Soc Jpn 75:1019–1031

Kitoh A, Ose T, Kurihara K, Kusunoki S, Sugi M (2009) Projection of changes in future weather extremes using super-high-resolution global and regional atmospheric models in the KAKUSHIN Program: Results of preliminary experiments. Hydrol Res Lett 3:49–53. doi:10.3178/hrl.3.49

Kitoh A, Endo H, Krishna Kumar K, Cavalcanti IFA, Goswami P, Zhou T (2013) Monsoons in a changing world: A regional perspective in a global context. J Geophys Res 118:3053–3065. doi:10.1002/jgrd.50258

Krishnan R, Sabin TP, Ayantika DC, Kitoh A, Sugi M, Murakami H, Turner AG, Slingo JM, Rajendran K (2013) Will the South Asian monsoon overturning circulation stabilize any further? Clim Dyn 40:187–211. doi:10.1007/s00382-012-1317-0

Kumar KK et al (2011) Simulated projection for summer monsoon climate over India by a high-resolution regional climate model (PRECIS). Curr Sci 101:312–326

Kusunoki S, Arakawa O (2012) Change in the precipitation intensity of the East Asian summer monsoon projected by CMIP3 models. Clim Dyn 38:2055–2072. doi:10.1007/s00382-011-1234-7

Kusunoki S, Mizuta R (2008) Future changes in the Baiu rain band projected by a 20 km mesh global atmospheric model: sea surface temperature dependence. SOLA 4:85–88. doi:10.2151/sola.2008-022

Kusunoki S, Mizuta R (2013) Changes in precipitation intensity over East Asia during the twentieth and twenty-first centuries simulated by a global atmospheric model with a 60 km grid size. J Geophys Res 118 11,007–011,016. doi:10.1002/jgrd.50877

Kusunoki S, Yoshimura J, Yoshimura H, Noda A (2006) Change of Baiu rain band in global warming projection by an atmospheric general circulation model with a 20 km grid size. J Meteor Soc Jpn 84:581–611

Kusunoki S, Mizuta R, Matsueda M (2011) Future changes in the East Asian rain band projected by global atmospheric models with 20 and 60 km grid size. Clim Dyn 37:2481–2493. doi:10.1007/s00382-011-1000-x

Lau K-M, Kim K-M (2006) Observational relationships between aerosol and Asian monsoon rainfall, and circulation. Geophys Res Lett 33:L21810. doi:10.1029/2006GL027546

Lau WKM, Kim K-M (2010) Fingerprinting the impacts of aerosols on long-term trends of the Indian summer monsoon regional rainfall. Geophys Res Lett 37:L16705. doi:10.1029/2010GL043255

Lau KM, Kim MK, Kim KM (2006) Aerosol induced anomalies in the Asian summer monsoon: the role of the Tibetan Plateau. Clim Dyn 26:855–864. doi:10.1007/s00382-006-0114-z

Lee J-Y, Wang B (2014) Future change of global monsoon in the CMIP5. Clim Dyn 42:101–119. doi:10.1007/s00382-012-1564-0

Levine RC, Turner AG, Marathayil D, Martin GM (2013) The role of northern Arabian Sea surface temperature biases in CMIP5 model simulations and future projections of Indian summer monsoon rainfall. Clim Dyn 41:155–172. doi:10.1007/s00382-012-1656-x

Ma J, Xie S-P (2013) Regional patterns of sea surface temperature change: A source of uncertainty in future projections of precipitation and atmospheric circulation. J Clim 26:2482–2501. doi:10.1175/jcli-d-12-00283.1

Ma J, Yu J-Y (2014) Paradox in South Asian summer monsoon circulation change: Lower tropospheric strengthening and upper tropospheric weakening. Geophys Res Lett 41:2934–2940. doi:10.1002/2014GL059891

May W (2004) Potential future changes on the Indian summer monsoon due to greenhouse warming: Analysis of mechanisms in a global timeslice experiment. Clim Dyn 22:389–414

Meehl GA, Arblaster JM (2003) Mechanisms for projected future changes in south Asian monsoon precipitation. Clim Dyn 21:659–675

Meehl GA et al (2007) Global climate projections. In: Solomon S et al (eds) Climate change 2007: the physical science basis. contribution of working group I to the fourth assessment report of the intergovernmental panel on climate change. Cambridge University Press, Cambridge, pp 747–845

Meehl GA, Arblaster JM, Collins WD (2008) Effects of black carbon aerosols on the Indian monsoon. J Clim 21:2869–2882. doi:10.1175/2007jcli1777.1

Mitchell TD, Jones PD (2005) An improved method of constructing a database of monthly climate observations and associated high-resolution grids. Int J Climatol 25:693–712

Mizuta R, Oouchi K, Yoshimura H, Noda A, Katayama K, Yukimoto S, Hosaka M, Kusunoki S, Kawai H, Nakagawa M (2006) 20 km-mesh global climate simulations using JMA-GSM model: Mean climate states. J Meteor Soc Jpn 84:165–185

Mizuta R et al (2012) Climate simulations using MRI-AGCM3.2 with 20 km grid. J Meteor Soc Jpn 90A:233–258. doi:10.2151/jmsj.2012-A12

Mizuta R, Arakawa A, Ose T, Kusunoki S, Endo H and Kitoh A (2014) Classification of CMIP5 future climate responses by the tropical sea surface temperature changes. SOLA 10. doi:10.2151/sola.2014-035

Ogata T, Ueda H, Inoue T, Hayasaki M, Yoshida A, Watanabe S, Kira M, Ooshiro M, Kumai A (2014) Projected future changes in the Asian monsoon: A comparison of CMIP3 and CMIP5 model results. J Meteor Soc Jpn 92:207–225. doi:10.2151/jmsj.2014-302

Rajendran K, Kitoh A (2008) Indian summer monsoon in future climate projection by a super high-resolution global model. Curr Sci 95:1560–1569
Rajendran K, Kitoh A, Srinivasan J, Mizuta R, Krishnan R (2012) Monsoon circulation interaction with Western Ghats orography under changing climate. Theor Appl Climatol 110:555–571. doi:10.1007/s00704-012-0690-2
Ramesh KV, Goswami P (2014) Assessing reliability of regional climate projections: the case of Indian monsoon. Sci Rep 4:4071. doi:10.1038/srep04071
Rowell DP (2012) Sources of uncertainty in future changes in local precipitation. Clim Dyn 39:1929–1950. doi:10.1007/s00382-011-1210-2
Sampe T, Xie S-P (2010) Large-scale dynamics of the Meiyu-Baiu rainband: environmental forcing by the westerly jet. J Clim 23:113–134. doi:10.1175/2009jcli3128.1
Sandeep S, Ajayamohan RS (2014) Poleward shift in Indian summer monsoon low level jetstream under global warming. Clim Dyn. doi: 10.1007/s00382-014-2261-y
Seo K-H, Ok J (2013) Assessing future changes in the East Asian summer monsoon using CMIP3 models: Results from the best model ensemble. J Clim 26:1807–1817. doi:10.1175/jcli-d-12-00109.1
Seo K-H, Ok J, Son J-H, Cha D-H (2013) Assessing future changes in the East Asian summer monsoon using CMIP5 coupled models. J Clim 26:7662–7675. doi:10.1175/jcli-d-12-00694.1
Song F, Zhou T (2014) Interannual variability of East Asian summer monsoon simulated by CMIP3 and CMIP5 AGCMs: skill dependence on Indian ocean–western pacific anticyclone teleconnection. J Clim 27:1679–1697. doi:10.1175/jcli-d-13-00248.1
Song F, Zhou T, and Qian Y (2014) Responses of East Asian summer monsoon to natural and anthropogenic forcings in the 17 latest CMIP5 models. Geophys Res Lett 41. doi:10.1002/2013GL058705
Sperber KR, Annamalai H, Kang IS, Kitoh A, Moise A, Turner A, Wang B, Zhou T (2013) The Asian summer monsoon: an intercomparison of CMIP5 versus. CMIP3 simulations of the late twentieth century. Clim Dyn 41:2711–2744. doi:10.1007/s00382-012-1607-6
Sugi M, Yoshimura J (2004) A mechanism of tropical precipitation change due to CO_2 increase. J Clim 17:238–243
Taylor KE, Stouffer RJ, Meehl GA (2012) An overview of CMIP5 and the experiment design. Bull Amer Meteor Soc 93:485–498. doi:10.1175/bams-d-11-00094.1
Trenberth KE, Stepaniak DP, Caron JM (2000) The global monsoon as seen through the divergent atmospheric circulation. J Clim 13:3969–3993
Turner AG, Annamalai A (2012) Climate change and the South Asian summer monsoon. Nat Clim Change 2. doi:10.1038/NCLIMATE1495
Ueda H, Iwai A, Kuwako K, Hori ME (2006) Impact of anthropogenic forcing on the Asian summer monsoon as simulated by eight GCMs. Geophys Res Lett 33:L06703. doi:10.1029/2005gl025336
Vecchi GA, Soden BJ (2007) Global warming and the weakening of the tropical circulation. J Clim 20:4316–4340. doi:10.1175/jcli4258.1
Wang B, Lin Ho (2002) Rainy season of the Asian-Pacific summer monsoon. J Clim 15:386–398
Wang B, Ding Q (2006) Changes in global monsoon precipitation over the past 56 years. Geophys Res Lett 33. doi:10.1029/2005gl025347
Wang B, Ding Q (2008) Global monsoon: Dominant mode of annual variation in the tropics. Dyn Atmos Oceans 44:165–183. doi:10.1016/j.dynatmoce.2007.05.002
Wang B, Wu Z, Li J, Liu J, Chang C-P, Ding Y, Wu G (2008) How to measure the strength of the East Asian summer monsoon. J Clim 21:4449–4463. doi:10.1175/2008jcli2183.1
Wang B, Liu J, Kim H-J, Webster PJ, Yim S-Y (2012) Recent change of the global monsoon precipitation (1979–2008). Clim Dyn 39:1123–1135. doi:10.1007/s00382-011-1266-z
Wang B, Yim S-Y, Lee J-Y, Liu J, Ha K-J (2014) Future change of Asian-Australian monsoon under RCP 4.5 anthropogenic warming scenario. Clim Dyn 42:83–100. doi:10.1007/s00382-013-1769-x
Wang C, Kim D, Ekman AML, Barth MC, Rasch PJ (2009) Impact of anthropogenic aerosols on Indian summer monsoon. Geophys Res Lett 36:L21704. doi:10.1029/2009GL040114

Xie P-P, Arkin PA (1997) Global precipitation: A 17 year monthly analysis based on gauge observations, satellite estimates and numerical model outputs. Bull Amer Meteorol Soc 78:2539–2558

Xie S-P, Deser C, Vecchi GA, Ma J, Teng H, Wittenberg AT (2010) Global warming pattern formation: sea surface temperature and rainfall. J Clim 23:966–986. doi:10.1175/2009jcli3329.1

Yatagai A, Kamiguchi K, Arakawa O, Hamada A, Yasutomi N, Kitoh A (2012) APHRODITE: Constructing a long-term daily gridded precipitation dataset for Asia based on a dense network of rain gauges. Bull Am Meteor Soc 93:1401–1415. doi:10.1175/BAMS-D-11-00122.1

Zhang L, Zhou T (2011) An assessment of monsoon precipitation changes during 1901–2001. Clim Dyn 37:279–296. doi:10.1007/s00382-011-0993-5

Chapter 5
The Australian Summer Monsoon in Current and Future Climate

Huqiang Zhang and Aurel Moise

Abstract As the counterpart of the Asian monsoon in the Northern Hemisphere, in this chapter the Australian summer monsoon covers a spatial domain encompassing tropical Sumatra and the Java Islands, and the adjacent waters in the west, extending south and eastward into the Timor and Timor Sea region and further penetrating into the tropical Australian continent. This chapter documents its observed features at a range of temporal and spatial scales, evaluates how well the current climate models can reproduce these fundamental features, and finally summarizes current projections of its potential changes in future and primary processes leading to such changes. The monsoon system shows pronounced seasonal variations of rainfall and prevailing wind, with its austral summer season rainfall being supported by the reversal of easterly trade winds into deep and moist westerlies. Its onsets are influenced by a number of factors including the Madden-Julian Oscillation (MJO), land-sea thermal contrast, the influence of middle latitude systems, and the inherent atmospheric instability. The inter-annual variations of the monsoon onset are correlated to El Niño-Southern Oscillation (ENSO), but the total summer monsoon rainfall is not. This is partially attributed to the seasonally varying air-sea interactions over the waters north of the Australian continent. The Asian aerosol and tropical SSTs near the continent have been used in explaining observed rainfall increases northwest of the tropical Australian continent. In fully coupled global climate model simulations, the broad features of the monsoon mean climate, its seasonal and inter-annual variations of rainfall, temperature and circulation, can be reasonably reproduced by a majority of the models, but there are very large variations in individual model skills. The relevant importance of primary large-scale drivers governing the monsoon variations differs significantly across current climate models, with some models having too strong an ENSO influence. There is great uncertainty in model projections of the changes in

H. Zhang · A. Moise (✉)
Bureau of Meteorology Research and Development, GPO Box 1289k, Melbourne, VIC 3001, Australia
e-mail: a.moise@bom.gov.au

H. Zhang
e-mail: h.zhang@bom.gov.au

© Springer International Publishing Switzerland 2016

L.M.V. de Carvalho and C. Jones (eds.), *The Monsoons and Climate Change*,
Springer Climate, DOI 10.1007/978-3-319-21650-8_5

the monsoon rainfall under global warming. A weak change in mean rainfall from multi-model ensemble averages is largely produced accompanied by large model discrepancies, with the number of the models showing likely increases in rainfall being matched by roughly the same number of the models showing decreased rainfall. There is a lack of consensus regarding the changes in the Australian monsoon onset/retreat, with studies using rainfall in defining the monsoon onset suggesting the onset comes earlier. However, for the studies using circulation as one of the criteria, they showed a possible delay due to the weakening and shifting of the atmospheric circulation. Future progress to improve the modelling skill and increase our confidence of the projection of the Australian monsoon relies on a number of key aspects, including the improved model physics and dynamics with increased model resolutions; improved representations of key drivers of the monsoon system, such as realistic MJO, ENSO and Indian Ocean Dipole (IOD) in climate models; and improved understanding of the model discrepancies.

Keywords Australian monsoon · Onset/retreat · Inter-annual variations · Large-scale drivers · Uncertainty

5.1 Introduction

This chapter has two purposes: the first is to document the fundamental characteristics of the Australian monsoon in the current climate and the skill of climate models in capturing these features. The second is to discuss its potential changes in future climate based on global model simulations. It begins with an overview of the monsoon system, including its spatial domain, seasonal rainfall and wind variations, and spatial and temporal evolution of the onset, break and retreat. The observed trends over the last several decades will also be included. Then we document underlying drivers of its variations, such as the influence of Madden-Julian Oscillation (MJO; Madden and Julian 1971, 1972), Asian winter monsoon cold surges, and middle-latitude intrusions on the onset/break and the intensity of the monsoon. Potential drivers including El Niño-Southern Oscillation (ENSO), the Indian Ocean Dipole (IOD), and the Pacific-Indian SST gradient will be discussed. Following that, we focus on diagnosing potential changes of the monsoon under global warming by summarizing the results from a suite of CMIP3/5 model studies including (1) changes in monsoon rainfall seasonality; (2) thermodynamic and dynamic contributions to such changes; and (3) potential changes to onset/retreat and the underlying processes. The challenge for better understanding and reducing the uncertainties in our current projection of the changes in the monsoon system under global warming will also be discussed.

There have been a number of monsoon monographs (e.g., Wang 2006; Chang et al. 2011; Lau and Waliser 2005, 2011) in which specific chapters have been

devoted to the Australian monsoon (e.g., Hendon et al. 2011; Wheeler and McBride 2005; 2011). What makes this chapter different from these publications is that we not only provide observational analyses of the Australian summer monsoon, but we also assess how the system is simulated by current climate models and the potential changes derived from some recent coupled modeling experiments that have been used in the recent IPCC scientific assessment reports (IPCC 2007, 2013).

5.2 Observed Features of the Australian Summer Monsoon Climate

The view of the monsoon in the global climate system has evolved in recent years, with a global monsoon concept being recognized in the scientific community. The essential characteristics are the reversal of the tropical and subtropical atmospheric circulations accompanied by remarkable seasonal changes in precipitation (e.g., Trenberth et al. 2000). Several regional monsoons are embedded within such a global system. In this regard, the Australian summer monsoon is part of the Australia–Asia monsoon system (Chang and Krishnamurti 1987; Wang 2006; Wheeler and McBride 2005, 2011), in which the wet season migrates from the boreal summer in the Northern Hemisphere into the maritime continent and then tropical Australia in the austral summer along with a reversal of the large-scale overturning atmospheric circulation in the Australia–Asian region (Trenberth et al. 2000).

Despite its name, then, the Australian summer monsoon in this context occurs beyond the Australian continent. It encompasses rapid rainfall and circulation transitions from dry to wet climate during austral late spring (September–October–November: SON) to summer season (December–January–February: DJF) in a spatial domain covering much of the northern part of the Australian continent and extending further northward, including South Sumatra, Java, and the Timor region and adjacent waters (Morton et al. 2009). In some studies, the Australian summer monsoon was distinguished from the Maritime Continent monsoon over the Indonesia, Malaysia, New Guinea and surrounding shallow waters (Wang 2006). Nevertheless, considering that the maritime continent part of the monsoon acts as the transition of the Asian summer monsoon into the Australian summer monsoon and the transition is continuous in time and space (Chang 2004), in this chapter we refer to it as the monsoon over both the maritime continent and northern Australia in the austral summer. To put the Australian summer monsoon into a much larger regional context, Fig. 5.1a shows the mean 850 hPa wind, precipitation and temperature climatology derived from ERA-Interim reanalysis, TRMM-3B43 and Climatic Research Unit (CRU) datasets during the Australian summer monsoon months of DJF. To highlight the degree of seasonality in the atmospheric circulation and the associated rainfall generation in the Australian summer monsoon, Fig. 5.1b displays changes in the mean circulation between January (i.e., monsoon

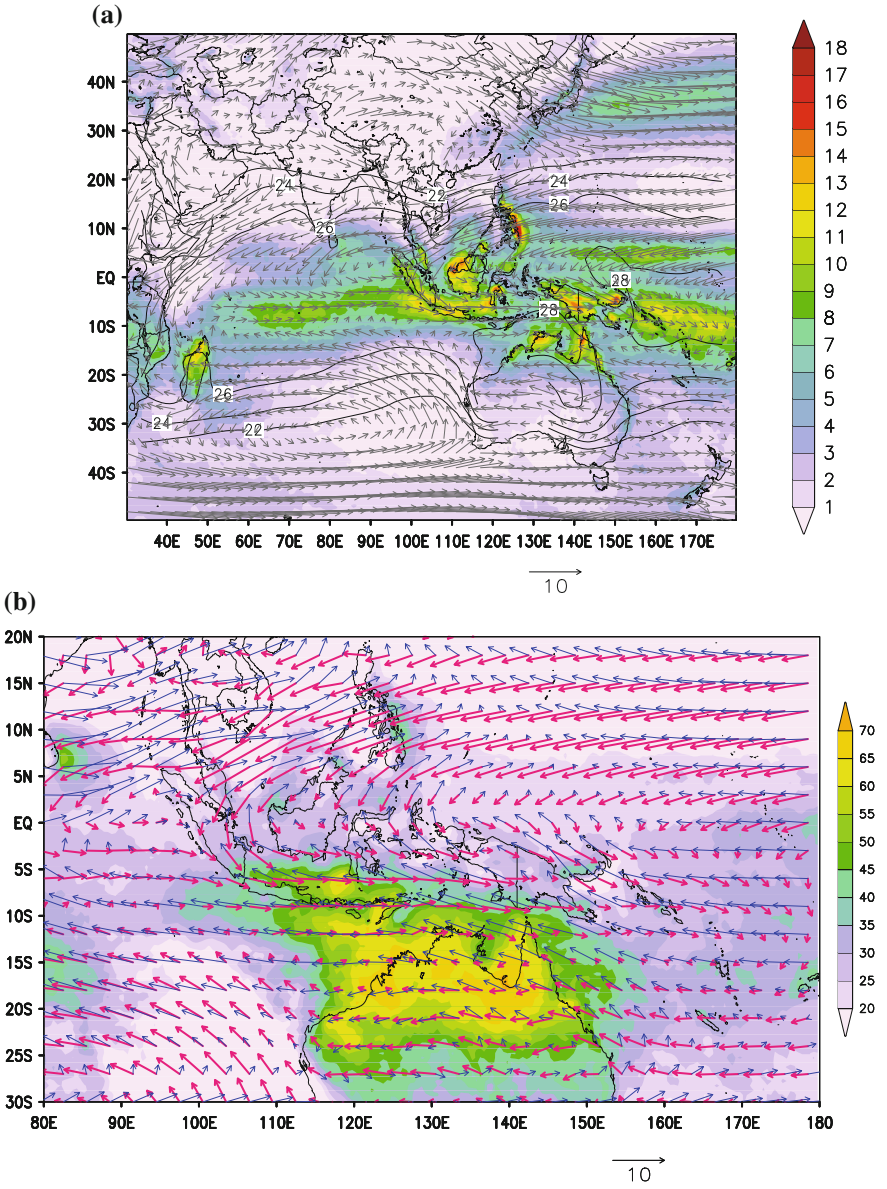

Fig. 5.1 **a** Observed DJF rainfall (mm/day; *shading*) averaged over 1998–2013, from the satellite-based data TRMM-3B43. The stream lines show the surface wind from the atmospheric reanalysis ERA-Interim (Dee et al. 2011) averaged over the same period. The black contour lines indicate the surface-air temperature from CRU (Kennedy et al. 2011) with corresponding labels (in °C). **b** Percent of annual total rainfall occurring during DJF (*shading*) and climatology of surface wind from the atmospheric reanalysis ERA-Interim for January (*pink vectors*) and July (*blue vectors*)

season) and July (i.e., dry season) together with the proportion of the total annual rainfall that occurs in DJF.

Firstly, the Australian summer monsoon is dominated by prevailing deep westerlies in the low-middle troposphere (referring to Fig. 5.2 for the vertical structure of the monsoon zonal wind) covering the southern part of the maritime continent, including the Java-Sumatra region, Java, and Timor Sea and nearby waters. It extends further eastward toward New Guinea and the Solomon Islands, where it is sometimes referred to as the "Western Pacific Monsoon" (e.g., Smith et al. 2012). Moisture-laden westerly winds that originate from the tropical Indian Ocean and South Asian waters are a prominent feature of the monsoon. The deep moist westerly is the most important circulation regime in generating tropical Australian summer rainfall revealed by several recent synoptic analyses (e.g., Pope et al. 2009). The large amount of warm and moist air transported into the region, together with the ascending motion created by the monsoon trough over northern Australia, produces heavy monsoon rainfall over the region.

From Fig. 5.1a one can also see a close atmospheric circulation linkage between the East Asian winter monsoon (EAWM) and the development of the Australian summer monsoon. The EAWM, often occurring in the November to March period, is characterized by a deep and strong cold-core anti-cyclonic circulation known as the "Siberian-Mongolian High," with intense low-level northeasterlies prevailing over the East Asian continent and northwest Pacific Ocean (Ding 1994). With southeastward movement of the high-pressure system towards the East China Sea

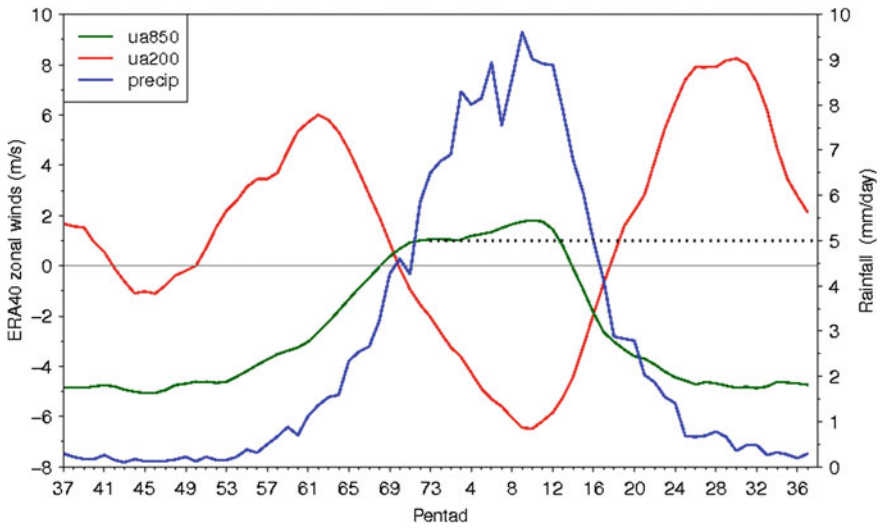

Fig. 5.2 Annual cycle of DJFM rainfall (*blue; right axis*), low level 850 hPa zonal winds (*green; left axis*) and upper level 200 hPa zonal winds (*red; left axis*) from pentad GPCP data (Adler et al. 2003) from 1979–2008 for rainfall and ERA-Interim from 1979–2002 for winds over tropical Australia (land only)

and northwest Pacific, massive cold air mass breakouts occur that encompass a large area from East Asia, to the west Pacific, and penetrate southward towards the South China Sea and the tropical west Pacific (Ding 1994; Chan and Li 2004; Chang 2004).

A number of synoptic analyses, such as Chang et al. (1979), Sumi and Murakami (1981) and Chen and Yen (1991) following the first Global Atmospheric Research Program Global Experiment (FGGE) Winter Monsoon Experiment (WMONEX) and the Australian Monsoon Experiment (AMEX) in 1986–1987, showed the impacts of EAWM on tropical convection and cross-equatorial flows, as well as the linkage between EAWM and Australian summer monsoon circulation. In a recent study, Zhang and Zhang (2010) further investigated the potential impacts of EAWM on the summer climate variability and predictability in the Australian monsoon region through Australia–Asia (A–A) monsoon interactions. Statistically significant correlations were established between the Australian summer monsoon and its rainfall variations with cross-equatorial flows penetrating from the South China Sea region and northerly flow in the EAWM. The underlying mechanism for such connections is the response of the position and intensity of the Hadley circulation to strong/weak EAWM. A strong EAWM is associated with an enhanced cross-equatorial flow crossing the maritime continent and strengthened Australia summer monsoon westerlies that affect rainfall and temperature variations in the northern and eastern parts of the Australian continent. Furthermore, they proposed that such interactions could potentially affect climate predictability in the region, as shown by some statistically significant lag correlations at monthly time scales. The results were attributed to the impacts of the EAWM on regional SST variations and its linkage to land surface conditions on the Eurasian continent.

So far, we have not given an objective definition of the spatial domain of the Australian summer monsoon. Given that the fundamental features of any regional monsoon include remarkable seasonal wind and rainfall variations, Fig. 5.1b highlights the wind and rainfall seasonality in the Australian monsoon region. It shows the January and July 850 hPa wind, together with the proportion of accumulated DJF seasonal rainfall to the annual total. If one uses rainfall seasonality in defining the monsoon domain such as Wang and Ding (2008) and Yim et al. (2014), then the Australian summer monsoon covers the south Sumatra and Java Islands and nearby Java Sea, extending southeastward towards the Lesser Sunda Islands, Timor Sea, and Arafura Sea and into the tropical Australia and Gulf of Capentaria regions. Over these regions, there are significant zonal wind reversals, with the prevailing wind changing from easterly trade winds in the winter months into the monsoon westerly in the summer months. The monsoon trough occurs over a large part of northern Australia, where the dry east-to-southeast trade winds meet the moisture-laden northwest monsoon winds. This forms favorable moisture and dynamical conditions for heavy rainfall generation.

There are a few notable features in the Australian monsoon domain. One of them is the limited southward penetration of the zonal monsoon westerly into the Australian continent. While the whole tropical Australia experiences significant rainfall seasonal variations, the averaged zonal wind remains largely easterlies

south of 15°S, as seen in Fig. 5.1b. Over the eastern part of the maritime continent, covering New Guinea and the Solomon Islands, there are significant wind seasonal variations as illustrated by McBride and Wheeler (2011), changing from south-easterly trade winds into the westerly associated with the cross-equatorial flow from the Northern Hemisphere. Nevertheless, the seasonal rainfall variation is relatively weak there, with its austral summer rainfall accounting for <35 % of the total annual rainfall received, so that there is not a universally agreed extension of the Australian summer monsoon, depending on the variables used in such definitions. This has some implications when we discuss the potential changes in the monsoon domain in future climate in Sect. 5.4.

Figure 5.2 shows the annual cycle of the rainfall and zonal winds averaged over the domain of 120–150°E and 20°S to the Equator. Clearly, when the low-to-middle level zonal wind changes from easterly to westerly at around the 69th pentad (∼mid-December), the upper level zonal wind also changes from westerly to easterly around the same time. Associated with the establishment of the monsoon circulation, rainfall in the domain increases rapidly. Towards early March (∼18th pentad), the Australian summer monsoon begins to retreat, with rainfall experiencing a rapid decline and the trade easterlies resuming the dominance in the low-middle level troposphere with westerlies in the upper levels.

The importance of the moist zonal westerly in feeding and sustaining the Australian summer monsoon is further illustrated in the correlation map (Fig. 5.3) between area-averaged summer rainfall over 20°S–7.5°S and 120°–150°E with the 850 hPa zonal wind. Clearly the Australian summer monsoon rainfall is largely dominated by the strength of the monsoon westerly, and this forms the basis for using zonal wind as one of the Australian monsoon indices (Wang 2006).

In recent years, there have been increasing numbers of studies on the onset and retreat of the Australian summer monsoon. This is largely because the timing of the start and end of the summer monsoon season can have significant social and economic impacts. There has been a variety of monsoon onset/retreat definitions, based on rainfall, wind, Outgoing Longwave Radiation (OLR), precipitable water or combinations of these (Holland 1986; Hendon and Liebmann 1990; Drosdowsky 1996; Wang and LinHo 2002; Li and Zeng 2003; Zeng and Lu 2004; Smith et al. 2008). However, there is no universally accepted method (see detailed reviews from Wang et al. 2004; Smith et al. 2008), since each definition has its own merits in capturing some of the characteristics associated with the monsoon. Holland (1986) used 850 hPa zonal westerly in defining the onset, and reported significant correlations with the Southern Oscillation Index (SOI) in the following austral spring. Hendon and Liebmann (1990) included rainfall as an additional variable to that definition and revealed the linkage between the eastward propagation of the MJO-like tropical deep convections to the onset of the Australian summer monsoon. Nevertheless, Drosdowsky (1996), using averaged deep-layer mean zonal wind (from surface up to 500 hPa), overlaid by upper level easterlies in defining the onset dates, found complex zonal wind-rainfall relationships. His study yielded a different onset-SOI relationship (onsets were correlated to the prior SOI values) and found no significant time scales for the onset/reoccurrence.

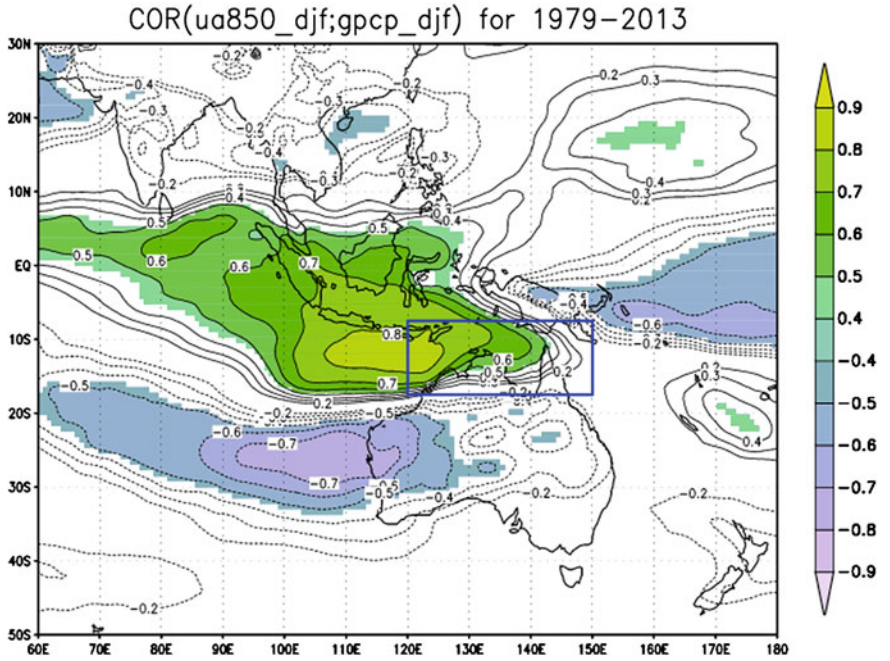

Fig. 5.3 Correlations of area-averaged DJF rainfall climatology (GPCP 1979–2013; averaged over *blue box*) with DJF low-level 850 hPa zonal wind climatology (ERA-Interim 1979–2013). Only correlations significant at the 99 % levels have been *shaded*

Zhang (2010) developed a method for defining monsoon onset/retreat that can be applied to global climate model results. For this purpose, he considered two conditions in the selections of variables to be used in the definition: one is that they should capture the fundamental features of the monsoon system, which includes significant rainfall and circulation seasonal variations; the other is that they can be reasonably simulated by current climate models. He combined the normalized atmospheric precipitable water as used in Zeng and Lu (2004) to reflect the rapid moistening processes and 850 hPa wind seasonal reversal to represent the establishment of the monsoon circulation in defining the monsoon onset.

Given the nature of the rapid transition of the summer monsoon, it is not surprising to see uncertainties of the onset dates using different methods. For instance, Fig. 5.4 compares four time series of the onset dates over Darwin for 1958/59–2009/2010: (1) from the definition of Drosdowsky (1996) using radiosonde wind data; (2) the rainfall-based onset dates from Lo et al. (2007), in which the wet-season onset date is defined based on the accumulation of rainfall to a pre-defined threshold; (3) using the same definition as in Lo et al. (2007) but with a different dataset (here we use the pentad rainfall data from CPC Merged Analysis of Precipitation (CMAP) for the period of 1979–2010); and, finally, (4) the onset dates near Darwin using the definition of Zhang (2010) based on the 850 hPa zonal wind

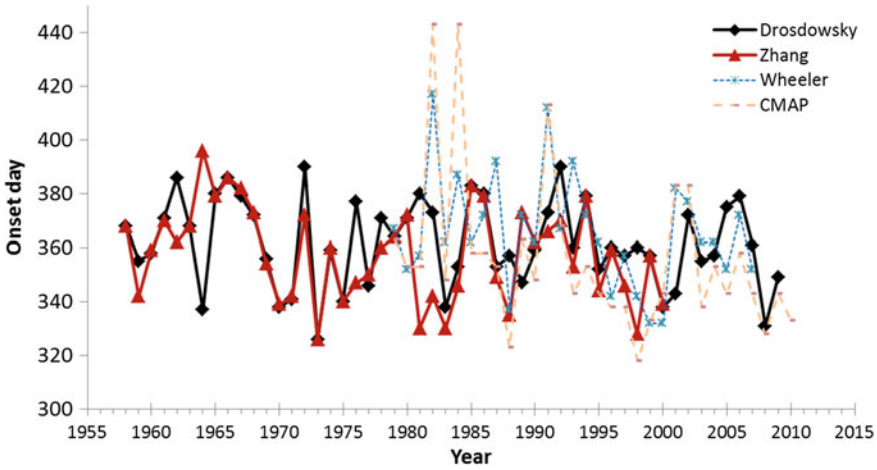

Fig. 5.4 Monsoon/wet season onset dates in Darwin from four different datasets: Drosdowsky (*black line*) for monsoon onset dates of Drosdowsky (1996) for the 1958–2009 period; Zhang (*red line*) for monsoon onset dates of Zhang (2010) for 1958–2000; Wheeler (*blue dashed line*) for the wet season onset of Lo et al. (2007) based on the Australian Water Availability Project (AWAP) rainfall data of Jones et al. (2009); CMAP (*yellow dotted line*) for the wet season onset as in Lo et al. (2007), but using pentad CMAP rainfall data of Xie and Arkin (1997), and the onset date is set in the middle of the pentad period

and normalized total precipitable water from ERA-40 reanalysis for 1958–2001. The onset dates from rainfall data only should be viewed as the wet season onset as it did not have any requirement for the monsoon circulation establishment in these definitions. Analysis of the Darwin wet season rainfall showed that extensive rainfall can also be produced in the wet easterly regime as shown in Pope et al. (2009).

The averaged onset dates are close to each other in these four datasets: Julian Day (JD) 362 for Drosdowsky (1996); JD358 for Zhang (2010); JD366 for the wet season onset of Lo et al. (2007); and JD357 for the wet season onset using the CMAP rainfall data. All the analyses point towards monsoon onset in the Darwin region at the end of December. There are significant inter-annual variations of the onset dates, and this will be discussed in the next section.

Using the ERA-40 reanalysis data, Zhang (2010) provided spatial patterns of the evolution of the Australian summer monsoon (Fig. 5.5). To give a broader picture of its development (particularly over the west Maritime Continent region, where there are no significant rainfall seasonal variations but there is a zonal wind reversal), in this updated figure we did not exclude the locations with less than a 45 mm difference between the mean precipitable water in January and July as

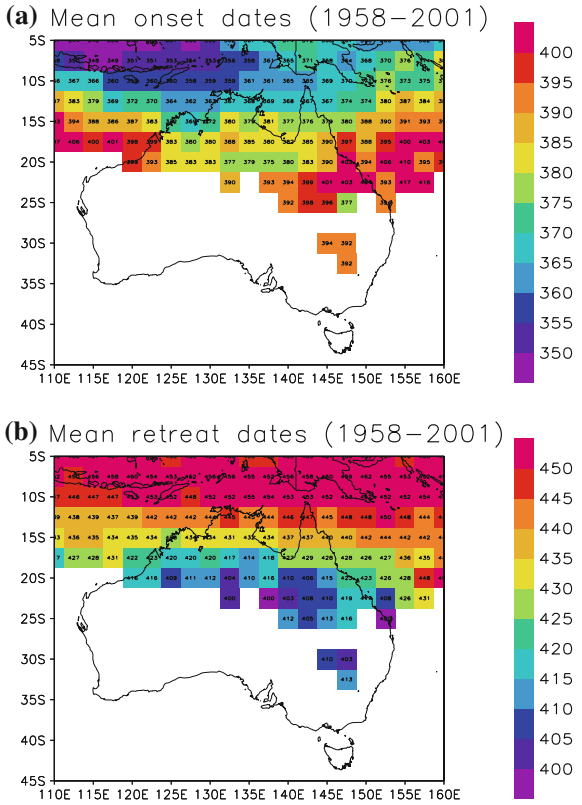

Fig. 5.5 **a** 43 year climatology of Australian summer monsoon onset dates derived from the current study using both PW and wind conditions in Zhang (2010). Time units are Julian days and numbers >365 indicate the following year; **b** as (**a**), but for retreat dates

required in Zhang (2010) for defining monsoon. The Australian summer monsoon first starts over the warm water of the south Sumatra-Java region and nearby Banda Sea, Arafura Sea, and Timor Sea in early to late December (JD340-360). Then, it penetrates southeastward, reaching the northern end of the Australian continent, Gulf of Carpentaria, and Coral Sea region by early January in the following year (JD370). For about half of the 43 year period, the summer monsoon penetrates southward down to latitudes around 17.5°S by mid- January (JD380). There were also years when the monsoon system reached further south—to around 25°S.

As discussed in Zhang (2010), the retreat of the Australian monsoon is more zonally orientated. It usually starts from the southern part of the monsoon region

(20°–25°S) around late February to early March and gradually withdraws northward. By early to middle March (JD435), the monsoon has retreated from the Australian continent and remains in the Timor Sea and adjacent regions. It further migrates into the Northern Hemisphere around April. Accordingly, most of the monsoons in the northern end of the Australian continent last about 40–50 days, while the average in the Timor Sea region is about 80 days.

5.3 Variations of the Australian Summer Monsoon and the Underlying Drivers

In Sect. 5.2, we mainly documented the observed mean climate of the Australian summer monsoon. Nevertheless, it also has pronounced variations at a range of time scales: with significant inter-annual variations of the monsoon onset, remarkable intra-seasonal rainfall and wind variations following the onset, and inter-annual and decadal rainfall variations. Exploring the underlying drivers leading to such variations has long been a focus in monsoon studies.

5.3.1 Variations in Monsoon Onset

As shown in Fig. 5.4, the onset of the Australian summer monsoon has significant inter-annual variation. For instance, the earliest onset date in Drosdowsky (1996) and Zhang (2010) is JD326 (November 22) in the 1973–1974 season, while the latest onset can be JD390 to JD396 (end of January) in these datasets. As pointed out by Hung and Yanai (2004), there are several major factors contributing to the onset, including the land-sea thermal contrast, barotropic instability in the tropics, the arrival of the MJO, and the intrusion of mid-latitude troughs.

The monsoon system has long been viewed as the product of land-sea thermal contrast (Wang 2006). However, as pointed out by Hung and Yanai (2004), the role of the elevated heating source from the high land in Asia leading to the reversal of the meridional temperature gradient in the middle to upper troposphere, and therefore the onset of the Asian summer monsoon does not exist in the Australian monsoon. Because of the lack of high land, such as the Tibetan Plateau in Asia, surface heating from the Australian continent is shallow (confined below 750 hPa). Yet, it can play an important role in building up a thermally induced meridional-vertical circulation change in the tropical Australian and nearby waters, which helps transport low-level moist air inland to intensify the monsoon circulation. Kawamura et al. (2002) suggested that such thermal heat lows can create a convectively unstable condition favorable for the onset of the Australian summer monsoon. Although the heating helps to set up the large-scale thermal and circulation structures for the establishment of the monsoon circulation, the sudden onset

of the monsoon itself typically requires some large-scale trigger. Both the studies including Kawamura et al. (2002), and Hung and Yanai (2004), identified the arrival of eastward-propagating MJO, and some times the intrusion of middle latitude trough as the primary triggers of the onset.

5.3.2 MJO and Monsoon Intra-seasonal Variations

An excellent review on the role of MJO on modulating the onset of the Australian summer monsoon has been provided by Wheeler and McBride (2005, 2011). First identified and documented by Madden and Julian (1971, 1972), the MJO in general refers to the planetary-scale eastward propagation of organized tropical deep convection originating over the tropical Indian Ocean and travelling towards the western tropical Pacific. It has a dominant 30–80 day oscillation in its frequency spectrum. Wheeler and Hendon (2004), using the combined EOF analysis of 850 and 200 hPa zonal wind together with OLR, have developed a pair of real-time multivariate indices in monitoring the MJO activities in the tropical Indo-Pacific region. As shown in Fig. 5.6, they divide the MJO lifecycle into eight phases, and during phases 4–6, intensive deep convection often occurs in the tropical Australian monsoon region.

There were some conflicting views on whether MJO affected the Australian monsoon onset. Hendon and Liebmann (1990) suggested that the onset near Darwin was closely associated with the 40–50 day MJO-like oscillation in the tropics, but Drosdowsky (1996) did not find any dominant time scales of the monsoon active/break periods. Wheeler and McBride (2011), using the updated onset dates from Drosdowsky (1996) and Pope et al. (2009) and their MJO index data (Wheeler and Hendon 2004), revisited the issue on the impacts of MJO on the monsoon onset. They found 85 % of the onset dates occurred in phases 4–7, when MJO low-level westerlies are around the tropical Australia monsoon region. They suggested that the MJO set up the large-sale favorable conditions for the onset, but it is only one of the factors determining the monsoon onset. Another factor contributing to the onset of the Australian monsoon is the intrusion of the middle latitude systems as shown by Davidson et al. (1983). Hung and Yanai (2004) further suggested that it had an even greater role when the MJO is weak or absent.

After the onset, the monsoon displays pronounced intra-seasonal variations. The early work of Troup (1961) documented significant sequences of bursts and breaks of monsoon westerlies and associated heavy rainfall events over northern Australia. Following the FGGE WMONEX and the Australian Monsoon Experiment (AMEX) in 1986–1987, more detailed synoptic analyses emerged that documented the characteristics of the monsoon rainfall and circulation variations on an intra-seasonal time scale. Wheeler and McBride (2005, 2011) have provided a comprehensive overview including the power spectrum analysis of daily OLR, zonal wind, and rainfall in tropical Australia. They showed that the MJO is the strongest mode of the intra-seasonal variation in the region. As shown in Fig. 5.6,

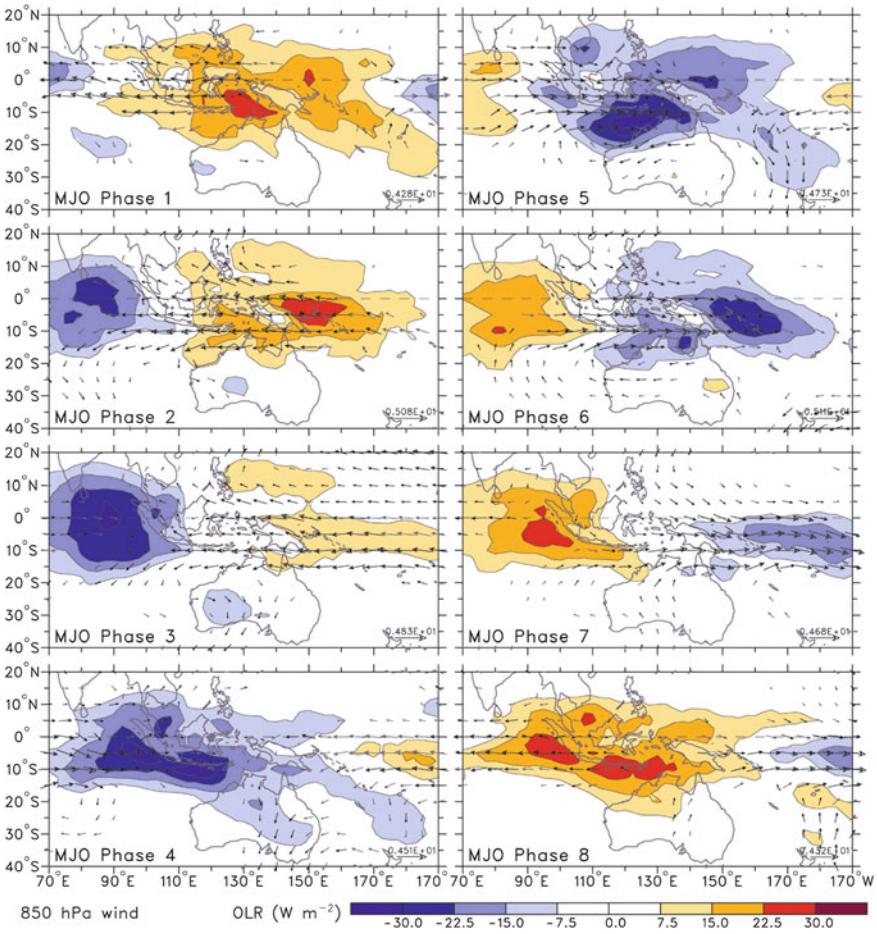

Fig. 5.6 MJO composites of OLR and 850 hPa wind anomalies for the December–January–February season (from Wheeler and McBride 2011)

different phases of the MJO set up different large-scale conditions for deep convection and heavy rainfall generation within the monsoon season (e.g., Wheeler et al. 2009). For the western part of the monsoon domain, heavy rainfall tends to be associated with MJO Phases 4 and 5. However, its impacts on the eastern part of the large islands are much smaller or even reversed (Wheeler and McBride 2011) because the process is complicated by the strong diurnal cycle of locally generated convection over the islands (Rauniyar and Walsh 2011). The MJO-monsoon burst/break connection also appears to vary from year to year; in some years, the MJO influence is very great, while in others there is a very weak linkage between the two, partly because MJO itself has inter-annual variations (Hendon et al. 1999).

In recent years, synoptic weather systems within the Australian monsoon have been studied, using the isentropic potential vorticity (PV) tracking method (Berry et al. 2012). The analysis showed that most synoptic systems originated within tropics, but at about a 700 hPa level, a high rate of systems were first detected near the east coast of the continent, where extra-tropical Rossby waves were seen to frequently break. The system propagates from east to west at approximately 6 ms^{-1} and has a characteristic length scale of 2,000 km. A composite analysis showed that rainfall is significantly enhanced ahead (west) of the synoptic PV maximum, and suppressed behind. Such results emphasize the influence of the middle latitude systems contributing to the monsoon intra-seasonal variations in the tropics.

5.3.3 The Inter-annual and Inter-decadal Variations

The Australian monsoon rainfall exhibits significant inter-annual and decadal variations. Figure 5.7 shows the standard deviation of the DJF summer land rainfall total for the period of 1950–2013 from the Global Precipitation Climate Centre (GPCC) rainfall data, with the linear trends in the last 30 and 50 year periods from data (GPCC) over land only, as well as the data from the Global Precipitation Climatology Project (GPCP), which covers data over both land and ocean. In Fig. 5.7a, the standard deviation is about 40–50 mm $month^{-1}$ over most of the Australian monsoon domain, with some coastal areas having higher values around 100 mm $month^{-1}$. They are roughly equivalent to about 30–50 % of the average rainfall in the season, illustrating remarkable year-to-year variations.

In addition, significant upward rainfall trends have been observed for the last half-century in northwest Australia, but a weak or even drying trend observed in some parts of northeast Australia (Fig. 5.7b). This was often termed as a "rainfall dipole trend" (Smith 2004; Shi et al. 2008; Li et al. 2013). As documented in the recent study by Li et al. (2013), in 30 years the upward rainfall trend is extended across the whole tropical Australian monsoon region. Using the GPCP dataset, which covers rainfall data over both the land and the ocean, this upward trend spatial pattern is also presented in Fig. 5.7d. Contour lines in Fig. 5.7 show regions with significant trends. The upward rainfall trend is extended into the nearby Indian Ocean offshore from northwest Australia. Another feature noted is that in contrast to the upward trend, summer rainfall over a large part of the Maritime Continent and west of New Guinea shows a downward trend. So far, there is limited understanding for such a heterogeneity in the observed rainfall trends, indicating the complexity of the processes dominating rainfall changes in the Australian monsoon region.

Efforts have been undertaken to explore the underlying processes leading to such significant year-to-year variations and long-term trends. Several large-scale drivers, primarily from the tropical Indian and Pacific Oceans, have been identified as accountable for part of the variability (Nicholls 1981; Nicholls et al. 1982; McBride and Nicholls 1983; Risbey et al. 2009; Klingaman et al. 2012; Watterson 2012;

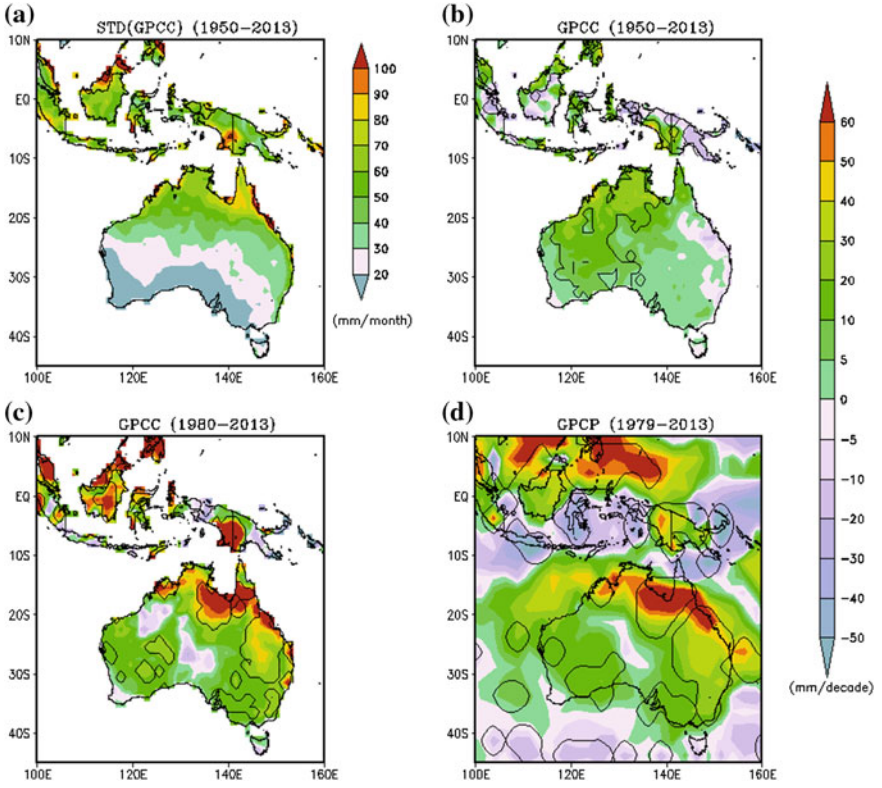

Fig. 5.7 **a** Observed December–January–February (DJF) rainfall (mm month^{-1}) standard deviation over the 1950–2013 period, from GPCC data (Rudolf et al. 2011); **b** linear trend (mm decade^{-1}) of DJF rainfall from GPCC over the period of 1950–2013; **c** as (**b**), but for the last 34 years of 1980–2013; **d** as (**b**), but for rainfall over land and ocean from GPCP data for 1979–2013. Contour *lines* in (**b**), (**c**), and (**d**) indicate regions where the trend is significant ($\alpha = 0.1$)

Zhang et al. 2013; Li et al. 2013). They include the ENSO, Indian Ocean Dipole and basin-wide warming, and the SST gradient between tropical west Pacific and Indian oceans.

First and foremost, ENSO has long been identified as the primary forcing of the climate variability in the Australian region (Nicholls 1981; Nicholls et al. 1982; McBride and Nicholls 1983; Risbey et al. 2009). However, the influence of ENSO on Australian summer monsoon has some unique features. Nicholls et al. (1982) showed that the onset of the wet season (using rainfall threshold) is highly correlated with El Niño. This is further confirmed by the monsoon onset data from Drosdowsky (1996), using zonal wind definition and the onset dates from Zhang (2010), using combined zonal wind and moisture indices. Taschetto et al. (2010) identified El Niño-Modoki leading to the delayed onset and earlier retreat of the Australian monsoon associated with the Pacific SST warming pattern. Figure 5.8a

shows correlations between the onset dates and the SOI from Zhang (2010). As in the studies of Drosdowsky (1996) and Smith et al. (2008), pre-monsoon SOI values in September–October–November (SON) were used in the calculations. The onset dates are overwhelmingly negatively correlated to SOI in nearly all the locations, suggesting later monsoon onsets during El Niño years (with negative SOI). Statistically significant correlations are seen in the Timor Sea, Coral Sea, and part of the northern Australian regions. Such results can be explained by (1) relatively cooler SSTs in these regions, which are not favorable for development of deep convection; and (2) the shift of the ascending branch of the Walker circulation over the maritime continent towards the central-west Pacific that is accompanied with easterly low-level wind anomalies. Both represent unfavorable conditions for monsoon development. Nevertheless, the correlations for retreat dates are much weaker and less coherent, with most of them not significant. This is consistent with the findings of Drosdowsky (1996) and Smith et al. (2008), which reported no significant correlations of monsoon and rainy season retreat with the SOI.

Although the monsoon onset is highly influenced by ENSO and even statistical models have been built for the prediction of wet season onsets in tropical Australia (Lo et al. 2007), its total rainfall during the monsoon is not (Hendon et al. 2011). McBride and Nicholls (1983) showed that the ENSO influence on the tropical Australian rainfall dramatically weakened, from a strong correlation between SON rainfall and SOI to a weak one in DJF. Similarly, Hendon et al. (2011) showed that the magnitude of the tropical Australian rainfall (north of 25°S) correlation with

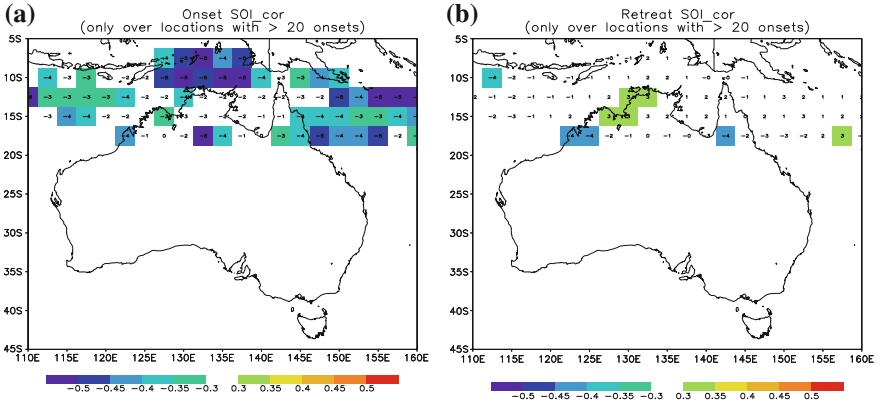

Fig. 5.8 **a** Correlations between monsoon onset dates in the Australian region with SOI in September–October–November. The calculations are only for the locations with more than a 20 year occurrence, and statistically significant correlations at 95 % confidence levels are *shaded*. Digit numbers are values of correlation x10; **b** as (**a**), but for retreat dates. Modified from Zhang (2010)

Nino 3.4 SST dropped from over −0.5 in SON to about −0.3 in DJF. In order to demonstrate the seasonality of such influence and highlight the complexity of processes dominating the Australian monsoon rainfall variations, in Fig. 5.9 we show the simultaneous correlations between Nino 3.4 SST and rainfall for the pre-monsoon or early monsoon season (SON), and during the monsoon season (DJF). As discussed earlier, rainfall in SON is highly negatively correlated with Nino 3.4 over much of the Australian monsoon domain, extending from the maritime continent to the tropical and eastern part of Australia (Fig. 5.9c). However, such significant influence is dramatically reduced in the DJF season (Fig. 5.9d). The discernible correlations are almost off the Australian continent and only remain strong in the South China Sea and Philippine Sea region. This collapse of the ENSO

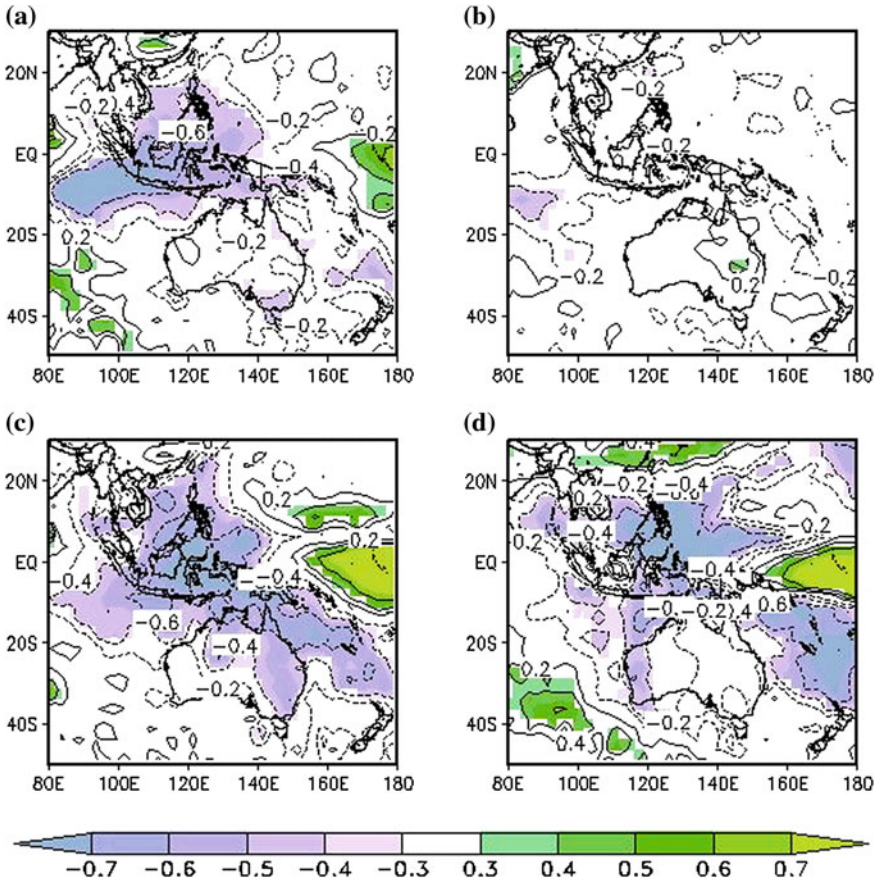

Fig. 5.9 Correlations between September–October–November (SON) and December–January–February (DJF) rainfall and IOD and El Niño 34. **a** SON–IOD. **b** DJF–IOD. **c** SON–NINO34. **D** DJF–NINO34

influences can be partly attributed to seasonally varying air-sea interactions in the tropical region north of Australia (Hendon et al. 2011). This is understood as such that prior to the monsoon season, the region is dominated by trade easterlies, and the eastward shift of the Walker circulation caused by the warming in the tropical eastern Pacific (El Niño phase) would enhance the easterly trade winds and cooling the SSTs (and reduced rainfall). It is therefore a strong positive air-sea feedback. However, once the monsoon is established, monsoon zonal westerlies dominate the region and the easterly anomalies by the tropical east Pacific warming effectively reducing the wind speed in the region, which in turn warms the SSTs by weakening the evaporative cooling, therefore dampening the pre-monsoon SST anomalies that build up. This leads to the collapse of the ENSO impacts on the summer monsoon rainfall.

In recent decades, the role of tropical Indian Ocean SSTs has been identified as another climate driver of the Australian climate variations. Although some of the Indian Ocean SST variations can be attributed to the influence from the tropical Pacific, many studies showed some degree of independence (Saji et al. 1999; Behera et al. 2006). The Indian Ocean Dipole (IOD) (Saji et al. 1999) SST anomaly pattern is, in particular, shown to be influential to Australian weather and climate, such as the formation of northwest cloud bands and the drought in the southeastern part of the Australian continent (Frederisken and Frederisken 1996; Cai et al. 2009a; Ummenhofer et al. 2009). A recent study by Taschetto et al. (2011) also emphasized the basin-wide warming mode in the Indian Ocean on the Australian summer climate. However, because of the significant seasonal phase lock of the IOD life cycle, such that it tends to develop in the austral winter season (JJA) and reaches its peak in SON before a rapid decline in the monsoon season, the impacts of IOD on the Australian monsoon have been less investigated. Nevertheless, several recent studies revealed some significant impacts of the IOD on the monsoon development (Zhang et al. 2013), especially the onset of the Australian monsoon that often occurs during and following the peak of the IOD.

As shown in Fig. 5.9a, indeed, the IOD is highly correlated to the SON rainfall in the eastern tropical Indian Ocean and nearby Sumatra-Java Islands and the Java and Timor Seas. This can be explained by two likely consequences. First, this is the region where the earliest onset occurs around early October (Moron et al. 2009) in the southern Sumatra-Java region. Positive IOD is often accompanied by strong easterly anomalies (Saji et al. 1999; Guan et al. 2003) and the easterly anomalies weaken the monsoon westerlies in the region and cause the rainfall decreases. During this season, the monsoon has not yet reached the Australian continent, so there is no significant correlation between the IOD and SON rainfall in the tropical Australian region. Progressing into DJF, the IOD diminishes quickly, as does its correlation with DJF rainfall (Fig. 5.9b). However, as pointed out by Zhang et al. (2013), its influences on the monsoon onset over the Australian continent are still significant. This can be understood by two aspects: one is that the monsoon system has a spatial coherence and the delay of the onset in the October–November–December season over the southern part of the Indonesia-Sumatra-Java region means the northwest-southeastward propagation of the monsoon will also be

weakened and slowed down; the other is that although the IOD tends to become weaker post-SON, there are still residual influences in the December–January period that can affect the monsoon onset over tropical Australia. Due to the fact that the IOD SST anomalous patterns cannot persist throughout the whole monsoon season, its influence on the seasonal rainfall total is therefore limited. Note that IOD is only one of the dominant SST modes in the Indian Ocean. Studies such as that of Taschetto et al. (2011) pointed out that the basin-wide warming during peak El Niño years can also significantly affect the tropical Australian rainfall through Gill-type atmospheric responses.

So far, we have only concentrated on the drivers of the Australian monsoon inter-annual variations. Studying the causes of the rainfall at decadal and longer time scales have also been an active research area in Australian monsoon research. In Fig. 5.7 we showed the summer rainfall increase in northwest tropical Australia and the rainfall decrease in the northeast part of the continent, and the reversal of the trend in the northeast region in the last three decades (Li et al. 2013). There have been a number of explanations for the possible causes of these trends. Using some simple AGCM sensitivity experiments, Wardle and Smith (2004) suggested that the rainfall increase in northwest Australia could be linked to enhanced Australian summer monsoonal circulation with increased land-sea temperature contrast. However, to what extent the land-sea thermal contrast can contribute to such rainfall increases and what can cause the increase in the thermal contrast still remain unanswered. Rotstayn et al. (2007, 2012) proposed the potential contribution of the Asian anthropogenic aerosol effect on the increased rainfall trend in northwestern Australia (NWA) by being able to reproduce the NWA increase with Asian aerosol forcing in a coupled GCM. They showed that the Asian aerosol can change the meridional temperature and pressure gradients over the tropical Indian Ocean, which in turn enhanced the monsoonal wind, resulting in more summer rainfall in the northwest. However, Shi et al. (2008) pointed out that such influences simulated by the model could be the result of an unrealistic relationship between Australian rainfall and eastern Indian Ocean sea-surface temperature (SST). Shi et al. (2008) further found that the observed positive trend is closely related to SST changes in the south Indian Ocean. Lin and Li (2012) even proposed that the remote effect of SST in the tropical Atlantic may partially contribute to the rainfall increases in this region. In summary, at present there is no universally agreed-upon explanation for the upward rainfall trend in the northwest.

Similarly, the reason for the decreasing rainfall in northeast tropical Australia is largely unknown. Li et al. (2012) found that the rainfall decrease in northeast Australia could be attributed to the warming trend of SST in the Wharton Basin, located in the northeast Indian Ocean (Li et al. 2012). A recent study of Li et al. (2013) further reported the disappearance of the dipole rainfall trend in the tropical Australian summer. They found that since the late 1980s, the upward rainfall trend has occurred across the whole tropical Australian continent. Indeed, this feature has also been clearly shown in Fig. 5.8. They reported that SST in the tropical western Pacific has replaced the SST in the south and northeast Indian Ocean as the controlling factor responsible for the recent rainfall increase in tropical Australia. They

proposed that direct thermal forcing by increasing SST in the tropical western Pacific leads to an anomalous Gill-type cyclone centered around northern Australia, leading to anomalously high rainfall.

5.4 The Australian Monsoon Simulated by Climate Models

Global climate models (GCMs) are the fundamental tools being used in understanding, modeling, predicting, and projecting the global climate system. Our confidence on the projected changes in the monsoon climate is largely built on the skill of these models in simulating the mean climate and its variations in the current condition (Randall et al. 2007; Flato et al. 2013). Therefore, many studies have been undertaken to evaluate the ability of these models to reproduce the observed monsoon characteristics described in Sects. 5.2 and 5.3. Note that this section, as well as the whole chapter, is more focused on climate aspects of the Australian monsoon than on the short-term Numerical Weather Prediction (NWP), intra-seasonal to seasonal modeling and predictions.

There have been great efforts made in forecasting the short-term weather systems embedded in the Australian monsoon. In the last decade or so, the concept of a "seamless prediction system" has been promoted; this implies consistency of the predictions across space and time scales (WCRP 2005; Hoskins 2012). Intra-seasonal and seasonal predictions of the Australian monsoon, such as the onset of the wet season and seasonal rainfall totals have been developed, based on coupled seasonal forecasting systems (Hendon et al. 2011; Drosdowsky and Wheeler 2014). However, discussions on the modeling skills of such systems will be brief in this section, as there have been a number of book chapters devoted to these aspects (Hendon et al. 2011; Wheeler and McBride 2011). Here we mainly document the skill of current climate models over the Australian monsoon region.

Most of the material here is based on studies analyzing the Coupled Model Intercomparison Project (CMIP) Phases 3 (CMIP3) and 5 (CMIP5) (Meehl et al. 2007; Taylor et al. 2012), which have been used for the IPCC Fourth and Fifth Scientific Assessment Reports (IPCC 2007; IPCC 2013). The skill of these models simulating various aspects of the Australian monsoon climate has been assessed by a large number of studies (Colman et al. 2011; Moise et al. 2012; Jourdain et al. 2013). Given the tremendous spatial and temporal variations of the Australian monsoon seen in Sect. 5.2, and the range of drivers responsible for such variations, modeling the Australian monsoon has been and still is a great challenge for global models. Nevertheless, progress has been made in the last few decades, with improved model physics and dynamics and increased model resolution (Flato et al. 2013).

5.4.1 Mean Monsoon Climate Simulated by Climate Models

Colman et al. (2011) specifically evaluated the skill of 23 CMIP3 models in simulating tropical Australian climate and aspects of the Australian monsoon. They evaluated the large-scale aspects, such as the mean distribution of rainfall and surface temperature, the seasonal variations of the atmospheric circulation and the inter-annual variations of the monsoon climate associated with ENSO. In the study by Jourdain et al. (2013), the results have been updated to include 35 CMIP5 models, and the impacts of ENSO and IOD on the modeled climate were discussed in more detail. The overall results showed that the fundamental seasonal variations of rainfall, temperature, and circulation can be captured by the majority of the models, but there are tremendous variations in individual model skill.

Figure 5.10 shows the multi-model ensemble averages of DJF rainfall and 850 hPa wind simulated by 23 CMIP3 and 45 CMIP5 models, compared with the observed climatology. The observed features of the summer monsoon circulation and rainfall distribution can be, by and large, captured by the model ensemble averages. Extreme monsoon rainfall occurs in the Sumatra-Java and nearby waters. It further penetrates into tropical Australia, with 3 mm day^{-1} contour lines in both CMIP3 and CMIP5 models looking similar in shape to the observed contour lines. There is no significant difference between the ensemble averages of the CMIP3 and CMIP5 models, except that the model biases over the New Guinea region become more significant in the CMIP5 models. As pointed out by Colman et al. (2011), the averaged CMIP model results have a dry bias in the northeast, with a wet bias further in the northwest of the continent. In addition, the modeled rainfall climatology spatial pattern over the maritime continent appears smoother than observed, with a number of high precipitation centers missing from such model ensembles. Insufficient resolution in global climate models is likely part of the problem, as localized land-sea contrast and topographic effects are important in the rainfall generation in the maritime continent (e.g., Rauniyar and Walsh 2011).

The skill of the rainfall ensemble averages from the CMIP3/5 models shown in Fig. 5.10 must be read with caution since there is enormous spread among the models, and the ensemble averages effectively average out these offsetting errors. Thus, the agreement between the model ensembles and the observations does not mean that the majority of the models have satisfactory monsoon rainfall simulations. This argument is clearly illustrated in Fig. 5.11, which shows seasonal averaged rainfall in DJF from 72 CMIP3 and CMIP5 models compared with the observation (CMAP: Xie and Arkin 1997). One can see that the extension of the monsoon heavy rainfall varies significantly among the models, with several of them showing very limited summer rainfall over tropical Australia.

This is further evident in the area-averaged rainfall in the tropical Australian land (120°–150°E and 20°–10°S) by a group of CMIP5 models (Fig. 5.12a). Of the 37 CMIP5 models examined, about half of them overestimated the summer rainfall during the DJF monsoon season, while the other half underestimated it. Taking the February rainfall as an example, the observed climatology is about 7 mm day^{-1}.

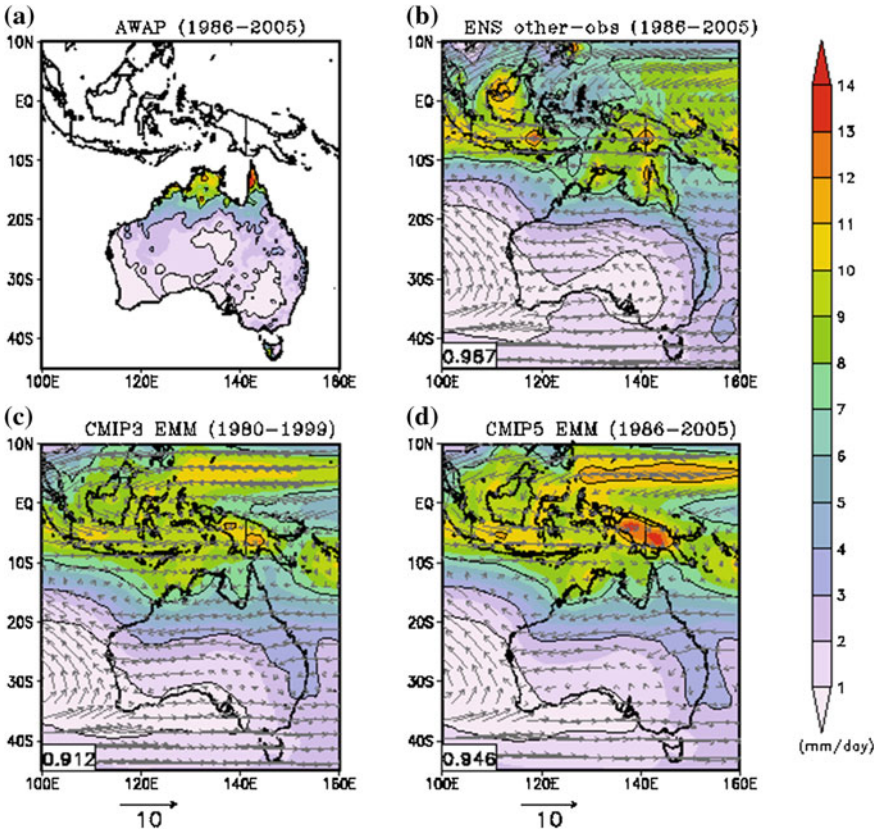

Fig. 5.10 Comparison of DJF rainfall and 850 hPa atmospheric circulation from observations and multi-model ensemble averages from 23 CMIP3 and 45 CMIP5 models. **a** The Australian Bureau of Meteorology high-quality rainfall observation (AWAP: Jones et al. 2009) for 1986–2005 (mm day^{-1}); **b** 850 hPa wind from ERA-40 together with the precipitation climatology averaged from three observational products to minimize the observational errors: the GPCP (Adler et al. 2003), GPCC (Rudolf et al. 2011), and CMAP (Xie and Arkin 1997); **c** CMIP3 model ensemble averages; **d** CMIP5 model ensemble averages

There are about eight models whose mean rainfall is more than 9 mm day^{-1}, which is $\sim$30 % more than the observed. In contrast, there are also a similar number of models whose mean values are <5 mm day^{-1} (30 % less than the observed).

Another message from Fig. 5.12a is that there was a significant model improvement from the early CMIP2 (roughly representing models in the late 1990s) to CMIP3 experiments (roughly representing models in the mid-2000s), but the model improvement in their simulated tropical Australian rainfall is less significant between the CMIP3 and the CMIP5 models, although the analysis by Jourdain et al. (2013) suggested that the best of the CMIP5 models have better skills than the best of the CMIP3 models. The ensemble averages from CMIP2 models severely

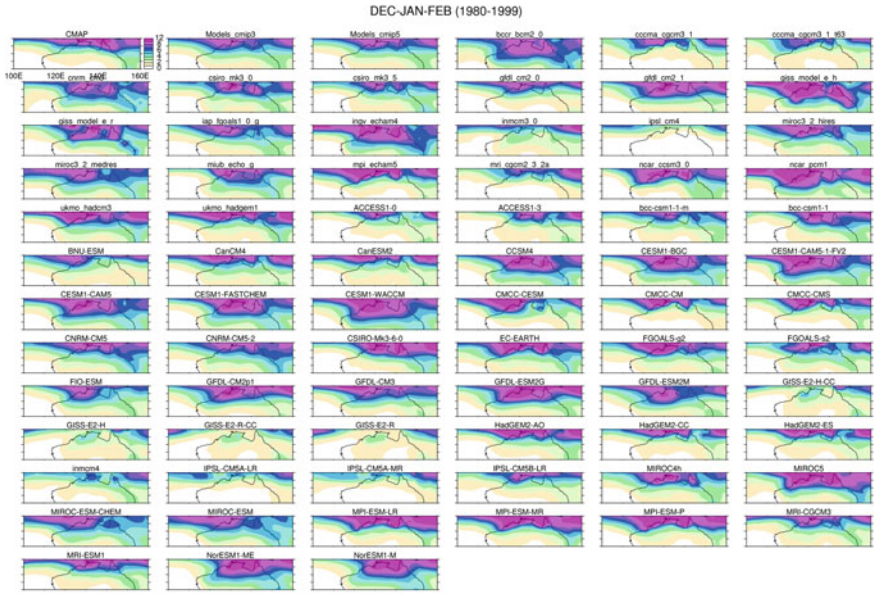

Fig. 5.11 December–January–February mean rainfall climatology (mm day^{-1}) from 1980–1999, from CMAP observational data (*first panel, top row*) from (Xie and Arkin 1997), the ensemble averages from 23 CMIP3 models (*second panel, top row*) and from 49 CMIP5 models (*third panel, top row*). The 23 CMIP3 models start from "bccr-bcm2" (*fourth panel, top row*) to "ukmo-hadgem1" (*second panel, fifth row*). The rest is for the 49 CMIP5 models. In the chapter, we focus on the common features from these models so no model descriptions are provided that can be obtained from the CMIP data webpage at http://www-pcmdi.llnl.gov/projects/cmip/

underestimated the monsoon season rainfall while it overestimated the rainfall in other seasons. In contrast, rainfall seasonality can be reasonably captured by the majority of the CMIP3 and CMIP5 models. This poor performance of the early CMIP2 models was also reported in the assessment of the uncoupled AGCM experiments from Zhang et al. (2002).

Similar conclusions can be drawn to the model-simulated low-level wind in the region. The multi-model ensemble results in Fig. 5.10 offer similar summer monsoon circulation patterns as in the reanalysis products, including the penetration of the zonal monsoon westerly in the region that is a critical feature of the Australian summer monsoon. Nevertheless, this does not imply that the monsoonal circulation is well simulated by most of the models. Figure 5.12b shows the area-averaged 850 hPa zonal wind over the domain of (120°–150°E and 20°–10°S). A large scatter among the 36 CMIP5 models is apparent. There are about 10 models whose averaged winds are easterly throughout the year, with no zonal westerly established. The CMIP5 model ensemble has a weaker monsoon westerly than in the reanalysis products. However, in contrast to the lack of robust improvements in the CMIP5 rainfall compared with CMIP3 models, the seasonality of the 850 hPa wind in the CMIP5 models appears much closer to the reanalysis-based observations than the

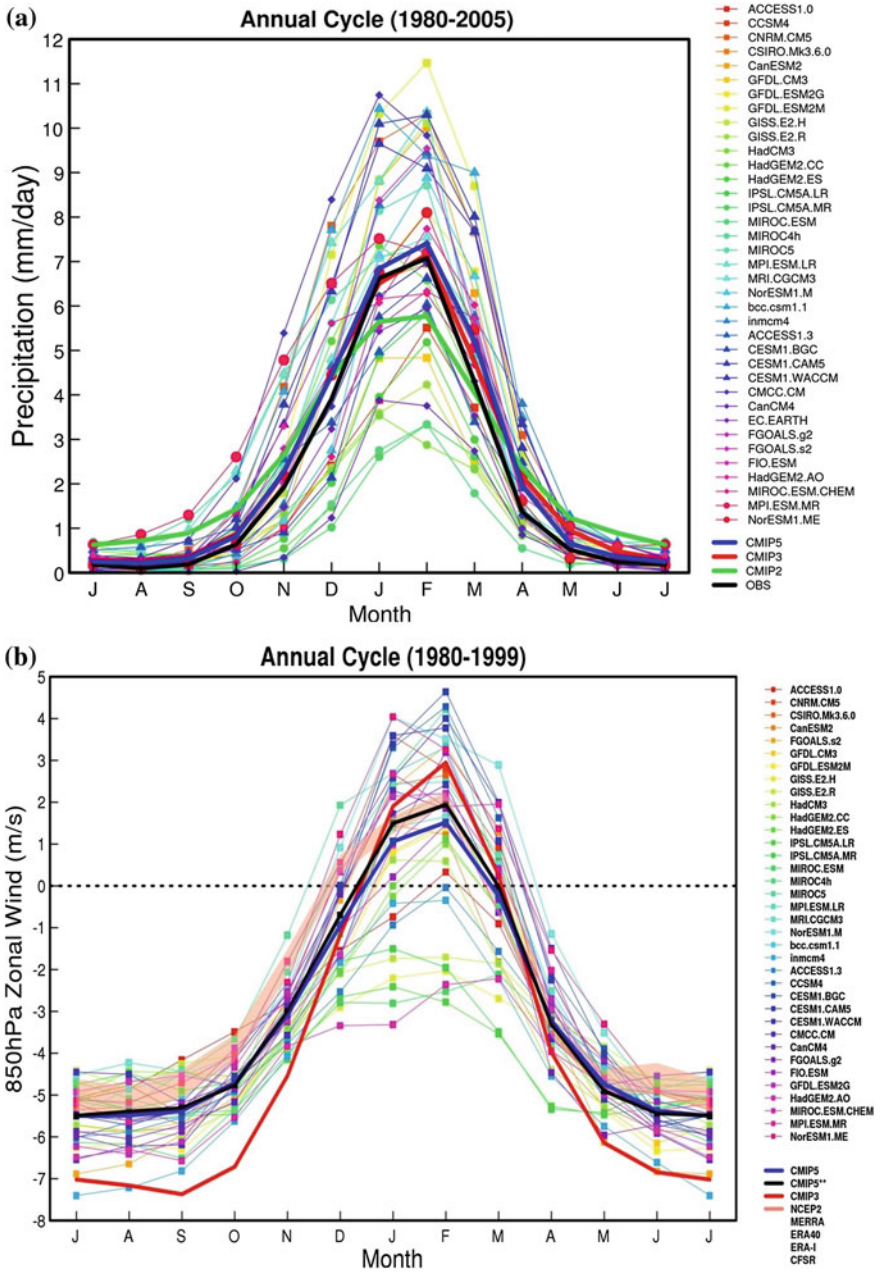
(a)
Annual Cycle (1980-2005)
Precipitation (mm/day)
Month
J A S O N D J F M A M J J
ACCESS1.0
CCSM4
CNRM.CM5
CSIRO.Mk3.6.0
CanESM2
GFDL.CM3
GFDL.ESM2G
GFDL.ESM2M
GISS.E2.H
GISS.E2.R
HadCM3
HadGEM2.CC
HadGEM2.ES
IPSL.CM5A.LR
IPSL.CM5A.MR
MIROC.ESM
MIROC4h
MIROC5
MPI.ESM.LR
MRI.CGCM3
NorESM1.M
bcc.csm1.1
inmcm4
ACCESS1.3
CESM1.BGC
CESM1.CAM5
CESM1.WACCM
CMCC.CM
CanCM4
EC.EARTH
FGOALS.g2
FGOALS.s2
FIO.ESM
HadGEM2.AO
MIROC.ESM.CHEM
MPI.ESM.MR
NorESM1.ME
CMIP5
CMIP3
CMIP2
OBS
(b)
Annual Cycle (1980-1999)
850hPa Zonal Wind (m/s)
Month
J A S O N D J F M A M J J
ACCESS1.0
CNRM.CM5
CSIRO.Mk3.6.0
CanESM2
FGOALS.s2
GFDL.CM3
GFDL.ESM2M
GISS.E2.H
GISS.E2.R
HadCM3
HadGEM2.CC
HadGEM2.ES
IPSL.CM5A.LR
IPSL.CM5A.MR
MIROC.ESM
MIROC4h
MIROC5
MPI.ESM.LR
MRI.CGCM3
NorESM1.M
bcc.csm1.1
inmcm4
ACCESS1.3
CCSM4
CESM1.BGC
CESM1.CAM5
CESM1.WACCM
CMCC.CM
CanCM4
FGOALS.g2
FIO.ESM
GFDL.ESM2G
HadGEM2.AO
MIROC.ESM.CHEM
MPI.ESM.MR
NorESM1.ME
CMIP5
CMIP5**
CMIP3
NCEP2
MERRA
ERA40
ERA-I
CFSR

◀ **Fig. 5.12** **a** Seasonal cycle of precipitation (mm day-1) averaged over 120°–150°E, 20°S–10° (land points only) from 1980–1999, simulated by 37 CMIP5 models. Also shown are the multi-model ensemble averages from 37 CMIP5 models (*thick blue line* CMIP5), 25 CMIP3 models (*thick red line* CMIP3) as in Colman et al. (2011), and 18 CMIP2 models (*thick green line*) as in Moise et al. (2005). The observed climatology (*thick black line* OBS) is from the GPCP for 1979–2010. **b** as (**a**), but for averaged 850 hPa zonal wind (ms^{-1}). It also shows the multi-model ensemble averages from 37 CMIP5 models (*thick purple line* CMIP5), and an average from the best 30 CMIP5 models (i.e., those simulating monsoon westerlies). The observations are shown as the light pink shaded band derived from ERA-40 (Dee et al. 2011), NCEP-CFSR (Saha 2010), ERA-interim (Dee et al. 2011), MERRA (Rienecker et al. 2011) and NCEP2 (Kalnay et al. 1996), in order to reflect uncertainty in observational datasets

CMIP3 models. This is mainly due to the reduced biases in the magnitude of the easterlies outside the monsoon season, which, to some degree, illustrates the improvement of the tropical circulation in the CMIP5 models despite of the fact that there are still sizeable errors in modeled rainfall distributions. It reflects the high complexity of the rainfall generation in the monsoon region and the difficulty of the current global models with relatively course resolutions and deficiencies in the model physics and dynamics in capturing the full picture of the monsoon rainfall processes. This is the rationale behind several studies, such as those of Zeng and Lu (2004) and Zhang (2010), which tried to use some large-scale variables essential to the monsoon development to diagnose the monsoon development, rather than directly using rainfall generated from these models.

Using 850 hPa zonal wind and normalized precipitable water in diagnosing the monsoon onset/retreat, Zhang et al. (2013) evaluated a suite of CMIP3 models in simulating the evolution of the Australian summer monsoon. As shown in Fig. 5.13, a majority of the models can capture the northwest-southeast evolution of the summer monsoon, which starts from the South Sumatra and Java region around late November and then progressively approaches the Australian continent in late December. However, there are significant biases in the modeled onset/retreat dates and the extent of the monsoon inland penetration. Table 5.1 shows the averaged onset dates along the northwest-southeast direction from (5°S, 110°E) to (20°S, 140°E), together with the results from the 13-model ensemble mean and the results derived from ERA-40 reanalysis. In this data, the monsoon starts from southern Sumatra and nearby warm waters around JD336; then the monsoon onset penetrates southeastward towards Java and the Java Sea around JD345 and progresses towards Timor and the Timor Sea area around JD352. Around JD360 it reaches the warm water north of the Australian continent, then approaches the continent shortly after that and moves further southeastward around JD375. The 13-model ensemble gives remarkably similar dates to the ones derived from ERA-40. However, there are variations across the models, with some of them having a much earlier onset—by as much as 20–25 days—while some have a delayed onset by about 30 days. Recently, Zhang et al. (2014) updated their CMIP3 analysis to more CMIP5 models, and the conclusions largely remain the same.

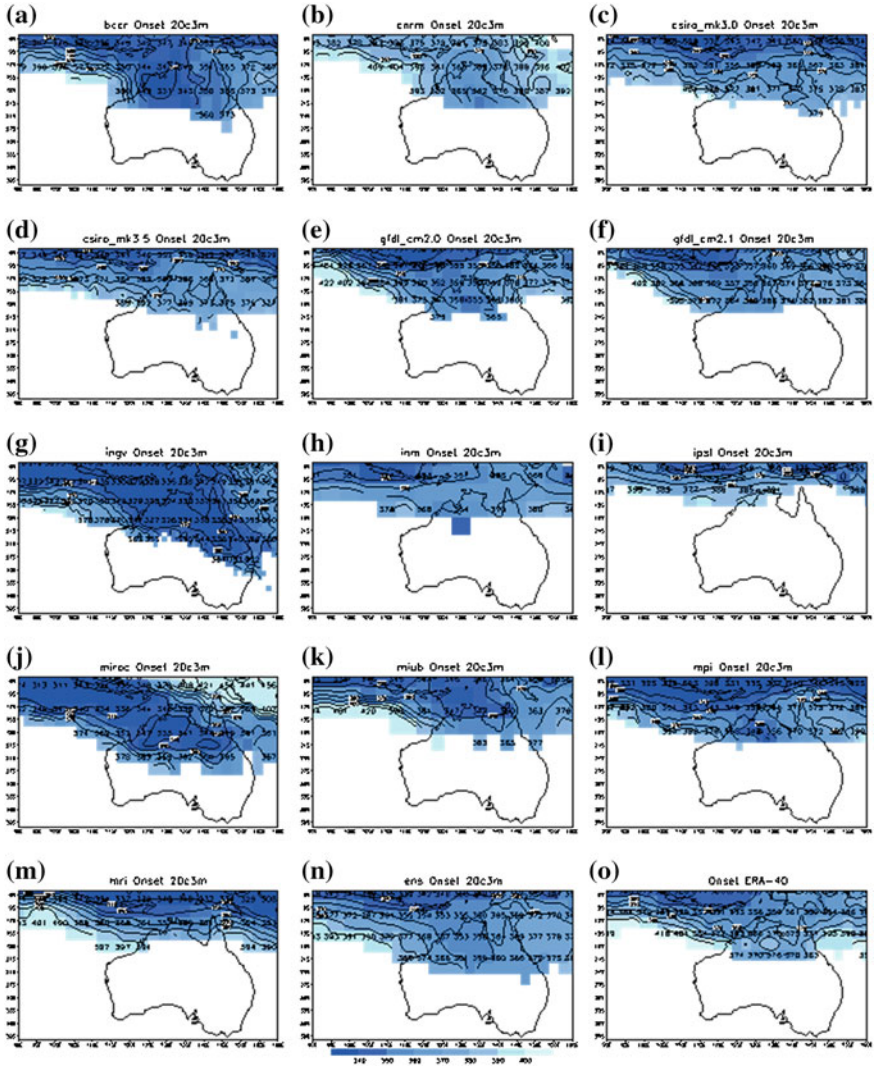

Fig. 5.13 **a**–**m** 19 year mean climatology of Australian monsoon onset dates (Julian day number) simulated by 13 CMIP3 models in their 20C3 M simulations between 1981 and 2000. The model names are as listed in Table 5.1. Only locations where at least 10 onsets have occurred in the 19 year period are plotted. **n** 13-model ensemble results after re-gridding the model data to common 2.5° × 2.5° resolution; **o** averaged onset dates derived from the same method using 43 year ERA-40 reanalysis data for 1959–2001. Modified from Zhang et al. (2013)

The spatial domain of the monsoon system represented by the climate models is also evaluated in a number of studies (Wang and Ding 2008; Wang et al. 2011; Colman et al. 2011). Using the monsoon domain definition as the region where the summer-winter rainfall difference exceeds 2.5 mm day^{-1} and this annual range

Table 5.1 Averaged onset dates (Julian Day, JD) at grid points along a northwest-southeast direction [starting from (5°S, 110°E) to (20°S, 140°E)] in the Australian monsoon region in the model 20C3 M runs

Model	5°S	7.5°S	10°S	12.5°S	15°S	17.5°S	20°S
	105–115°E	110–120°E	115–125°E	120–130°E	125–135°E	130–140°E	135–145°E
bccr	313	339	345	346	340	346	350
cnrm	378	378	377	374	367	362	358
csiro_mk3.0	326	340	349	356	371	373	368
csiro_mk3.5	335	354	354	360	370	371	377
gfdl_cm2.0	316	331	346	355	355	357	360
gfdl_cm2.1	332	340	350	356	362	368	376
ingv	314	328	330	328	322	331	337
inm	342	347	351	366	363	366	
ipsl	345	344	367	386	393		
miroc	331	329	330	344	335	338	339
miub	345	353	353	354	357	356	374
mpi	322	331	339	350	352	350	360
mri	320	334	348	360	379		
ensemble	337	345	354	358	355	357	361
ERA-40	336	345	352	360	369	379	374

Results are averaged over a 10° zonal band at each location. Adapted from Zhang et al. (2013)

exceeds 55 % of the annual rainfall total (the same as we used in Fig. 5.1b), Lee and Wang (2012) showed that the monsoon domain is reasonably simulated by the model ensembles of 20 CMIP5 models in their analysis; however, it is unclear how the individual model performs. Another way to evaluate the monsoon domain in the models is to examine the location of the monsoonal circulation pattern. Colman et al. (2011) evaluated the low-level wind shear lines associated with the Australian monsoon simulated by CMIP3 models. The monsoon shear line is simply defined as the occurrence of zero mean zonal wind at low levels, which corresponds to the transition from easterlies to westerlies. Figure 5.14 shows an updated version representing the 925 hPa shear lines simulated by a group of CMIP5 models, together with the results derived from a number of reanalysis products that represent the uncertainty in these "observational" datasets. The ensemble mean shear lines are derived from the model averaged winds simulated in the CMIP5 historical runs (for current climate) and RCP8.5 runs (for future climate).

For most of the models, the southwest/northeast orientation of the low level shear line in the tropical Australian region is well captured, but it is slightly Equatorward of the observed, as also noted in Colman et al. (2011). The shear line over Papua New Guinea and the tropical west Pacific Ocean is, however, quite different from the reanalysis data. There is a significant lack of the southward penetration. Enormous spread across an individual model is seen in the Papua New Guinea region, and Colman et al. (2011) found even greater model differences in early monsoon season (December). The severe underestimation of the westerlies in this part of the tropics by the CMIP models was also reported in the analysis of Smith et al. (2012). This is

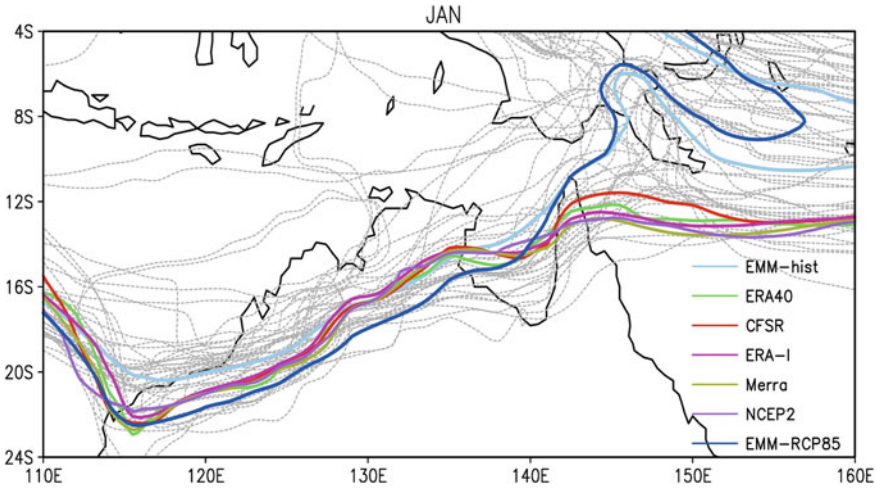

Fig. 5.14 Monsoon shear line (defined as the latitude of zero values of the monthly mean 925 hPa zonal wind) in January for 1980–1999 for 40 CMIP5 models (*gray lines*), along with that of the ensemble mean model (*heavy light blue line* EMM-hist). To show the uncertainty in observations, the corresponding results from ERA-40, NCEP-CFSR, ERA-interim, MERRA and NCEP2 reanalysis products are included. Results from the 40 model RCP85 ensemble averages are shown in heavy blue (EMM-RCP85)

also consistent with the results of Brown et al. (2013) that the position of the CMIP model-simulated South Pacific Convergence Zone was too zonally oriented towards the Equator. Possible reasons for such results include (a) coarse model resolution (e.g., Smith et al. 2013 showed improved model performance in the region with dynamically downscaled modeling experiments), and (b) the tropical SST biases in these models (the too-far westward extension of the tropical SST cold tongue would inhibit the convection development in the region and therefore cause eastward penetration of the summer monsoon). Such differences in the simulated monsoon circulation are eventually transferred into the modeled precipitation errors; Colman et al. (2011) demonstrated that the models with stronger monsoon zonal westerlies often produced larger summer rainfall totals.

Besides the documentation of the modeling errors in the model-simulated mean rainfall and temperature climatology, great efforts have been made to gain some understanding of the potential causes of such errors. For instance, Colman et al. (2011) used 500 hPa vertical velocity to examine the monsoon rainfall generation under various vertical motion (representing atmospheric convections) regimes. In this way, total precipitation can be decomposed into two components: one is the relative occurrence of particular convective regimes, and the other is how much precipitation on average falls for a particular vertical motion regime. They found that models that overestimated the summer monsoon rainfall over Australia had both stronger westerlies and were systematically more "convective." At the same time, they showed too much precipitation from both moderately convective and

suppressed conditions in these models. In contrast, models with underestimated monsoon rainfall showed not just suppressed regional convection, but too little precipitation for all convective and suppressed conditions.

5.4.2 *Monsoon Variations Simulated by Climate Models*

It is essential that climate models have reasonable skill in simulating monsoon variability in the current climate if we are to apply them for projections in a greenhouse-warmed climate. Such skill largely depends on the skill of model ability to represent the large-scale drivers governing its variations documented in Sect. 5.3. Most such analyses have focused on inter-annual variations, although there have been several studies documenting the skill of climate models in modeling the intra-seasonal monsoon variations in some monsoon domains (e.g., Lin et al. (2008) for the Asian monsoon).

As documented in Sect. 5.3, MJO is a primary cause of the monsoon intra-seasonal variations but it is still a challenge for climate models (Lin et al. 2008; Xavier 2012; IPCC 2013), and most models have weak coherence in their MJO propagation. As a consequence, most models show weak intra-seasonal rainfall variations and a lack of eastward propagation in the Asian monsoon domain (Lin et al. 2008). There is a lack of such detailed analyses for the Australian monsoon in coupled climate models, but several published studies documented such skills from a fully coupled seasonal forecasting model (Predictive Ocean Atmosphere Model for Australia–POAMA) used for intra-seasonal forecasts (Hudson et al. 2011). Marshall et al. (2011) showed that the model was skillful in simulating the pattern and intensity of the summer weekly rainfall variations in the tropical Indo-Pacific region associated with the MJO, but it performed poorly over the maritime continent as commonly seen in other models (Peatman et al. 2013). This has consequences, for example, in the prediction of extreme heat waves during the summer monsoon season in tropical Australia (Marshall et al. 2013).

At a seasonal time scale, both statistical and coupled seasonal forecasting models tend to have lower skill in forecasting seasonal mean rainfall of the Australian summer monsoon than other seasons (Drosdowsky and Chambers 2001; Hendon et al. 2011). Hendon et al. (2011) found that the POAMA system was able to provide some skillful seasonal forecasts of regional climate in tropical Australia at lead times up to a few months in its cool and transition seasons. However, forecasts from POAMA for summer rainfall were no better than climatology, even at short lead time. As discussed in Sect. 5.3, they attributed this commonly seen feature among several forecasting models to the seasonally varying air-sea interactions in the seas around northern Australia that promotes seasonal predictability prior to monsoon onset and breaks down once the onset has occurred. For the onset of the summer wet season in tropical Australia (which was defined as the date when a threshold rainfall accumulation of 50 mm is reached from September 1st), Drosdowsky and Wheeler (2014) reported that POAMA can skillfully predict the variability of onset, with reasonable probabilistic

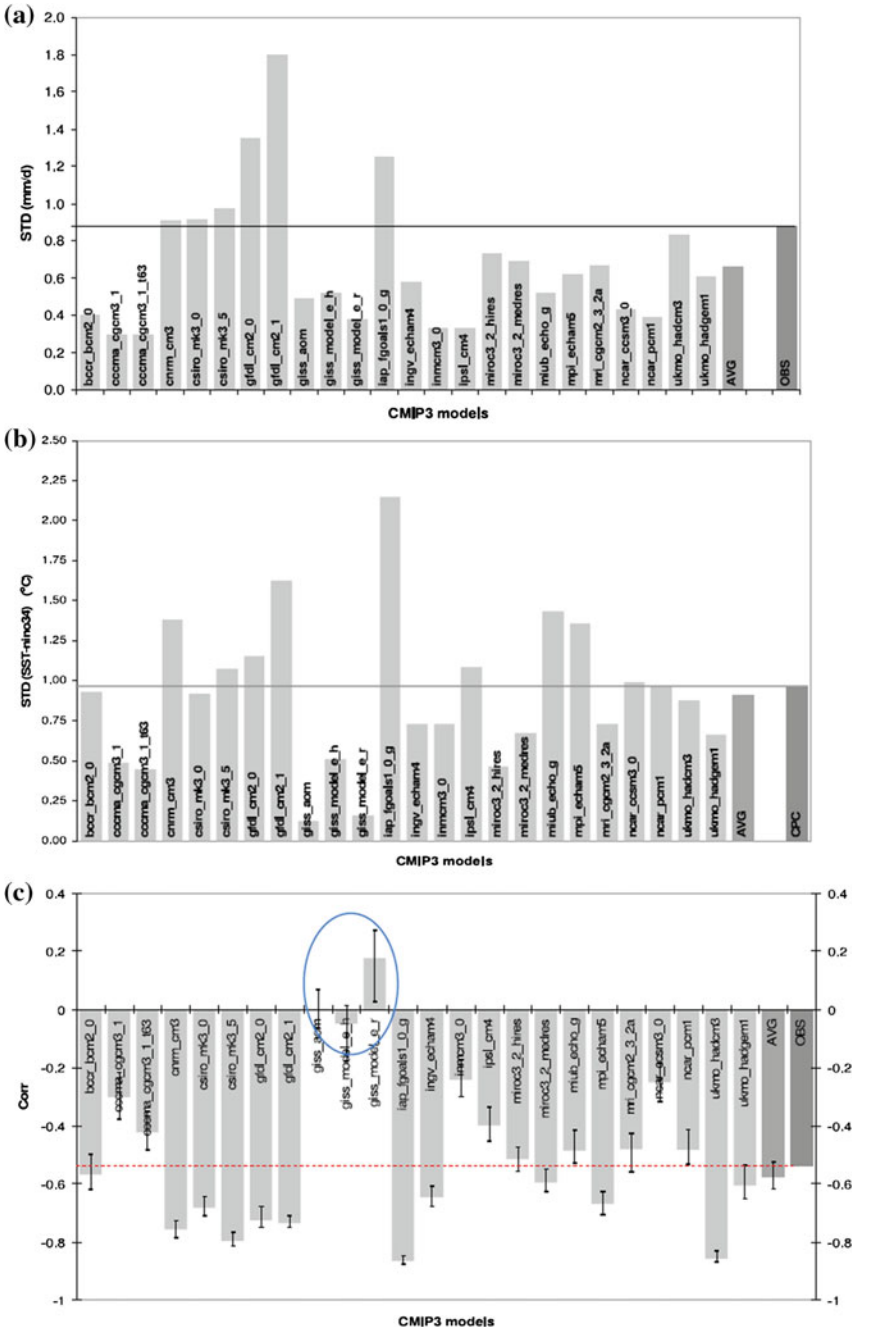
(a)
STD (mm/d)
2.0
1.8
1.6
1.4
1.2
1.0
0.8
0.6
0.4
0.2
0.0
bccr_bcm2_0
ccsm_cgcm3_1
ccsm_cgcm3_1_t63
cnrm_cm3
csiro_mk3_0
csiro_mk3_5
gfdl_cm2_0
gfdl_cm2_1
giss_aom
giss_model_e_h
giss_model_e_r
iap_fgoals1_0_g
ingv_echam4
inmcm3_0
ipsl_cm4
miroc3_2_hires
miroc3_2_medres
miub_echo_g
mpi_echam5
mri_cgcm2_3_2a
ncar_ccsm3_0
ncar_pcm1
ukmo_hadcm3
ukmo_hadgem1
AVG
OBS
CMIP3 models
(b)
STD (SST-nino34) (°C)
2.50
2.25
2.00
1.75
1.50
1.25
1.00
0.75
0.50
0.25
0.00
bccr_bcm2_0
ccsm_cgcm3_1
ccsm_cgcm3_1_t63
cnrm_cm3
csiro_mk3_0
csiro_mk3_5
gfdl_cm2_0
gfdl_cm2_1
giss_aom
giss_model_e_h
giss_model_e_r
iap_fgoals1_0_g
ingv_echam4
inmcm3_0
ipsl_cm4
miroc3_2_hires
miroc3_2_medres
miub_echo_g
mpi_echam5
mri_cgcm2_3_2a
ncar_ccsm3_0
ncar_pcm1
ukmo_hadcm3
ukmo_hadgem1
AVG
CPC
CMIP3 models
(c)
Corr
0.4
0.2
0
-0.2
-0.4
-0.6
-0.8
-1
bccr_bcm2_0
ccsm_cgcm3_1
ccsm_cgcm3_1_t63
cnrm_cm3
csiro_mk3_0
csiro_mk3_5
gfdl_cm2_0
gfdl_cm2_1
giss_aom
giss_model_e_h
giss_model_e_r
iap_fgoals1_0_g
ingv_echam4
inmcm3_0
ipsl_cm4
miroc3_2_hires
miroc3_2_medres
miub_echo_g
mpi_echam5
mri_cgcm2_3_2a
ncar_ccsm3_0
ncar_pcm1
ukmo_hadcm3
ukmo_hadgem1
AVG
OBS
CMIP3 models

◀ **Fig. 5.15** **a** Standard deviation of (detrended) precipitation anomalies (mm/d) for the entire wet season (October to April) for Australian tropics (120°E–150°E, 10°S–20°S land points) for the 1950–1999 50 year period. Also shown is the average of the models (AVG) and the observations (Bureau of Meteorology) (OBS). **b** Standard deviation of (detrended) Nino 3.4 SST anomalies for September to November (SON) for 1950–1999. Shown are individual models, model mean (AVG) and CPC observations (*dark gray*). **c** Correlations between SON Nino 3.4 SST anomalies and full wet season (ONDJFMA) tropical Australian precipitation. Shown are individual models, mean of models with negative correlations (AVG), and observations (*dark gray*). The 90 % confidence interval for each model is indicated by the black error bars, and the circle shows the three models with non-significant correlations (a = 0.10 two-tailed) (from Colman et al. 2011)

forecasting skill, over about a third of Australia's Northern Territory. This skill is higher than that from an ENSO-based statistical method (Lo et al. 2007), suggesting that it gains from additional sources of predictability from air-sea coupling.

There is a large body of research assessing the skill of current climate models in representing the Australian monsoon inter-annual variations. Because of the important role of tropical Indian and Pacific ocean SSTs at this time scale, such skills largely depend on dominant SST patterns, such as the ENSO, IOD, Indian Ocean basin-wide warming, and the Indian-Pacific SST temperature gradient simulated by these models. Numerous individual modeling studies evaluated such modeling skill, but here we extensively refer results from two studies on CMIP3 and CMIP5 model simulations by Colman et al. (2011) and Jourdain et al. (2013).

Colman et al. (2011) examined the rainfall inter-annual variations and their associations with ENSO. Figure 5.15 compares standard deviations of the wet season (defined as October to April) precipitation in tropical Australian land in the 1980 to 1999 period from the CMIP3 models and from the observations. Observed standard deviation in this period is 0.9 mm d^{-1} (which is about 20–30 % of mean total precipitation over the region, as also shown in Fig. 5.7). Most of the modeled variability is weaker than observed, with standard deviations around three-quarters of the observed value (0.65 mm day^{-1}). There are only a few models that have substantially too strong variability. In that study, the relationship with ENSO was reflected by the correlations between SON Nino 3.4 index with whole wet season precipitation. First of all, as shown in Fig. 5.15b, the SST variations in the Nino 3.4 region were quite different across the models, which indicates that the strength of the ENSO varies greatly in these models. Most of the CMIP3 models tend to show a weak ENSO, as detailed by Guilyardi et al. (2009). Figure 5.15c displays the correlations between SON Nino 3.4 and the wet season rainfall totals. Models with weak/strong Nino 3.4 variability tend to show weak/strong correlations, consistent with the findings of Cai et al. (2009b). However, more than half of the models have correlations that are too strong. Thus, despite inter-annual variability being too weak on average for both total precipitation and Nino 3.4 SST variability, correlations between the two are stronger than observed in the majority of CMIP3 models.

Jourdain et al. (2013) substantially updated the analysis of Colman et al. (2011) by analyzing 59 models in the CMIP3 and CMIP5 in simulating the Australian summer monsoon and its variations associated with ENSO and IOD. As found by Colman et al. (2011), the standard deviation of the Australian monsoon rainfall

based on the multi-model mean is in remarkable agreement with observations in both CMIP3 and CMIP5. However, this hides a wide spread in the simulated amplitude of the inter-annual variability in both CMIP3 and CMIP5. They found that the model spread is 36 % higher in CMIP3 than in CMIP5 for tropical Australian land rainfall totals. Another interesting result is that they found that the correlation between the mean and the inter-annual variability among the models was relatively weak, underlining the importance of evaluating a model both with regard to its mean and its variability. For some models, they may have a realistic mean Australian monsoon rainfall, but its inter-annual variability could be far from observed.

For all tropical Australia rainfall, as in the CMIP3 analysis of Colman et al. (2011), Jourdain et al. (2013) showed (Fig. 5.16) that most models reproduced the observed Australian monsoon-ENSO connections, but the strength of the relationship depended on the strength of the simulated ENSO in individual models. They pointed out that the models can largely reproduce the observed features that the preceding JJA SST anomalies in the tropical Pacific can provide, some predicting skills for the tropical Australian summer monsoon rainfall, with the lag correlations remaining around −0.3. Over the Maritime Continent, the simulated monsoon-ENSO connection was generally weaker than observed, depending on the ability of an individual model to realistically reproduce the ENSO signature in the warm pool region. They further showed that a large part of this bias came from the New Guinea region, where moisture convergence seemed to be particularly affected by this SST bias.

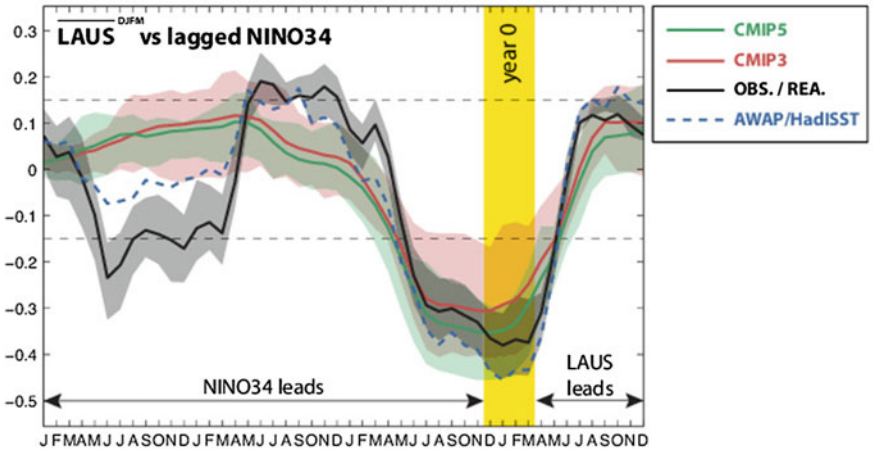

Fig. 5.16 Lag correlation between LAUS averaged in DJFM of year 0 and monthly Nino 3.4 values. Thick lines are the means over the observations/reanalyses (*black*), CMIP3 (*red*), and CMIP5 (*green*). Semi-transparent areas show the upper and lower quartiles. The dashed thick blue line represents results calculated from observed rainfall and observed SST data. The *yellow* area indicates the reference time ($t = 0$), and its width shows the DJFM months over which each index is averaged (provided by A. Jourdain, according to Jourdain et al. 2013)

Despite significant wind anomalies in the Indian Ocean related to the IOD, based on partial correlation analysis, they claimed that the monsoon-IOD relationship was relatively weak—both in the observations and in the models. Such a weak correlation could be due to two factors. Firstly, Jourdain et al. (2013) correlated SON IOD with DJFM tropical Australian land rainfall. Therefore the impacts of the IOD on the early stage of the Australian monsoon may be averaged out in their analysis. For instance, Zhang et al. (2013) found the impacts of the IOD on Australian monsoon onset simulated by the CMIP3 models. Secondly, we know that ENSO and IOD are closely related, but ENSO does not uniquely determine the IOD development, and some studies (e.g., Luo et al. 2010) showed impacts of the IOD on subsequent ENSO development. Thus, simple partial correlations treating IOD impacts as a residual signal after excluding the ENSO impacts may have underestimated the contribution of IOD and some other Indian Ocean SST variations to the Australian summer monsoon.

5.5 Model Projected Changes in the Australian Monsoon Under Global Warming

Assessing potential changes to both the monsoon rainfall and circulation under global warming has attracted a good deal of attention in recent years; much of it has motivated the development of regional climate change projections. As pointed out in the previous two sections, most projections are based on the CMIP experiments used in the development of IPCC Fourth and Fifth Climate Change Scientific Assessment Reports (IPCC 2007, 2013). Despite consensus on large-scale climate changes induced by increasing greenhouse gases (e.g., Power et al. 2012), there are great uncertainties at regional levels, particularly for rainfall (IPCC 2007, 2013). This is especially true for the Australian monsoon region, for a number of reasons: (1) the complexity of the monsoon system, which varies significantly over a range of spatial and temporal scales; (2) the range of underlying drivers as summarized in Sect. 5.3; (3) variations in the representation of different rivers by different models; and (4) uncertainty about how these drivers will change in the future.

Significant efforts have been made in developing regional climate change projections for Australia (CSIRO and Bureau of Meteorology 2007, 2012), with a number of studies particularly devoted to changes in the monsoon (Colman et al. 2011; Moise et al. 2012; Rotstayn et al. 2012; Suppiah et al. 2013; Watterson 2013). In this section we summarize a number of studies that have investigated the CMIP3/5 model-simulated changes in the Australian summer monsoon (Moise et al. 2012; Zhang et al. 2013; Jourdain et al. 2013; Kitoh et al. 2013; Lee and Wang 2012). The recent IPCC AR5 report includes projections of the Australian monsoon (Christensen et al. 2013; Collins et al. 2013) that are in fact derived from these studies.

Following the evaluation of CMIP3 model-simulated Australian monsoon climate, Moise et al. (2012) documented 19 CMIP3 model projections of the changes

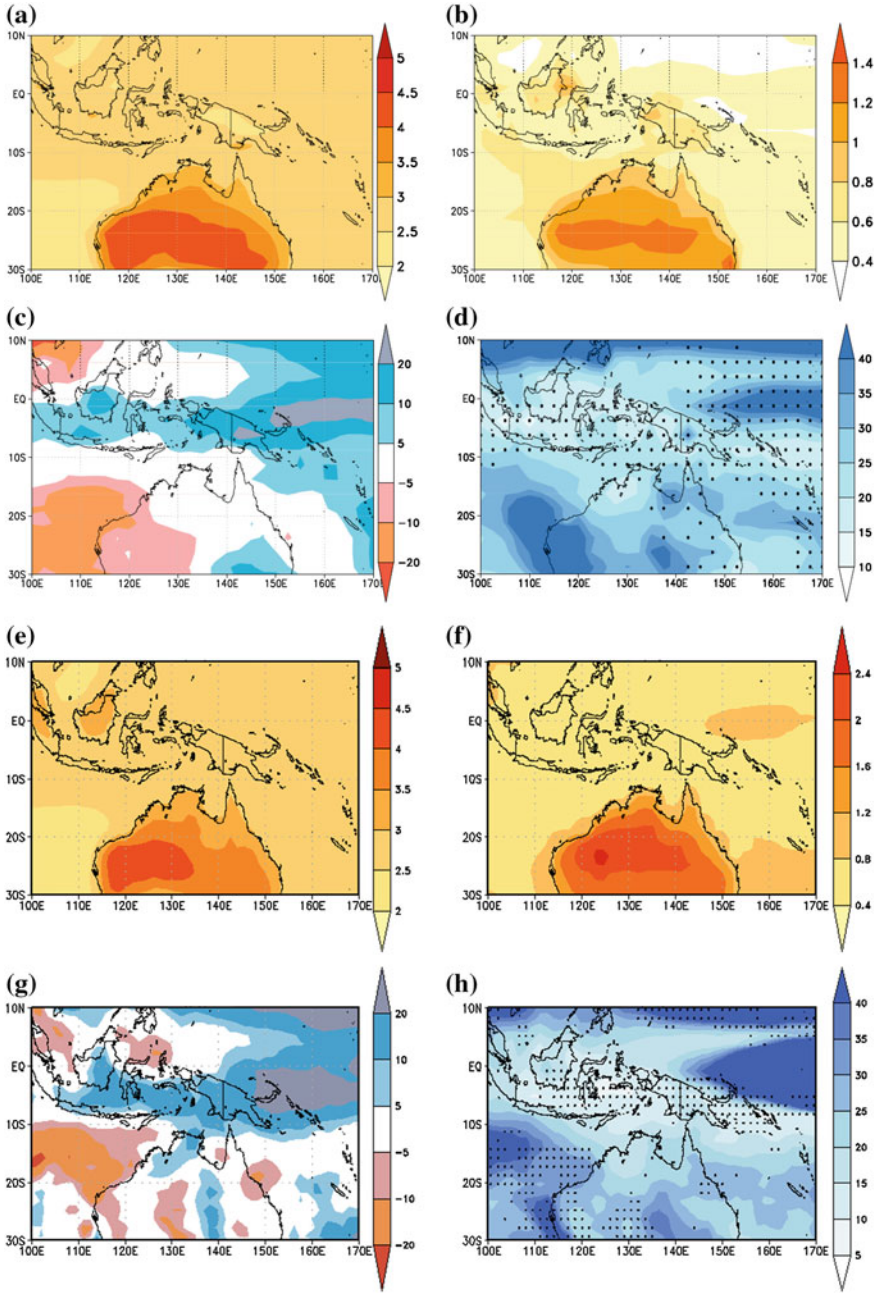
(a)
(b)
(c)
(d)
(e)
(f)
(g)
(h)
10N
EQ
10S
20S
30S
100E
110E
120E
130E
140E
150E
160E
170E
5
4.5
4
3.5
3
2.5
2
1.4
1.2
1
0.8
0.6
0.4
20
10
5
−5
−10
−20
40
35
30
25
20
15
10
2.4
1.6

◀ **Fig. 5.17** Ensemble mean changes in (**a**) surface air temperature (°C) and (**c**) precipitation (%) for December–February seasonal means. Compared are averages from 2080–2099 from the SRES-A2 scenario, versus the 1980–1999 period from the 20c3 m runs. Also shown are measures for intermodal variation: standard deviation of changes in (**b**) surface-air temperature (°C) and (**d**) precipitation (in % of 2080–2099 average). The stippling in (**d**) occurs where more than 66 % of the models agree on the direction of the change. Figures (**a**) to (**d**) are modified from Moise et al. (2012); (**e**) to (**h**) are the same as (**a**) to (**d**), but for the results from 40 CMIP5 models, RCP8.5 runs against their historical runs

in the Australian monsoon under the A2 (high greenhouse gas emission) scenario. These results are, by and large, highly consistent with the CMIP5 derived projections reported by Irving et al. (2012). Figure 5.17 shows projected changes in surface temperature and precipitation for the DJF season from CMIP3 models in Moise et al. (2012) and the CMIP5 models. The overall patterns of the projected changes are very similar between CMIP3 and CMIP5. Over the equatorial regions to the north of Australia, the multi-model ensemble indicates increased rainfall at the end of the twenty-first century, but there is no big change over northern Australia. Moise et al. (2012) pointed out that the clear signal of increased precipitation (+10 to +15 %) in the deep tropics near the Equator and decreased precipitation outside this belt in the subtropics was one of the robust results that emerged from the previous IPCC AR4 report (IPCC 2007). The relatively small change over tropical Australia is caused by the fact that there is a large spread in model simulations of precipitation change, with both large positive and large negative anomalies.

This issue was explicitly addressed in Power et al. (2012), in assessing uncertainty among climate model simulations. The model spread is illustrated by Fig. 5.18, which shows that the models are nearly equally divided in the sign of their simulated changes in monsoon precipitation in three CMIP5 emission scenarios. Consequently the ensemble averages produce a potentially misleading result and in this type of situation, the multi-model mean results can be meaningless (Smith et al. 2013). Moise et al. (2012) further showed that when they grouped the CMIP3 models into different groups according to how well total wet season rainfall over tropical Australia was simulated, the relatively dry models simulated an increase in precipitation across the entire wet season, while for the relatively wet models they tended to show a decrease during some months of the wet season, suggesting a possible shift in seasonality. For all these groups, rainfall at the end of the wet season was increased—which was interpreted as an indication of a more prolonged monsoon season.

Another method for synthesizing multi-model results is to take into account of the skill of each model in simulating both the mean and variability of the observed climate. For instance, in an analysis by Jourdain et al. (2013) for CMIP3 and CMIP5 model-simulated Asia-Australian monsoon, they excluded a large number of CMIP3 and CMIP5 models. From a total of 56, only 10 models were deemed skillful to project future changes. They selected the models based on skill in representing the statistical properties of the Indian and Australian monsoon and

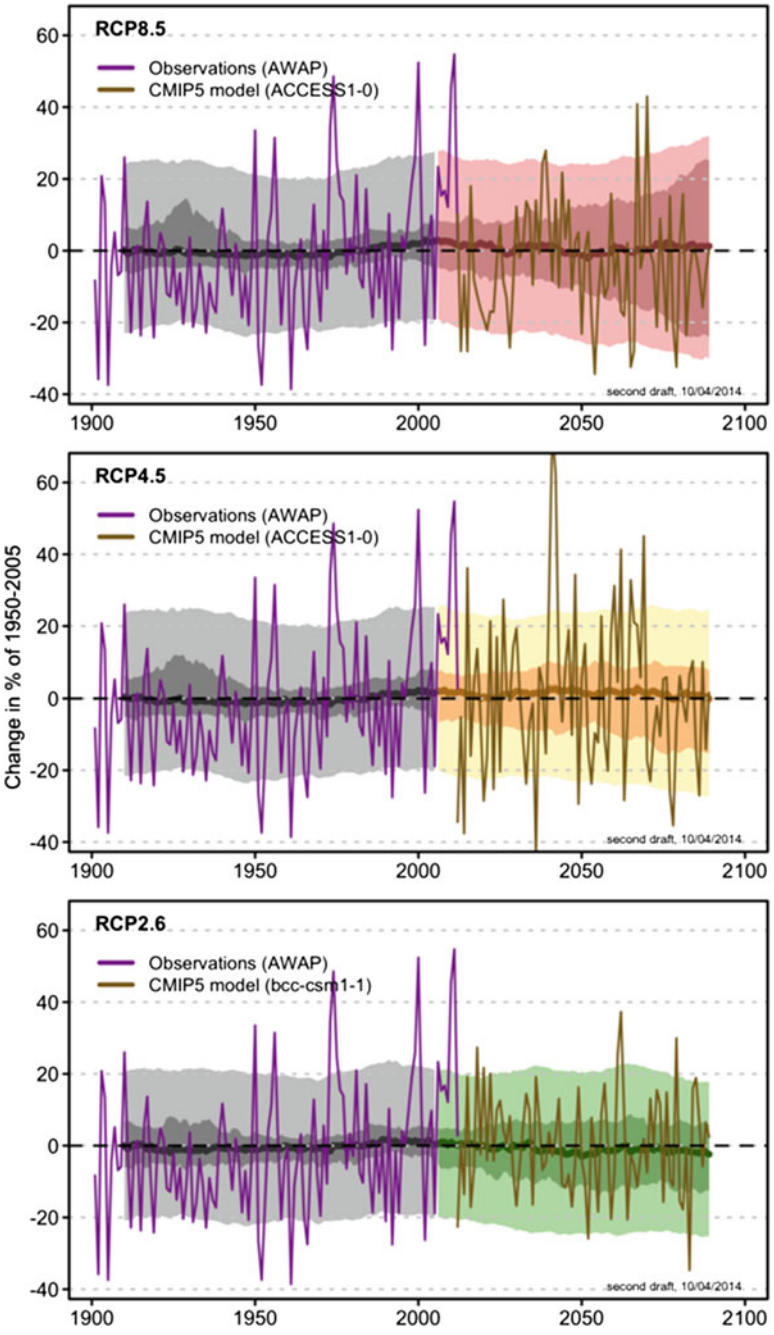
RCP8.5
Observations (AWAP)
CMIP5 model (ACCESS1-0)
second draft, 10/04/2014
RCP4.5
Observations (AWAP)
CMIP5 model (ACCESS1-0)
second draft, 10/04/2014
Change in % of 1950-2005
RCP2.6
Observations (AWAP)
CMIP5 model (bcc-csm1-1)
second draft, 10/04/2014
60
40
20
0
-20
-40
1900
1950
2000
2050
2100

◀ **Fig. 5.18** Time series for precipitation over Australian tropics (20°S-0) for 1900–2100 as simulated in CMIP5 models, relative to the 1950–2005 mean. The central line is the median value, and the shading is the 10 and 90 percentile range of 20 year means (*inner*) and single year values (*outer*). The gray shading indicates the period of the historical simulation, while three future scenarios (Talor et al. 2012) are shown with color-coded shading: *pink* RCP8.5, *orange* RCP4.5, and *green* RCP2.6. The Bureau of Meteorology observations (AWAP) are shown in purple and projected series from a typical model (ACCESS1-0) are shown into the future

features of the ENSO-monsoon relationship. Then 7 of these 10 models showed a significant rainfall increase of about +12 to +22 % at the end of the twenty-first century, as compared to the 1850–1899 period. The three remaining models did not show a significant trend. There was no clear consensus between these 10 models concerning the future monsoon rainfall over the Maritime Continent, highlighting the lack of understanding of rainfall and convection processes over the warm pool and maritime continent region. Similarly, Lee and Wang (2014) ranked models according to their representation of the dominant annual cycle modes of the monsoon and its intensity for selecting the best models for projections of the monsoon changes in a moderate greenhouse gas emission scenario (RCP4.5). They found that the best models yielded a summer monsoon rainfall increase in the Australian region, with the percentage to the annual rainfall total falling in summer also increased. However, the factional summer rainfall increase was much less than that seen over the Asian domain.

Because of potential changes in the dominant patterns of tropical SST variations under global warming, monsoon inter-annual variability could also be altered. Both the IPCC AR4 and AR5 reports, and many CMIP modeling studies, showed the potential for changes to ENSO and IOD in a warmed climate (IPCC 2007 and 2013; Cai et al. 2009c; Yeh et al. 2009; Wang et al. 2013). Moise et al. (2012) examined projected changes in rainfall variability across tropical Australia. As shown in Fig. 5.19a, of the 20 models they examined, the standard deviation of summer rainfall tended to decrease. All models that simulated near-observed or stronger precipitation variability in the twentieth century period showed reduced variability by the end of the twenty first century, while those models showing skillful precipitation amounts in the current climate also generally showed a decrease in variability. Nevertheless, there is a lack of understanding of such changes, as the increased inter-annual variability of monsoon rainfall was reported over western Pacific and south Asian monsoon (Brown et al. 2013; Turner and Annamalai 2012). In addition, the correlations between the tropical Australian wet season (October to April) rainfall and the preceding spring (September to November) Nino 3.4 sea surface temperature anomalies (Fig. 5.19b) revealed a slight weakening of the ENSO-monsoon connections under global warming, but very few of these changes were statistically significant. Thus, such results indicate a need for more thorough analysis and modeling studies.

A large number of studies have investigated the possible response of the large-scale overturning circulation to global warming, and these studies indicated a weakening of tropical overturning as the climate warms (Vecchi and Soden 2007;

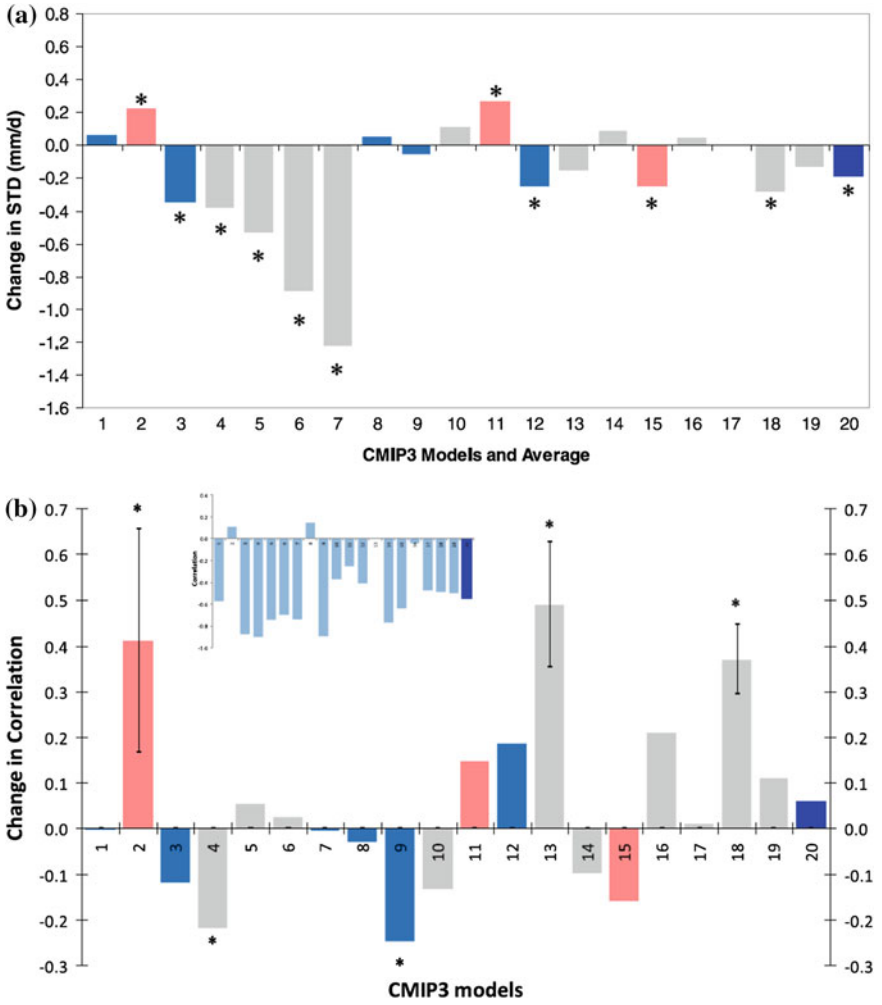

Fig. 5.19 **a** Change in inter-annual standard deviation of precipitation (STD, in mm day^{-1} between wet season (October to April, inclusive) from 1980–1999 to 2080–2099 under the SRES-A2 scenario for 19 CMIP3 models. Model mean change is shown in *dark blue* on the *right*. Colors represent models that are more than one standard deviation below (*blue*), above (*pink*) total wet season observed precipitation for the 1980–1999 period. Gray bars indicate models that are within one standard deviation of the observations. The asterisk denotes that these changes are significant ($p = 0.05$) using a t-test (from Moise et al. 2012); **b** Change in correlation between SON Niño 34 SSTs and wet season (October to April, inclusive) precipitation across tropical Australia from the 1980–1999 until the 2080–2099 periods for the SRES-A2 scenario. Also shown are the 2080–2099 period correlations themselves in the insert, as shown in Fig. 5.15c (adapted from Moise et al. 2012)

IPCC 2007 and 2013). CMIP3 model results showed a remarkable agreement in simulating a weakening of the tropical atmospheric overturning circulation (Vecchi and Soden 2007) which is also seen in the CMIP5 results (Chadwick et al. 2013). Furthermore, the Walker circulation is projected to weaken under global warming (Power and Kociuba, 2011) more than the Hadley Circulation (Vecchi and Soden 2007). Such changes in the Walker and Hadley cells may have direct implications for changes to the monsoon circulation. Nevertheless, more studies have been conducted for the Asian monsoon than its Australian counterpart. Despite an intensification of precipitation in the Asian monsoon region, the Asian summer monsoon circulation tends to weaken (Ueda et al. 2006; Kripalani et al. 2007; Cherchi et al. 2011).

Several studies specifically addressed the changes in the Australian monsoon circulation. Rotstayn et al. (2012) performed detailed simulations with a coupled climate model aimed at investigating the effects of greenhouse gas and aerosol changes on the summer rainfall and circulation in the monsoon region. Greenhouse-gas forcing alone led to a strong summer rainfall decrease over northwest tropical Australia, and in fact the reduction extended over most of the monsoon region. The inclusion of Asian aerosol forcing in the model significantly offset the rainfall decreases. The aerosol changes induced a cyclonic circulation trend off the coast of northwest Australia (enhanced monsoon flows) but greenhouse gas change led to an anticyclonic circulation trend (weakened monsoon flows). They further explained that such results shift to both the Walker circulation and local Hadley circulation as well as a Rossby wave response to tropical convective heating anomalies. Suppiah et al. (2013) did a separate analysis of the CMIP5 experiments using the same model, but it was more focused on the Australian monsoon. They reported a weakened Australian summer monsoon circulation and reduced rainfall in the region with the RCP4.5 and RCP8.5 forcing. They attributed such changes to the Pacific Indian Ocean Dipole (PID) SST warming patterns simulated by the model. This model showed a greater warming over the east of Papua New Guinea and less warming in the eastern Indian Ocean. However, the detailed processes linking the SST changes to the weakened monsoon were not discussed. Note that the weakening of the Australian monsoon circulation with increased greenhouse gases was seen in other modeling studies (e.g., Cherchi et al. 2011).

Despite these findings, significant uncertainty still surrounds projected changes in the monsoon circulation. As a consequence, confidence in the projections is classified as medium to low, as acknowledged in recent IPCC report (Christensen et al. 2013). Moise et al. (2012) summarized monsoon projections from 19 CMIP3 models. As shown in Fig. 5.20a of the multi-model ensemble mean, in the lower troposphere there are modest westerly anomalies across northern Australia, and in the north of the continent, stronger westerlies and a steady cross equatorial flowing west of Papua New Guinea are apparent. The westerly anomalies (Fig. 5.20a) are also reflected by a

slightly further southward penetration of the monsoon shear lines presented in Fig. 5.14. In addition, the equatorial easterly anomalies over Indonesia, coupled with the westerly anomalies over Papua New Guinea and adjacent regions, indicate low-level divergence over the warm pool regions, which are consistent with a weakening and shifting of the tropical overturning circulation (Vecchi and Soden 2007). However, the results of the enhanced low-level westerlies in Fig. 5.20a must be viewed carefully as an indication of the enhanced monsoon circulation because they are not matched by changes in the upper tropospheric circulation. Figure 5.20b

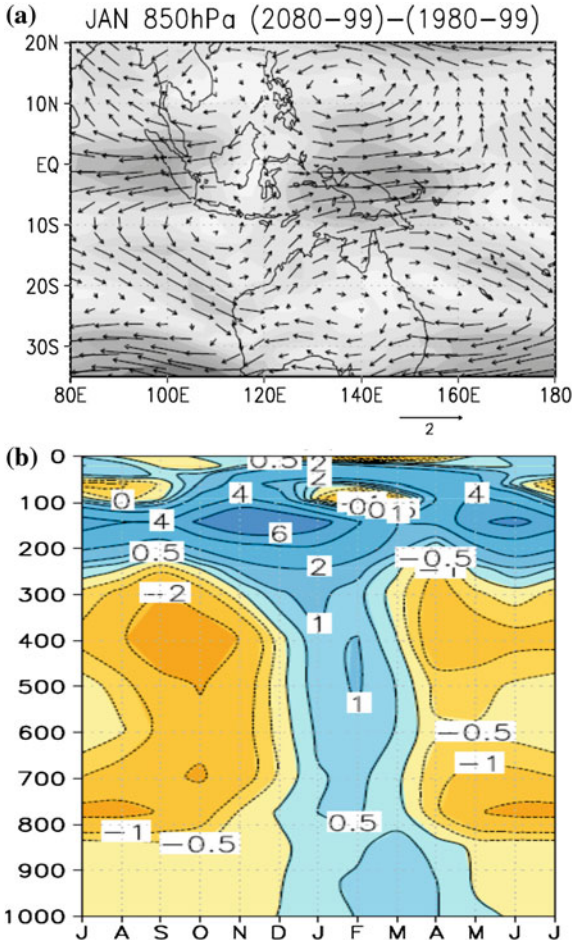

Fig. 5.20 **a** change in January 850 hPa zonal wind between SRES-A2 (2080–2099) and 20c3 m (1980–1999) ensemble means of CMIP3 model simulations in Moise et al. (2012). Shown are the magnitude (*shading*) and directions (*vectors*). **b** as (**a**), but for zonal wind vs pressure annual cycles over tropical Australia (land areas north of 20°S) from the CMIP3 model ensemble mean. *Unit* m s^{-1}

shows a weakening of the easterlies in the upper levels (also found in Cherchi et al. 2011), which does not indicate an overall enhanced monsoon circulation.

The question about the linkage between modelled changes in the monsoon rainfall and its circulation has been investigated in a number of studies. Following the method of Bony et al. (2004), Moise et al. (2012) decomposed projected rainfall changes into three components: (1) a dynamic component linked to precipitation changes associated with changes to the atmospheric circulation, (2) a thermodynamic component related to the changes in rainfall due to the changes in the atmospheric thermodynamical structure, (such as an increase in moisture content with higher air temperatures) and (3) a term describing the co-variation of first two. This type of analysis helps better understanding of the reasons for the uncertainty in projected changes in the monsoon rainfall climate. Results from the CMIP3 models (Fig. 5.21) show that the thermodynamic component of precipitation change is positive virtually everywhere, and particularly strong over the Maritime Continent. The dynamic term is negative over most of the region (with the exception of the ocean north of Papua New Guinea), with strongest contributions to the immediate north and northwest of Australia. Changes in the covariant term are relatively weak and broadly follow the pattern of the dynamic term. The models agree well in the results, with all the models indicating the decrease in the number of strong convective regimes but increased precipitation for such convection, irrespective of model climate biases.

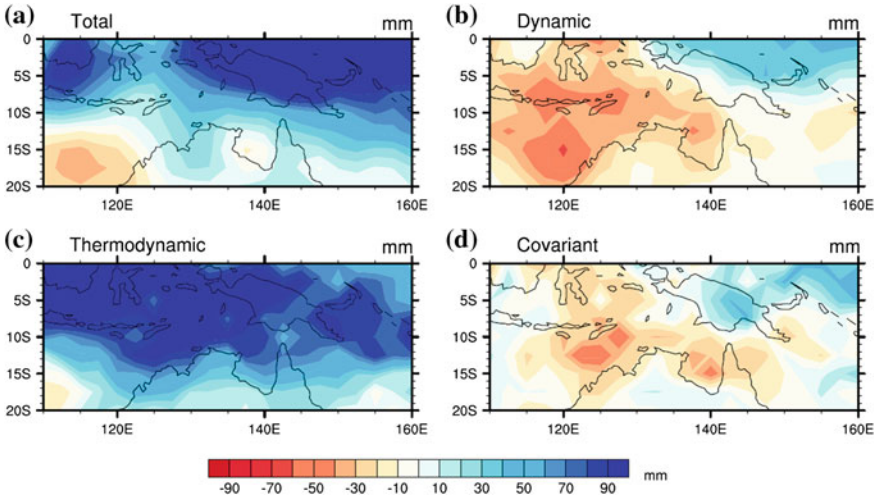

Fig. 5.21 **a** DJF precipitation change (mm) under SRES-A2 scenario: 2080–2099 minus 1980–1999 averages, as simulated by the CMIP3 ensemble mean model and the three components contributing to the overall change: **b** dynamic, (**c**) thermodynamic, and **d** covariant. Refer to Moise et al. (2012) for details

Other aspects of possible changes to the Australian summer monsoon include its spatial domain, onset/retreat dates and rainfall extremes. For changes in the monsoon domain, nearly all the analyses used a rainfall seasonality measurement by Wang and Ding (2008) in calculating the area of the monsoon domain. They defined the monsoon domain as the region where the summer-winter rainfall difference exceeds 2.5 mm day^{-1} and this annual range exceeds 55 % of the annual total rainfall. With this definition, Lee and Wang (2014) found no discernible change in the Australian monsoon land domain based on their selected four best models but some expansion over the oceans to the east. This expansion was largely caused by the increased percentage of the summer monsoon rainfall to the annual totals. Similar results are found in Kitoh et al. (2013) for 29 CMIP5 model results and Hsu et al. (2012), using relatively high resolution uncoupled AGCM experiments. While all these studies used a similar definition for the monsoon domain based on rainfall alone, it is unclear whether such expansions are supported by changes in the monsoon circulation. The uncertainty among these model simulations is also largely unknown in these studies; thus the projected expansions of the Australian monsoon over the SPCZ region needs to be further investigated.

Several studies have evaluated the potential changes in the monsoon onset and retreat dates. For example, the increased March–April rainfall in the Australian domain, together with the enhancement of the low-level westerly and more southward location of the monsoon shear line during this time, prompted Moise et al. (2012) to suggest a delayed retreat of the Australian monsoon. Similarly, Lee and Wang (2014) used the rainfall changes from May to September to estimate possible changes of the Asian monsoon onset/retreat. However, given the abruptness of the onset process, the use of monthly data in these analyses may be able to reveal only approximate changes to the onset/retreat.

In recent years, more thorough analyses of the monsoon onset/retreat have been conducted using CMIP3 and CMIP5 model daily data. Based on the model daily rainfall climatology and using the definition by Wang and LinHo (2002), Kitoh et al. (2013) found that the Australian monsoon has earlier onset dates, later retreat dates, and longer durations. Again, significant uncertainties accompany these model results, and Kitoh et al. (2013) explicitly noted that models' limited ability to reproduce the present monsoon climate and the large scatter among the model projections limited the confidence in the results. As discussed in Sect. 5.2, some of these rainfall-based changes are not monsoon-related because significant rainfall can be generated in the deep moist easterly in the region prior to the monsoon onset (Pope et al. 2009).

Bearing this in mind, Zhang et al. (2013) used daily 850 hPa and volumetric precipitable water data to analyze the change in the monsoon onset following the definition of Zhang (2010) as described in Sect. 5.2. They analysed 13 CMIP3 models over a 20-year period. Here we briefly present the published CMIP3 analysis by Zhang et al. (2013), although in a more recent study (Zhang et al. 2014) they have updated the analysis to 26 CMIP5 models over a 50-year period—and results largely remain the same. The whole analysis was not just for documenting

the modelled changes in the onset/retreat, but rather focusing more on understanding such modelling results and the likely reasons behind such uncertainty.

Under global warming, Fig. 5.22 shows that most models indicated a delayed onset, with model-ensemble results showing a delay of 10–20 days in the tropics, and around seven days over the Australian continent. There were very large model discrepancies in their projected changes, but the disagreement was relatively smaller than the results for the Asian monsoon (Zhang et al. 2012). Furthermore, the models tended to show different combinations of changes in onset and retreat, with some models showing delayed onset and early retreat, some showing delayed onset and delayed retreat, and a number of them showing various changes over land compared to over sea. The combined results were such that the majority of the models produced shortened duration, particular in the tropical Sumatra-Java and nearby waters.

Simple correlation analyses were conducted and results suggested that both ENSO and IOD play important roles in determining variations of the Australian monsoon onset and retreat dates. The extent of these influences varies significantly among the models. A number of models show very strong ENSO-like SST correlation patterns, but this feature is not shared by others. A large number of the models have IOD-like SST correlation patterns, with positive IOD-like patterns being associated with delayed monsoon onset. As shown in Fig. 5.23b, this linkage is reflected by the correlations of IOD with 850 hPa wind, with weakened zonal westerlies over the tropical eastern Indian Ocean and Sumatra-Java region, which are not favorable for monsoon onset.

Under a global warming scenario, the mean SST warming in the pre-monsoon season has a positive IOD-like pattern in a large proportion of the models, with the warming over the eastern tropical Indian Ocean near Sumatra-Java area being relatively weaker than in the west (Fig. 5.23a). This is consistent with studies suggesting that global warming could be in favor for the development of more positive IODs (e.g., Cai et al. 2009a). Most models produced zonal easterly anomalies in the region that are consistent with the effects of a weakened upward branch of the tropical Walker circulation (Vecchi and Soden 2007; Power and Kociuba 2011) and positive IOD-like induced circulation anomalies in the east Indian Ocean (Guan et al. 2003, and refer to Fig. 5.23b). This appears to be one of the reasons that the models show a delayed onset and shortened duration. Although the study by Jourdain et al. (2013) showed very limited impacts of IOD on summer season rainfall totals, our analysis suggests an important role of Indian Ocean SSTs on the development of the monsoon.

Several studies have assessed the likely changes to climate extremes in the Australian monsoon region. In their study, Kitoh et al. (2013) calculated several precipitation indices from modeled daily rainfall data to describe the potential changes in the monsoon rainfall extremes, such as the precipitation daily intensity index (defined as the total precipitation divided by the number of days with precipitation greater than or equal to 1 mm), seasonal maximum five day precipitation total (the seasonal maximum precipitation total in five consecutive days), and seasonal maximum consecutive dry days (defined as the seasonal maximum number

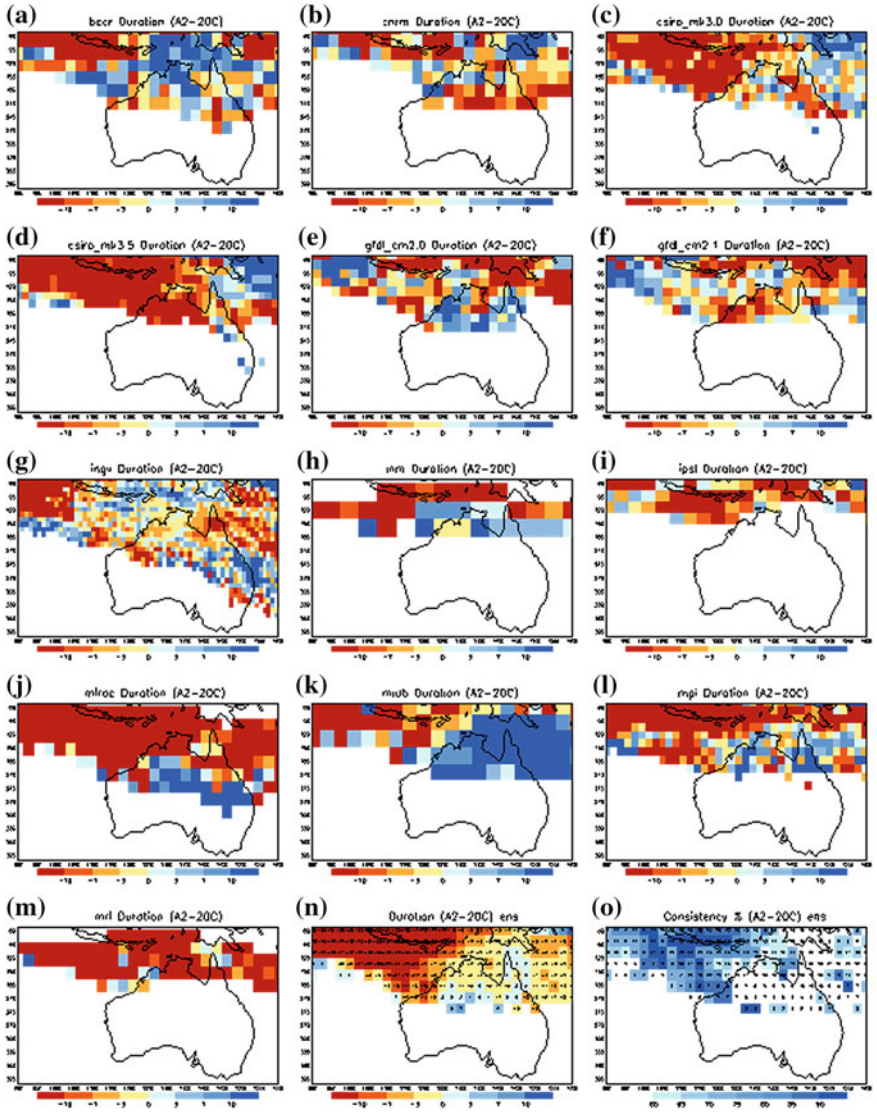

Fig. 5.22 **a**–**m** changes in Australian monsoon onset (*unit* days) between the model 20 year A2 (2081–2100) and 20C3 M simulations. **n** 13-model ensemble results after re-gridding the model data into common 2.5° × 2.5° resolution; **o** consistency (%) measured by the percentage of the number of models that simulated the same sign as the ensemble changes that are derived from all the models simulating changes in monsoon onset at each grid. Detailed model references can be found in Zhang et al. (2013)

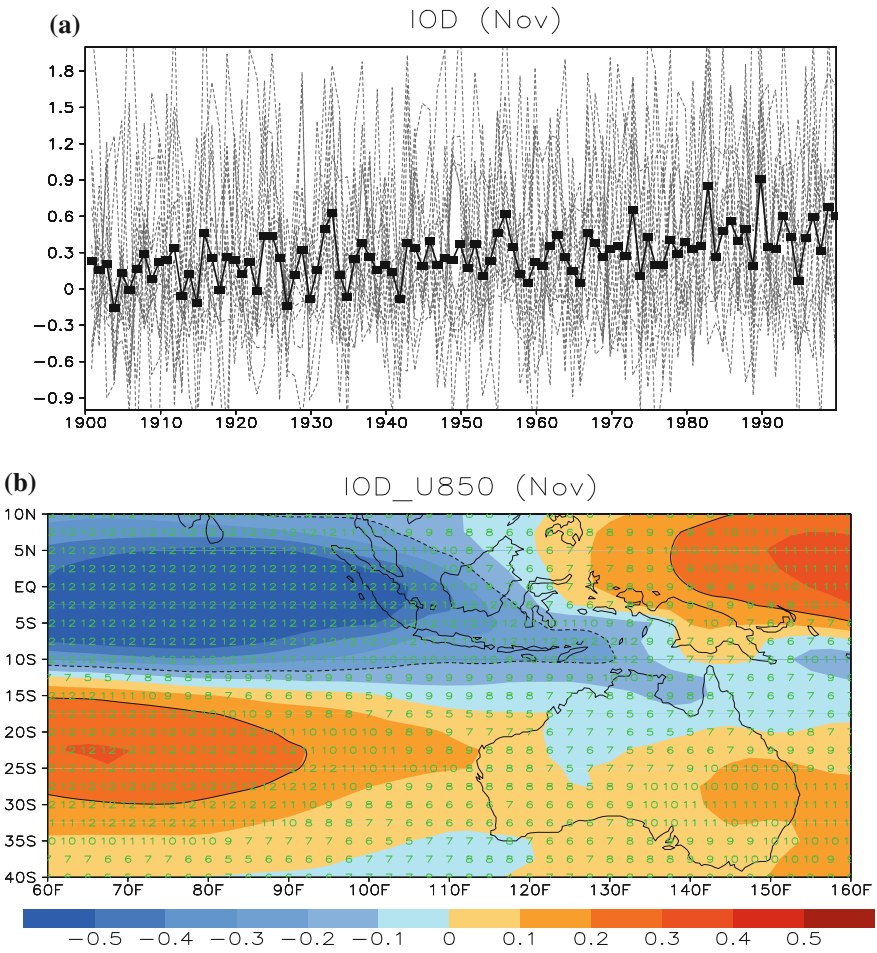

Fig. 5.23 **a** Changes in monthly Indian Ocean Dipole index simulated by the 13 CMIP3 models during the 100 year 20C3 M and A2 simulations in Zhang et al. (2013); **b** averaged IOD and U850 correlations in November from the 13 CMIP3 model 20C3 M experiment. Digital numbers give the total number of models showing the same sign of the averaged values

of consecutive dry days with precipitation <1 mm). Over the Australian monsoon domain (land only), associated with a slight increase in seasonal rainfall total, the precipitation daily intensity index and the seasonal rainfall maximum all showed increases in the majority of the CMIP5 models, together with consecutive dry days showing a slight decrease. In the analysis of CMIP3 models in Zhang et al. (2013), although they found that the monsoon duration was shortened overall, they found the total precipitation within the period between onset and retreat was in fact increased; they attributed this to the increases in the rainfall extremes. Results from the precipitation regime sorting analysis of Moise et al. (2012) also showed that a

warmer climate induced decreased numbers of deep convections, but increased precipitation intensity for such convections. All these studies likely suggest more frequent occurrences of heavy rainfall extremes during the monsoon season under global warming, largely caused by the increased atmospheric moisture content that can partially offset the effect of circulation weakening.

5.6 Conclusions

We have structured this chapter around three key goals: (1) to document the observed features of the Australian monsoon; (2) to assess how well the current climate models can reproduce these fundamental features; and (3) to summarize current projections of its potential changes in future and primary processes leading to such changes. Although brief discussions have been made about some synoptic features of the monsoon system and the skill from an Australian operational model in forecasting its activities at intra-seasonal to seasonal time scales, the primary focus of this chapter has been on the documentation of the climatic features of the Australian monsoon.

We acknowledge that within this chapter, we have not been able to address *all* the aspects of the monsoon climate, nor have we summarized results from *all* the published studies on the Australian monsoon climate. The IPCC scientific assessment reports have also included specific statements on the monsoon system, while in this chapter we have expanded the scientific background supporting such statements in detail and focused on discussing the underlying processes. The information presented in this chapter can be summarized as follows:

(1) The Australian summer monsoon, as the counterpart of the Asian monsoon in the Northern Hemisphere, covers a spatial domain encompassing the tropical Sumatra and Java Islands and the adjacent waters in the west, extending south and eastward into the Timor and Timor Sea region and further penetrating into the tropical Australian continent. It has pronounced seasonal variations of rainfall and prevailing winds, with its austral summer season (DJFM) rainfall accounting for more than half of the annual totals. This is mainly supported by the reversal of easterly trade winds into deep and moist westerlies. The development of the monsoon system shows coherent features in time and space, with its onset progressing in a northwest-southeast orientation. In this chapter we did not break it down further into more detailed geographic domains, such as the Maritime Continent monsoon and western Pacific monsoon, although there are some different features over these regions associated with localized land-sea contrast and topographic effects.

(2) The Australian monsoon has remarkable variations at a wide range of time scales. Its onsets are influenced by a number of factors, with recent studies suggesting that the MJO is the primary trigger, although the contributions from land-sea thermal contrast, the influence of middle latitude systems, and

the atmospheric instability cannot be ignored. MJO appears to be the strongest mode of the intra-seasonal variations of the tropical Australian monsoon. The inter-annual variations of the monsoon onset are correlated to ENSO but the total summer monsoon rainfall is not. This is partially attributed to the seasonally varying air-sea interactions over the waters north of the Australian continent. On a longer time scale, increases in summer rainfall have been observed in the northwest of the tropical Australian continent, while rainfall declined in the northeast part until late last century. The role of Asian aerosol and the warming of tropical SSTs near the continent have been used in explaining such trends.

(3) Based on the analyses of fully coupled global climate model simulations in the CMIP3 and 5 experiments, we have shown that the broad features of the monsoon mean climate, its seasonal and inter-annual variations of rainfall, temperature, and circulation, can be reasonably reproduced by a majority of the models, but there are tremendous variations in individual model skill. Some of the models overestimated rainfall in the monsoon region, with the atmosphere too convective, precipitation too intense, and the monsoon shear line too southward, while there are also models showing the opposite. The offsetting errors in these models result in a remarkable agreement between the multi-model ensemble averages and observations, but such an agreement must be viewed carefully when assessing the overall performance of the current models.

(4) The relevant importance of the primary large-scale drivers governing the monsoon variations differs significantly across current climate models, with some models having too strong an ENSO influence, while in others the ENSO influence is very weak. IOD has no discernible impacts on the inter-annual variations of the summer monsoon rainfall total in the models, but its impacts on variations of the monsoon onset can be significant in the model simulations.

(5) While significant warming over the monsoon region is simulated by all the models with the increased atmospheric greenhouse gas concentrations, there is much uncertainty in model projections of the changes in the monsoon rainfall. Multi-model ensemble averages tend to suggest a weak change in mean rainfall, but this is mostly produced accompained by large model discrepancies, with the number of the models showing likely increases in rainfall being matched by roughly the same number of the models showing decreased rainfall. How to best address the uncertainty in such modeled results is a key task for the climate change projection in the monsoon region. One way is to select a few models with good skill in reproducing the observed mean climate and its variations. Using this approach, results tend to suggest a slightly weakened Australian summer monsoon circulation but a slight increase in monsoon rainfall due to the increases in the atmospheric moisture conditions. Associated with the increases in atmospheric moisture content with warmed climate, models also tend to show the increased likelihood of extreme monsoon rainfall events. There is no consensus on the changes in the Australian

monsoon onset/retreat, with studies using rainfall in defining the monsoon onset, suggesting that the onset comes earlier. However, for the studies using circulation as one of the criteria, they showed a possible delay due to the weakening and shifting of the atmospheric circulation and various SST warming patterns in the tropical oceans.

Future progress to improve the modeling skill and increase our confidence of the projection of the Australian monsoon relies on a number of key aspects: (1) the improved model physics and dynamics. There are a number of significant challenges ahead, such as improving the rainfall diurnal cycle in the models over the land and ocean and reducing the systematic modeling errors over the maritime continent, which have regional and global consequence; (2) improved representations of key drivers of the monsoon system, such as realistic ENSO and IOD and the presentation of MJO in the climate models; and (3) improved understanding of the model discrepancies and how to best represent such uncertainty in the projected changes in the monsoon climate.

Acknowledgments The authors thank Drs. Rob Colman and Ian Smith for their very thoughtful and detailed comments and suggestions during the internal review process. We also thank Dr. Wenju Cai of the CSIRO Marine and Atmospheric Research for encouraging us to contribute this chapter. Part of the research was conducted with the support of the Australian Climate Change Science Program (ACCSP) Monsoon Project. Dr. F. Delage of CAWCR provided Fig. 5.11. Collaborations with Dr. Ping Liang and Mr. Guangtao Dong of Shanghai Regional Climate Centre, Dr. Ying Xu, and Dr. Cunjie Zhang of the National Climate Center of China Meteorological Administration are also acknowledged.

References

Adler RF, Huffman GJ, Chang A, Ferraro R, Xie P, Janowiak J, Rudolf B, Schneider U, Curtis S, Bolvin D, Gruber A, Susskind J, Arkin P, Nelkin E (2003) The Version 2 Global Precipitation Climatology Project (GPCP) Monthly Precipitation Analysis (1979-Present). J Hydrometeor 4:1147–1167

Behera SK, Luo JJ, Masson S, Rao SA, Sakuma H, Yamagata T (2006) A CGCM study on the interaction between IOD and ENSO. J Clim 19:1688–1705

Berry GJ, Reeder MJ, Jakob C (2012) Coherent synoptic disturbances in the Australian monsoon. J Clim 25:8409–8421

Bony S, Dufresne JL, Treut HL, Morcrette JJ, Senior C (2004) On dynamic and thermodynamic components of cloud changes. Clim Dyn 22:71–86. doi:10.1007/s00382-003-0369-6

Brown JR, Colman RA, Moise AF, Smith IN (2013) The western Pacific monsoon in CMIP5 models: Model evaluation and projections. J Geophys Res 118:12458–12475

Cai W, Cowan T, Sullivan A (2009a) Recent unprecedented skewness towards positive Indian Ocean Dipole occurrences and its impact on Australian rainfall. Geophys Res Lett 36:L11705. doi:10.1029/2009GL037604

Cai W, Sullivan A, Cowan T (2009b) Rainfall teleconnections with Indo-Pacific variability in the WCRP CMIP3 models. J. Climate 22:5046–5071

Cai W, Cowan T, Sullivan A (2009c) Climate change contributes to more frequent consecutive positive Indian Ocean Dipole events. Geophys Res Lett 36:L23704

Chan JCL, Li CY (2004) The East Asian winter monsoon, in East Asian Monsoon. In: Chang C-P (ed), World scientific series on meteorology of East Asia, vol. 2. World Scientific, pp 54–106
Chadwick R, Boutle I, Martin G (2013) Spatial patterns of precipitation change in CMIP5: Why the rich don't get richer in the tropics. J Clim 26:3803–3822
Chang CP (2004) East Asian Monsoon. World Scientific, 564 pp
Chang CP, Krishnamurti TN (eds) (1987) Monsoon meteorology. Oxford University Press, Oxford, 544 pp
Chang CP, Erickson JE, Lau KM (1979) Northeasterly cold surges and near- equatorial disturbances over the winter MONES area during Dec. 1974. Part I: Synoptic aspects. Mon Wea Rev 107:812–829
Chang C-P, Ding Y, Lau N-C (eds) (2011) The global monsoon system: research and forecast. World Scientific, 594 pp
Chen T-C, Yen M-C (1991) Intraseasonal variations of the tropical easterly jet during the 1979 northern summer. Tellus 43A:213–225
Cherchi A, Alessandri A, Masina S, Navarra A (2011) Effects of increased CO_2 levels on monsoons. Clim Dyn 37:83–101
Christensen JH, Krishna Kumar K, Aldrian E, An S-I, Cavalcanti IFA, de Castro M, Dong W, Goswami P, Hall A, Kanyanga JK, Kitoh A, Kossin J, Lau N-C, Renwick J, Stephenson DB, Xie S-P, Zhou T (2013) Climate phenomena and their relevance for future regional climate change. In: Stocker TF, Qin D, Plattner G-K, Tignor M, Allen SK, Boschung J, Nauels A, Xia Y, Bex V, Midgley PM (eds) Climate change 2013: the physical science basis. Contribution of Working Group I to the Fifth assessment report of the intergovernmental panel on climate change. Cambridge University Press, Cambridge, United Kingdom and New York, NY, USA
Collins, M., Knutti R, Arblaster J, Dufresne J-L, Fichefet T, Friedlingstein P, Gao X, Gutowski WJ, Johns T, Krinner G, Shongwe M, Tebaldi C, Weaver AJ, Wehner M (2013) Long-term climate change: projections, commitments and irreversibility. In: Stocker TF, Qin D., Plattner GK, Tignor M, Allen SK, Boschung J, Nauels A, Xia Y, Bex Y, Midgley PM (eds) Climate change 2013: the physical science basis. Contribution of Working Group I to the Fifth assessment report of the intergovernmental panel on climate change. Cambridge University Press, Cambridge, United Kingdom and New York, NY, USA
Colman RA, Moise AF, Hanson LI (2011) Tropical Australian climate and the Australian monsoon assimulated by 23 CMIP3 models. J Geophys Res 116:D10116. doi:10.1029/2010JD015149
CSIRO and Bureau of Meteorology (2007) Climate Change in Australia: Technical Report, 140 pp., http://www.climatechangeinaustralia.gov.au
CSIRO and Bureau of Meteorology (2012) State of the climate 2012. 12 pp., http://www.csiro.au/Outcomes/Climate/Understanding/State-of-the-Climate.aspx
Davidson NE, McBride JL, McAvaney BJ (1983) The onset of the Australian monsoon during winter MONEX: synoptic aspects. Mon Weather Rev 111:496–516
Dee DP, Uppala SM, Simmons AJ, Berrisford P, Poli P, Kobayashi S, Andrae U et al (2011) The ERA-Interim reanalysis: configuration and performance of the data assimilation system. Q J R Meteorol Soc 137(656):553–597
Ding YH (1994) Monsoons over China. Kluwer Academic Publisher, Dordrecht, Boston, London 419 pp
Drosdowsky W (1996) Variability of the Australian Summer Monsoon at Darwin: 1957–1992. J. Climate 9:85–96
Drosdowsky W, Chambers LE (2001) Near global sea surface temperature anomalies as predictors of Australian seasonal rainfall. J. Climate 14:1677–1687
Drosdowsky W, Wheeler MC (2014) Predicting the onset of the north Australian wet season with the POAMA dynamical prediction system. Wea Forecast 29:150–161
Flato G, Marotzke J, Abiodun B, Braconnot P, Chou SC, Collins W, Cox P, Driouech F, Emori S, Eyring V, Forest C, Gleckler P, Guilyardi E, Jakob C, Kattsov V, Reason C, Rummukainen M (2013) Evaluation of climate models. In: Stocker TF, Qin D, Plattner G-K, Tignor M,

Allen SK, Doschung J, Nauels A, Xia Y, Bex V, Midgley PM (eds) Climate change (2013) The physical science basis. Contribution of Working Group I to the Fifth assessment report of the intergovernmental panel on climate change. Cambridge University Press, Cambridge, pp 741–882

Frederiksen Carsten S, Frederiksen Jorgen S (1996) A theoretical model of Australian Northwest Cloudband Disturbances and Southern Hemisphere Storm Tracks: The Role of SST Anomalies. J Atmos Sci 53:1410–1432

Guan Z, Ashok K, Yamagata T (2003) Summertime response of the tropical atmosphere to the Indian Ocean Dipole sea surface temperature anomalies. J. Meteo. Soci. Jpn 81:533–561

Guilyardi E, Wittenberg A, Fedorov A, Collins M, Wang C, Capotondi A, Van Oldenborgh G, Stockdale T (2009) Understanding El Nin˜o in ocean—atmosphere general circulation models. Bull Am Meteorol Soc 90:325–340

Hendon HH, Liebmann B (1990) A composite study of onset of the Australian summer monsoon. J Atmos Sci 47:2227–2240

Hendon HH, Zhang C, Glick JD (1999) Interannual variation of the Madden–Julian oscillation during austral summer. J. Climate 12:2538–2550

Hendon HH, Lim E, Wheeler MC (2011) Seasonal prediction of Australian summer monsoon rainfall. In: Chang C-P, Ding YH, Lau N-C, Johnson N-C, Wang B, Yasunari T (eds) The global monsoon system: research and forecast, (2nd edn). World Scientific Series on Asia-Pacific Weather and Climate, vol 5, pp 73–84

Holland Greg J (1986) Interannual variability of the Australian Summer Monsoon at Darwin: 1952–82. Mon Wea Rev 114:594–604

Hoskins B (2012) The potential for skill across the range of the seamless weather climate prediction problem: a stimulus for our science. Q J Roy Meteorol Soc 139:573–584

Hsu PC, Li T, Luo JJ, Murakami H, Kitoh A, Zhao M (2012) Increase of global monsoon area and precipitation under global warming: a robust signal? Geophys Res Lett 39:L0670

Hudson D, Alves O, Hendon HH, Marshall AG (2011) Bridging the gap between weather and seasonal forecasting: intraseasonal forecasting for Australia. Q J Roy Meteorol Soc 137:673–689. doi:10.1002/qj.769

Hung C, Yanai M (2004) Factors contributing to the onset of the Australian summer monsoon. Q J Roy Meteor Soc 130(597):739–758

Intergovernmental Panel on Climate Change (IPCC) (2007) Climate Change 2007: the physical science basis. Contribution of Working Group I to the Fourth assessment report of the IPCC. In: Solomon S et al (eds) Cambridge Univ. Press, Cambridge, UK

Intergovernmental Panel on Climate Change (IPCC) (2013) Climate Change 2013: the physical science basis. Contribution of Working Group I to the Fifth Assessment Report of the IPCC. In: Stocker et al (eds) Cambridge Univ. Press, Cambridge, UK

Irving DB, Whetton P, Moise AF (2012) Climate projections for Australia: a first glance at CMIP5. Aust Meteorol Oceanogr J 62:211–225

Jones DA, Wang W, Fawcett R (2009) High-quality spatial climate data-sets for Australia. Aust Meteorol Oceanogr J 58:233–248

Jourdain NC, Sen Gupta A, Taschetto AS, Ummenhofer CC, Moise AF, Ashok K (2013) The Indo-Australian monsoon and its relationship to ENSO and IOD in reanalysis data and the CMIP3/CMIP5 simulations. Clim Dyn 41:3073–3102

Kalnay E, Kanamitsu M, Kistler R, Collins W, Deaven D, Gandin L, IredellM Saha S, WhiteG Woollen J et al (1996) TheNCEP/NCAR 40 year reanalysis project. Bull Am Meteorol Soc 77:437–472

Kawamura R, Fukuta Y, Ueda H, Matsuura T, Iizuka S (2002) A mechanism of the onset of the Australian summer monsoon. J Geophys Res 107:D14. doi:10.1029/2001JD001070

Kennedy JJ, Rayner NA, Smith RO, Saunby M, Parker DE (2011) Reassessing biases and other uncertainties in sea-surface temperature observations measured in situ since 1850 part 2: biases and homogenisation. J Geophys Res 116:D14104. doi:10.1029/2010JD015220

Kitoh A, Endo H, Krishna Kumar K, Cavalcanti IFA, Goswami P, Zhou T (2013) Monsoons in a changing world regional perspective in a global context. J Geophys Res Atmos 118. doi:10.1002/jgrd.50258

Klingaman N, Woolnough S, Syktus J (2012) On the drivers of inter-annual and decadal rainfall variability in Queensland, Australia. Int J Climatol. ISSN 0899-8418 doi:10.1002/joc.3593

Kripalani RH, Oh JH, Kulkarni A, Sabade SS, Chaudhari HS (2007) South Asian summer monsoon precipitation variability: Coupled climate model simulations and projections under IPCC AR4. Theor Appl Climatol 90:133–159

Lau WKM, Waliser DE (eds) (2005) Intraseasonal variability of the atmosphere-ocean climate system. Springer, Heidelberg, p 474

Lau WKM, waliser de (eds) (2011) intraseasonal variability of the atmosphere-ocean climate system, 2nd edn. Springer, Heidelberg, p 613

Lee J-Y, Wang B (2014) Future change of global monsoon in the CMIP5, Clim Dyn 42:101–119

Lee J-Y, Wang B (2012) Future change of global monsoon in the CMIP5. Clim Dyn 42:101–119, doi: 10.1007/s00382-012-1564-0

Li J, Feng J, Li Y (2012) A possible cause of decreasing summer rainfall in northeast Australia Int JClimatol 32: 995–1005, doi:10.1002/joc.2328

Li J, Zeng Q (2003) A new monsoon index and the geographical distribution of the global monsoons. Adv Atmos Sci 20:299–302

Lin Z, Li Y (2012) Remote influence of the tropical Atlantic on the variability and trend in north west Australia summer rainfall. J Clim 25:2408–2420

Li X-F, Yu J, Li Y (2013) Recent summer rainfall increase and surface cooling over Northern Australia since the Late 1970s: a response to warming in the tropical western pacific. J Clim 26 (18):7221–7239

Lin J-L et al (2008) Subseasonal variability associated with asian summer monsoon simulated by14 IPCC AR4 Coupled GCMs. J. Clim 21:4541–4567

Lo F, Wheeler MC, Meinke H, Donald A (2007) Probabilistic forecasts of the onset of the north Australian wet season. Mon Wea Rev 135:3506–3520

Luo Jing-Jia, Zhang Ruochao, Behera Swadhin K, Masumoto Yukio, Jin Fei-Fei, Lukas Roger, Yamagata Toshio (2010) Interaction between El Niño and Extreme Indian Ocean Dipole. J Clim 23:726–742

Madden RA, Julian PR (1971) Detection of a 40–50 day oscillation in the zonal wind in the tropical Pacific. J Atmos Sci 28:702–708

Madden RA, Julian PR (1972) Description of global-scale circulation cells in the tropics with a 40–50 day period. J Atmos Sci 29:1109–1123

Marshall AG, Hudson D, Wheeler MC, Hendon HH, Alves O (2011) Assessing the simulation and prediction of rainfall associated with the MJO in the POAMA seasonal forecast system. Clim Dyn 37:2129–2141

Marshall AG, Hudson D, Wheeler M, Alves O, Hendon HH, Pook MJ, Risbey JS (2013) Intra-seasonal drivers of extreme heat over Australia in observations and POAMA-2. Clim Dyn. doi:10.1007/s00382-013-2016-1

McBride JL, Nicholls N (1983) Seasonal relationships between Australian rainfall and the Southern Oscillation. Mon Wea Rev 111:1998–2004

Meehl GA, Covey C, Delworth T, Latif M, McAvaney B, Mitchell JFB, Stouffer RJ, Taylor KE (2007) The WCRP CMIP3 multimodel dataset. Bull Amer Meteor Soc, 88(9):1383–1394

Moise AF, Colman RA, Zhang H, and Participating CMIP2 modeling groups (2005) Coupled Model Simulations of Current Australian Surface Climate and Its Changes under Greenhouse Warming: An Analysis of 18 CMIP2 Models, Australian Met Mag, 54, 4

Moise AF, Colman RA, Brown JR (2012) Behind uncertainties in projections of Australian tropical climate: Analysis of 19 CMIP3 models. J Geophys Res 117:D10103. doi:10.1029/2011JD017365

Moron V, Robertson AW, Boer R (2009) Spatial coherence and seasonal predictability of monsoon onset over Indonesia. J Clim 22:840–850

Nicholls N (1981) Air-sea interaction and the possibility of long-range weather prediction in the Indonesian Archipelago. Mon Wea Rev 109:2435–2443

Nicholls N, McBride JL, Ormerod RJ (1982) On predicting the onset of the Australian west season at Darwin. Mon Wea Rev 110:14–17

Peatman SC, Mattews AJ, Stevens DP (2013) Propagation of the Madden–Julian Oscillation through the Maritime Continent and scale interaction with the diurnal cycle of precipitation. Q J R Meteorol Soc. doi:10.1002/qj.2161

Pope M, Jakob C, Reeder MJ (2009) Regimes of the North Australian wet season. J Clim 22:6699–6715

Power SB, Kociuba G (2011) What caused the observed twentieth-century weakening of the walker circulation? J Clim 24:6501–6514

Power SB, Delage F, Colman R, Moise A (2012) Consensus on 21st century rainfall projections in climate models more widespread than previously thought. J Clim 25:3792–3809. doi:10.1175/JCLID-11-00354.1

Randall DA, Wood RA, Bony S, Colman R, Fichefet T, Fyfe J, Kattsov V et al (2007) Cilmate models and their evaluation. In: Climate change 2007: the physical science basis. Contribution of working Group I to the fourth assessment report of the intergovernmental panel on climate change. Cambridge University Press, Cambridge, United Kingdom and New York

Rauniyar SP, Walsh KJE (2011) Scale interaction of the diurnal cycle of rainfall over the Maritime Continent and Australia: Influence of the MJO. J Clim 24:325–348

Risbey JS, Pook MJ, McIntosh PC, Wheeler MC, Hendon HH (2009) On the remote drivers of rainfall variability in Australia. Mon Weather Rev 137:3233–3253

Rienecker MM, Suarez MJ, Gelaro R, Todling R, Bacmeister J, Liu E, Bosilovich MG et al (2011) MERRA: NASA's modern-era retrospective analysis for research and applications. J Clim 24 (14):3624–3648

Rotstayn LD, Cai WJ, Dix MR, Farquhar GD, Feng Y, Ginoux P, Herzog M, Ito A, Penner JE, Roderick ML, Wang M (2007) Have Australian rainfall and cloudiness increased due to the remote effects of Asian anthropogenic aerosols? J Geophys Res Atmos 112 (D9, D09202). doi:10.1029/2006JD007712

Rotstayn LD, Jeffrey SJ, Collier MA, Dravitzki SM, Hirst AC, Syk-tus JI, Wong KK (2012) Aerosol- and greenhouse gas-induced changes in summer rainfall and circulation in the Australasian region: a study using single-forcing climate simulations. Atmos Chem Phys 12:6377–6404. doi:10.519/acp-12-6377-2012

Rudolf B, Becker A, Schneider U, Meyer-Christoffer A, Ziese M (2011) New Full Data Reanalysis Version 5 provides high-quality gridded monthly precipitation data. GEWEX News, Vol. 21, No. 2, 4–5

Saha S (2010) The NCEP Climate Forecast System Reanalysis. Bull. Amer Meteor Soc 91(8), 1015–1057 (DOI: 10.1175/2010BAMS3001.1)

Saji B, Goswami N, Vinayachandran PN, Yamagata T (1999) A dipole mode in the tropical Indian Ocean. Nature 401:360–363

Shi G, Cai W, Cowan T, Ribbe J, Rotstayn L, Dix M (2008) Variability and trend of north west Australia rainfall: Observations and coupled climate modeling. J Clim 21:2938–2959

Smith I, Moise A, Katzfey J, Nguyen K, Colman R (2013) Regional-scale rainfall projections: Simulations for the New Guinea region using the CCAM model. J Geophys Res Atmos 118:1271–1280, doi:10.1002/jgrd.50139

Smith I (2004) An assessment of recent trends in Australian rainfall. Aust Meteor Mag 53:163–173

Smith IN, Wilson L, Suppiah R (2008) Characteristics of the northern Australian rainy season. J Clim 21:4298–4311

Smith IN, Moise AF, Colman RA (2012) Large-scale circulation features in the tropical western Pacific and their representation in climate models. J Geophys Res 117:D04109. doi:10.1029/2011JD016667

Sumi A, Murakami T (1981) Large-scale aspects of the 1978–1979 winter circulation over greater MONEX region, Part I: monthly and season mean fields. J Meteor Soc Jpn 59:625–645

Suppiah R, Collier MA, Rotstayn LD, Syktus JI, Wong KK (2013) Simulated and projected summer rainfall in tropical Australia: links to atmospheric circulation using the CSIRO Mk3.6 climate model. Aust Meteorol Oceanogr J 63:15–26

Taschetto AS, Haarsma RJ, Sen Gupta A, Ummenhofer CC, England MH (2010) Teleconnections associated with the intensification of the Australian monsoon during El Niño Modoki events. IOP Conf. Series: Earth and Environmental Science, 11: 012031, doi:10.1088/1755-1315/11/1/012031

Taylor KE, Stouffer RJ, Meehl GA (2012) An overview of CMIP5 and the experiment esign. Bull Am Meteorol Soc 93(4):485–498

Trenberth KE, Stepaniak DP, Caron JM (2000) The global monsoon as seem through the divergent atmospheric circulation. J. Clim 13:3969–3993

Troup AJ (1961) Variations in upper tropospheric flow associated with the onset of the Australian summer monsoon. Indian J Meteorol Geophys 12:217–230

Taschetto AS, Sen Gupta A, Hendon HH, Ummenhofer CC, England MH (2011) The contribution of Indian Ocean sea surface temperature anomalies on Australian summer rainfall during El Niño events. J Clim 24(14):3734–3747

Turner AG, Annamalai H (2012) Climate change and the South Asian summer monsoon. Nat Clim Change 2:587–595

Ueda H, Iwai A, Kuwako K, Hori ME (2006) Impact of anthropogenic forcing on the Asian summer monsoon as simulated by eight GCMs. Geophys Res Lett 33. doi:10.1029/2005gl025336

Ummenhofer CC, England MH, McIntosh PC, Meyers GA, Pook MJ, Risbey JS, Gupta AS, Taschetto AS (2009) What causes southeast Australia's worst droughts? Geophys Res Lett 36: L04706. doi:10.1029/2008GL036801

Vecchi GA, Soden BJ (2007) Global warming and the weakening of the tropical circulation. J Clim 20:4316–4340. doi:10.1175/JCLI4258.1

Wang B (2006) The Asian monsoon. Springer, Heidelberg 787 pp

Wang B, LinHo (2002) Rainy season of the Asian-Pacific summer monsoon. J Clim 15:386–398

Wang B, Ding QH (2008) Global monsoon: dominant mode of annual variation in the tropics. Dyn Atmos Oceans 44:165–183

Wang B, Kim HJ, Kikuchi K, Kitoh A (2011) Diagnostic metrics for evaluation of annual and diurnal cycles. Clim Dyn 37:941–955

Wang B, Liu J, Kim H-J, Webster PJ, Yim S-Y, Xiang B (2013) Northern Hemisphere summer monsoon intensified by mega-El Niño/southern oscillation and Atlantic multidecadal oscillation. PNAS 110(14):5347–5352. doi:10.1073/pnas.1219405110

Wang B, Zhang Y, Lu M-M (2004) Definition of South China Sea Monsoon Onset and Commencementof the East Asia Summer Monsoon. J Clim 17: 699–710

Watterson IG (2012) Understanding and partitioning future climates for Australian regions from CMIP3 using ocean warming indices. Clim Change 111:903–922

Watterson IG (2013) Climate change simulated by full and mixed-layer ocean versions of CSIRO Mk3.5 and mk3.0: the Asia-Pacific region. Asia Pac J Atmos Sci 49:287–300

WCRP (2005) The world climate research programme strategic framework 2005–15. WCRP-123, WMO/TD-No.1291. World Meteorological Organization: Geneva

Wheeler M, McBride JL (2005) Australian-indonesian monsoon region. In: Lau KM, Waliser DE (eds) Intraseasonal variability of the atmosphere-ocean climate system. Springer, Heidelberg

Wheeler M, McBride JL (2011) Australasian monsoon. In: Lau WKM, Waliser DE (eds) Intraseasonal variability in the atmosphere-ocean climate system. Springer, Berlin, 646 pp

Wheeler MC, Hendon HH (2004) An all-season real-time multivariate MJO index: Development of an index for monitoring and prediction. Mon Wea Rev 132:1917–1932

Wheeler MC, Hendon HH, Cleland S, Meinke H, Donald A (2009) Impacts of the Madden–Julian oscillation on Australian rainfall and circulation. J Clim 22:1482–1498

Xavier PK (2012) Intraseasonal convective moistening in CMIP3 models. J Clim 25:2569–2577

Xie P, Arkin PA (1997) Global precipitation: a 17 year monthly analysis based on gauge observations, satellite estimates, and numerical model outputs. Bull Am Meteorol Soc 78 (11):2539–2558

Yeh S-W, Kug J-S, Dewitte B, Kwon M-H, Kirtman BP, Jin F-F (2009) El Niño in a changing climate. Nature 461:511–514

Yim S-Y, Wang B, Liu J, Wu Z (2014) Regional monsoon indices, Climate Dynamics (in press)

Zeng X, Lu E (2004) Globally unified monsoon onset and retreat indexes. J Clim 17:2241–2248

Zhang H (2010) diagnosing Australia-Asian monsoon onset/retreat using large-scale wind and moisture indices. Clim Dyn 35:601–618

Zhang CJ, Zhang H (2010) Potential impacts of east Asian winter monsoon on climate variability and predictability in the Australian summer monsoon region. Theor Appl Climatol. doi:10.1007/s00704-009-0246-2

Zhang H, Henderson-Sellers A, Irannejad P, Sharmeen S, Phillips T, McGuffie K (2002) Land-surface modelling and climate simulations: results over the Australian region from sixteen AMIP2 models. Bureau of Meteorology Research Centre Report, No. 89

Zhang H, Liang P, Moise A, Hanson L (2012) Diagnosing potential changes in Asian summer monsoon onset and duration in IPCC AR4 model simulations using moisture and wind indices. Clim Dyn 39:2465–2486

Zhang H, Moise A, Liang P, Hanson L (2013) The response of summer monsoon onset/retreat in Sumatra-Java and tropical Australia region to global warming in CMIP3 models. Clim Dyn 40:377–399

Zhang H, Dong G, Moise A, Colman R, Hanson L, Smith I, Liang P, Ye H (2014) The onset, duration and intensity of the Australian monsoon in 26 CMIP5 models, Climate Dynamics (to be submitted)

Chapter 6
The South American Monsoon System (SAMS)

Leila Maria Véspoli de Carvalho and Iracema F.A. Cavalcanti

Abstract The South American Monsoon System (SAMS) is the most important climatic feature of the continent. It provides water resources for millions of people living in rural and urban areas, and is a dominant control on both agriculture and on hydroelectric power generation, which is the primary source of electricity in South America. SAMS exhibits variations on a broad range of scales, which further depend on complex multi-system interactions, feedback and teleconnections. Global warming plays a major role in modifying monsoonal circulations and coupled modes of variability in the tropics and extratropics, with potential to alter the SAMS characteristics. South America has been experiencing progressive warming that may critically impact the continent's hydrological cycle. This chapter reviews the main characteristics of the SAMS and discusses observational and modeling studies investigating ongoing and future projections of climatic changes.

Keywords South american monsoon system · South atlantic convergence zone · CMIP5 simulations · Precipitation · Climate change · Global warming

L.M.V. de Carvalho (✉)
Department of Geography, University of California, Santa Barbara, CA, USA
e-mail: leila@eri.ucsb.edu

L.M.V. de Carvalho
Earth Research Institute, University of California, Santa Barbara, CA, USA

I.F.A. Cavalcanti
Climate Prediction and Weather Forecast Center, National Institute of Space Research (CPTEC/INPE), Cachoeira Paulista, Brazil
e-mail: iracema.cavalcanti@cptec.inpe.br

© Springer International Publishing Switzerland 2016

L.M.V. de Carvalho and C. Jones (eds.), *The Monsoons and Climate Change*,
Springer Climate, DOI 10.1007/978-3-319-21650-8_6

6.1 Introduction

The dominant climatic feature of tropical South America is the pronounced seasonal change in precipitation and moisture that accompanies variations in the trade winds, diabatic heating, surface pressure, thermodynamic instability, cross-equatorial moisture transport, low-level convergence and upper-level divergence of mass in the atmosphere (Fig. 6.1). Unlike other monsoon systems that exhibit pronounced differences in seasonal mean wind direction, easterly winds dominate all year over northern South America and the tropical Atlantic. For this reason, it was not until the end of the twentieth century that this climatic feature was finally recognized as a monsoon. It has since been observed that when the annual mean is removed from the winter and summer mean circulation, a clear reversal in the low-level circulation monthly anomalies becomes evident and resembles the seasonal change in the wind

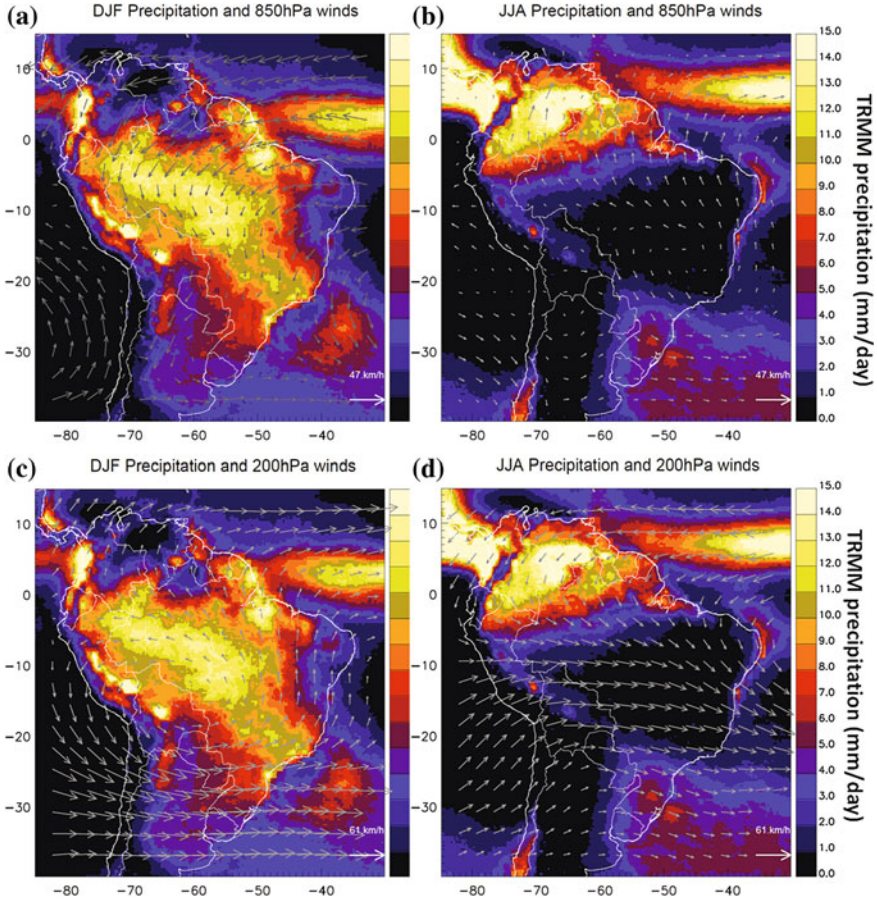

Fig. 6.1 TRMM mean daily precipitation and 850 hPa winds in DJF (**a**) and JJA (**b**); TRMM mean daily precipitation and 200 hPa winds in DJF (**c**) and JJA (**d**)

direction observed in other monsoon systems (Zhou and Lau 1998). SAMS is currently regarded as one of the most important monsoon systems in the world.

Other characteristic features of the SAMS are an upper tropospheric anticyclone located approximately over the Bolivian Altiplano (Fig. 6.1), known as the Bolivian High (Silva Dias et al. 1983), the stretching of the atmospheric column and conversion of low-level potential energy into upper-level divergent kinetic energy, and the interaction between divergent and rotational winds at the upper level that transform divergent kinetic energy into rotational kinetic energy (Wang and Fu 2002). Additional distinctive features are the Northeast Trough (Silva Dias et al. 1983; Lenters and Cook 1997, 1999), the low-level Gran-Chaco Low (Gandu and Silva Dias 1998), the northerly low-level jet (LLJ) east of the Andes (Marengo et al. 2004), and the South Atlantic Convergence Zone (SACZ) (Kodama 1992).

Differential heating between South America and the Atlantic Ocean is the main driver of the SAMS seasonal cycle. The considerable expanse of South American landmass within tropical latitudes, adjoined by the South Atlantic to the east and the Andes, (the world's longest continental mountain range with an average elevation of 4,000 m) to the west, combine to create and maintain this powerful monsoon engine (Fu et al. 1999; Fu et al. 2001; Fu and Li 2004; Rickenbach et al. 2011).

The South Atlantic Convergence Zone (SACZ) is the SAMS's unique and most important component. Characterized by persistent cloudiness and northwest-southeast oriented precipitation (Fig. 6.1), the SACZ results from low-level convergence of winds and moisture transport from the Amazon toward the subtropical South Atlantic Ocean (Kodama 1992; Liebmann et al. 1999; Liebmann et al. 2001; Carvalho et al. 2002b; Carvalho et al. 2004; Nieto Ferreira and Chao 2013). The SACZ activity is largely modulated by transient disturbances (Nogues-Paegle and Mo 1997; Liebmann et al. 1999; Nogues-Paegle et al. 2000; Cunningham and Cavalcanti 2006) and precipitation on its oceanic portion is frequently disassociated from convection over the continent (Carvalho et al. 2004, 2011a; Muza et al. 2009). The SACZ variability and change strongly affect the climate of southeastern South America, one of the most densely populated areas of the continent.

The life cycle of the SAMS has been investigated with multiple approaches and data sets. Of particular interest is the determination of the onset, duration and demise of the monsoon. Given the numerous distinct methods and/or variables that have been proposed to identify the monsoon cycle, it is not uncommon to find discrepancies among results. For instance, in early studies using outgoing longwave radiation (OLR) as a proxy for precipitation and convection (Kousky 1988; Horel et al. 1989), the identification of the onset and demise of the wet season was subject to the chosen OLR threshold in each method.

Liebmann and Marengo (2001) proposed a new methodology to determine the SAMS onset and demise based on the time-variability of the integral of daily increments of the seasonal precipitation anomalies (annual mean removed) between two dry seasons. According to this method, the wet season at a particular location begins when the increments become positive and ends when they become negative. The onset and demise dates of the wet season may vary by a few days, depending on the criterion used to smooth the resulting incremental integral (Bombardi and

Carvalho 2009). Moreover, it can be successfully applied only in locations with a pronounced seasonal cycle of rainfall. Bombardi and Carvalho (2009) applied this methodology to the Global Precipitation Climatology Project (GPCP) 5-day average (pentad) data and found that the median onset of the monsoon over central and central-eastern Brazil is between mid-October and early November.

Other methods have been developed to describe the large-scale life cycle of the SAMS. Gan et al. (2004) defined the onset (demise) of the wet season as the date for which rainfall is above (below) 4 mm/day for at least 75 % of the subsequent pentads and the first occurrence of 850 hPa westerly (easterly) winds at 60°W and 10–20°S latitudes. Gan et al. (2006) investigated four indices to determine the onset, demise, and intra-seasonal variations of the monsoon over central-west Brazil. They suggested that indices based on low-level circulation (850 hPa) are more efficient for these purposes in comparison to similar indices obtained with precipitation. Other methods incorporated multiple variables that describe the monsoon cycle according to Zhou and Lau (1998). Silva and Carvalho (2007) proposed a multivariate index based on combined empirical orthogonal function analysis (CEOF) of precipitation, specific humidity, and low-level atmospheric circulation anomalies (long-term mean removed) to describe the large-scale characteristics of SAMS. This index, named Large-scale Index for South American Monsoon (LISAM), is continuous in time and exhibits variations on synoptic to multi-annual time scales (Carvalho et al. 2011a; Carvalho et al. 2011b). Raia and Cavalcanti (2008) applied a different criterion, based on the atmospheric humidity flux over an area recognized as the monsoon core, where the zonal wind reverses and humidity exhibits pronounced seasonal variability between winter and summer. This method shows less variability in the onset and demise dates compared to Silva and Carvalho (2007) and Gan et al. (2004). In spite of the differences in methodologies, there is a general consensus that the mean onset of the wet season over the Brazilian High Plains is between mid-October and mid-November, with some regional differences (Nieto-Ferreira and Rickenbach 2011). The peak of monsoonal precipitation is between December and February and its withdrawal occurs between March and April.

The SAMS and SACZ exhibit complex interactions and feedback with the land-surface, biosphere, and oceans that result in variations on a broad range of spatial and temporal scales. Like other monsoon systems, SAMS undergoes persistent active and inactive ("break") periods in the intensity of rainfall that accompany changes in low-level circulation and moisture transport and affect the characteristics and diurnal cycles of convective systems over tropical South America (Carvalho et al. 2002a; Cifelli et al. 2002; Herdies et al. 2002; Jones and Carvalho 2002; Petersen et al. 2002; Liebmann et al. 2004a; Carvalho et al. 2011b). Tropical intra-seasonal oscillations (i.e., oscillations roughly between 20 and 100 days), which are sometimes associated with the Madden-Julian Oscillation (MJO) (Madden and Julian 1994), control these alternating wet and dry periods (Liebmann et al. 2004a, b; Carvalho et al. 2004; Jones and Carvalho 2002). Similarly, the variability of the SACZ is largely modulated by oscillations on subseasonal time scales that depend on tropical-extratropical interactions (Casarin and Kousky 1986; Nogues-Paegle and Mo 1997; Liebmann et al. 1999; Carvalho et al. 2004; Cunningham and Cavalcanti 2006; Muza et al. 2009; Carvalho et al. 2011b). An

important feature emerging from the SACZ variability is the well-documented dipole ("seesaw") in precipitation and circulation between southeastern Brazil and southern Brazil, Uruguay-northeastern Argentina. This pattern has been associated with the propagation of mid-latitude wave trains east of South America that modify circulation and moisture transport in the tropics and subtropics (e.g., Carvalho et al. 2004; Liebmann et al. 1999; Nogues-Paegle and Mo 1997).

Most of the explained inter-annual variability of the SAMS precipitation comes from the El Niño Southern Oscillation (ENSO) (Nogues-Paegle and Mo 2002; Grimm 2003, 2004, 2011; Marengo et al. 2012), with impacts that vary throughout the monsoon season (Grimm et al. 2007; Grimm and Zilli 2009). These variations suggest that regional surface-atmosphere interactions compete with remote influences during the wet season (Grimm et al. 2007). Land-surface and land-cover processes also impact inter-annual variations of the SAMS (Collini et al. 2008; Ma et al. 2011). Moreover, there is evidence that ENSO modulates the intensity and position of the SACZ and the occurrence of extreme precipitation along the southeast coast of Brazil (Liebmann et al. 2001; Carvalho et al. 2002b).

The tropical South Atlantic also plays a significant role in the inter-annual variability of the SAMS's and the SACZ's precipitation (Venegas et al. 1997; Robertson and Mechoso 2000; Robertson et al. 2003; De Almeida et al. 2007; Taschetto and Wainer 2008; Bombardi et al. 2014). Cold (warm) sea surface temperature (SST) anomalies over the tropical South Atlantic along with warm (cold) SST anomalies over the extratropical South Atlantic have been associated with early (late) onsets (Bombardi and Carvalho 2011) and increased (decreased) total daily precipitation over southeastern Brazil (Misra 2008; Bombardi et al. 2014). Modeling studies have suggested significant ocean-atmosphere feedback over the southwestern tropical Atlantic acting upon the organization of the SACZ (Chaves and Nobre 2004; Misra 2008). The SAMS's variability on multi-annual to decadal time scales is less known, largely due to limited observations in the Amazon Basin and surrounding areas. Krishnamurthy and Misra (2010) found two modes of the SAMS variability on decadal time scales that suggest associations with the Atlantic Multidecadal Oscillation (AMO) and the Pacific Decadal Oscillation (PDO). Moreover, instrumental data and sediment records have shown evidence of the early 1970s climate shift affecting SAMS (Robertson and Mechoso 1998; Piovano et al. 2002; Carvalho et al. 2011a; Jacques-Coper and Garreaud 2014).

Assessing, attributing and quantifying the effects of increased global CO_2 levels on future changes in the SAMS's hydrological cycle is critical for the future of water resources in South America, but problematic for various reasons. The variability of the SAMS and the SACZ depends on complex interactions of phenomena on a broad range of scales, and multiple approaches are necessary to properly identify and predict future changes. Precipitation regimes vary on regional-to-local scales, imposing limits on projected climate change scenarios. The sparseness of observations and their relatively short records are among the major obstacles to recognizing and characterizing climatic changes in South America. In addition, land-ocean-atmosphere interactions are not completely understood and remain poorly represented in climate models. In spite of these difficulties, recent studies

have considerably advanced our understanding of climate change in the SAMS. The following sections present some of the recent results regarding observed trends and future projections based on climate modeling.

6.2 Observed Changes in the SAMS

There is compelling evidence that the total monsoon precipitation has increased globally in the past 30 years as a response to the increase in the global mean surface temperature (Hsu et al. 2011). It is argued that the expansion of the monsoon regions occurs primarily at their poleward edges, between 20°–30° north and south. The Climate Forecast System Reanalysis (CFSR) (Saha et al. 2010) and the National Center for Environmental Prediction/National Center for Atmospheric Research (NCEP/NCAR) Reanalysis-1 (Kalnay et al. 1996) indicate a progressive increase in low-level tropospheric temperatures over tropical South America, more specifically over eastern Brazil (Fig. 6.2) during the monsoon season. These trends can potentially alter ocean-land differential heating and thus the monsoonal circulation and moisture transport from the tropics to the subtropics.

Liebmann et al. (2004b) investigated seasonal linear trends of precipitation from rain gauges and gridded rainfall and found an increase in the number of days with precipitation and in the amount of precipitation per event south of 20°S during the January-February season. Additionally, recent studies (Dufek and Ambrizzi 2008; Teixeira and Satyamurty 2011; Silva Dias et al. 2012; Marengo et al. 2013; Pinto et al. 2013; Skansi et al. 2013; Raimundo et al. 2014) found positive trends in the frequency of heavy and extreme rainfall events in southern and southeastern Brazil. All of these findings seem consistent with Hsu et al. (2011) hypotheses. It is also worth mentioning, however, that a large number of rain gauge stations that are considered in these studies are located near or within large urban centers. The effect of the growth of the cities on changes in the diurnal cycle of precipitation is difficult to evaluate and to separate from other signals (Kalnay and Cai 2003).

Long-term changes in total and extreme rainfall in South America between 1960 and 2000 (Haylock et al. 2006) reveal a general pattern that somewhat agrees with Liebmann et al. (2004b) and Hsu et al. (2011): increase in precipitation (total and extremes) in Ecuador and northern Peru and the region of southern Brazil, Paraguay, Uruguay, and northern and central Argentina, whereas a decrease is observed over southern Peru and southern Chile. The authors argue that the spatial patterns of trends in the rainfall indices show similarities with ENSO teleconnection patterns over South America and suggest that a more negative Southern Oscillation Index (SOI) in the 1990s may have had an important effect on regional rainfall trends observed in that four-decade study. Nonetheless, the scarcity of precipitation indices investigated by Haylock et al. (2006) over central Brazil and in the Amazon limits the evaluation of trends over large portions of the SAMS' domain.

However, the attribution of the SAMS's observed trends to ENSO contradicts the findings of Zhou et al. (2011). These authors investigated trends in global

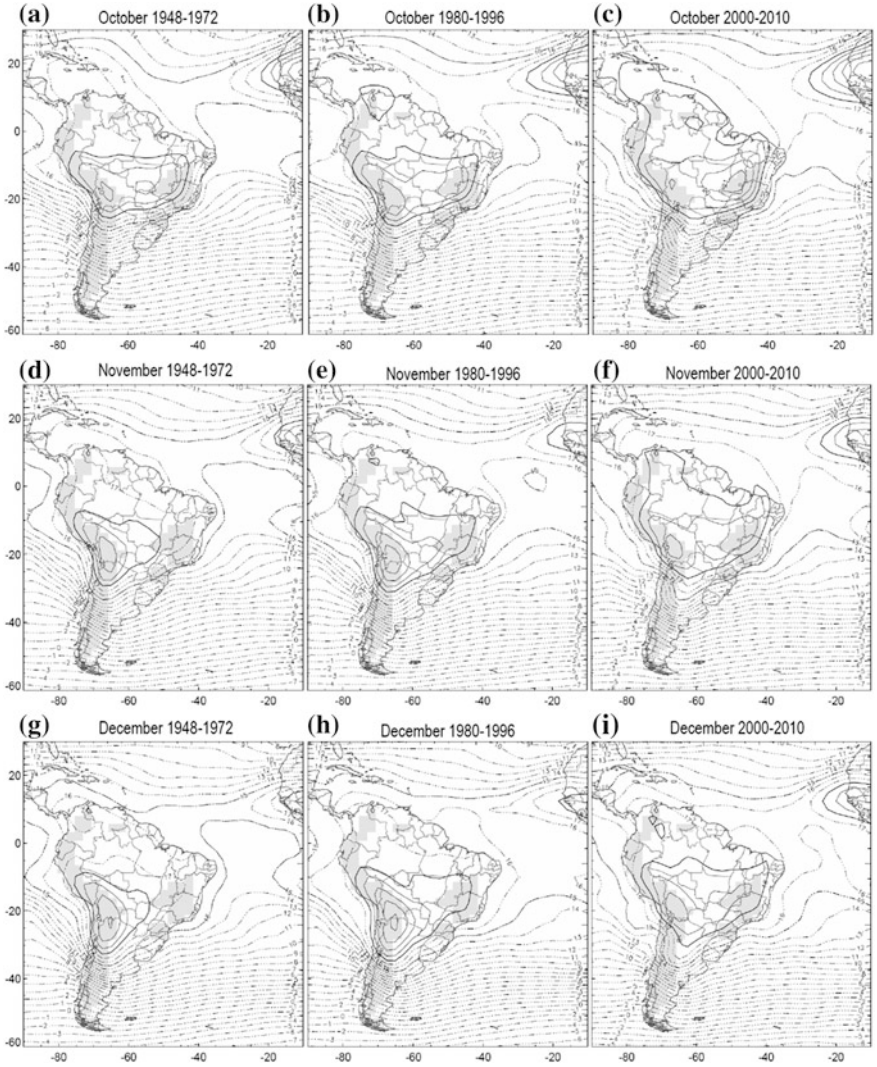

Fig. 6.2 Average temperatures at 850 hPa during three distinct periods: 1948–72 (**a**, **d**, **g**), 1980–96 (**b**, **e**, **h**), 2000–2010 (**c**, **f**, **i**) and for October (**a**, **b**, **c**), November (**d**, **e**, **f**) and December (**g** ,**h**, **i**). *Solid lines* show temperatures ≥18 °C. *Dashed lines* indicate temperatures <18 °C. The 18 and 15 °C isotherms are emphasized by *thick lines*. *Shades* indicate topography above 500 m. Data is obtained from the National Centers for Environmental Prediction/National Center for Atmospheric Research (NCEP/NCAR) reanalysis-1 (Kalnay et al. 1996)

precipitation using GPCP estimates from 1979 to 2007, after removing ENSO effects using regression based on the Niño 3.4 index. They found that the majority of tropical areas exhibit increasing trends in precipitation, and that these trends are pronounced in areas of enhanced convection, such as the Intertropical Convergence

Zone (ITCZ). Contrastingly, areas climatologically associated with suppressed precipitation exhibit decreasing trends in precipitation. This mechanism has been ubiquitously referred to as "the wet get wetter, and the dry get drier" (Held and Soden 2006). However, when land and oceans are considered separately, this hypothesis may fail or even reverse. Greve et al. (2014) investigated the strength of this paradigm by examining various datasets to identify the increase in aridity/humidity based on the relative deviation in precipitation (ΔP) and evaporation (ΔE), at the grid-box level, between 1948 and 1968 and 1985 and 2005. For South America, their results seem consistent with previous studies that have demonstrated the increase in dry conditions over central and eastern Brazil, a region also influenced by SAMS (wet gets drier), (e.g., Bombardi and Carvalho 2009) and the increase in precipitation over parts of the Amazon (wet gets wetter) and subtropical South America (Liebmann et al. 2004b; Jones and Carvalho 2013). These trends, which should continue into the future, are discussed in the following section.

Marengo (2009) examined rainfall and river indices over both the northern and southern Amazon to identify long-term trends in these variables. Most records were obtained between the early 1920s and 1995. Interestingly, this research concluded that in both sub-regions, the long-term variations characterized decadal to multi-decadal cycles (such as the PDO) rather than a long-term trend. Moreover, this study also shows that precipitation regimes in both regions are "out-of-phase." Nevertheless, different scenarios seem to emerge as more data, longer records, and larger areas are included in the analyses of trends in precipitation over South America.

Skansi et al. (2013) investigated a large network of stations over all of South America and found clear and significant wetting and intensified rainfall between 1950 and 2010. According to that study, the annual total precipitation averaged over the continent increased by about 92 mm in the last decade compared to the 1950s. This trend is observed alongside increasing trends in heavy precipitation events, particularly those exceeding the 95th percentile. Their study also shows that the region encompassing southeast South America (103 rain gauge stations) exhibited the highest rates of change in annual rainfall, followed by Amazonia (77 rain gauge stations). On the other hand, western South America (32 rain gauge stations) and northeast Brazil (30 rain gauge stations) experienced moderate and weak non-significant reductions in total precipitation, respectively. Similar trends are observed for several extreme precipitation indices. Interestingly enough, these results seem to agree with Greve et al. (2014).

These observational studies reveal, among other issues, how peculiar and complex the South American Monsoon is. Most importantly, SAMS exhibits precipitation characteristics and trends that differ from place to place despite similar radiative forcing. These aspects are difficult to assess with intermittent records and/or coarse resolution data. The following section investigates present and future changes in SAMS, based on climate modeling, highlighting relevant findings, and identifying existing challenges.

6.3 The SAMS in Model Simulations and Projections

As discussed before, the most remarkable characteristic of SAMS is the pronounced seasonal difference in precipitation and other atmospheric variables. Atmospheric Global Circulation Models (AGCMs) are capable of simulating these characteristics with varying degrees of skill. Examples of studies using AGCMs to investigate SAMS include, among others, Cavalcanti et al. (2002), who used the Center of Weather Forecasting and Climate Studies/Center for Ocean-Land-Atmospheric Studies model (CPTEC/COLA); Liebmann et al. (2007), who used ECHAM 4.5 to investigate the onset and end of the rainy season; and Kitoh et al. (2011), who used the Meteorological Research Institute (MRI) AGCM at varying resolutions. However, the AGCMs have systematic biases over South America, such as the deficits of rainfall in the Amazon and excessive rainfall in the SACZ. These atmospheric models are forced with prescribed observed SST boundary conditions and thus are not able to represent air-sea interactions. Chaves and Nobre (2004), using the CPTEC/COLA AGCM, demonstrated that South Atlantic SSTs influence SACZ intensity; they further hypothesized that cloud cover associated with the SACZ, in turn, reduce regional SST. This feedback explains the observed negative correlation between precipitation and SST where the SACZ persists.

Coupled ocean-atmosphere models, which are able to include air-sea interactions, have been used in global experiments such as the Coupled Model Intercomparison Project Phase 3(CMIP3), (Meehl et al. 2007). Results obtained from CMIP3 models were used in the Intergovernmental Panel on Climate Change (IPCC) Assessment Report (AR4) (Solman et al. 2013), following the Special Report on Emissions Scenarios (SRES) (Nakićenović 2000). There are four SRES families of emission scenarios in the AR4 that project global average surface temperature warming under varying degrees of anthropogenic influence in the twenty-first century: *A*1, *A*2, *B*1, and *B*2. The *A*1 scenario's key assumptions are rapid economic growth, a global population that reaches 9 billion in 2050 and then gradually declines, the quick spread of new and efficient technologies, and extensive social and cultural interactions worldwide. The *B*1 scenario projects a "convergent world with the same global population as in the *A*1 but with rapid changes in economic structures toward a service and information economy, reductions in materials intensity, and the introduction of clean and resource-efficient technologies. The *A*2 emission scenario assumes a very heterogeneous world. The underlying theme is the strengthening regional cultural identities with an emphasis on family values and local traditions, high population growth, and less concern for rapid economic development. The *B*2 scenario emphasis is on local solutions to economic, social, and environmental sustainability. It is again a heterogeneous world with less rapid, and more diverse technological change that depends on community initiative and social innovation to find local, rather than global solutions. These scenarios, which are frequently combined, represent the future levels of greenhouse gas emissions that are used to force climate models.

Studies of South American climate projections used mainly A1B (considered intermediate between A1 and B1) and A2 SRES scenarios. These simulations, characterizing the climate of the twentieth century (20C3 M experiments), generally available from 1960 to 2000, were used to evaluate climatological features including SAMS. The difference between January, February, and March (JFM) and July, August, and September (JAS) climatological precipitation was represented by most CMIP3 models, particularly the relatively high precipitation in JFM compared to JAS (Vera et al. 2006). However, only four out of seven CMIP3 models reproduced the SACZ configuration in JFM. It is known that the SACZ occurs more frequently during the mature stage of the SAMS, from December through February (DJF); therefore, we expect the identification of features related to this system in model simulations to improve during these months. In fact, the SACZ configuration in DJF was represented by nine out of ten CMIP3 models in Bombardi and Carvalho (2009). Regional models also reproduce climatic differences between DJF and June, July, and August (JJA) over South America (Chou et al. 2012; Solman et al. 2013).

Besides model's representations of the mean climatological differences between summer and winter and the SACZ, there are other critical aspects of the monsoon that need to be evaluated in simulations: the ability to realistically simulate the seasonal cycle of precipitation, the monsoon life cycle (onset, demise, and duration), precipitation intensity, and SAMS subseasonal-to-decadal variability. The skill of models in representing SAMS variability also depends on how they simulate the mechanisms associated with changes in the monsoon, such as tropical-extratropical interactions, intra-seasonal oscillations, ENSO and respective teleconnections, the Pacific Decadal Oscillation (PDO), and the Atlantic Dipole, among many other coupled modes (Bombardi and Carvalho 2011; Kim et al. 2012; Kim and Yu 2012; Gillett and Fyfe 2013; Polade et al. 2013).

The annual cycle of precipitation in the core of SAMS is very well represented in CMIP3 models (Bombardi and Carvalho 2009; Seth et al. 2010) and also in regional models forced with ensemble global climate models (Chou et al. 2012, Solman et al. 2013). Humidity flux plays an important role in the development and maturity of the SAMS, as it is linked to SAMS' life cycle and precipitation intensity (Wang and Fu 2002; Carvalho et al. 2011b). Gulizia et al. (2013) showed that 20 CMIP3 models were able to represent the dominant mode of vertically integrated moisture transport and patterns of humidity flux over South America. Regarding precipitation variability, a number of CMIP3 models were able to simulate the standard deviation of rainfall over South America in the early-to-mature stage (October, November, and December − OND) and mature-to-late stage of the monsoon cycle (January, February, and March—JFM), but with different intensities compared to observations (Vera and Silvestri 2009).

Variations and changes in the monsoon life cycle in model simulations depend on the criterion adopted to evaluate onset, duration, and demise and, to a large extent, the model's ability to realistically represent the monsoon's characteristics. Therefore, future projections of the onset, duration and demise of SAMS should be interpreted with caution. In general though, AGCMs simulate well the SAMS climatological onset and demise. One example is shown in Liebmann et al. (2007), who

used 24 members of ECHAM4.5 AGCM simulations to identify the onset and demise of the South American rainy season by applying the method that was discussed in Liebmann and Marengo (2001). The onset dates identified were close to the onset estimated with observed gridded precipitationin the southern Amazon, which for most purposes can be considered to be the core of SAMS. Seth et al. (2010) showed that the multi-model mean of nine CMIP3 models represented pre-monsoon (September, October, November—SON) and mature stage (DJF) precipitation reasonably well, but failed to simulate realistic precipitation intensities in the oceanic SACZ during DJF. Using the method of Liebmann and Marengo (2001), Bombardi and Carvalho (2009) showed that the onset dates of SAMS were reasonably well simulated by CMIP3 models in central Brazil, but the duration of the rainy season was overestimated over western South America and underestimated over central Brazil. Most importantly, that study identified a considerable discrepancy among CMIP3 models in representing the seasonal cycle over the northwest and northeast Amazon. These problems seem to result from the misrepresentation of the ITCZ and its seasonal cycle in some models, which is critical to assessing the hydrological cycle in these regions.

6.4 Monsoon Features in CMIP5 Models

The new generation of Global Climate Earth System Models, which include ocean-atmosphere coupling, ocean and atmosphere chemistry, ecosystems, dynamical vegetation, the carbon cycle, and other physical processes in the atmosphere and ocean, as well as improved parameterization schemes, have been used to simulate past and present climates (referred to as "historic runs," commonly referring to the 1950-2005 period), and to provide projections for future climate change. Results from these models were organized by the Coupled Model Intercomparison Project Phase 5 − CMIP5 (Taylor et al. 2012). The representation of the SAMS, and particularly its precipitation patterns, is markedly improved in results from CMIP5 compared to CMIP3.

As shown in Sect. 6.3, the main features of the SAMS, such as the differences between summer and winter precipitation, humidity, atmospheric circulation at low- and upper-levels, and moisture flux are generally well represented by models. For instance, the ensemble mean of five CMIP5 models (HadGEM2-ES—Jones et al. (2011); CSIRO—Rotstayn et al. (2010); IPSL—Dufresne et al. (2013); MRI—Yukimoto et al. (2012); and MIROC—Watanabe et al. (2011)) exhibits patters of precipitation over South America, during the summer and winter, that compare well with observations (Fig. 6.3). These CMIP5 models were chosen on account of their ability to represent summer precipitation over South America. Their ensemble mean indicates that in DJF, considered the peak of the SAMS, precipitation exceeding 4 mm/day covers large areas of tropical South America. However, maximum rainfall intensity is observed over central Brazil, south of the Amazon, approximately between 10–15°S and 55°W (Fig. 6.3c), indicating that the core with maximum precipitation is displaced southeastward relative to observations (Fig. 6.3a). Additionally, excessive

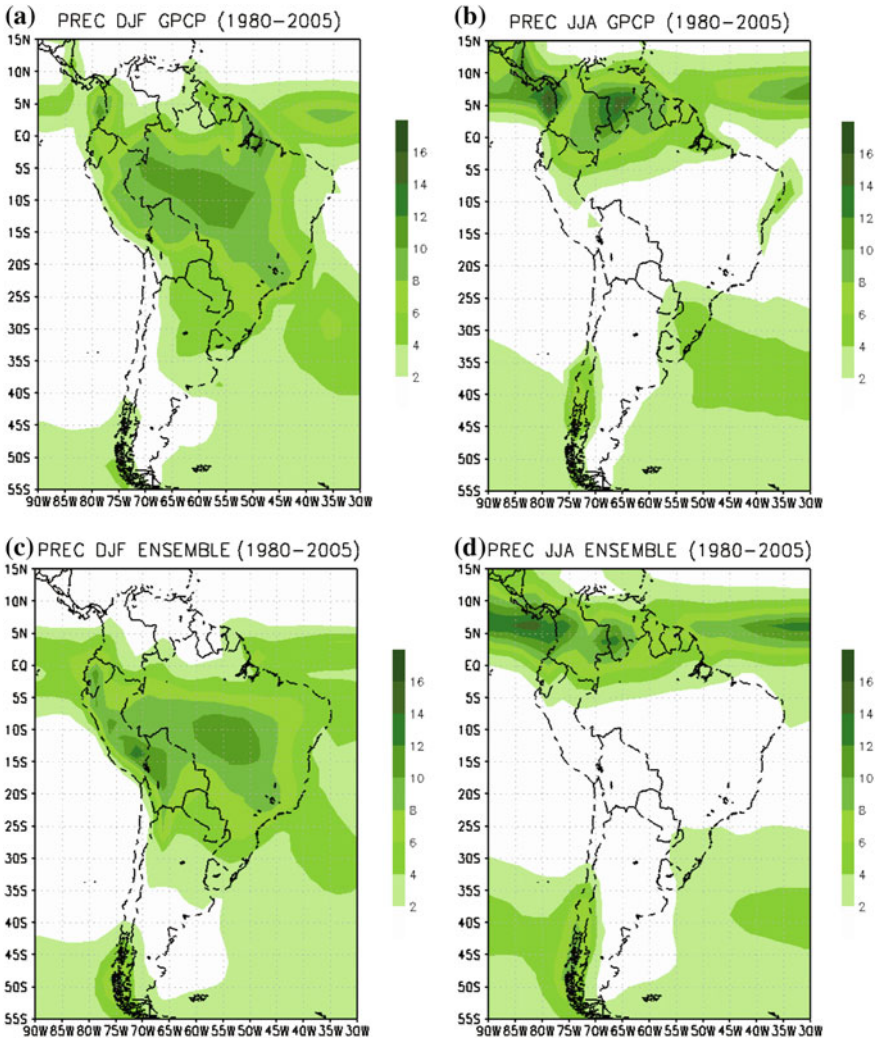

Fig. 6.3 Precipitation from **a**, **b** GPCP and **c**, **d** model ensemble [HadGEM2-ES, CSIRO, IPSL, MRI and MIROC], (1980–2005) for summer (DJF) and winter (JJA)

precipitation is simulated along the eastern slopes of the Peruvian and Bolivian Andes. Despite these issues, the elongated northwest-southeast band of precipitation extending from the Amazon basin toward the Atlantic Ocean, resembling the SACZ, is evident in the ensemble mean (Fig. 6.3c).

In JJA (Fig. 6.3b), following the seasonal cycle of solar radiation, areas of intense rainfall are positioned north of the Equator, and the location of their maxima, at approximately 5°N, indicates the region of enhanced convective activity in the Atlantic and Pacific ITCZ. These features in the models are remarkably realistic

when compared against observations (Fig. 6.3d). At this time, the wet season over land peaks over northwestern South America and Central America, and the average precipitation over the SAMS region is below 2.0 mm/day. Southern Brazil, Uruguay, and southern Chile do not exhibit similar seasonal differences. Although the ensemble seems to represent well the seasonal migration of convection over the continent and the displacement of the ITCZ, unrealistic excessive precipitation is observed over northeast Brazil in DJF, and there is indication of a "double ITCZ" in the Atlantic; both features are likely related. Furthermore, the models do not represent the observed precipitation over northeast Brazil in JJA, which indicates the ensemble's deficiency in representing the seasonal cycle of precipitation east of the Amazon, a problem that seems to persist with respect to CMIP3 models (e.g., Bombardi and Carvalho 2009). However, it is clear that the differences between summer and winter are well simulated by the ensemble (Fig. 6.4) as indicated by the areas where the magnitude of the differences equals or exceeds 2.5 mm/day, considered to be monsoon regions by Wang et al. (2011) and Kitoh et al. (2013).

It is also evident that the mean annual cycle of precipitationin the core of SAMS (65°W–55°W, 10°S–15°S), in the individual models and the ensemble mean, compares reasonably well with observed estimates from GPCP (Fig. 6.5), although, as noted earlier, the spatial extent of the core is smaller in the ensemble. December-March is the rainiest season, with precipitation above or equal to 9 mm/day, whereas June-August is the driest season, with precipitation less than or equal to 1 mm/day. Despite biases in the mean intensity of precipitation, the mean seasonal cycle is well captured by all models.

When considering the entire SAMS domain, the CMIP5 multi-model average precipitation resembles the observations; however, the onset of the monsoon appears earlier than in observations, as noted by Kitoh et al. (2013). This study also showed that extreme precipitationindices in the SAMS region were well simulated by the multi-model ensemble. However, the definition of the SAMS life cycle largely

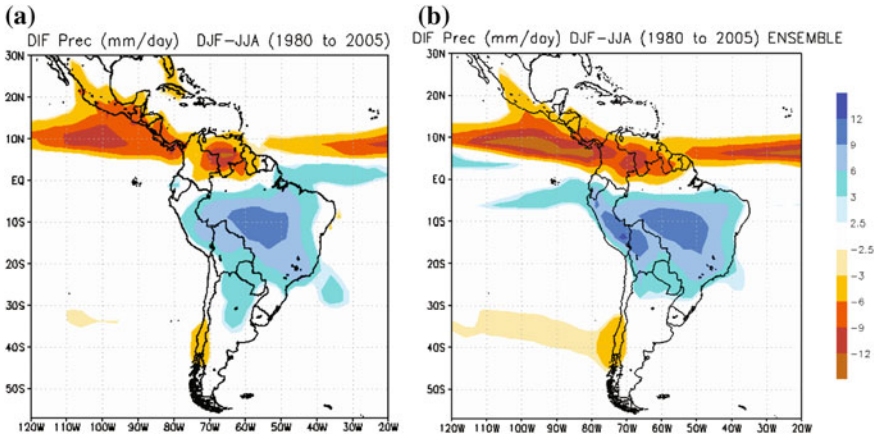

Fig. 6.4 Precipitation difference between the 2 seasons **a** GPCP, **b** model ensemble

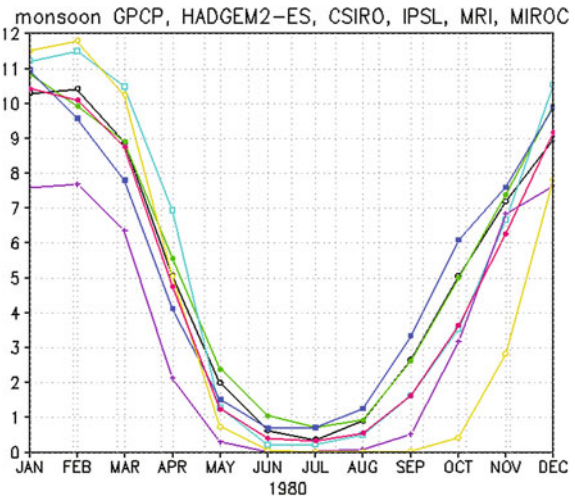

Fig. 6.5 Annual cycle of precipitation in the SAMS core. GPCP (*black line*), HadGEM2-ES (*blue line*), CSIRO (*green line*), IPSL (*yellow line*), MRI (*cyan line*), MIROC (*purple line*) and the ensemble (*red line*)

depends on the adopted methodology. Large-scale characteristics of SAMS's life cycle and amplitude in the CMIP5 models were investigated by Jones and Carvalho (2013). For this purpose, the authors calculated the Large-scale Index for the South American Monsoon (LISAM) (Silva and Carvalho 2007), explained in the introductory section of this chapter. LISAM is well correlated with precipitation over the core of the monsoon. CMIP5 model simulations for the historical run showed signals of climate change in South America that were consistent with reanalyses and indicated an overall intensification in the amplitude of SAMS and a multi-decadal trend of progressive early onsets and late demises in the climate of the twentieth century. It is worth noting that LISAM cannot properly characterize any location-shift that the core of the monsoon may have undergone during this time. Moreover, LISAM "onset" and "demise" refer to the entire monsoonal system (precipitation, circulation, moisture and temperature) and should be understood within this context.

In addition to the simulated increase in SAMS amplitude and duration, South America has experienced a dramatic warming of tropical regions in recent decades (Fig. 6.2). The increase of low-level (850 hPa) temperature and specific humidity between 1951 and 2005 (Fig. 6.2) were realistically simulated in most CMIP5 "historical runs." Of particular importance was the increase in area and magnitude of the 85th percentile of continental temperatures and specific humidity at 850 hPa in the last decade (1996–2005). The region that experienced the most pronounced warming was central-eastern Brazil. Among the factors that could explain this is the decrease in cloudiness, possibly associated with decreasing precipitation over this area and intensive land-use-cover-change (Carvalho and Jones 2013). This study also emphasizes the large discrepancy among models' simulations of daily mean precipitation during DJF over tropical South America. Some models simulate unrealistically excessive precipitation near the ITCZ, shifting the maxima north of central South America, where the core of monsoonal precipitation should be.

It is also evident that some models outperform others in representing the main characteristics of SAMS in the twentieth century. The appropriate evaluation of the skill of the model in reproducing SAMS should include a detailed examination of the main modes of variability driving SAMS's changes on a broad range of scales. As discussed in the introduction of this chapter, among SAMS's most important and characteristic features is a dipole of suppression and enhanced precipitation between southeastern Brazil and southern Brazil, Uruguay-northeastern Argentina that is frequently observed in association with SACZ variability. This "seesaw" has been associated with the Pacific South America (PSA) mode that explains patterns of teleconnections between the tropics and extratropics (Cunningham and Cavalcanti 2006). The simulations of CMIP5 HadgEM2-ES of South America's recent climate (1979–2004) indicate a good performance by the model in reproducing the main features of seasonal precipitation, temperature, and atmospheric circulation variability over South America. The model also reproduces the dipole in precipitation anomalies (Fig. 6.6) and respective teleconnections patterns (PSA, Fig. 6.7) that have been associated with subseasonal variability of the SACZ (Cavalcanti and Shimizu 2012). Moreover, this model simulates realistic monsoonal circulation, such as the cross equatorial low-level northerly winds over northern South America that turn southeastward as they encounter the Andes over central Brazil in DJF (see Fig. 6.1). The seasonal changes in wind from summer to winter over South America are also well simulated. During JJA southeasterly winds dominate over tropical South America as the South Atlantic Subtropical High intensifies and shifts westward during the winter. At upper levels, the Bolivian High and the Atlantic trough in DJF, as well as the westerlies over the continent in JJA, are also well simulated.

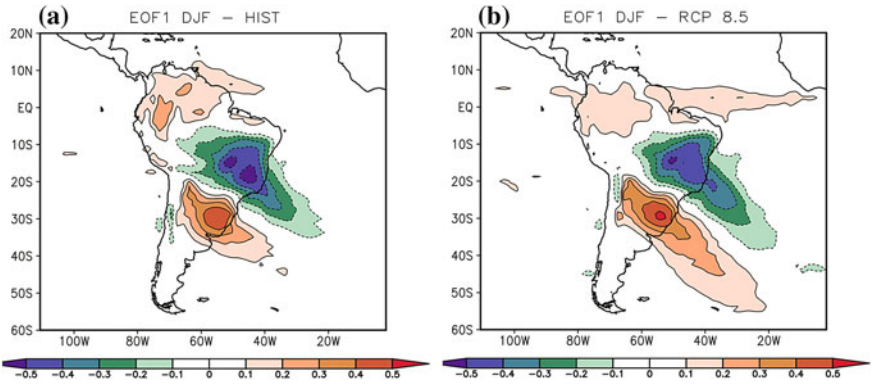

Fig. 6.6 First EOF of daily anomaly precipitation in DJF **a** HadGEM2-ES (1979–1980 to 2004–2005); **b** HadGEM2-ES (2073–2074 to 2098–2099). The seesaw pattern over southeastern South America and precipitation anomalies over northwestern South America with opposite sign of anomalies over southeastern Brazil are realistic features observed in the present climate associated with subseasonal variations in the SACZ (from Cavalcanti and Shimizu 2012)

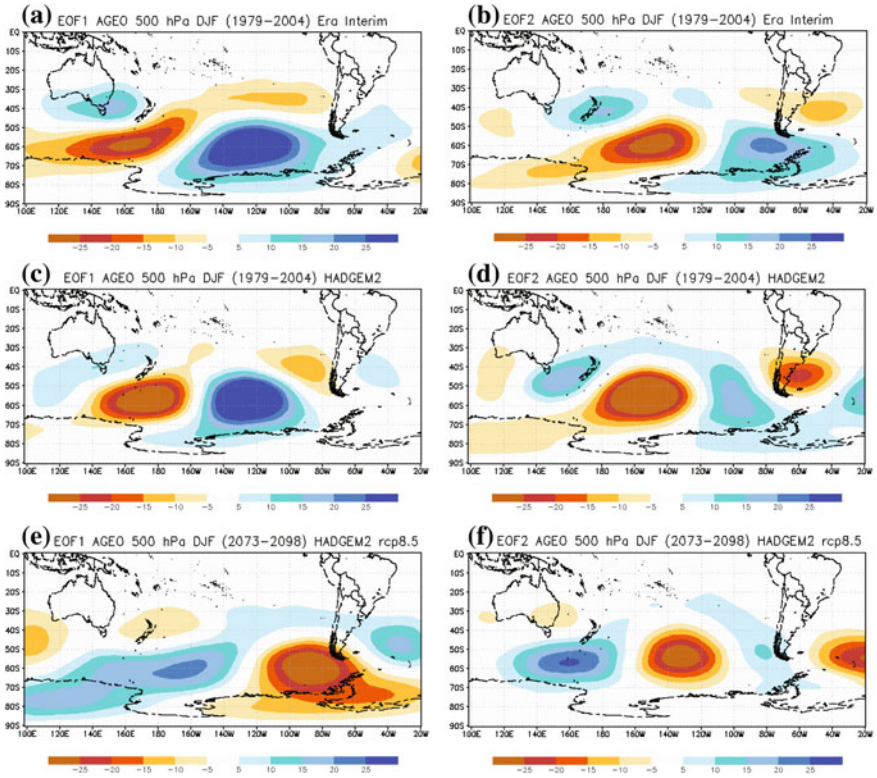

Fig. 6.7 EOF 1 (*first column*) and EOF2 (*second column*) of zonal asymmetric geopotential anomaly at 500 hPa (ERA-Interim (*top*), HadGEM2-ES (*middle*), (HadGEM2-RCP8.5 (*bottom*) associated with the dipole of precipitation shown in Fig. 6.6. Notice that the model reproduces the main observed PSA features in the present climate. PSA1 and PSA2 show an evolution of the tropical-extratropical wave train. In the future climate, the wave train is displaced eastward in PSA1, consistent with a warmer equatorial Pacific, and EOF2 displays a zonal wave train that is not typical of PSA (from Cavalcanti and Shimizu 2012)

The differences in precipitation over South America from winter to summer are associated with changes in wind flow and humidity, which are visible in vertically integrated moisture flux represented by the HadGEM2-ES model (Fig. 6.8c, d) and compared to ERA-Interim reanalysis (Fig. 6.8a, b). This model exhibits the best performance in representing the observed precipitation fields among the five CMIP5 models analyzed in the previous section. The cross-hemispheric flux of humidity from the tropical North Atlantic toward the Amazon, turning southeastward in DJF, and the seasonal reversal in JJA, characterized by moisture fluxes from the tropical South Atlantic toward the northwest and east Amazon, are well captured, although their magnitudes are overestimated.

The annual cycle of moisture transport at the Equator, calculated from ERA Interim reanalysis, is also well represented by HadGEM2-ES (Fig. 6.9a, b). From November

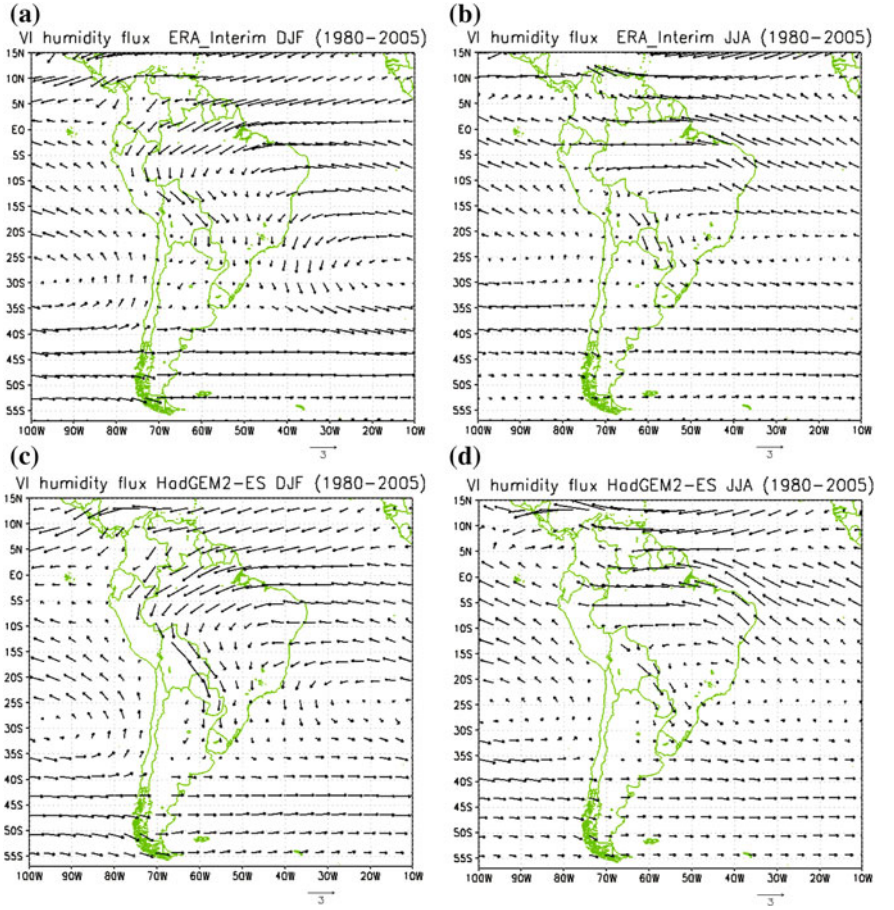

Fig. 6.8 Vertically integrated humidity flux **a**, **c** summer (DJF) and **b**, **d** winter (JJA). ERA Interim (*top*) and HadGEM2-ES (*bottom*)

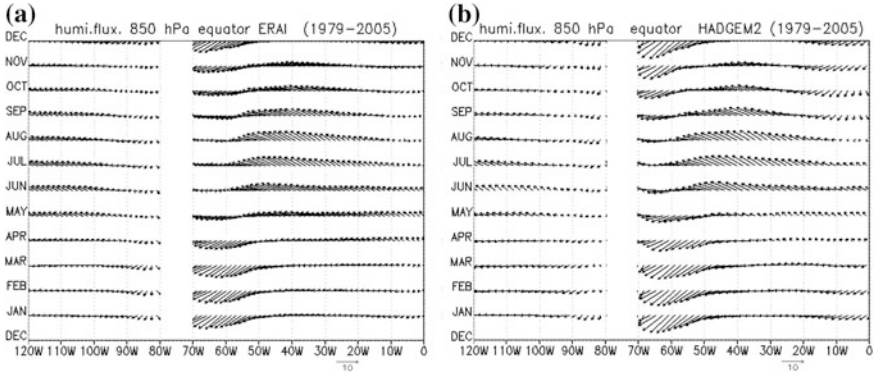

Fig. 6.9 Climatological annual cycle of 850 hPa humidity flux at the Equator **a** ERA Interim, **b** HadGEM2-ES

to April, northeasterly flux crosses northern South America, while from June to September, southeasterly flux crosses the Equator toward the North Atlantic Ocean. May and October are transition months, characterized by minimal moisture flux.

6.5 Climate Change Projections

In CMIP5 projections, future climate scenarios were characterized by their representative concentration pathway (RCP), determined by radiative forcing (Taylor et al. 2012). The rising radiative forcing pathway leading to 8.5 W/m^2 in 2100 is known as the RCP 8.5. It corresponds to the strongest global warming (and worst-case scenario) at the end of the century and has been investigated in several analyses. Figure 6.10 compares SAMS regions in projections (RCP 8.5) at the end of the twenty-first century (contour) and in the historical simulation (shaded blue) from the CMIP5 five-member ensemble discussed earlier in this chapter. The most striking features are the expansion of the SAMS area westward over the Pacific and eastward over the Atlantic, near the equator, and the southward shift of the oceanic SACZ toward subtropical latitudes. Smaller expanded areas in similar regions were obtained by Hsu et al. (2011) and Kitoh et al. (2013). Hsu et al. (2012) discussed the expansion of the Global Monsoon Area (GMA) and increased Global Monsoon Precipitation (GMP) in future climate projections using high resolution AGCMs, with SST derived from SRES-A1B CMIP3 models. Kitoh et al. (2013) confirmed these results and also identified this expansion in the CMIP5 RCP 8.5 scenario. Jones and Carvalho (2013), using the LISAM index, also discussed the expansion of the SAMS area in CMIP5 models. The positive trends in GMA and GMP from 1979 to 2008, found by Hsu et al. (2011) with observations, are believed to be related to the increase of moisture convergence and surface evaporation due to the thermodynamic effect resulting from global warming. These effects seem particularly important over

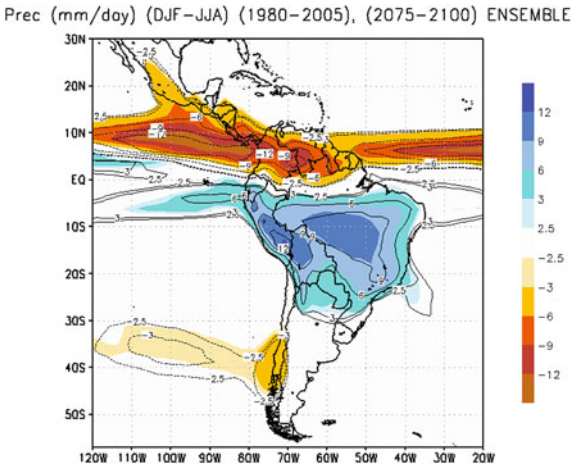

Fig. 6.10 Difference between summer and winter simulated during the 1980–2005 period (*shaded*) and projected during the 2075–2100 period (contour) for the ensemble of five CMIP5 models

South America (Carvalho and Jones 2013). Notice that the precipitation differences in the SAMS core in Fig. 6.10 does not change, but the maximum intensities are increased northeastward and southeastward.

Idealized experiments with a coupled ocean-atmosphere model subjected to increasing carbon dioxide show intensification of the precipitation difference between summer and winter in the global monsoon regions, including the SAMS region (Cherchi et al. 2011). Projections of precipitation extremes in the SAMS region by CMIP5 models indicate an increase in daily precipitation indices, such as the simple precipitation daily intensity index, maximum five-day total precipitation, and maximum consecutive dry days (Kitoh et al. 2013).

The difference (%) between future projections of precipitation in the RCP 8.5 scenario (2075–2100) and present simulations (1980–2005) in DJF, obtained with the same five CMIP5 ensemble mean, is shown in Fig. 6.11. The most dramatic differences are observed over the Amazon, in the Atlantic ITCZ, and oceanic SACZ. The ensemble difference indicates minimal precipitation change over SAMS's core (<5 %) and 10–20 % increases over the center of the La Plata Basin, southern Peru, Colombia, and parts of northeast Brazil. On the other hand, a reduction of around 40 % of DJF rainfall is projected over northern South America and Chile (Fig. 6.11a). The difference in humidity flux between the two periods shows an increase of moisture flux over the Amazon and toward southeastern South America in the future climate, consistent with the precipitation increase in that region (Fig. 6.11b). The pattern of precipitation change in DJF obtained from the five models is similar to that obtained from a larger subset of CMIP5 models for October to March and periods of 2081–2100 and 1986–2005, used in the IPCC Fifth Assessment Report (IPCC-AR5) (Fig. 6.12). The larger subset exhibits smaller percentage changes and up to 10 % precipitation reduction in the central-north Amazon. The hatched areas identify regions where the changes are

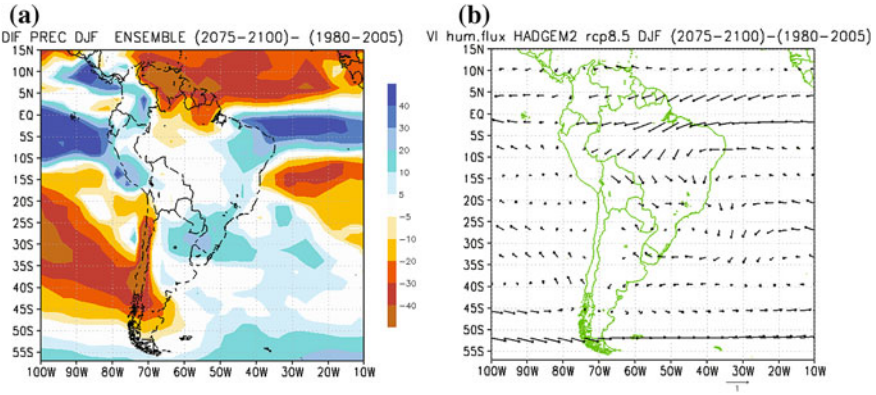

Fig. 6.11 Difference (%) between future projections in scenario rcp 8.5 (2075–2100) and present simulation (1980–2005) in DJF. **a** Precipitation from the ensemble of five CMIP models, **b** humidity flux at 850 hPa

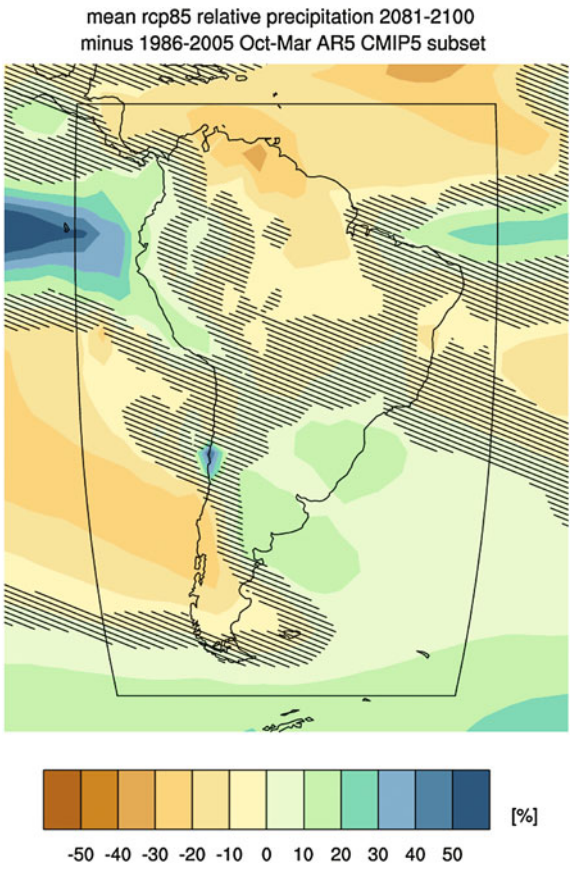

Fig. 6.12 Difference (%) between future projections in scenario rcp 8.5 (2081–2100) and present simulation (1986–2005) in ONDJFM from CMIP5 models of IPCC-AR5. Hatching shows areas where the changes are small, compared with internal variability (less than one standard deviation of internal variability)

small compared to internal variability. These areas extend over a large portion of the SAMS domain, particularly central Brazil and the SACZ region. However, over southeastern South America, which includes part of the SAMS area, the changes are larger than one standard deviation of internal variability (IPCC 2013).

Projections of the annual cycle of precipitation in the SAMS core area, by the five models under the RCP 8.5 scenario, show little dispersion among three members, while the remaining two members demonstrate considerable differences during the mature phase of SAMS (Fig. 6.13a). Compared to the historical 1980–2005 period, the annual cycle of the ensemble in the SAMS core area in the future projection in the 2075–2100 period produces more (less) precipitation in DJ (SOND) (Fig. 6.13b). This is consistent with previous studies of CMIP3 multi-model projections that show increased (reduced) rainfall in the mature (pre-) monsoon phase (Seth et al. 2011). These changes were attributed to decreased moisture convergence in the austral spring and enhanced convergence during the summer. The warmer troposphere and increased stability due to global warming (Chou and Chen 2010), act as a remote mechanism to reduce precipitation over

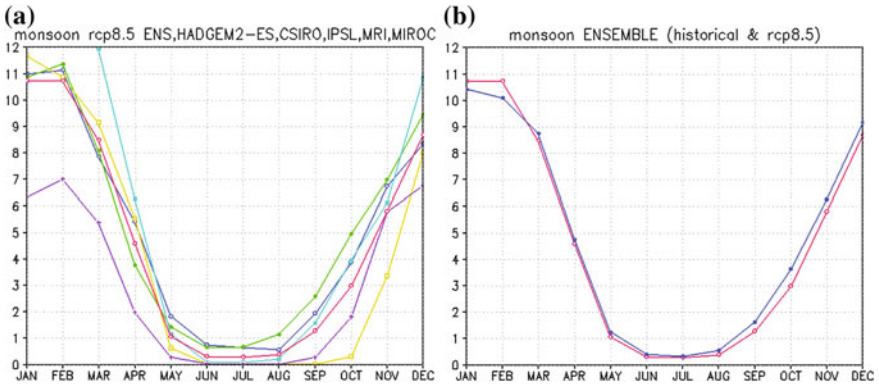

Fig. 6.13 Annual cycle of precipitation in the SAMS core **a** projected by HadGEM2-ES (*blue line*), CSIRO (*green line*), IPSL (*yellow line*), MRI (*cyan line*), MIROC (*violet line*) and the ensemble (*red line*), **b** ensemble of historical period (*blue line*) and future projection under rcp 8.5 scenario (*red line*)

South America in the winter. During the summer, local mechanisms, such as increased evaporation and decreased stability, contribute to increased precipitation. Both mechanisms seem to reduce precipitation during spring, when there is increased atmospheric stability and insufficient soil moisture.

The median onset and demise of the monsoon in future projections was similar to that of the twentieth century, or one pentad later, in the central monsoon region, as estimated with CMIP3 models and the Liebmann and Marengo (2001) method (Bombardi and Carvalho 2009). However, when the entire SAMS region is considered, and assuming the areas of summer minus winter precipitation difference equal or exceed 2.5 mm/day, CMIP5 projections show minor precipitation increases and little change in onset and demise, compared to the twentieth century (Kitoh et al. 2013). Conversely, using the Large-Scale Index for the South America Monsoon (LISAM), Jones and Carvalho (2013) indicated an earlier onset and later demise, and thus a longer duration, of the SAMS by the end of the twenty-first century (2081 to 2100). The warming and moistening of the continent has extended the summer season, compared to the winter season. However, although monsoonal circulation begins earlier, this does not necessarily guarantee an increase in precipitation over the core of the monsoon early in the season, as many complex local mechanisms are necessary to trigger deep convection. Spatial changes in precipitation maxima and increasing trends in precipitation south of 20°S are in good agreement among model projections.

6.6 Conclusions

The multiplicity of dynamic and physical processes and intricate interactions that affect the variability of the SAMS and the SACZ on a broad range of scales demonstrate the challenges in understanding future climate change in tropical South

America. Moreover, the scarce observations over large areas where the monsoon is more active hamper the signal of climate change and add substantial uncertainty to the validation of climatic predictions. The rapid modification of land use and land cover in vast areas of tropical South America and their implications for heat budget and the hydrological cycle, are among the major complications in climate modeling. Moreover, biomass burning in the Amazon introduces large quantities of aerosols into the atmosphere, with potential effects on precipitation, cloud properties, and radiative balance (Dias et al. 2002; Jiang et al. 2006; Levin and Cotton 2009).

Unfortunately, these effects are difficult to quantify, evaluate, and simulate (Lin et al. 2006). Furthermore, teleconnections with coupled modes, such as ENSO and the South Atlantic Dipole on inter-annual time scales, and the PDO and AMO on decadal to multi-decadal time scales, need to be properly simulated in coupled models in order to produce realistic scenarios of climate variations and changes in the SAMS. In addition, the MJO, which is the most important source of intra-seasonal variation in both SAMS and the SACZ, remains a significant obstacle to achieving accurate simulations in coupled models.

In spite of these challenges, there has been a significant advance in our current understanding of climate change in tropical South America. Although observations have been largely limited to the last 3–5 decades and are often intermittent and with restricted spatial coverage, there has been increasing evidence of changes in precipitation and particularly its extremes. The most consistent results, that are independent of data and methodology, are the positive trends in the frequency of heavy and extreme rainfall events in southern and southeastern Brazil and the La Plata Basin, substantiating the hypothesis that SAMS is intensifying poleward of 20°S. However, there is great uncertainty regarding changes in precipitation over the Amazon Basin, suggesting that local factors may compete with remote influences in this region. In addition, the steep topography of the Andes to the west and the scarce number of rain gauge stations over vast areas of the Amazon forest are among the problematic factors that reduce confidence in these findings.

When considering ocean and land together, there is observational evidence suggesting that wet areas are becoming wetter, whereas dry regions (largely dominated by anticyclones) are becoming drier: the "wet-get-wetter and the dry-get-drier" paradigm. However, when land is separated from the ocean, some wet areas seem to be getting drier and vice versa. This seems to be occurring in eastern Brazil, an area that is under the influence of the SAMS and largely impacted by the SACZ during the summer. The boundary between the "wet-get-wetter" and the "wet-get-drier" is virtually unknown, and given the uncertainty, a simple paradigm to generalize climate change seems inappropriate. However, with respect to temperature, there is solid evidence that tropical South America has experienced a progressive warming in recent decades, especially in the northeast. These changes, already in place, may increasingly alter land-ocean gradients with significant impact on changes in precipitation regimes on large and regional scales that are not yet completely understood.

With respect to modeling, there has been recognized improvement between the CMIP3 and CMIP5 simulations of precipitation in South America. The seasonal

variability in precipitation, circulation and moisture transport has been well represented in the climate of the twentieth century when compared against observations, but large biases in the magnitude of daily and seasonal precipitation remain in many regions. A number of models adequately represent important tropical-extratropical teleconnection patterns and respective response on precipitation. However, the representation of precipitation over the Amazon and the "double ITCZ" remains problematic for some models. These issues have impacted the correct simulation of seasonal and inter-annual precipitation in the semi-arid regions east of the Amazon, an area known for sustaining great poverty and vulnerability to changes in precipitation regimes.

While CMIP5 projections all agree that the warming and dampening of the lower troposphere will be more pronounced at low latitudes, the impacts on daily and seasonal precipitation are much more complex. The five best performing CMIP5 models, with respect to the climate of South America, indicate the expansion of the SAMS area westward over the Pacific and eastward over the Atlantic, near the equator, and the southward shift of the oceanic SACZ toward subtropical latitudes by the end of the twenty-first century (from 2075 until 2100), relative to the historical simulations (from 1980 until 2005) in DJF. There is an overall agreement that precipitation in the ITCZ will become more intense ("wet-get-wetter"). However, projections of the total seasonal precipitation, onset and demise of the monsoon depend on the adopted methodology, as some studies have different definitions for the "monsoon season." The most consistent result seems to be the continued trend in wet conditions south of 20°S. Large uncertainties are observed equatorward of this latitude, including the core of the monsoon and over eastern Brazil. The continued international effort to improve coupled and earth system models and propose new methods will be crucial for promoting mitigation and further adaptation to the potential impacts of climate change in South America.

Acknowledgments Leila Maria Véspoli de Carvalho acknowledges the support of the Climate and Large-Scale Dynamics Program from the National Science Foundation (AGS-1053294 and AGS 1116105), the NOAA Climate Program Office (NA10OAR4310170), the CGIAR Research Program on Climate Change, Agriculture and Food Security (CCAFS), and the International Potato Center in Lima, Peru (SB120184). I.F.A. Cavalcanti acknowledges CNPq for research support. The authors are grateful to Forest Cannon for the thorough review of this chapter.

References

Bombardi RJ, Carvalho LMV (2009) IPCC Global coupled climate model simulations of the South America monsoon system. Clim Dyn 33:893–916

Bombardi RJ, Carvalho LMV (2011) The South Atlantic dipole and variations in the characteristics of the South American monsoon in the WCRP-CMIP3 multimodel simulations. Clim Dyn. doi:10.1007/s00382-010-0836-9,36,2091-2210

Bombardi RJ, Carvalho LMV, Jones C, Reboita MS (2014) Precipitation over eastern South America and the South Atlantic sea surface temperature during neutral ENSO periods. Clim Dyn 42:1553–1568

Carvalho LMV, Jones C (2013) CMIP5 simulations of low-level tropospheric temperature and moisture over tropical Americas. J Clim 26:6257–6286

Carvalho LMV, Jones C, Silva Dias MAF (2002a) Intraseasonal large-scale circulations and mesoscale convective activity in tropical South America during the TRMM-LBA campaign. J Geophys Res Atmos 107. doi:10.1029/2001JD000745

Carvalho LMV, Jones C, Liebmann B (2002b) Extreme precipitation events in Southeastern South America and large-scale convective patterns in the South Atlantic convergence zone. J Clim 15:2377–2394

Carvalho LMV, Jones C, Liebmann B (2004) The South Atlantic convergence zone: Intensity, form, persistence, and relationships with intraseasonal to interannual activity and extreme rainfall. J Clim 17:88–108

Carvalho LMV, Jones C, Silva AE, Liebmann B, Dias PLS (2011a) The South American monsoon system and the 1970s climate transition. Int J Climatol 31:1248–1256. doi:10.1002/joc.2147

Carvalho LMV, Silva AE, Jones C, Liebmann B, Rocha H (2011b) Moisture transport and intraseasonal variability in the South America monsoon system. Clim Dyn 36:1865–1880. doi:10.1007/s00382-00010-00806-00382

Casarin DP, Kousky VE (1986) Anomalias de precipitação no sul do Brasil e variações na circulação atmosférica *Rev*. Bras Met 1:83–90

Cavalcanti IAF, Shimizu MH (2012) Climate fields over South America and variability of SACZ and PSA in HadGEM2-ES. Am J Clim Change 1:132–144

Cavalcanti IFA et al (2002) Global climatological features in a simulation using the CPTEC-COLA AGCM. J Clim 15:2965–2988

Chaves RR, Nobre P (2004) Interactions between sea surface temperature over the South Atlantic ocean and the South Atlantic convergence zone. Geophys Res Lett 31. doi:10.1029/2003GL018647

Cherchi A, Alessandri A, Masina S, Navarra A (2011) Effects of increased CO_2 levels on monsoons. Clim Dyn 37:83–101

Chou C, Chen C-A (2010) Depth of convection and the weakening of tropical circulation in global warming. J Clim 23:3019–3030

Chou S et al (2012) Downscaling of South America present climate driven by 4-member HadCM3 runs. Clim Dyn 38:635–653

Cifelli R, Petersen WA, Carey LD, Rutledge SA, Dias MAFD (2002) Radar observations of the kinematic, microphysical, and precipitation characteristics of two MCSs in TRMM LBA. J Geophys Res-Atmos 107

Collini EA, Berbery EH, Barros VR, Pyle ME (2008) How does soil moisture influence the early stages of the South American monsoon? J Clim 21:195–213

Cunningham CAC, Cavalcanti IFD (2006) Intraseasonal modes of variability affecting the South Atlantic convergence zone. Int J Climatol 26:1165–1180

De Almeida, RAF, Nobre P, Haarsma RJ, Campos EJD (2007) Negative ocean-atmosphere feedback in the South Atlantic convergence zone. Geophys Res Lett 34. doi 10.1029/2007gl030401

Dias MAF et al (2002) Cloud and rain processes in a biosphere-atmosphere interaction context in the Amazon region. J Geophys Res-Atmos 107

Dufek AS, Ambrizzi T (2008) Precipitation variability in Sao Paulo State, Brazil. Theoret Appl Climatol 93:167–178

Dufresne JL et al (2013) Climate change projections using the IPSL-cm5 earth system model: from CMIP3 to CMIP5. Clim Dyn 40:2123–2165

Fu R, Li W (2004) The influence of the land surface on the transition from dry to wet season in Amazonia. Theoret Appl Climatol 78:97–110

Fu R, Zhu B, Dickinson RE (1999) How do atmosphere and land surface influence seasonal changes of convection in the tropical amazon? J Clim 12:1306–1321

Fu R, Dickinson RE, Chen MX, Wang H (2001) How do tropical sea surface temperatures influence the seasonal distribution of precipitation in the equatorial Amazon? J Clim 14:4003–4026

Gan MA, Kousky VE, Ropelewski CF (2004) The South America monsoon circulation and its relationship to rainfall over West-Central Brazil. J Clim 17:47–66
Gan MA, Rao VB, Moscati MCL (2006) South American monsoon indices. Atmos Sci Lett 6:219–223
Gandu AW, Silva Dias PL (1998) Impact of tropical heat sources on the South American tropospheric upper circulation and subsidence. J Geophys Res Atmos 103:6001–6015
Gillett NP, Fyfe JC (2013) Annular mode changes in the CMIP5 simulations. Geophys Res Lett 40:1189–1193
Greve P, Orlowsky B, Mueller B, Sheffield J, Reichstein M. Seneviratne SI (2014) Global assessment of trends in wetting and drying over land. Nature Geosci, advance online publication
Grimm AM (2003) The El Nino impact on the summer monsoon in Brazil: regional processes versus remote influences. J Clim 16:263–280
Grimm AM (2004) How do La Nina events disturb the summer monsoon system in Brazil? Clim Dyn 22:123–138
Grimm AM (2011) Interannual climate variability in South America: impacts on seasonal precipitation, extreme events, and possible effects of climate change. Stoch Env Res Risk A 25:537–554
Grimm AM, Zilli MT (2009) Interannual variability and seasonal evolution of summer monsoon rainfall in South America. J Clim 22:2257–2275
Grimm AM, Pal JS, Giorgi F (2007) Connection between spring conditions and peak summer monsoon rainfall in South America: role of soil moisture, surface temperature, and topography in eastern Brazil. J Clim 20:5929–5945
Gulizia C, Camilloni I, Doyle M (2013) Identification of the principal patterns of summer moisture transport in South America and their representation by WCRP/CMIP3 global climate models. Theoret Appl Climatol 112:227–241
Haylock MR et al (2006) Trends in total and extreme South American rainfall in 1960–2000 and links with sea surface temperature. J Clim 19:1490–1512
Held IM, Soden BJ (2006) Robust responses of the hydrological cycle to global warming. J Clim 19:5686–5699
Herdies, DL, da Silva A, Silva Dias MAF, Ferreira RN (2002) Moisture budget of the bimodal pattern of the summer circulation over South America. J Geophys Res Atmos 107
Horel JD, Hahmann AN, Geisler JE (1989) An investigation of the annual cycle of convective activity over the tropical Americas. J Clim 2:1388–1403
Hsu PC, Li T, Wang B (2011) Trends in global monsoon area and precipitation over the past 30 years. Geophys Res Lett 38
Hsu PC, Li T, Luo JJ, Murakami H, Kitoh A., Zhao M (2012) Increase of global monsoon area and precipitation under global warming: A robust signal? Geophys Res Lett 39
IPCC (2013) The physical sience basis. In: Stocker TF, Qin D, Plattner G-K, Tignor M, Allen SK, Boschung J, Nauels A, Xia Y, Bex V, Midgley PM (eds) Contributions of working group i to the fifth assessment report of the intergovernmental panel on climate change. Cambridge University Press, Cambridge, UK and New York, USA, 1535 pp
Jacques-Coper M, Garreaud RD (2014) Characterization of the 1970s climate shift in South America. Int J Climatol
Jiang HL, Xue HW, Teller A. Feingold G, Levin Z (2006) Aerosol effects on the lifetime of shallow cumulus. Geophys Res Let 33
Jones C, Carvalho LMV (2002) Active and break phases in the South American monsoon system. J Clim 15:905–914
Jones C, Carvalho LMV (2013) Climate change in the South American monsoon system: present climate and CMIP5 projections. J Clim 26:6660–6678
Jones CD et al (2011) The HadGEM2-ES implementation of CMIP5 centennial simulations. Geosci Model Dev 4:543–570
Kalnay E, Cai M (2003) Impact of urbanization and land-use change on climate. Nature 423: 528–531

Kalnay E et al (1996) The NCEP-NCAR 40 Year reanalysis project. Bull Am Meteorol Soc 77:437–471
Kim H-M, Webster PJ, Curry JA (2012) Evaluation of short-term climate change prediction in multi-model CMIP5 decadal hindcasts. Geophys Res Lett 39:L10701
Kim ST, Yu J-Y (2012) The two types of ENSO in CMIP5 models. Geophys Res Lett 39:L11704
Kitoh A, Kusunoki S. Nakaegawa T (2011) Climate change projections over South America in the late 21st century with the 20 and 60 km mesh Meteorological Research Institute atmospheric general circulation model (MRI-AGCM). J Geophys Res Atmos 116
Kitoh A, Endo H, Kumar KK, Cavalcanti IFA, Goswami P, Zhou TJ (2013) Monsoons in a changing world: a regional perspective in a global context. J Geophys Res Atmos 118:3053–3065
Kodama YM (1992) Large-scale common features of subtropical precipitation zones (The Baiu Frontal Zone, the SPCZ, and the SACZ). Characteristics of subtropical frontal zones. J Meteorol Soc Jpn 70:813–836
Kousky VE (1988) Pentad outgoing longwave radiation climatology for the South American sector. Rev Bras Met 3:217–231
Krishnamurthy V, Misra V (2010) Observed ENSO teleconnections with the South American monsoon system. Atmospheric Science Letters 11:7–12
Lenters JD, Cook KH (1997) On the origin of the bolivian high and related circulation features of the South American Climate. J Atmos Sci 54:656–678
Lenters JD, Cook KH (1999) Summertime precipitation variability over South America: role of the large-scale circulation. Mon Weather Rev 127:409–431
Levin Z, Cotton WR (2009) Aerosol pollution impact on precipitation: a scientific review. Springer, New York
Liebmann B, Marengo J (2001) interannual variability of the rainy season and rainfall in the Brazilian Amazon basin. J Clim 14:4308–4318
Liebmann B, Jones C, Carvalho LMV (2001) Interannual variability of daily extreme precipitation events in the state of Sao Paulo, Brazil. J Clim 14:208–218
Liebmann B, Kiladis GN, Marengo JA, Ambrizzi T, Glick JD (1999) Submonthly convective variability over South America and the South Atlantic convergence zone. J Clim 12:1877–1891
Liebmann B, Kiladis GN, Vera CS, Saulo AC, Carvalho LMV (2004a) Subseasonal variations of rainfall in South America in the vicinity of the low-level jet east of the Andes and comparison to those in the South Atlantic convergence zone. J Clim 17:3829–3842
Liebmann B et al (2004b) An observed trend in central South American precipitation. J Clim 17:4357–4367
Liebmann B et al (2007) Onset and end of the rainy season in South America in observations and the ECHAM 4.5 atmospheric general circulation model. J Clim 20:2037–2050
Lin JC, Matsui T, Pielke RA, Kummerow C (2006) Effects of biomass-burning-derived aerosols on precipitation and clouds in the Amazon Basin: a satellite-based empirical study. J Geophys Res Atmos 111:D19204
Ma HY, Ji X, Neelin JD, Mechoso CR (2011) Mechanisms for precipitation variability of the Eastern Brazil/SACZ convective margin. J Clim 24:3445–3456
Madden RA, Julian PR (1994) Observations of the 40-50-Day tropical oscillation—a review. Mon Weather Rev 122:814–837
Marengo JA (2009) Long-term trends and cycles in the hydrometeorology of the Amazon basin since the late 1920s. Hydrol Process 23:3236–3244
Marengo JA, Valverde MC, Obregon GO (2013) Observed and projected changes in rainfall extremes in the Metropolitan area of Sao Paulo. Clim Res 57:61–72
Marengo JA, Soares WR, Saulo C, Nicolini M (2004) Climatology of the low-level jet east of the Andes as derived from the NCEP-NCAR reanalyses: characteristics and temporal variability. J Clim 17:2261–2280
Marengo JA et al (2012) Recent developments on the South American monsoon system. Int J Climatol 32:1–21

Meehl GA et al (2007) The WCRP CMIP3 multimodel dataset—a new era in climate change research. Bull Am Meteorol Soc 88, 1383–1394
Misra V (2008) Coupled air, sea, and land interactions of the South American monsoon. J Clim 21:6389–6403
Muza MN, Carvalho LMV, Jones C, Liebmann B (2009) Intraseasonal and interannual variability of extreme dry and wet events over Southeastern South America and subtropical Atlantic during the Austral summer. J. Climate 22:1682–1699
Nakićenović N, Swart R (eds) (2000) Special report on emissions scenarios: a special report of working group iii of the intergovernmental panel on climate change. Cambridge University Press, ISBN:0-521-80081-1, 978-052180081-5
Nieto-Ferreira R, Rickenbach TM (2011) Regionality of monsoon onset in South America: a three-stage conceptual model. Int J Climatol 31:1309–1321
Nieto Ferreira R, Chao WC (2013) Aqua-planet simulations of the formation of the South Atlantic convergence zone. Int J Climatol 33:615–628
Nogues-Paegle J, Mo KC (1997) Alternating wet and dry conditions over South America during summer. Mon Weather Rev 125:279–291
Nogues-Paegle J, Mo KC (2002) Linkages between summer rainfall variability over south America and sea surface temperature anomalies. J Clim 15:1389–1407
Nogues-Paegle J, Byerle LA, Mo KC (2000) Intraseasonal modulation of South American summer precipitation. Mon Weather Rev 128:837–850
Petersen WA, Nesbitt SW, Blakeslee RJ, Cifelli R, Hein P, Rutledge SA (2002) TRMM observations of intraseasonal variability in convective regimes over the Amazon. J Clim 15:1278–1294
Pinto O, Pinto IRCA, Ferro MAS (2013) A study of the long-term variability of thunderstorm days in southeast Brazil. J Geophys Res Atmos 118:5231–5246
Piovano EL, Ariztegui D, Moreira SD (2002) Recent environmental changes in Laguna Mar Chiquita (central Argentina): a sedimentary model for a highly variable saline lake. Sedimentology 49:1371–1384
Polade SD, Gershunov A, Cayan DR, Dettinger MD, Pierce DW (2013) Natural climate variability and teleconnections to precipitation over the Pacific-North American region in CMIP3 and CMIP5 models. Geophys Res Lett 40:2296–2301
Raia A, Cavalcanti IFD (2008) The life cycle of the South American monsoon system. J Clim 21:6227–6246
Raimundo CC, Sansigolo CA, Molion LCB (2014) Trends of rainfall classes in the metropolitan region of São Paulo. Revista Brasileira de Meteorologia 29:397–408
Rickenbach TM, Nieto-Ferreira R, Barnhill RP, Nesbitt SW (2011) Regional contrast of mesoscale convective system structure prior to and during monsoon onset across South America. J Clim 24:3753–3763
Robertson AW, Mechoso CR (1998) Interannual and decadal cycles in river flows of southeastern South America. J Clim 11:2570–2581
Robertson AW, Mechoso CR (2000) Interannual and interdecadal variability of the South Atlantic convergence zone. Mon Weather Rev 128:2947–2957
Robertson AW, Farrara JD, Mechoso CR (2003) Simulations of the atmospheric response to South Atlantic sea surface temperature anomalies. J Clim 16:2540–2551
Rotstayn LD et al (2010) Improved simulation of Australian climate and ENSO-related rainfall variability in a global climate model with an interactive aerosol treatment. Int J Climatol 30:1067–1088
Saha S et al (2010) The NCEP climate forecast system reanalysis. Bull Am Meteorol Soc 91:1015–1057
Seth A, Rojas M, Rauscher SA (2010) CMIP3 projected changes in the annual cycle of the South American monsoon. Clim Change 98:331–357
Seth A, Rauscher SA, Rojas M, Giannini A, Camargo SJ (2011) Enhanced spring convective barrier for monsoons in a warmer world? Clim Change 104:403–414

Silva AE, Carvalho LMV (2007) Large-scale index for South America MONSOON (LISAM). Atmospheric Science Letters 8:51–57

Silva Dias, MAF, Dias J, Carvalho LMV, Freitas ED, Dias PLS (2012) Changes in extreme daily rainfall for São Paulo, Brazil. Clim Change. doi:10.1007/s10584-10012-10504-10587

Silva Dias PL, Schubert WH, DeMaria M (1983) Large-scale response of the tropical atmosphere to transient convection. J Atmos Sci 40:2689–2707

Skansi MM et al (2013) Warming and wetting signals emerging from analysis of changes in climate extreme indices over South America. Global Planet Change 100:295–307

Solman SA et al (2013) Evaluation of an ensemble of regional climate model simulations over South America driven by the ERA-Interim reanalysis: model performance and uncertainties. Clim Dyn 41:1139–1157

Taschetto AS, Wainer I (2008) The impact of the subtropical South Atlantic SST on South American precipitation. Ann Geophys 26:3457–3476

Taylor KE, Stouffer RJ, Meehl GA (2012) An overview of Cmip5 and the experiment design. Bull Am Meteorol Soc 93:485–498

Teixeira MD, Satyamurty P (2011) Trends in the frequency of intense precipitation events in Southern and Southeastern Brazil during 1960–2004. J Clim 24:1913–1921

Venegas SA, Mysak LA, Straub DN (1997) Atmosphere-Ocean coupled variability in the South Atlantic. J Clim 10:2904–2920

Vera C, Silvestri G (2009) Precipitation interannual variability in South America from the WCRP-CMIP3 multi-model dataset. Clim Dyn 32:1003–1014

Vera C. Silvestri G, Liebmann B, Gonzalez P (2006) Climate change scenarios for seasonal precipitation in South America from IPCC-AR4 models. Geophys Res Lett 33. doi:10.1029/2006GL025759

Wang B, Kim HJ, Kikuchi K, Kitoh A (2011) Diagnostic metrics for evaluation of annual and diurnal cycles. Clim Dyn 37:941–955

Wang H, Fu R (2002) Cross-equatorial flow and seasonal cycle of precipitation over South America. J Clim 15:1591–1608

Watanabe S et al (2011) MIROC-ESM 2010: model description and basic results of CMIP5-20c3 m experiments. Geosci Model Dev 4:845–872

Yukimoto S et al (2012) A new global climate model of the Meteorological Research Institute: MRI-CGCM3-model description and basic performance. J Meteorol Soc Jpn 90A:23–64

Zhou JY, Lau KM (1998) Does a monsoon climate exist over South America? J Clim 11: 1020–1040

Zhou YP, Xu KM, Sud YC, Betts AK (2011) Recent trends of the tropical hydrological cycle inferred from Global Precipitation Climatology Project and International Satellite Cloud Climatology Project data. J Geophys Res Atmos 116

Chapter 7
Recent and Possible Future Variations in the North American Monsoon

Andrew Hoell, Chris Funk, Mathew Barlow and Shraddhanand Shukla

Abstract The dynamics and recent and possible future changes of the June–September rainfall associated with the North American Monsoon (NAM) are reviewed in this chapter. Our analysis as well as previous analyses of the trend in June–September precipitation from 1948 until 2010 indicate significant precipitation increases over New Mexico and the core NAM region, and significant precipitation decreases over southwest Mexico. The trends in June–September precipitation have been forced by anomalous cyclonic circulation centered at 15°N latitude over the eastern Pacific Ocean. The anomalous cyclonic circulation is responsible for changes in the flux of moisture and the divergence of moisture flux within the core NAM region. Future climate projections using the Coupled Model Intercomparison Project Phase 5 (CMIP5) models, as part of the Intergovernmental Panel on Climate Change (IPCC) Fifth Assessment Report (AR5), support the observed analyses of a later shift in the monsoon season in the presence of increased greenhouse gas concentrations in the atmosphere under the RCP8.5 scenario. The CMIP5 models under the RCP8.5 scenario predict significant NAM-related rainfall decreases during June and July and predict significant NAM-related rainfall increases during September and October.

Keywords Observed precipitation increases · Projected later season

A. Hoell (✉) · C. Funk · S. Shukla
Department of Geography, University of California, Santa Barbara, CA, USA
e-mail: hoell@geog.ucsb.edu

C. Funk
Earth Resources Observation Systems Data Center,
U.S. Geological Survey, Reston, USA

M. Barlow
Department of Environmental, Earth and Atmospheric Sciences,
University of Massachusetts, Lowell, MA, USA

S. Shukla
University Corporation of Atmospheric Research, Boulder, CO, USA

© Springer International Publishing Switzerland 2016

L.M.V. de Carvalho and C. Jones (eds.), *The Monsoons and Climate Change*,
Springer Climate, DOI 10.1007/978-3-319-21650-8_7

7.1 Introduction and Data

7.1.1 Overview

The North American Monsoon refers to the land-atmosphere interactions and atmospheric dynamics responsible for the contrast between the pronounced maximum in rainfall during June–September (Fig. 7.1) and dry conditions during October–May over the southwest portion of the continent of North America. Due to the large spatial expanse of the North American Monsoon and its extent across geographic and political borders, the North American Monsoon has been previously referred to as the Mexican Monsoon, the Arizona Monsoon, and the Southwest United States Monsoon. Here, the term "North American Monsoon" (NAM) is all-inclusive.

During June–September, long-term average precipitation totals in excess of 550 mm (Fig. 7.1a) are associated with the NAM along the spine of the Sierra Madre Occidental, extending between Nayarit and Sonora, and accounting for more than 70 % of the annual average precipitation (Fig. 7.1b). Lesser precipitation amounts, in the order of 200–350 mm, fall north of 30°N, in areas such as northwest Mexico, southern Arizona, and southern Utah (Fig. 7.1).

Due to the large spatial extent of the NAM region, the climatological onset and ending dates of the NAM greatly vary region-wide. Over Mexico, the onset of the NAM is during late May and early June (Vera et al. 2006). Over the southwest United States, the onset of the NAM is during early July (Fig. 7.2b), as areas such as Arizona and New Mexico observe an average onset date of July 3–14 (Vera et al. 2006). The maximum monthly average precipitation falls during July and August (Fig. 7.2b, c) and the termination of the NAM-related rains occurs regionally during September, first over the southwestern United States, and finally over northwest Mexico.

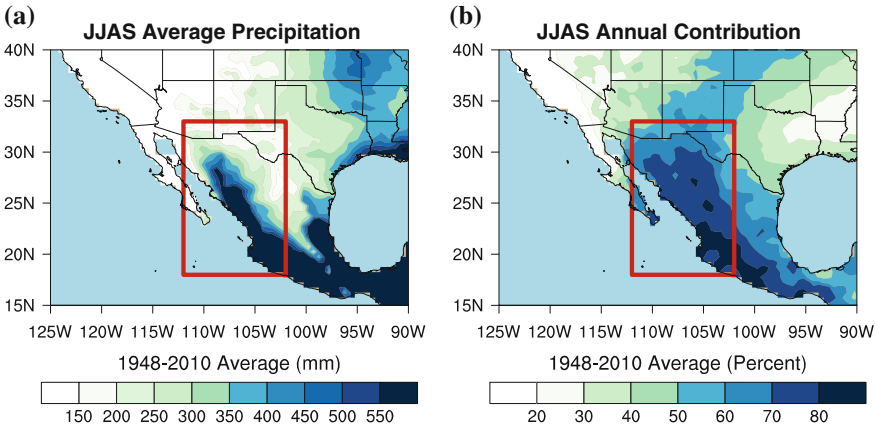

Fig. 7.1 **a** Mean June–September 1948–2010 precipitation (mm) and **b** percent contribution of June–September precipitation to the annual total

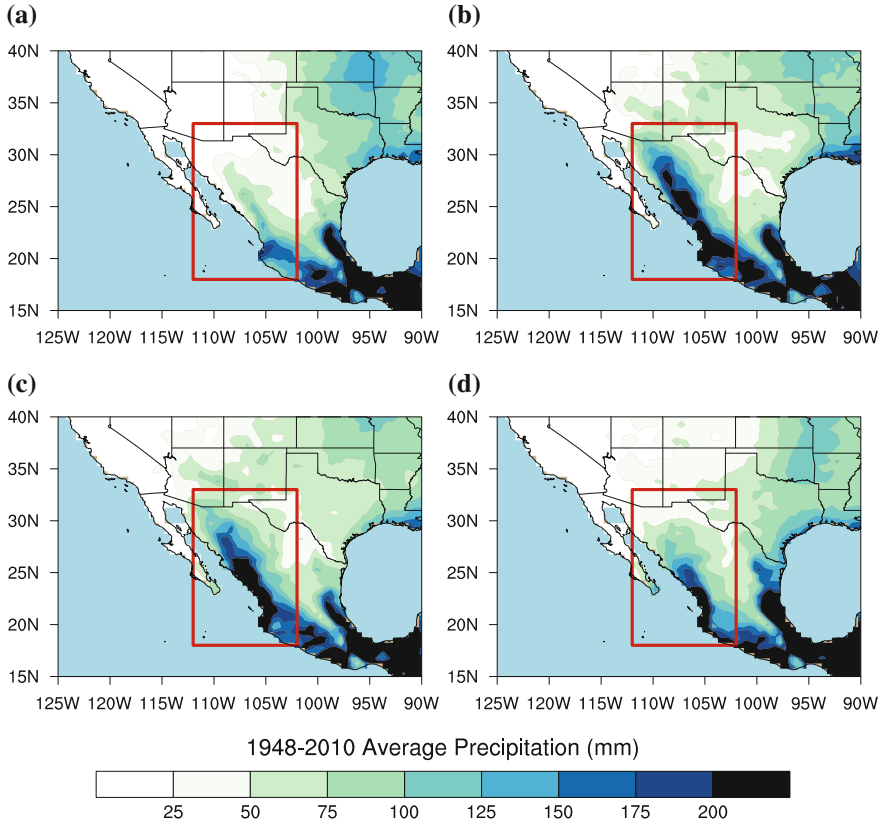

Fig. 7.2 Mean 1948–2010 precipitation during **a** June, **b** July, **c** August and **d** September

Multi-decadal climate variability during the twentieth century has been observed in terms of long-term changes in regional precipitation over southwestern North America (e.g., McCabe 2004; Seager et al. 2005; Weiss et al. 2009; Seager and Hoerling 2014). During June–September over the NAM region, a later onset and withdrawal of the NAM-related precipitation has been observed over the Southwest United States in recent decades (Grantz et al. 2007). Future climate projections using the Coupled Model Intercomparison Project Phase 5 (CMIP5) models, as part of the Intergovernmental Panel on Climate Change (IPCC) Fifth Assessment Report (AR5), support the observed analyses of a later shift in the monsoon season in the presence of increased greenhouse gas concentrations in the atmosphere (Cook and Seager 2013). In this chapter, we review the recent literature examining the observed multi-decadal changes in the June–September rains associated with the NAM during the last half of the twentieth century, and possible projected changes of the NAM associated with increased greenhouse gas concentrations in the atmosphere in the future.

7.1.2 Data

Observed monthly precipitation was drawn from the Global Precipitation Climatology Centre (GPCC) precipitation dataset for 1948–2010 on a 0.5° × 0.5° fixed latitude-longitude grid (Becker et al. 2013). Observed atmospheric dynamics, shown in terms of stream function, pressure vertical velocity, and vertically integrated moisture flux, were drawn from the 6 hourly National Center for Environmental Prediction—National Center for Atmospheric Research (NCEP-NCAR) reanalysis for 1948–2010 on a 2.5° × 2.5° fixed latitude-longitude grid (Kalnay et al. 1996).

Possible changes of the June–September rains associated with the NAM for the duration of the current century were drawn from the CMIP5 RCP8.5 scenario using the methods of Cook and Seager (2013); they analyzed 41 ensemble simulations over 11 coupled global climate models from the RCP8.5 scenario for 2005–2099, and the historical scenario for 1980–2004. The climate of the RCP8.5 simulations was forced with strong concentrations of greenhouse gases in the atmosphere, while the historical simulations are forced by observed conditions within the instrumental period, such as incoming solar radiation and greenhouse gas concentrations. The models used and the number of ensembles included for each model is shown in Table 1 of Cook and Seager (2013).

7.2 Mean Monsoon Dynamics

The NAM system is usually considered to include the monsoon-like heavy summer rainfall centered in northwest Mexico and extending into the southwestern United States, as well as its regional continental linkages in circulation and precipitation. The basic aspects of the NAM system have been examined in several papers (Webster 1987; Douglas et al. 1993; Adams and Comrie 1997; Higgins et al. 1997; Barlow et al. 1998; Higgins et al. 1999; Higgins and Gochis 2007), and consist of a core area of precipitation with monsoonal characteristics—including a single precipitation season led by the highest surface temperatures, seasonal reversal of winds, deep tropical heating associated with an upper-level anticyclone, and associated changes to circulation over much of the United States (and to precipitation in the central United States in particular). Although the winds in the Gulf of California undergo a seasonal reversal, the change is not of a sufficient magnitude and scale to meet the criteria of Ramage (1971) for a monsoon, at least in existing large-scale data products. Recent work has suggested that the circulation response to the monsoon onset may, counter-intuitively, play a role in limiting its northward advance once it reaches the westerlies (Saini et al. 2013). In a larger-scale context, the NAM system is part of a regional monsoon system (Vera et al. 2006) which, in turn, is part of the global monsoon system (Trenberth et al. 2000; Wang and Ding 2008). Here, we briefly discuss the dynamical mechanisms responsible in forcing the June–September rainfall associated with the NAM before reviewing the recent and possible future changes of the NAM, the primary topic of this chapter.

The NAM-related reversal of seasonal wind responsible for the copious precipitation during June–September over southwest North America is forced by the surface pressure difference between the land surface and the adjacent Pacific Ocean. During the Northern Hemisphere summer, intense solar radiation heats the land surface faster than the ocean due to differences in the capacity of each body to store energy. As a result of the temperature contrast between the land and ocean, a surface low pressure area (often referred to as a "thermal low" (Fig. 7.3) develops along the northwest coast of Mexico, resulting in onshore flow and a flux of moisture toward land from the Gulf of California and the Gulf of Mexico (Fig. 7.4).

The rainy season associated with the NAM begins in late May and early June over southern Mexico (Fig. 7.2a). The band of rain penetrates northward over the Sierra Madre Occidental during the months of June–August (Fig. 7.2a–c), associated with the northward progression of the thermal low pressure area (contours in Fig. 7.3a–d) caused by increased land-ocean differential heating, anticylonic circulation in the middle troposphere (shading in Fig. 7.3a–d), and reduced transient storm activity over the United States. The NAM-related precipitation begins over Northwest Mexico

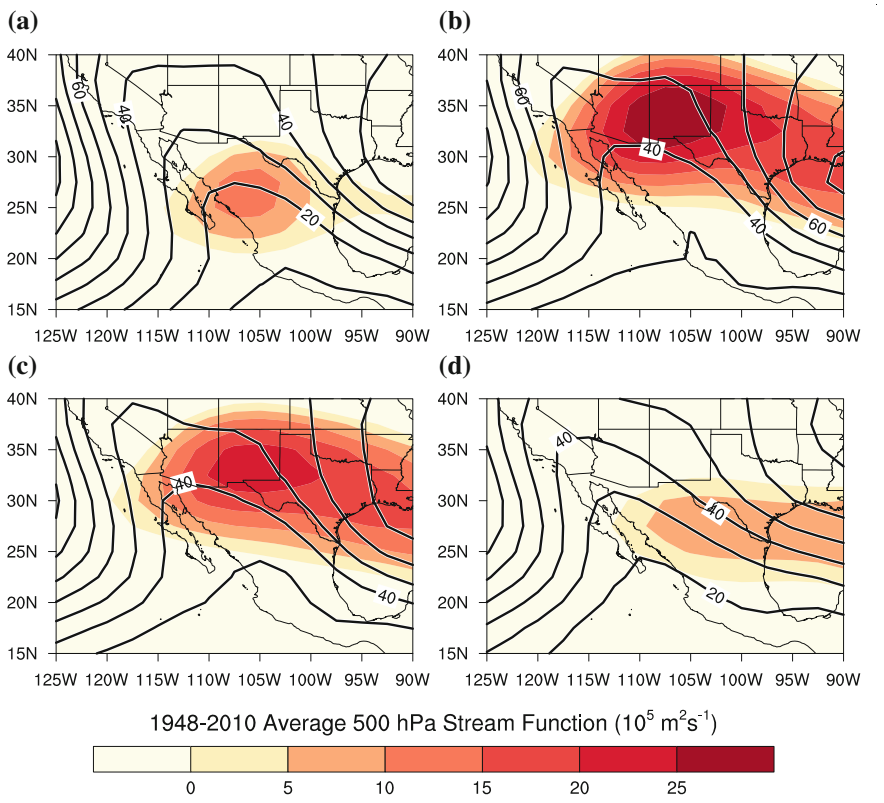

Fig. 7.3 Mean 1948–2010 stream function during **a** June, **b** July, **c** August and **d** September at 500 hPa (*shading*) and 1000 hPa (*contour*) in units of m^2 s^{-1}

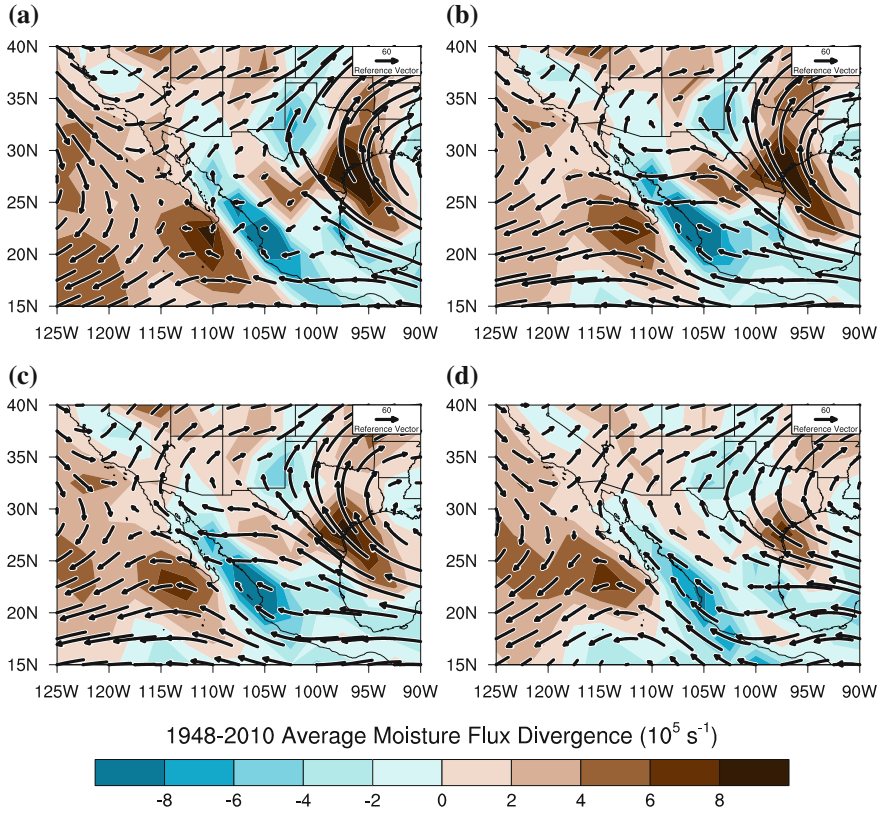

Fig. 7.4 Mean 1948–2010 vertically integrated moisture flux (vector; m s^{-1}) and vertically integrated moisture flux divergence (s^{-1}) during **a** June, **b** July, **c** August and **d** September

during June and over the southwest United States during early July. The vertical movement of moisture by convection supplies the moisture required for rainfall during June–September (Fig. 7.5). The northernmost extent of the NAM-related rains reaches Arizona and New Mexico, but rains over these areas are much lighter in comparison to the elevated parts of the Pacific coastal areas of Mexico.

The moisture source responsible for NAM-related rainfall remains unclear. There are two hypotheses: one that the primary moisture source is from the Gulf of Mexico (Bryson and Lowry 1955; Sellers and Hill 1974) and the other that moisture originates from the Gulf of California. Schmitz and Mullen (1996) showed that moisture responsible for NAM-related precipitation is provided by both the Gulf of Mexico and the Gulf of California, as upper tropospheric moisture is supplied from the Gulf of Mexico and lower tropospheric moisture is supplied from the Gulf of California. As shown by vectors in Fig. 7.4, the horizontal transport of vertically-integrated moisture does not show a clear source when averaged monthly, especially during June and July. However, despite the weak flux of moisture around the rainiest areas

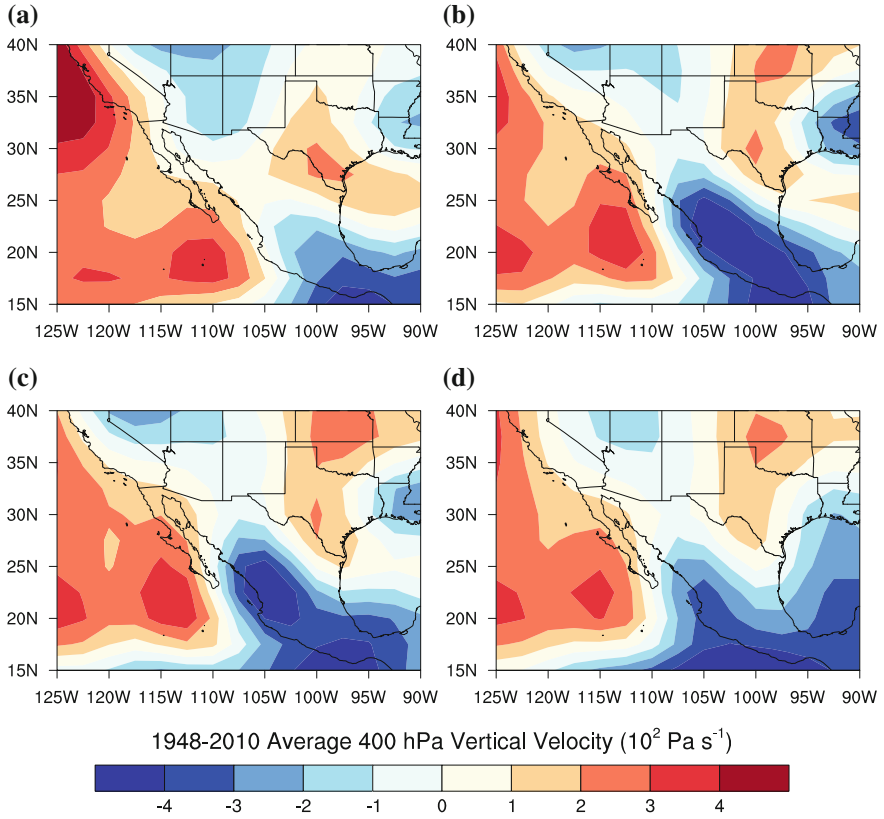

Fig. 7.5 Mean 1948–2010 pressure vertical velocity during **a** June, **b** July, **c** August and **d** September at 400 hPa in units of hPa s^{-1}

associated with the NAM, there is strong horizontal moisture flux convergence during June–September over intense precipitation areas (shading in Fig. 7.4).

During late summer, the NAM-related precipitation weakens and regresses southward in an opposing pattern to the onset phase. The decrease of precipitation is associated with weakening middle tropospheric high pressure over Texas and New Mexico (Fig. 7.3d) and increased precipitation over adjacent areas. The NAM-related rainfall ends over the southwest United States during September.

7.3 Observed and Projected Changes

Significant precipitation increases during June–September have been observed over Arizona and New Mexico (Anderson et al. 2009); however, no significant precipitation trends have been observed over the rest of the NAM region

(Anderson et al. 2009; Arriaga-Ramírez and Cavazos 2010). The regional variation of the long-term NAM-related precipitation trend has been attributed to changes in intensity and frequency of precipitation episodes, and to changes in the length of the NAM-related precipitation season (Englehart and Douglas 2006). Western Mexico precipitation during June–September is perhaps influenced differently from the rest of the core NAM region because of differences in moisture transports and preceding hydrological conditions (Gochis et al. 2007). In terms of the timing of NAM-related precipitation, Grantz et al. (2007) identified delays in the onset, peak, and cessation of precipitation over the southwestern United States, which implies a later shift in seasonality of the monsoon. Here, we investigate the linear trends in atmospheric pressure (in terms of stream function), moisture flux, and vertical motions for June–September 1948–2010 to examine the possible long-term forcing of NAM-related precipitation.

The linear trend in June–September 1948–2010 precipitation is shown in Fig. 7.6, and indicates significant precipitation increases over New Mexico and the core NAM region, and significant precipitation decreases over southwest Mexico. The significant precipitation changes over the southwestern United States and

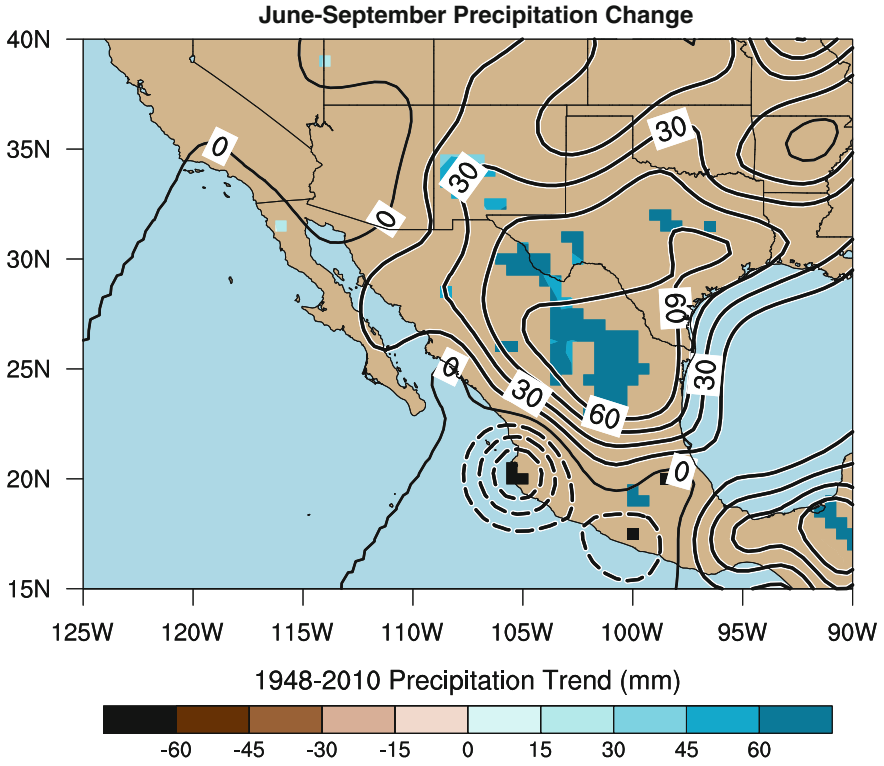

Fig. 7.6 Linear precipitation trend during June–September 1948–2010 contoured every 15 mm. Trends significant at $p < 0.10$ using a t-test are shaded

southwest Mexico are corroborated by Anderson et al. (2009) and Gochis et al. (2007), respectively.

The linear 1948–2010 trend in NAM-related June–September precipitation is forced by the regional teleconnection generated by anomalous cyclonic circulation (Fig. 7.7) centered at 15°N latitude over the eastern Pacific Ocean. The anomalous cyclonic circulation, a low pressure area, is responsible for the significant trend in ascending air over southern Mexico and the eastern tropical Pacific Ocean (Fig. 7.8), which does not appear to have a strong influence on the NAM-related precipitation during June–September.

The anomalous cyclonic circulation is clear in the 1948–2010 trend of vertically integrated moisture flux (vectors in Fig. 7.9). The circulation on the eastern side of the anomalous cyclone is responsible for the significant trend in vertically integrated moisture flux convergence (shading in Fig. 7.9) over the eastern tropical Pacific, northwestern Mexico, Gulf of California, and Baja California, which forces the increasing regional precipitation trends (Fig. 7.6) during June–September. Alhough moisture flux divergence is not shown in the 1948–2010 trend over southwestern Mexico for June–September, the diffluence of the trend in vertically integrated moisture flux helps to explain why a significant decreasing trend in precipitation is observed (Fig. 7.6). Off of the coast of southwestern Mexico, the curvature of the trend in vertically integrated moisture flux is tight and cyclonic

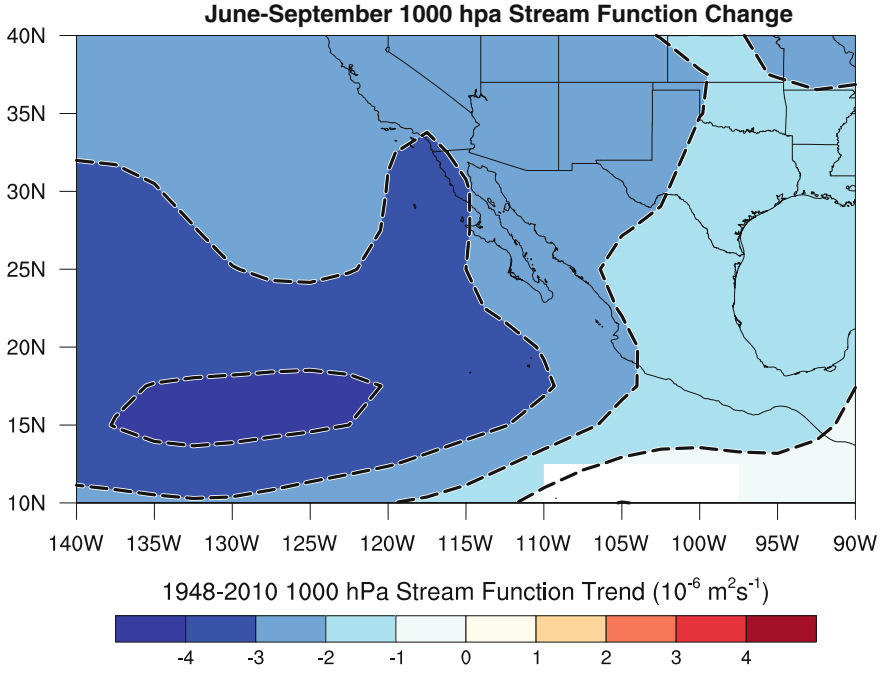

Fig. 7.7 Linear 1000 hPa trend during June–September 1948–2010 contoured every 1×10^6 m^2 s^{-1}. Trends significant at $p < 0.10$ using a t-test are shaded

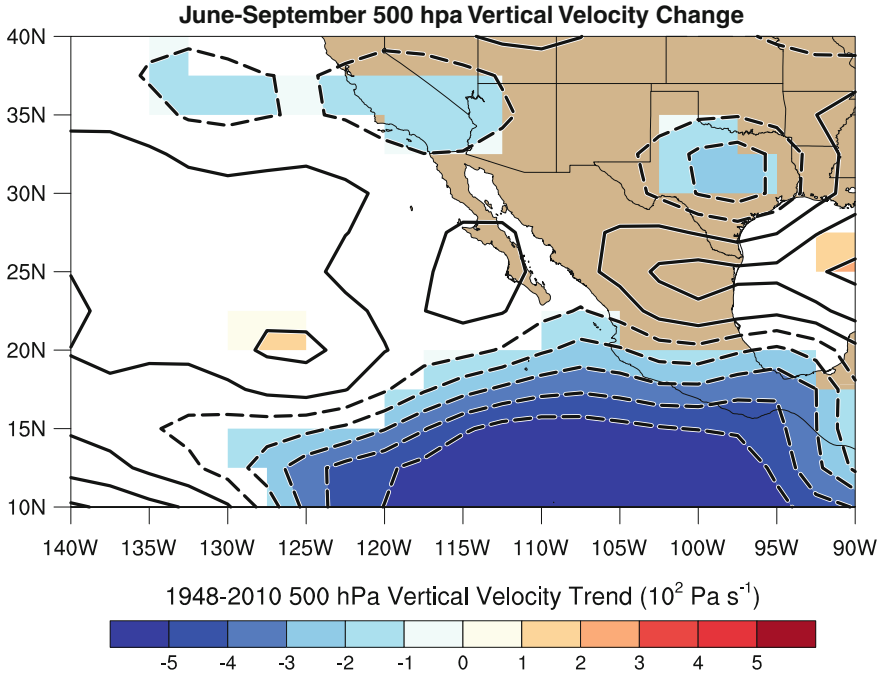

Fig. 7.8 Linear 500 hPa pressure vertical velocity trend during June–September 1948–2010 contoured every 1×10^{-2} Pa s^{-1}. Trends significant at $p < 0.10$ using a t-test are shaded

(a southeast wind), but just to the east of the curvature is a southerly flow that results in diffluence and contributes to precipitation reductions.

Cook and Seager (2013) examined the RCP8.5 scenarios of 41 ensemble simulations from 11 coupled global climate models to determine whether the recent observed changes that support a later start and end to the NAM-related rains were reproduced in a climate with increased atmospheric greenhouse gas concentrations. Figure 7.10 shows the area-averaged precipitation time series from these same 41 simulations (see Cook and Seager 2013 for details) from 1980 to 2099 over the core NAM region of Cook and Seager (2013), defined as a box bound by the points 18° N–33°N, and 112°W–102°W (red boxes in Figs. 7.1 and 7.2). In Fig. 7.10, the historical simulations are shown for 1980–2004, while the RCP8.5 simulations are shown for 2005–2099.

The CMIP5 precipitation declines over the core NAM region for 1980–2099 are around 15 % during June and July, and the linear least squares regression decreases for each month are significant at $p < 0.05$ (Cook and Seager 2013). During June, the precipitation decreases are strong across the entire core NAM region as well as Baja California, Arizona, and New Mexico (Fig. 7.7 of Cook and Seager 2013). During July, the precipitation decreases are strongest along the Sierra Madre Occidental and along the shores of the Gulf of California, but are mixed elsewhere within the core NAM region (Fig. 7.7 of Cook and Seager 2013).

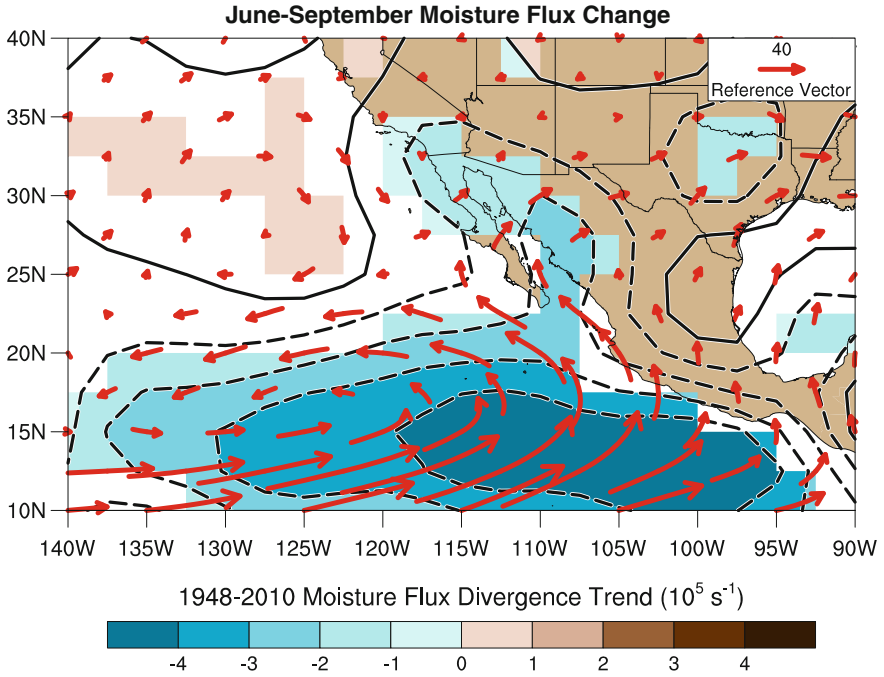

Fig. 7.9 Linear vertically integrated moisture flux trend (vector; m s^{-1}) and moisture flux divergence trend (contour; 1 × 10^{-5} s^{-1}) during June–September 1948–2010 contoured every 1 × 10^{-5} s^{-1}. Trends of vertically-integrated moisture flux significant at $p < 0.10$ using a t-test are shaded

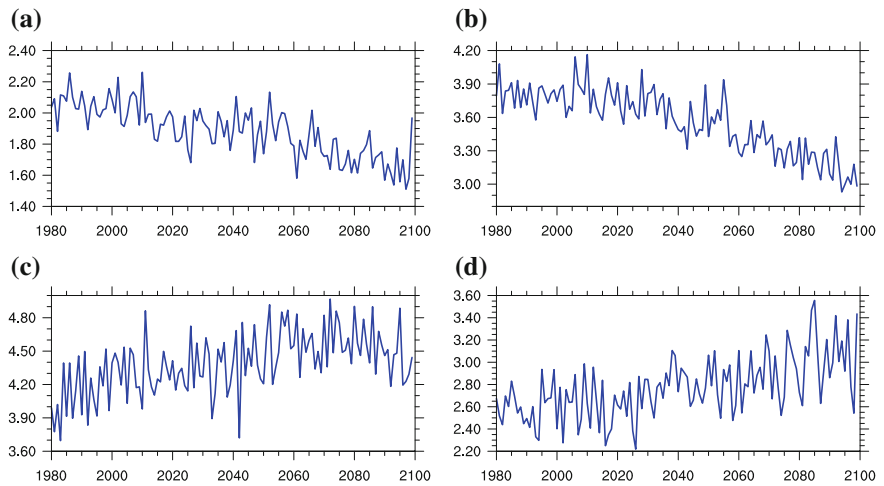

Fig. 7.10 Ensemble average CMIP5 precipitation projections from the RCP8.5 scenario averaged over the boxed regions in Figs. 7.1–7.2 (18°N–33°N; 112°W–102°W) in mm day^{-1}. (According to Cook and Seager 2013). **a** June. **b** July. **c** September. **d** October

The CMIP5 precipitation increases over the core NAM region for 1980–2099 are around 14 and 6 % during September and October, respectively. The linear least squares regression increases during both September and October are significant at $p < 0.05$ (Cook and Seager 2013). During September and October, the precipitation increases are strongest over southeastern portions of the core NAM region, while precipitation changes are weak elsewhere (Fig. 7.7 of Cook and Seager 2013).

Reduced precipitation over the core NAM region during June and July, and enhanced precipitation over the core NAM region during September and October, imply a shift to a later monsoon in the presence of increased greenhouse gases within the RCP8.5 scenarios of the CMIP5 simulations. The decreases in rainfall during June and July in the RCP8.5 scenarios are caused by increases in the vertical stability of the atmosphere due to atmospheric warming and reduced available moisture at the surface (Cook and Seager 2013), despite an increase in the temperature contrast between the continental and oceanic areas (Torres-Alvarez et al. 2014). The increases in rainfall during September and October in the RCP8.5 scenarios are forced by increases in moisture convergence (Cook and Seager 2013).

Global climate models capture the large-scale circulation and seasonal cycle of the NAM (Liang et al. 2008; Gutzler 2009). However, due to the complexity of the NAM and its sensitivity to processes that are poorly resolved by global climate models, global climate models poorly simulate the finer-scale features of the NAM (Castro et al. 2007, Cerezo-Mota et al. 2011). The coupled climate system models have made no improvements in their simulations of the NAM between the CMIP Phase 3 (CMIP3) and CMIP Phase 5 (CMIP5) activities (Geil et al. 2013). Therefore, future projections of the NAM, using modeling approaches, must be interpreted with caution.

Acknowledgments This research was supported by a U.S. Geological Survey (USGS) cooperative agreement #G09AC000001, the USGS Land Change Science Program, and the UCAR Postdocs Applying Climate Expertise (PACE) Fellowship Program.

References

Adams DK, Comrie AC (1997) The North American Monsoon. Bull Am Meteor Soc 78:2197–2213. doi:10.1175/1520-0477(1997)078<2197:TNAM>2.0.CO;2

Anderson BT, Wang J, Salvucci G, Gopal S, Islam S (2009) Observed trends in summertime precipitation over the southwestern United States. J Clim 23:1937–1944. doi:10.1175/2009JCLI3317.1

Arriaga-Ramírez S, Cavazos T (2010) Regional trends of daily precipitation indices in northwest Mexico and southwest United States. J Geo Res Atmos 115:D14111. doi:10.1029/2009JD013248

Barlow M, Nigam S, Berbery EH (1998) Evolution of the North American Monsoon System. J Clim 11:2238–2257. doi:10.1175/1520-0442(1998)011<2238:EOTNAM>2.0.CO;2

Becker A, Finger P, Meyer-Christoffer A, Rudolf B, Schamm K, Schneider U, Ziese M (2013) A description of the global land-surface precipitation data products of the global precipitation

climatology centre with sample applications including centennial (trend) analysis from 1901—present. Earth Syst Sci Data 5:71–99. doi:10.5194/essd-5-71-2013
Bryson RA, Lowry WP (1955) The synoptic climatology of the Arizona summer precipitation singularity. Bull Am Meteor Soc 36 329–339
Castro CL, Pielke RA, Adegoke JO, Schubert SD, Pegion PJ (2007) Investigation of the summer climate of the contiguous United States and Mexico using the Regional Atmospheric Modeling System (RAMS). Part II: model climate variability. J Clim 20:3866–3887. doi:10.1175/JCLI4212.1
Cerezo-Mota R, Allen M, Jones R (2011) Mechanisms controlling precipitation in the northern portion of the North American monsoon. J Clim 24:2771–2783. doi:10.1175/2011JCLI3846.1
Cook BI, Seager R (2013) The response of the North American monsoon to increased greenhouse gas forcing. J Geophys Res Atmos 118:1690–1699. doi:10.1002/jgrd.50111
Douglas MW, Maddox RA, Howard K, Reyes S (1993) The Mexican monsoon. J Clim 6:1665–1677. doi:10.1175/1520-0442(1993)006<1665:TMM>2.0.CO;2
Englehart PJ, Douglas AV (2006) Defining intraseasonal rainfall variability within the North American monsoon. J Clim 19:4243–4253. doi:10.1175/JCLI3852.1
Geil KL, Serra YL, Zeng X (2013) Assessment of CMIP5 model simulations of the North American monsoon system. J Clim 26:8787–8801. doi:10.1175/JCLI-D-13-00044.1
Gochis DJ, Brito-Castillo L, James Shuttleworth W (2007) Correlations between sea-surface temperatures and warm season streamflow in northwest Mexico. Int J Climatol 27:883–901. doi:10.1002/joc.1436
Grantz K, Rajagopalan B, Clark M, Zagona E (2007) Seasonal shifts in the North American monsoon. J Clim 20:1923–1935. doi:10.1175/JCLI4091.1
Gutzler DS et al (2009) Simulations of the 2004 North American monsoon: NAMAP2. J Clim 22:6716–6740. doi:10.1175/2009JCLI3138.1
Higgins RW, Yao Y, Wang XL (1997) Influence of the North American monsoon system on the U.S. Summer Precipitation Regime J Clim 10:2600–2622. doi:10.1175/1520-0442(1997)010<2600:IOTNAM>2.0.CO;2
Higgins RW, Chen Y, Douglas AV (1999) Interannual variability of the North American warm season precipitation regime. J Clim 12:653–680. doi:10.1175/1520-0442(1999)012<0653:IVOTNA>2.0.CO;2
Higgins RW et al (2003) Progress in pan American CLIVAR Research: the North American monsoon system. Atmosfera 16:29–65
Higgins W, Gochis D (2007) Synthesis of results from the North American Monsoon Experiment (NAME) process study. J Clim 20:1601–1607. doi:10.1175/JCLI4081.1
Kalnay E et al (1996) The NCEP/NCAR 40 Year reanalysis project. Bull Am Meteor Soc 77:437–471. doi:10.1175/1520-0477(1996)077<0437:TNYRP>2.0.CO;2
Liang X-Z, Zhu J, Kunkel KE, Ting M, Wang JXL (2008) Do CGCMs simulate the North American monsoon precipitation seasonal-interannual variability? J. Clim 21:4424–4448. doi:10.1175/2008JCLI2174.1
McCabe GJ, Palecki MA, Betancourt JL (2004) Pacific and Atlantic Ocean influences on multidecadal drought frequency in the United States. Proc Natl Acad Sci 101:4136–4141
Ramage CS (1971) Monsoon meteorology. Academic Press, New york, p 296
Saini R, Barlown M, Hoell A (2013) Is the North American monsoon self-limiting?. Geophys Res Lett 40:4442–4447. doi:10.1002/grl.50801
Schmitz JT, Mullen SL (1996) water vapor transport associated with the summertime North American monsoon as depicted by ECMWF analyses. J Clim 9:1621–1634. doi:10.1175/1520-0442(1996)009<1621:WVTAWT>2.0.CO;2
Seager R, Hoerling M (2014) Atmosphere and ocean origins of North American droughts. J Clim 27:4581–4606. doi:10.1175/JCLI-D-13-00329.1
Seager R, Kushnir Y, Herweijer C, Naik N, Velez J (2005) Modeling of tropical forcing of persistent droughts and pluvials over Western North America: 1856–2000*. J Clim 18:4065–4088. doi:10.1175/JCLI3522.1

Sellers WD, Hill RH (1974) The Arizona climate, 1931–1972. The University of Arizona Press, Tucson p 616

Torres-Alavez A, Cavazos T, Turrent C (2014) Land-Sea thermal contrast and intensity of the North American monsoon under climate change conditions. J Clim 27:4566–4580. doi:10.1175/JCLI-D-13-00557.1

Trenberth KE, Stepaniak DP, Caron JM (2000) The global monsoon as seen through the divergent atmospheric circulation. J Clim 13:3969–3993. doi:10.1175/1520-0442(2000)013<3969:TGMAST>2.0.CO;2

Vera C, Coauthors (2006) Toward a unified view of the American monsoon systems. J Clim 19:4977–5000. doi:10.1175/JCLI3896.1

Wang B, Ding Q (2008) Global monsoon: dominant mode of annual variation in the tropics. Dyn Atmos Oceans 44:165–183. doi:10.1016/j.dynatmoce.2007.05.002

Webster PJ (1987) The elementary monsoon. Monsoons, Wiley, New york pp 3–32

Weiss JL, Castro CL, Overpeck JT (2009) Distinguishing pronounced droughts in the Southwestern United States: seasonality and effects of warmer temperatures. J. Clim 22:5918–5932. doi:10.1175/2009JCLI2905.1

Chapter 8
The East African Monsoon System: Seasonal Climatologies and Recent Variations

Chris Funk, Andrew Hoell, Shraddhanand Shukla, Greg Husak and Joel Michaelsen

Abstract This chapter briefly reviews the complex climatological cycle of the East African monsoon system, paying special attention to its connection to the larger Indo-Pacific-Asian monsoon cycle. We examine the seasonal monsoon cycle, and briefly explore recent circulation changes. The spatial footprint of our analysis corresponds with the "Greater Horn of Africa" (GHA) region, extending from Tanzania in the south to Yemen and Sudan in the north. During boreal winter, when northeast trade winds flow across the northwest Indian Ocean and the equatorial moisture transports over the Indian Ocean exhibit strong westerly mean flows over the equatorial Indian Ocean, East African precipitation is limited to a few highland areas. As the Indian monsoon circulation transitions during boreal spring, the trade winds over the northwest Indian Ocean reverse, and East African moisture convergence supports the "long" rains. In boreal summer, the southwesterly Somali Jet intensifies over eastern Africa. Subsidence forms along the westward flank of this jet, shutting down precipitation over eastern portions of East Africa. In boreal fall, the Jet subsides, but easterly moisture transports support rainfall in limited regions of the eastern Horn of Africa. We use regressions with the trend mode of global sea surface temperatures to explore potential changes in the seasonal monsoon circulations. Significant reductions in total precipitable water are indicated in Kenya, Tanzania, Rwanda, Burundi, Uganda, Ethiopia, South Sudan, Sudan, and Yemen,

C. Funk (✉)
US Geological Survey Center for Earth Resources and Observation (EROS) Center, Reston, USA
e-mail: chris@geog.ucsb.edu; cfunk@usgs.gov

C. Funk · A. Hoell · S. Shukla · G. Husak · J. Michaelsen
Santa Barbara Climate Hazards Group, University of California, Santa Barbara, CA, USA
e-mail: hoell@geog.ucsb.edu

S. Shukla
e-mail: shrad@geog.ucsb.edu

G. Husak
e-mail: husak@geog.ucsb.edu

J. Michaelsen
e-mail: michaelsen@geog.ucsb.edu

© Springer International Publishing Switzerland 2016

L.M.V. de Carvalho and C. Jones (eds.), *The Monsoons and Climate Change*,
Springer Climate, DOI 10.1007/978-3-319-21650-8_8

with moisture transports broadly responding in ways that reinforce the climatological moisture transports over the Indian Ocean. Over Kenya, southern Ethiopia and Somalia, regressions with velocity potential indicate increased convergence aloft. Near the surface, this convergence appears to manifest as a surface high pressure system that modifies moisture transports in these countries as well as Uganda, Tanzania, Rwanda, and Burundi. An analysis of rainfall changes indicates significant declines in parts of Tanzania, Rwanda, Burundi, Uganda, Kenya, Somalia, Ethiopia, and Yemen.

Keywords East Africa monsoon system · Precipitation · CHIRPS

8.1 Introduction

For thousands of years, scientists and philosophers have pondered the motions of winds and clouds, and our understanding of monsoons is based on these early foundations. Aristotle was one of the first to put these thoughts to paper. In his *Meteorology* (Aristotle 350 B.C.), he explores the mystery of the atmosphere and meteors, and begins to describe the links between heating, evaporation, and the forces that drive the winds: "The explanation of these and many other phenomena is this. When the sun warms the earth the evaporation which takes place is… of two kinds…. One kind is rather of the nature of vapour, the other of the nature of a windy exhalation. That which rises from the moisture contained in the earth and on its surface is vapour, while that rising from the earth itself, which is dry, is like smoke. Of these the windy exhalation, being warm, rises above the moister vapour, which is heavy and sinks below the other." While still vague, concepts such as these would evolve into modern meteorology and our modern view of monsoon circulations. The ancient Greeks and Romans used the seasonally reversing Indian trade winds to travel between the Middle East, East Africa, and India (Fig. 8.1). Coined "mawsim" ("timely" and "appropriate") by Arab traders, these monsoon winds, and the Indo-Pacific circulation that drives them, still strongly influence the climate of food-insecure and drought-prone East Africa.

In this chapter we explore the seasonal variation of the Indo-Pacific monsoon circulation together with the associated climate of East Africa, which we define as the region stretching from Tanzania in the south to Eritrea, Djibouti, and Yemen in the north. Longitudinally, our focus is on food-insecure countries exhibiting monsoonal rains that depend on moisture transports from the Indian Ocean: Tanzania, Rwanda, Burundi, Uganda, Kenya, Somalia, Ethiopia, Djibouti, Eritrea, and Yemen. Our main objectives are to describe the mean seasonal climatological variations across eastern Africa, and to examine recent changes in atmospheric circulation and rainfall.

Fig. 8.1 Seventeenth-century map depicting the locations of the Periplus of the Erythraean Sea. Map created on December 31, 1596, by Abraham Ortelius (1527–1598) for *Periplus Maris Erythraei*, originally written in Greek in the first century CE. A Periplus is an account that lists, in order, coastal ports and landmarks

8.2 Background

The seasonal progression and reversal of the Indian Monsoon circulation (Ramage 1971) modifies East African climate by affecting patterns of moisture transport, subsidence, and precipitation (Riehl 1979). These links can help us understand East Africa's seasonal cycle, seasonal climate variability, and climate trends. During boreal winter and fall, easterly sub-tropical Indian trade winds in both the Northern and Southern Hemispheres turn rapidly into westerlies over the western Indian Ocean, flowing back to the east at about 5–10°S (Hastenrath et al. 2007, 2011). Since the conservation of angular momentum induces easterly tendencies in most tropical flows, these mean westerly winds are quite remarkable, and can be considered as part of the equatorially-trapped Rossby wave response of the tropical atmosphere to a steady source of heating in the tropical Indo-Pacific Warm Pool (Gill 1980, 1982). From this perspective, warm pool heating drives westerly flows reducing onshore moisture supplies into East Africa, helping to explain the region's

climatologically dry conditions. As we will see, this classic Gill-Matsuno-like response (Gill 1980, 1982) only holds climatologically during the boreal fall and winter. During the spring and summer, the cross-equatorial monsoonal circulation brings heavy cross-equatorial flows and easterly moisture supplies into Kenya and Ethiopia.

Modulations of Indo-Pacific Warm Pool heating can affect East Africa, either through inter-annual variations such as the El Niño-Southern Oscillation (ENSO) (Camberlin 1995; Camberlin and Philippon 2002; Funk et al. 2013; Hastenrath et al. 2007, 2011; Hoell and Funk 2013a; Hoell et al. 2014; Ogallo et al. 1988; Okoola 1999; Williams et al. 2011; Williams and Funk 2011); the Indian Ocean Dipole (IOD) (Goddard and Graham 1999; Saji et al. 1999); lower frequency warming trends (Cook and Vizy 2013; Funk et al. 2005, 2008, 2013; Hoell and Funk 2013b; Rowell et al. 1995; Williams et al. 2011; Williams and Funk 2011); or Pacific Decadal Variability (Lyon and DeWitt 2012; Lyon et al. 2013; Yang et al. 2014).

What this new research suggests is that Walker circulation-like climate variations are primary drivers of East African drought. As opposed to Hadley circulation analyses, which examine meridional (north-south) circulation averages, the Walker circulation (Bjerknes 1969) looks at zonal (east-west) climate averages taken near the Equator. These averages reveal that very warm regions (the "warm pool") in and over the eastern Indian and western Pacific Oceans are associated with high rates of precipitation and moisture and heat convergence (Bjerknes 1969). The energy associated with this heavy convection, however, is transported aloft to the eastern Pacific and East Africa, where it can result in subsiding air and low-level high pressure.

Conceptually, this view suggests a more zonal (Walker cell-like) understanding of the drivers of aridity in East Africa and the Sahel climate, as opposed to a focus on a meridional (Hadley circulation-like) progression (Rodwell and Hoskins 1996). It is interesting to note, for example, that a relatively simple hydrostatic primitive equation model, forced with diabatic forcing representing the Asian Monsoon during boreal summer, recreates many important features of the Indo-Asian-African summer climate (Rodwell and Hoskins 1996): the curved cross-equatorial monsoonal winds, and patterns of ascent and subsidence consistent with rainfall maxima over India/East Asia and Sudan/Ethiopia as well as rainfall minima over eastern and southern Africa.

The "Walker Cell" depiction seems to fit East Africa fairly well in boreal fall and winter (Hastenrath et al. 2007), when the mean circulation has a westerly mean, lower level winds over the equatorial Indian Ocean. This changes as the "monsoonal" Somali Jet (Findlater 1969) forms over East Africa during boreal spring and summer. Instead of turning east to form equatorial westerlies over the Indian Ocean, the low level winds cross from the Southern Hemisphere and recurve towards India.

The Somali Jet is thought to arise through the interaction of differential land-ocean heating contrast, the influence of the East African and Madagascar

highlands, and the "beta effect" (Krishnamurti et al. 1976). This jet, one of the most vigorous and constant low-level jet patterns, links the East African and Indian Monsoons (Vizy and Cook 2003). The Somali Jet plays a dual role in the East African climate, providing both a key source of moisture, but also a source of subsidence. Between March and April, as the Somali Jet shifts northward (Findlater 1969), East Africa experiences a rapid "monsoon jump" as the locus of rainfall shifts rapidly from southern to eastern Africa (Riddle and Cook 2008), bringing onshore moisture transports (Viste and Sorteberg 2013) and rapid increases in precipitation during the boreal spring "long" rains. As the zonal branch of the Somali Jet forms during boreal summer, moisture is advected eastward towards the Indian monsoon. Low-level diffluence along the Somali Jet's westward flank produces subsidence, reducing rainfall across eastern East Africa. These large-scale climate controls, the seasonal migration of warming from insolation, and the local influences of lakes and mountains, combine to produce the extremely complex timing and intensity of East African rainfall (Liebmann et al. 2012).

Given the tremendous complexity of East Africa's precipitation, it should not be too surprising that considerable uncertainty surrounds projections for East African climate change. In general, the latest coupled ocean-atmosphere simulations produced for the Phase 5 Coupled Model Intercomparison Project (CMIP5) indicate wetter conditions in East Africa (IPCC 2014). These increases in rainfall appear to be at odds with observations of decreased precipitation during boreal spring, which appears to be linked to increases in ocean temperatures and convection over the Indian (Funk et al. 2008, 2005; Verdin et al. 2005) or Indo-Pacific (Funk 2012; Lyon and DeWitt 2012; Williams et al. 2011; Williams and Funk 2011) Oceans. Recent experiments with global atmospheric circulation models (Funk 2012; Funk et al. 2013; Hoell and Funk 2013a, b; Lyon and DeWitt 2012; Yang et al. 2014) suggest that increased western Pacific sea surface temperatures (SST) and SST gradients, as well as enhanced warm pool convection, contribute to more frequent East African droughts.

Some East African mesoscale model simulations also indicate drying (Cook and Vizy 2013). Cook and Vizy (2013) drive the Weather Research and Forecast regional model (WRF) with 32 vertical levels and 90 km resolution. Cook and Vizy contrast WRF simulations forced with 1981–2000 boundary conditions and WRF simulations forced with 2041–2060 boundary conditions derived from nine coupled global climate models. During boreal spring, the difference between these two sets of simulations indicates a weakening Somali Jet, westerlies over the equatorial Indian Ocean, and reduced rainfall over Ethiopia, Somalia, Kenya, and Tanzania. These simulations also indicate an increase in the Arabian high pressure cell.

One likely source of discrepancy between the global CMIP5 model results for East Africa and the results produced by atmospheric global circulation models (AGCMs) and regional models is the tendency for CMIP5 models to predict an increase in El Niño-like SST and precipitation in the central Pacific (Chadwick et al.

2012), while the observed climate has shifted towards El Niño-like warming in the opposite direction (Cane et al. 1997; Compo and Sardeshmukh 2010; L'Heureux et al. 2013; Solomon and Newman 2012). El Niño-like SSTs are anomalously warm in the central and eastern equatorial Pacific.

While it has been suggested that warming in the CMIP5 models in the eastern/central Pacific is tied to a slowing of the global atmospheric circulation (Held and Soden 2006), there is little observational evidence for a corresponding shift towards stronger or more frequent ENSO events (Giese and Ray 2011), and stronger Pacific trade winds appear to have slowed warming in the Eastern Pacific by advecting heat into the extra-tropical Pacific (England et al. 2014). New research suggests that the El Niño-like tendency of the CMIP5 ensembles is primarily a function of the models' weakening zonal Pacific SST gradient (Sandeep et al. 2014), which is caused by preferential warming in the central and eastern equatorial Pacific. This differs substantially from the slowing of global convective mass flux explanation offered by Held and Soden (2006). Using AGCMs driven with ENSO and ENSO-residual SST, Sandeep et al. show that while both components indicate a slowing of global convective mass flux, the ENSO and ENSO-residual components indicate, respectively, a weakening and strengthening of the Walker Circulation, with the latter forcing dominating. In this chapter, we examine observed circulation changes, based on regressions with global "trend mode" SST principal component time series.

8.3 Data

We examine reanalysis fields (Kalnay et al. 1996) from the National Center for Environmental Prediction and the National Center for Atmospheric Research (NCEP/NCAR), precipitation observations from the Climate Hazards Group Infrared Precipitation with Stations (CHIRPS) dataset, and the National Ocean and Atmospheric Administration's Extended Reconstructed sea surface temperatures (NOAA ERSST Smith et al. 2008); we also briefly examine SST from eight CMIP5 simulations (Table 8.1).

The CHIRPS data set is a 30+ year quasi-global rainfall dataset (Funk et al. 2014). Spanning 50°S–50°N (and all longitudes), CHIRPS begins in 1981 and extends to the near present. The data set combines 0.05° resolution satellite imagery with in situ station data to create gridded rainfall time series for trend analysis and seasonal drought monitoring. For East Africa, CHIRPS is comparable (Shukla et al. 2014a) to the research quality Global Precipitation Climatology Centre (GPCC) product (Schneider et al. 2013), but is updated in near real time to support drought early warning applications.

Table 8.1 CMIP5 simulations used in this study

Modeling group and model name	Model acronym	Historical simulations
Canadian Centre for Climate Modelling and Analysis *Canadian Earth System Model, version 2*	CanESM2	5
National Center for Atmospheric Research *Community Climate System Model, version 4*	CCSM4	4
Community Earth System Model Contributors *Community Earth System Model version with Community Atmospheric Model, version 5*	CESM1-CAM5	2
Centre National de Recherches Météorologiques/Centre Européen de Recherche et Formation Avancée en Calcul Scientifique *Centre National de Recherches Météorologiques (CNRM) Coupled Global Climate Model, version 5*	CNRM-CM5	4
NOAA Geophysical Fluid Dynamics Laboratory *Geophysical Fluid Dynamics Laboratory Earth System Model, version 2 with with modular ocean model version 4.1*	GFDL-ESM2 M	1
Institut Pierre-Simon Laplace *IPSL Community Model version 5*	IPSL-CM5A-LR	3
Atmosphere and Ocean Research Institute (University of Tokyo), National Institute for Environmental Studies, and Japan Agency for Marine-Earth Science and Technology *Model for Interdisciplinary Research on Climate, version 5*	MIROC5	3
Max-Planck-Institut für Meteorologie (Max Planck Institute for Meteorology) *MPI Earth System Model Low Resolution*	MPI-ESM-LR	3
Total Ensemble		**25**

8.4 Methods

We seek to better understand links between East African climate and climate change, and variations in the larger scale Indo-Pacific monsoon system. Our analysis focuses first on the mean East African seasonal climate during January–February–March (JFM), April–May–June (AMJ), July–August–September (JAS) and October–November–December (OND). We examine seasonally averaged CHIRPS precipitation and National Center for Atmospheric Research/National Center for Environmental Prediction (NCAR/NCEP) reanalysis: (1) vertically integrated precipitable water; (2) vertically integrated moisture transports; (3) upper tropospheric (0.21 sigma) velocity potential; and (4) divergent wind fields.

We next analyze regressions between integrated precipitable water, moisture transports, velocity potential and divergent wind fields, and the first principal component of global ENSO-residual SST. The empirical orthogonal function

(EOF) associated with this first principal component, hereinafter referred to as the "trend mode," primarily corresponds to an estimate of the warming in the Indo-Pacific. Several recent studies have examined trends and empirical orthogonal functions (EOFs) of global SST with the influence of ENSO removed (Compo and Sardeshmukh 2010; Solomon and Newman 2012). Removing ENSO-related variations reduces the influence of inter-annual fluctuations and increases the level of agreement among trend fields calculated from different SST data sets.

Here, we have represented ENSO as the first principal component of NOAA Extended Reconstructed (ER) (Smith et al. 2008) tropical Pacific SST (125°E–115°W, 15°S–15°N) over the 1900–2014 time period. Using regression, we isolated and removed 1900–2014 ENSO-related SST variations, then defined the trend mode of variability as the first covariance-matrix-based EOF of global (70°S–70°N) seasonal (JFM, AMJ, JAS, OND) SST anomalies. The 1900–2014 seasonal SST grids were converted to anomalies, weighted by cosine-based weights to account for latitudinal variations in area, and used to compute the covariance matrix and associated eigenvector and principal component. An identical procedure is applied to 25 CMIP5 simulations (Table 8.1) and compared with results obtained from the NOAA ER SST data set.

8.5 The Seasonal Progression of the East African Monsoon

The East African climate is very complex (Liebmann et al. 2012). Over East Africa, the seasonal migration of moisture transports and large-scale patterns of atmospheric convergence and divergence interact with the region's complex topography to produce patterns of rainfall that can vary by orders of magnitude over hundreds of kilometers. Figure 8.2 shows mean CHIRPS precipitation for JFM, AMJ, JAS, and OND. At the largest scale, there is a clear seasonal progression, as the Inter-tropical Front transitions from a Southern Hemisphere maximum in JFM to a Northern Hemisphere maximum in JAS. The bulk of these rains, however, fall to the southwest or northwest of East Africa. Most of East Africa relies on two relatively meager "bimodal" rainy seasons: the "long rains" during boreal spring (AMJ in this study), and the boreal fall "short rains" (OND).

The seasonal progression of East Africa's precipitation is largely driven by changes in mean moisture transports and large-scale patterns of subsidence. These changes, in turn, are tightly coupled to seasonal variations in, over, and around the Indian Ocean and western Pacific Warm Pool. We use vertically integrated NCEP/NCAR reanalysis specific humidity (referred to as total precipitable water) and moisture transports to track these seasonal migrations. These moisture transports (Fig. 8.3) closely follow the monsoonal variations of the Indian trade winds. During austral summer (JFM and OND), monsoon winds sweep from the Western Ghat mountains of India towards Somalia. During boreal summer (AMJ and JAS), these winds reverse.

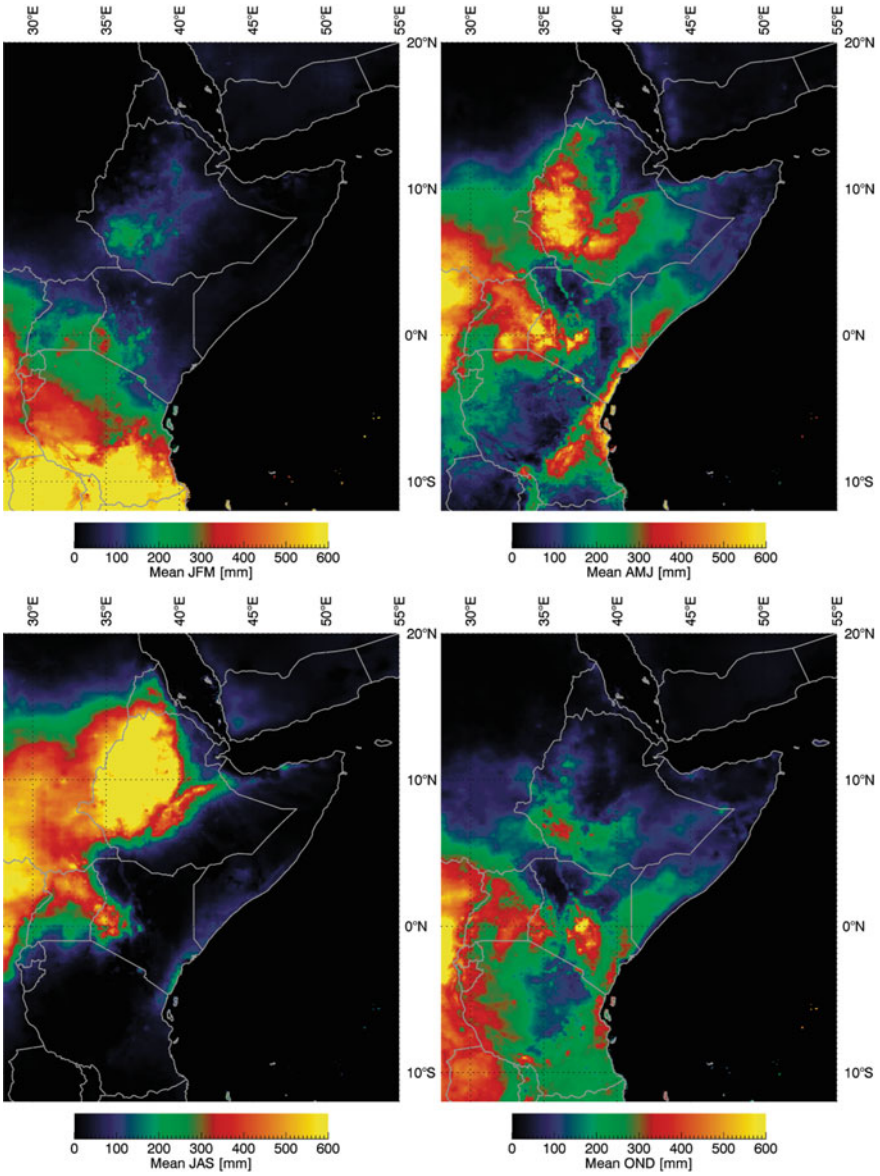

Fig. 8.2 1981–2013 mean CHIRPS

During each season, much of the moisture from the Indian Ocean is redirected to the east before reaching East Africa (Fig. 8.3). In JFM, a strong equatorial westerly jet (Hastenrath et al. 2011) to the northeast of Madagascar helps to drive lower tropospheric convergence and convection over the eastern Indian Ocean and western equatorial Pacific. A surface high pressure resides over Yemen. During AMJ, the

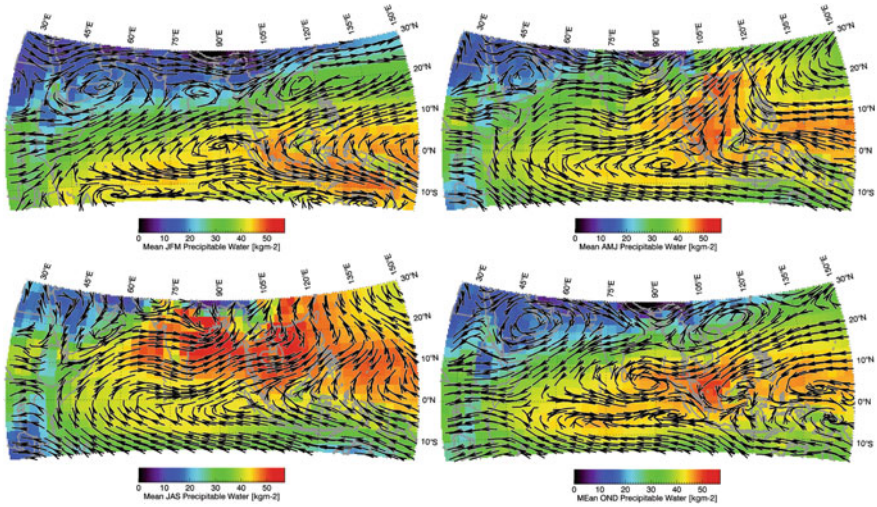

Fig. 8.3 Mean 1981–2010 NCEP/NCAR reanalysis total precipitable water and moisture transports

zonal westerlies over the Indian Ocean weaken, and moisture flows across East Africa, supporting the long rains (Viste and Sorteberg 2013). As these winds cross the Equator, conservation of angular momentum turns them towards India, helping to initiate the Indian Monsoon (Vizy and Cook 2003). As this monsoon intensifies in JAS, the southwesterly Somali Jet across eastern Africa intensifies and shifts eastward, reducing the onshore flow of moisture and producing subsidence across parts of eastern Kenya, southern Ethiopia, and Somalia. During OND, the Indian monsoon subsides and the reversing Indian trades bring moisture to feed the East African short rains. As the surface low pressure system over the south equatorial Indian Ocean intensifies in JFM, these transports diminish, and the seasonal cycle repeats. The seasonal cycle of East African climatology, therefore, is tightly coupled to the tropical Indo-Pacific and Indian Monsoon circulations.

The Indo-Pacific and Indian Monsoon circulations help create the conditions that give much of East Africa a semi-arid or arid climate. In general, East Africa does not receive bountiful rains because low pressure, along with temperature and moisture convergence over the warm equatorial Indo-Pacific, pull the bulk of the moisture transports to the east. This has long been understood as part of the "Walker circulation," first described by Bjerknes (1969), and named after the British meteorologist Sir Gilbert Walker, who first described the Southern Oscillation (Walker 1923). Following Bjerknes (1969), Fig. 8.4 shows a schematic diagram of the east-west (zonal) circulation. The bottom of the figure represents the earth's surface, and the top of the diagram, the tropopause. The left of the image describes the climatological conditions typical for much of East Africa. In the upper troposphere, winds converge into an area of upper-level low geopotential heights, producing subsidence. This subsidence reinforces a high pressure cell near the

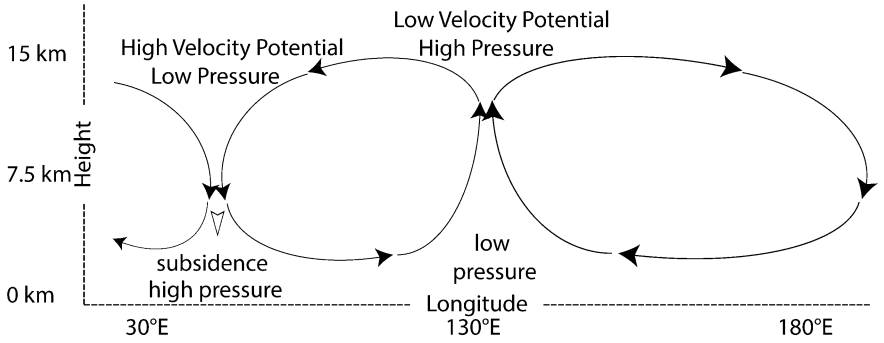

Fig. 8.4 Height by longitude schematic describing velocity potential

surface, which in turn supports low-level moisture divergence and dry conditions. Over the eastern Indian Ocean and western Pacific (located in the center of our schema), conditions are reversed, producing a convergence of moisture and heat, increasing the moist static energy and driving large-scale convection and precipitation. The convergence of latent and sensible heat increase geopotential heights aloft, producing an upper-level high.

These types of circulation features can be effectively visualized using a "velocity potential" field; this is a scalar field defined such that the divergent (non-geostrophic) wind field flows along (perpendicular to) the velocity potential field, flowing from low-velocity potential regions to high-velocity potential areas. Thus, near the Equator, the upper-level divergent wind will flow from an area of high geopotential heights, and low-velocity potential to areas of low geopotential heights and high velocity potential. Figure 8.5 shows climatological velocity potential and divergent wind streamlines for East Africa, estimated near the top of the tropopause (the 0.21 sigma ≈ level 200 hPa).

Figure 8.5 gives us additional insight into the march of seasons that drives the various stages of the East African monsoon. In general, in each season we find low-velocity potentials over the Indian Ocean and higher velocity potentials over East Africa (this intensifies during JAS). These velocity potential gradients are associated with easterly divergent winds. During JFM and JAS, these upper-level winds converge, respectively, over North Africa and the Middle East and over Southern Africa. During AMJ and JAS, upper-level convergence weakens over Sudan and the rest of the Sahel, and upper-level conditions are fairly conducive to rainfall over Yemen and most of East Africa. During OND, strong upper-level convergence stretches from eastern Tanzania across Kenya, eastern Ethiopia, and Yemen. While the Middle East is already under the influence of a low-level high pressure cell (Fig. 8.3), East Africa, during the OND "short rains," receives onshore moisture transports from over the northeast Indian Ocean. When El Niño (Indeje et al. 2000) or positive Indian Ocean Dipole (IOD) events (Saji et al. 1999) affect the zonal Indo-Pacific circulation, the region can experience heavy OND rainfall.

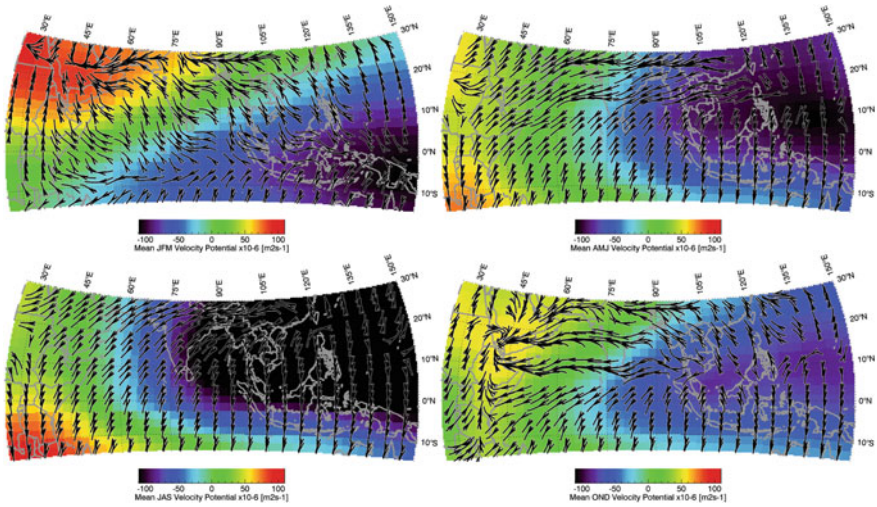

Fig. 8.5 Mean 1981–2010 NCEP/NCAR reanalysis 0.21 sigma velocity potential heights and divergent wind fields

In addition to large-scale circulation controls, the East African climate is also heavily influenced by local topography and Lake Victoria. The influence of these features can create great changes in mean climate over short distances. In general, rainfall at higher elevations is typically much higher than at lower elevations. Air temperatures exhibit an inverse relationship; thus much of East Africa contains hot, dry lowlands interspersed with cool, wet highland areas. Food-insecure populations and environments can often be found along the edges of these gradients, in between the very wet regions that receive consistent rains, and the arid lands that are consistently dry.

8.6 Relating Circulation Trends to Large-Scale Warming Patterns

The next section of this chapter will examine the relationship between the regional circulation and large-scale warming trends. We use total precipitable water and moisture transports to represent the lower atmosphere. The upper atmosphere is represented by upper-level (0.21 sigma) velocity potential fields. We examine trends in these fields by regressing them against the first principal component of global sea surface temperatures, after the influence of ENSO has been removed. We refer to this as the "trend mode" of global SST. While the overall SST trends and atmospheric responses in the CMIP5 models tend to represent an El Niño-like shift in the mean climate (Chadwick et al. 2012), this tendency appears to be closely related to the CMIP5 model's tendency to warm SSTs in the eastern Pacific more

rapidly than in the western (Sandeep et al. 2014). While both observations and the CMIP5 simulations indicate a warming central and eastern Pacific, the magnitude of the CMIP5 warming is substantially greater. We can see this by examining principal component time series (Fig. 8.6) and eigenvectors calculated over the 1900–2013 seasonal (AMJ) tropical Pacific (125°E–65°W, 15°S–15°N) SST in the NOAA ER SST observations and our CMIP5 ensemble (Table 8.1). While the overall magnitude and timing of the observed and CMIP5-simulated time series (Fig. 8.6a) is quite similar (except for decadal fluctuations in the observations about the CMIP5 ensemble mean), the CMIP5 ENSO response, as represented by the CMIP5 eigenvectors (Fig. 8.6b), is much greater. Together, Fig. 8.6a, b suggest that the CMIP5 models over-estimate the strength of warming in the eastern equatorial Pacific. This warming, and the resulting change in SST gradients, seem to be largely responsible for the slowing of the CMIP5 Walker Circulation.

Here, we focus on the empirical relationships between the NCEP/NCAR reanalysis and the observed trend mode first principal component. The observed and CMIP5 modeled trend mode changes are substantially more congruent than changes related to ENSO. As described in the background section, this ENSO-residual "trend mode" isolates a component of large-scale climate variability (the non-ENSO warming trend) that appears consistent across datasets (Cane et al. 1997; Compo and Sardeshmukh 2010; Solomon and Newman 2012).

Figure 8.7a shows the recent annual trend mode SST changes between 1999–2013 and 1979–1998, based on observed data (the NOAA ER SST). The 1999–2013 and 1979–1998 break periods were chosen to correspond with recent analyses describing a "Pacific Shift" in SST (Lyon et al. 2013). One key characteristic of the observed trend mode SST, the stronger western-to-central Pacific equatorial SST

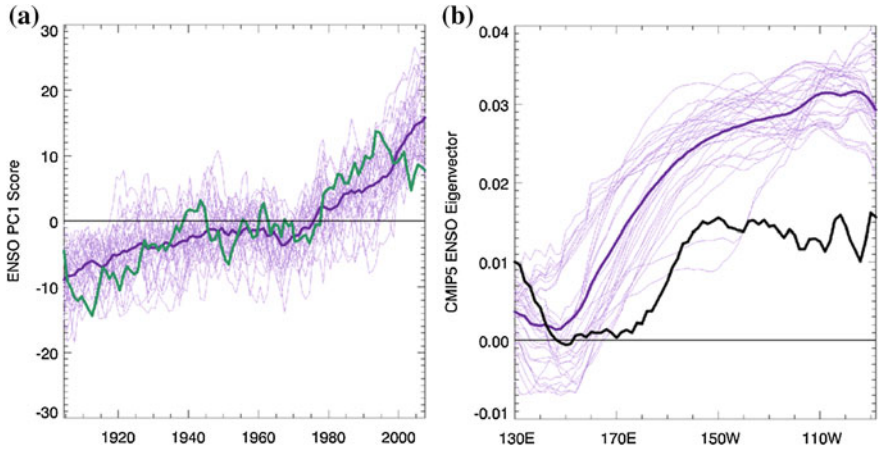

Fig. 8.6 **a** Ten-year averaged time series of observed (*blue*) and simulated CMIP5 (*purple*) ENSO principal component scores. **b** Meridionally averaged eigenvectors of tropical Pacific SST (15°S–15°N). In both **a** and **b,** individual simulations are shown with *thin purple lines*, while the *thick purple lines* indicate the ensemble averages

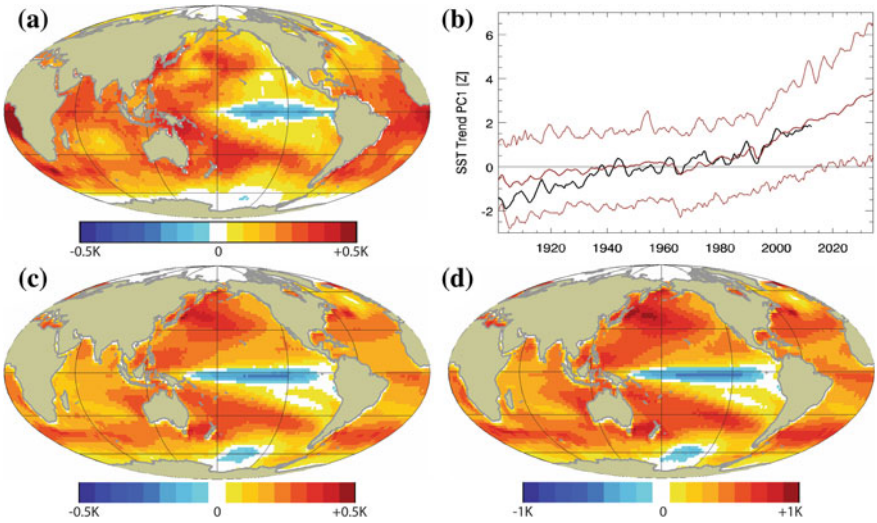

Fig. 8.7 **a** Change in SST associated with the observed trend mode between 1999–2013 and 1979–1998. **b** Time series of standardized observed and CMIP5 trend mode PCs, together with the minimum and maximum CMIP5 PC scores. **c** CMIP5 ensemble mean trend mode changes between 1999–2013 and 1979–1998. **d** Same as **c**, but for 2026–2035 compared to 1979–1998

gradient, has been described in a number of ENSO-residual trend studies, beginning with Cane et al. (1997), followed by Compo and Sardeshmukh (2010) and Solomon and Newman (2012). These stronger gradients tend to reduce the long rains over East Africa (Liebmann et al. 2014) and intensify the impacts of La Niña events (Hoell and Funk 2013a; Hoell et al. 2014), contributing to the greater rainfall deficits associated with more modern La Niña conditions (Williams and Funk 2011). Warming in the equatorial Indian Ocean (Funk et al. 2008) and western Pacific (Funk 2012) track very closely with CMIP5 SST predictions, and these warm waters have warmed substantially over the last 30 years.

The timing of the observed and CMIP5-estimated changes in the smoothed (10 year running mean) trend mode principal component scores is shown in Fig. 8.7b. While the minima-to-maxima spread of CMIP5 ensemble is quite large, the ensemble mean tracks very closely with the observed NOAA ER principal component time series. Both the observations and CMIP5 simulations indicate substantial increases between 1979 and 2013. Figure 8.7c combines the changes in these principal components with the CMIP5 eigenvectors to produce estimates of 1999–2013 versus 1979–1998 trend mode SST changes. Both the observations (Fig. 8.7a) and models (Fig. 8.7b) indicate substantial warming in the equatorial western Pacific and sub-tropics. The CMIP5 ENSO-residual trend mode also expresses slight cooling in the central Pacific, consistent with prior ENSO-residual empirical trend analyses (Cane et al. 1997; Compo and Sardeshmukh 2010; Solomon and Newman 2012).

By 2026–2035, continued trend mode warming could lead to even greater warming in the western equatorial Pacific (Fig. 8.7d), where climatological SSTs exceed 29 °C. SST patterns similar to Fig. 8.7a, b, d have been shown to produce drying across eastern Africa (Lyon and DeWitt 2012), and continued warming along these lines could intensify convection and precipitation over the warm pool, potentially influencing the monsoon circulations over East Africa.

We next use regressions between seasonal trend mode principal components (derived from the 1900–2013 NOAA ER SST) and NCEP/NCAR reanalysis total precipitable water, moisture transports, upper troposphere (0.21 sigma) velocity potential, and divergent wind fields to explore potential changes in the East African monsoon. Figure 8.8 shows the seasonal moisture and moisture transport regressions. Statistical significance in the figures is estimated at $p = 0.1$, based on a two-sided t-test with 64 degrees of freedom. Figure 8.9 contains similar seasonal velocity potential regression maps. The seasonal responses vary substantially, yet also indicate interesting similarities.

8.6.1 Seasonal Similarities for Sudan and Western Ethiopia

During all seasons, and particularly during JFM, the precipitable water regressions (Fig. 8.8) suggest atmospheric moisture declines in two primary locations: (1) across eastern Kenya, Tanzania, and Ethiopia, and southern Somalia, and

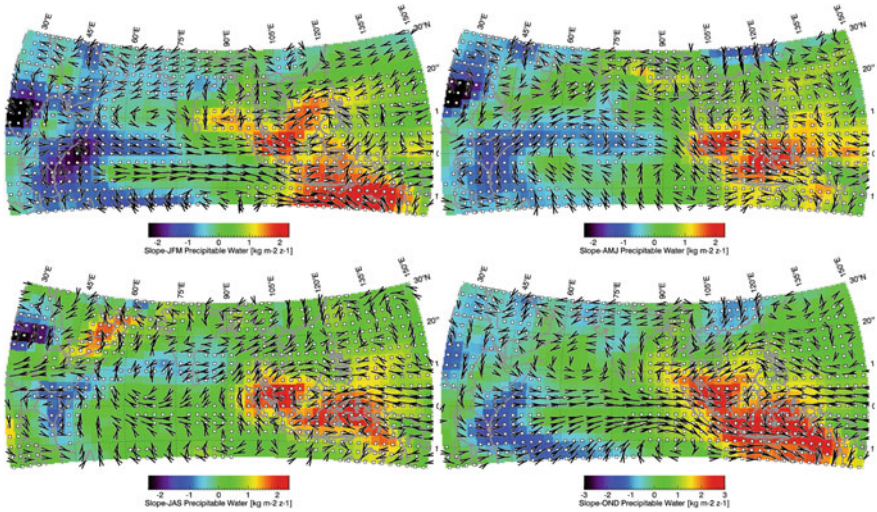

Fig. 8.8 1948–2013 regression between the trend mode first principal component and NCEP/NCAR reanalysis total precipitable water and moisture transport fields. Velocity potential slopes not significant as $p = 0.1$ were set to 0

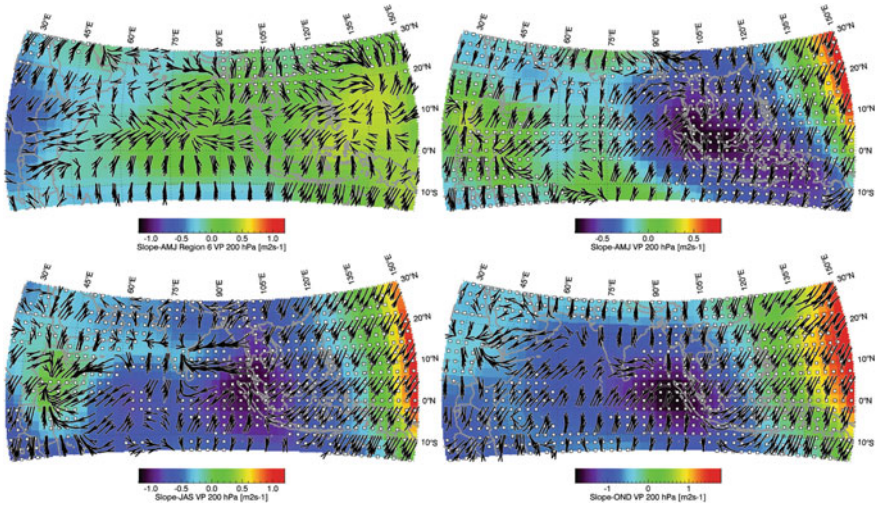

Fig. 8.9 1948–2013 regression between the trend mode first principal component and NCEP/NCAR reanalysis 0.21 sigma velocity potential heights and divergent wind fields. Velocity potential slopes not significant at $p = 0.1$ were set to 0

(2) across Sudan. The negative relationship to Sudan's total precipitable water appears related to a near surface high pressure cell, and anticyclonic circulation patterns that increase dry northerly transports while reducing moist flows out of the Congo basin. This region (and far western Ethiopia) has been found to be associated with 1990–2009 versus 1960–1989 rainfall declines during the main boreal summer rainy seasons, and appears to exhibit some of the most dramatic warming rates in East Africa and the Sahel (Funk et al. 2012). More discussion of the disruption of Congo moisture transports can be found in Williams et al. (2011), Jury and Funk (2012), and Viste and Sorteberg (2013). This surface high pressure cell and associated anticyclonic moisture transport responses appears to be supported by upper-level convergence in the divergent wind field responses (Fig. 8.9). In JFM and OND, the velocity potential response appears broadly similar to the velocity potential climatology; the response to the long-term warm trend (as represented by the trend principal component) may act to exacerbate the meridional (north-south) velocity potential gradient between the Sahara and southern Africa. Such a pattern would be associated with more (less) subsidence over the Sahara (southern Africa). The velocity potential regressions appear more complicated during AMJ and JAS. During AMJ and JAS, the climatological upper level divergent winds (Fig. 8.5) over Africa reverse, blowing into southern Africa and resembling the converse of the low-level monsoon trades across the northeast Indian Ocean (Fig. 8.3). During these seasons, the pattern of upper-level convergence (and increasing velocity potential) over Sudan appears to merge with subsidence over Ethiopia, Somalia, and Kenya.

8.6.2 Seasonal Similarities for Kenya, Tanzania, Somalia and Southern Ethiopia

We will now briefly discuss the seasonal moisture and velocity potential responses in "eastern East Africa," i.e., portions of Kenya, Tanzania, Somalia, and Ethiopia. While substantial declines in total precipitable water are indicated in each season, the spatial structure of the moisture transport responses varies substantially. During JFM and OND, the mean moisture flow across the Indian Ocean is the most zonal (Fig. 8.3), and one finds very large westerly mean transports between 5°N and 10°S. The trend mode responses during these boreal winter seasons (Fig. 8.8) resemble the climatological flows over the Indian Ocean (Fig. 8.3). During boreal winter, the link between these zonal winds and East African drought is well established (Hastenrath et al. 2011), and there is a strong link between El Niño (La Niña) and increased (decreased) East African rainfall. The low frequency trend mode principal component appears consistent with a La Niña-like change in boreal winter moisture transports.

As the Indian monsoon begins during the late portion of AMJ, the structure of both mean moisture transports (Fig. 8.3) and moisture transport responses (Fig. 8.8) change dramatically. Climatologically, ridging over the northwest Indian Ocean weakens, and monsoon trade winds cross into the Northern Hemisphere and recurve to the east, conserving angular momentum. Over the western Indian Ocean, the AMJ and JAS moisture transport responses appear to reinforce these climatological conditions. The southerly trade winds, and their local East African counterpart (the Somali Jet) are divergent along their western flanks, and this may be exacerbated by the intensified monsoonal trade patterns indicated during AMJ and JAS in Fig. 8.8. In the upper troposphere, in boreal spring and summer, we find strong upper-level convergence over Kenya, Ethiopia, Somalia and South Sudan, consistent with higher surface pressures.

8.7 Changes in CHIRPS Precipitation

We conclude with a brief examination of recent changes in CHIRPS precipitation (Fig. 8.10), which shows the recent (1999–2013 vs. 1981–1998) changes in standardized seasonal CHIRPS precipitation. Locations without significant (p = 0.1) precipitation changes or climatological precipitation with a standard deviation of <10 mm are not shown. Significance was estimated via a two-sided difference-of-means t-test. There has been a recent (1998) shift in Pacific SSTs that is thought to impact East African rainfall; we therefore examine here the differences in 1998–2013 and 1981–1997 mean rainfall. These changes have been divided by the 1981–2013 standard deviation to show changes in standardized precipitation. Changes not significant at $p = 0.1$ are not shown as a values in regions with seasonal rainfall standard deviations of <10 mm.

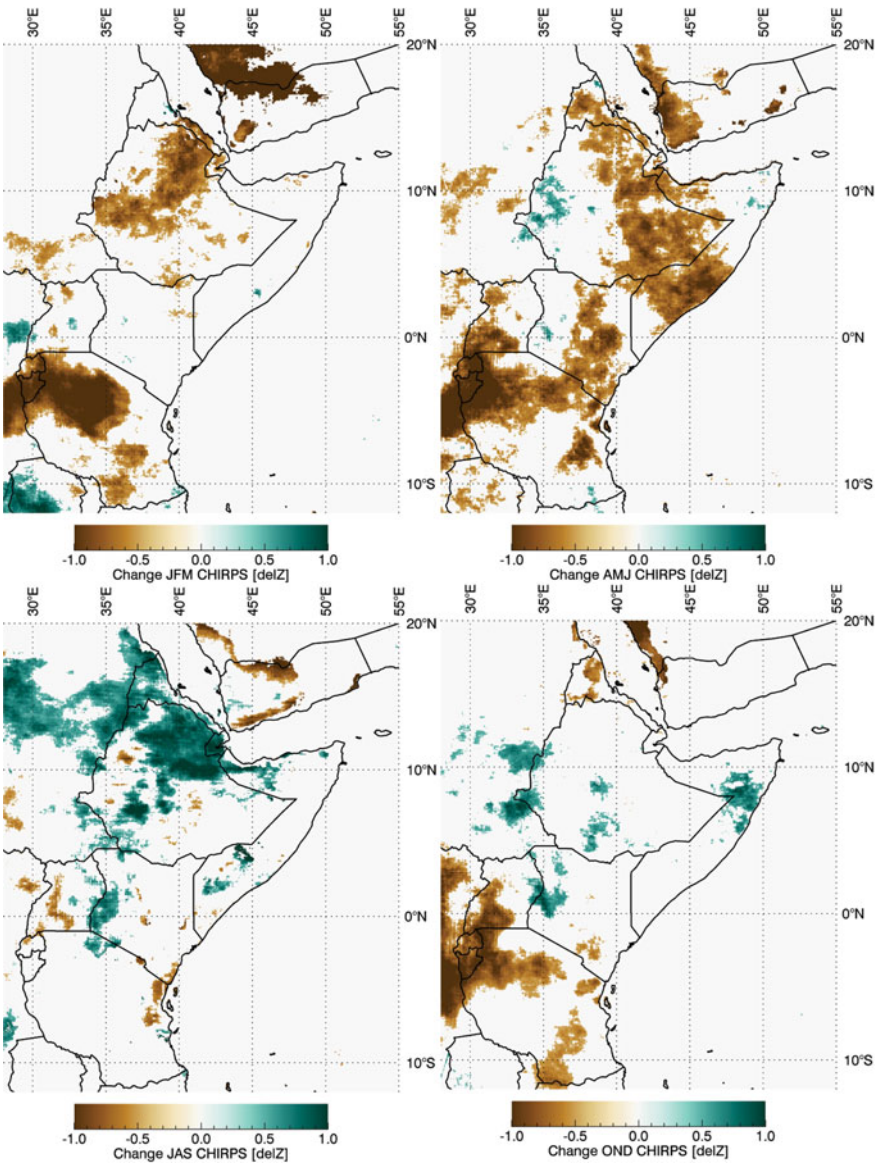

Fig. 8.10 Change in CHIRPS mean precipitation between 1998–2013 and 1981–1997, expressed in standardized deviations. Changes not significant at $p = 0.1$, based on a two-sided difference of means t-test, have been set to zero

During JFM, substantial drying is identified in Tanzania, Rwanda, Burundi, northern Ethiopia, and parts of the Middle East. The changes in Tanzania, Rwanda, and Burundi are probably much more significant, given the importance of this season climatologically. This region, in fact, exhibits substantial drying also in AMJ

and OND (i.e., all the seasons in which it typically receives rainfall). While the spatial agreement is not perfect, the reanalysis (Fig. 8.8) does indicate significant reductions in total precipitable water and onshore moisture transports in these seasons as well. In the CHIRPS data, this drying appears associated with rainfall reductions in Uganda in AMJ and OND as well. As suggested by Cook and Vizy (2013), drying in this region appears linked to changes in total precipitable water.

Kenya-Ethiopia-Somalia rainfall changes during AMJ, on the other hand, seem likely to be tied to changes in the Somali Jet, moisture supplies, and subsidence. If the Somali Jet has intensified, as suggested by Fig. 8.8, then dry boreal summer conditions may be arriving earlier in eastern Kenya, Ethiopia, and Somalia, resulting in more frequent droughts. Linking these droughts to enhanced Pacific SST gradients (Liebmann et al. 2014) may create opportunities for prediction (Shukla et al. 2014b).

During JAS, both the reanalysis moisture fields (Fig. 8.8) and CHIRPS precipitation (Fig. 8.10) show substantial increases across northern Ethiopia, as previously noted (Funk et al. 2012; Viste et al. 2012; Williams et al. 2011). Given that the large-scale circulation changes (Fig. 8.9) indicate upper-level convergence, this increase in precipitation appears associated with the lower troposphere. Changes in JAS total precipitable water and moisture transports indicate a strengthening of the Afar convergence zone, which stretches from the northern Ethiopian highlands to Yemen (Viste and Sorteberg 2013); the greatest moisture supply into northern Ethiopia comes from the north, and an intensified Afar convergence zone and associated low pressures would increase these flows. Across southern Ethiopia, the JAS transport regressions indicate an easterly shift, presumably increasing moisture transports into the highlands.

8.8 Conclusions

This chapter has briefly reviewed the complex climatological cycle of the East African monsoon system, paying special attention to its connection to the larger Indo-Pacific-Asian monsoon cycle. This perspective helps explain why parts of East Africa are dry, and why some of these locations are getting drier. The seasonal stage of the Indian monsoon system strongly influences moisture transports. When the winds across the northeast Indian Ocean reverse, the larger pattern transforms dramatically.

During "austral" summer (OND and JFM), cross-equatorial moisture transports are limited, and the key feature (over the Indian Ocean) is a strong westerly jet near the Equator (Hastenrath et al. 2011) that is caused by warm pool convection (Gill 1980, 1982) and modulated by ENSO. During OND, as the Intertropical Convergence Front moves quickly south, Indian trade winds from both the Northern and Southern Hemispheres converge over eastern Africa, and the region experiences its "short" rainy season. The climatological upper level velocity potential for this season, however, tends to produce convergence over the Greater

Horn of Africa, which may help explain this season's high variability and teleconnectivity. For Kenya and Ethiopia, there seems to be little recent change in OND rainfall. OND rainfall changes also seem to be model-dependent. For example, Hoell and Funk (2013) found substantial OND declines in simulations with the Global Forecast System model. On the other hand, Liebmann et al. (2014) found increases. The interpretation provided in the Liebmann study was that the short rains were influenced positively by warming in the northern Indian Ocean but also negatively by warming in the western Pacific, with the former having a slightly stronger influence.

During AMJ and JAS, the South Asian Monsoon begins, and the moisture transport patterns change dramatically. The jet over the equatorial Indian Ocean disappears, and the southeasterly trade winds sweep north across the eastern Indian Ocean and East Africa. For parts of eastern East Africa, these winds bring both a blessing and a burden. Forming the Somali Jet, they bring moisture onshore. This jet, however, produces subsidence on its westward flank, suppressing rainfall. The most bountiful rains occur in the west or at higher elevations, where orographic processes produce uplift. During AMJ, moisture transport regressions indicate stronger southerly monsoon winds at about 50°E; subsidence to the west (over East Africa) might be supported both by these low-level changes in the monsoon winds and upper-level changes in velocity potential and divergent wind fields. Across the southern Middle East, lower-level geopotential heights seem to be rising, and rainfall has also declined in Eritrea, Yemen, and Djibouti. During JAS, however, the Afar convergence zone appears to be intensifying, potentially adding to moisture transports into northern Ethiopia, where rainfall has been increasing.

One compelling result, identified in all seasons, is a tendency towards lower total precipitable water in Tanzania, Kenya, and Somalia. This seems to indicate a low-level ridging tendency. Focusing on Tanzania, Rwanda, Burundi, and Uganda, we see that these countries exhibit substantial rainfall declines during OND, AMJ, and JFM. One likely contributor to these precipitation decreases would be reduction in the onshore transports that typically flow onshore south of the Equator. Ridging tendencies between 10°S and the Equator appear to be reducing these flows in all seasons.

The future of the East African climate is and will be uncertain, given the incredible complexity of the processes that drive both mean and anomalous weather. More and better modeling studies will be needed. This brief chapter has emphasized the connection of East Africa's climate with the South Asian Monsoon and the Walker Circulation, connections that may help us better understand both the mean climate and recent changes in that climate. The results presented here suggest that a strengthening of the Walker circulation (as represented by the first principal component of global SSTs) influences the East African climate in complex but significant ways. Continued monitoring, modeling, and analysis will help us better identify, interpret, and predict those changes.

References

Aristotle (350 B.C.) Meteorology
Bjerknes J (1969) Atmospheric teleconnections from the equatorial Pacific. Mon Weather Rev 97:163–172
Camberlin P (1995) June–September rainfall in North-Eastern Africa and atmospheric signals over the tropics: a zonal perspective. Int J Climatol 15:773–783
Camberlin P, Philippon N (2002) The East African March–May rainy season: associated atmospheric dynamics and predictability over the 1968–97 period. J Clim 15:1002–1019
Cane MA et al (1997) Twentieth-century sea surface temperature trends. Science 275:957–960
Chadwick R, Boutle I, Martin G (2012) Spatial patterns of precipitation change in CMIP5: why the rich do not get richer in the tropics. J Clim 26:3803–3822
Compo GP, Sardeshmukh PD (2010) Removing ENSO-related variations from the climate record. J Clim. doi:10.1175/2009JCLI2735.1, 1957–1978
Cook KH, Vizy EK (2013) Projected Changes in East African rainy seasons. J Clim 26:5931–5948
England MH et al (2014) Recent intensification of wind-driven circulation in the Pacific and the ongoing warming hiatus. Nat Clim Change
Findlater J (1969) A major low-level air current near the Indian Ocean during the northern summer. Quart J R Meteorol Soc 95:362–380
Funk C (2012) Exceptional warming in the Western Pacific-Indian Ocean warm pool has contributed to more frequent droughts in Eastern Africa. Bull Am Meteorol Soc 7:1049–1051
Funk C, Michaelsen J, Marshall M (2012) Mapping recent decadal climate variations in precipitation and temperature across Eastern Africa and the Sahel. In: Wardlow B, Anderson M, Verdin J (eds) Remote sensing of drought: innovative monitoring approaches. CRC Press, p 25
Funk C, Dettinger MD, Michaelsen JC, Verdin JP, Brown ME, Barlow M, Hoell A (2008) Warming of the Indian Ocean threatens eastern and southern African food security but could be mitigated by agricultural development. Proc Natl Acad Sci USA 105:11081–11086
Funk C et al (2005) Recent drought tendencies in Ethiopia and equatorial-subtropical eastern Africa
Funk C et al (2013) Attribution of 2012 and 2003–12 rainfall deficits in eastern Kenya and southern Somalia. Bull Am Meteorol Soc 94:45–48
Funk C et al (2014) A quasi-global precipitation time series for drought monitoring 832, p 4
Gill AE (1980) Some simple solutions for heat-induced tropical circulation. Quart J R Meteorol Soc 106:447–462
Gill AE (1982) Atmosphere-ocean dynamics, vol 30. Academic Press, 662 pp
Giese BS, Ray S (2011) El Niño variability in simple ocean data assimilation (SODA), 1871–2008. J Geophys Res Oceans 1978–2012:116
Goddard L, Graham NE (1999) Importance of the Indian Ocean for simulating rainfall anomalies over eastern and southern Africa. J Geophys Res 104:19099–19116
Hastenrath S, Polzin D, Mutai CC (2007) Diagnosing the 2005 drought in equatorial East Africa. J Clim 20:4628–4637
Hastenrath S, Polzin D, Mutai C (2011) Circulation mechanisms of Kenya rainfall anomalies. J Clim 24:404–412
Held IM, Soden BJ (2006) Robust responses of the hydrological cycle to global warming. J Clim 19:5686–5699
Hoell A, Funk C (2013a) The ENSO-related West Pacific Sea surface temperature gradient. J Clim 26
Hoell A, Funk C (2013b) Indo-Pacific sea surface temperature influences on failed consecutive rainy seasons over eastern Africa. Clim Dyn 1–16
Hoell A, Funk C, Barlow M (2014) La Nina Diversity and the Forcing of Northwest Indian Ocean Rim Teleconnections. Clim Dyn

Indeje M, Semazzi FH, Ogallo LJ (2000) ENSO signals in East African rainfall seasons. Int J Climatol 20:19–46

IPCC (2014) Climate change 2014: impacts, adaptation, and vulnerability. Part B: regional aspects. Contribution of working Group II to the fifth assessment report of the intergovernmental panel on climate change. Cambridge University Press

Kalnay E et al (1996) The NCEP/NCAR 40-year reanalysis project. Bull Am Meteorol Soc 77:437–471

Krishnamurti TN, Molinari J, Pan HL (1976) Numerical simulation of the Somali jet. J Atmos Sci 33:2350–2362

L'Heureux ML, Lee S, Lyon B (2013) Recent multidecadal strengthening of the Walker circulation across the tropical Pacific. Nat Clim Change

Lyon B, DeWitt DG (2012) A recent and abrupt decline in the East African long rains. Geophys Res Lett 39(2). L02702

Lyon B, Barnston AG, DeWitt DG (2013) Tropical pacific forcing of a 1998–1999 climate shift: observational analysis and climate model results for the boreal spring season. Clim Dyn 1–17

Liebmann B et al (2012) Seasonality of African precipitation from 1996 to 2009. J Clim 25:4304–4322

Liebmann B et al (2014) Understanding recent Eastern horn of Africa rainfall variability and change. J Clim (in press)

Ogallo LJ, Janowiak JE, Halpert MS (1988) Teleconnection between seasonal rainfall over East Africa and global sea surface temperature anomalies. J Meteorol Soc Jpn 66:807–822

Okoola RE (1999) A diagnostic study of the eastern Africa monsoon circulation during the Northern Hemisphere spring season. Int J Climatol 19:143–168

Ramage C (1971) Monsoon meteorology, vol 296. Academic, San Diego

Riddle EE, Cook KH (2008) Abrupt rainfall transitions over the greater horn of Africa: observations and regional model simulations. J Geophys Res Atmos 1984–2012:113

Riehl H (1979) Climate and weather in the tropics. Academic Press, UK

Rodwell MJ, Hoskins BJ (1996) Monsoons and the dynamics of deserts. Quart J R Meteorol Soc 122:1385–1404

Rowell DP, Folland CK, Maskell K, Ward MN (1995) Variability of summer rainfall over tropical north Africa (1906–92): observations and modelling. Quart J R Meteorol Soc 121:669–704

Saji NH, Goswami BN, Vinayachandran PN, Yamagata T (1999) A dipole mode in the tropical Indian Ocean. Nature 401:360–363

Sandeep S, Stordal F, Sardeshmukh P, Compo G (2014) Pacific walker circulation variability in coupled and uncoupled climate models. Clim Dyn 43:103–117

Schneider U, Becker A, Finger P, Meyer-Christoffer A, Ziese M, Rudolf B (2013) GPCC's new land surface precipitation climatology based on quality-controlled in situ data and its role in quantifying the global water cycle. Theor Appl Climatol 1–26

Shukla S, Funk C, Hoell A (2014) Using constructed analogs to improve the skill of March–April–May precipitation forecasts in equatorial East Africa. Environ Res Lett 9.9:094009

Shukla S, McNally A, Husak G, Funk C (2014) A seasonal agricultural drought forecast system for food-insecure regions of East Africa. Hydrol Earth Syst Sc 18(10):3907-3921

Smith TM, Reynolds RW, Peterson TC, Lawrimore J (2008) Improvements to NOAA's historical merged land-ocean surface temperature analysis (1880–2006). J Clim 21:2283–2296

Solomon A, Newman M (2012) Reconciling disparate twentieth-century Indo-Pacific ocean temperature trends in the instrumental record. Nat Clim Change 2:691–699

Verdin J, Funk C, Senay G, Choularton R (2005) Climate science and famine early warning. Philos Trans R Soc B 360:2155–2168

Viste E, Sorteberg A (2013) Moisture transport into the Ethiopian highlands. Int J Climatol 33:249–263

Viste E, Korecha D, Sorteberg A (2012) Recent drought and precipitation tendencies in Ethiopia. Theor Appl Climatol 112:535–551

Vizy EK, Cook KH (2003) Connections between the summer East African and Indian rainfall regimes. J Geophys Res Atmos 108:4510

Walker GT (1923) Correlation in seasonal variations of weather, VIII. A Preliminary study of world weather. Memoirs of the Indian Meteorological Department
Williams P, Funk C (2011) A westward extension of the warm pool leads to a westward extension of the walker circulation, drying eastern Africa. Clim Dyn
Williams A et al (2011) Recent summer precipitation trends in the greater horn of Africa and the emerging role of Indian Ocean sea surface temperature. Clim Dyn 1–22
Yang W, Seager R, Cane MA, Lyon B (2014) The East African long rains in observations and models. J Clim

Chapter 9
The Connection Between the North and South American Monsoons

Rong Fu, Paola A. Arias and Hui Wang

Abstract We review evidence for a potential link between the North American Monsoon (NAM) and the South American Monsoon (SAM). Such a link is poorly documented in the literature, but if it were to exist, it could involve the influence of a monsoon onset on the cross-equatorial flow, atmospheric wave responses, and oceanic feedback to monsoon heating anomalies, which could in turn influence the decaying monsoon. With such a link, the variability of the NAM demise could be influenced by that of the SAM onset (or vice versa), in addition to its known dependence on regional land surface and adjacent oceans. The historical correlation between the NAM and the SAM appears to be mainly a consequence of both being dependent on tropical oceanic variability, such as El Niño-Southern Oscillation (ENSO), but an inter-monsoon link could be important for understanding the future climate variability of the American monsoons when the effects of anthropogenic forced change become more dominant—e.g., through reduction of evapotranspiration (ET) due to CO_2 fertilization of the rainforest and large-scale land use over the Amazon. These effects might perhaps not only delay the onset of the SAM, but also impact the demise of the NAM.

Keywords North American Monsoon · South American Monsoon · Inter-hemispheric connection · Monsoon variability

R. Fu (✉)
Jackson School of Geosciences, University of Texas at Austin, Austin, TX, USA
e-mail: rongfu@jsg.utexas.edu

P.A. Arias
Grupo de Ingeniería Y Gestión Ambiental (GIGA), Escuela Ambiental, Universidad de Antioquia, Medellín, Colombia
e-mail: paola.arias@udea.edu.co

P.A. Arias
Departamento de Geofísica, Universidad de Chile, Santiago, Chile

H. Wang
NOAA/NWS/NCEP/Climate Prediction Center, College Park, MD, USA

H. Wang
Innovim, Greenbelt, MD, USA

© Springer International Publishing Switzerland 2016

L.M.V. de Carvalho and C. Jones (eds.), *The Monsoons and Climate Change*,
Springer Climate, DOI 10.1007/978-3-319-21650-8_9

9.1 Why Do We Care About Inter-monsoon Connections?

Monsoon systems influence the livelihoods of more than half the world's population, and occur in areas of rapid population growth. Consequently, understanding their causes and variability has been an important focus of climate research, and substantial progress has been made in clarifying the dynamics of individual monsoon systems and of global monsoons in general. In contrast, relatively little attention has been paid to the potential inter-connections among various monsoon systems. Consequently, it is still unknown whether there are such connections among the different monsoon systems, and, if so, which mechanisms are responsible for them and how important they are in determining the variability of the monsoon systems, especially in a changing climate. The aim of this chapter is to explore these questions with a focus on the American monsoons, which serve as an example to illustrate the importance of investigating inter-monsoon connections.

Why do we focus on the American monsoons? First, the land masses over the American sector are more symmetric between the Northern and Southern Hemispheres than those of the Asia-Australian and African sectors, and so give rise to a relatively symmetric inter-hemispheric contrast of surface heating between land and oceans during the equinox seasons. Several processes could be involved in linking the inter-hemisphere monsoons: Firstly, the onset of a monsoon in one hemisphere could accelerate the reversal of the cross-equatorial flow, and the latter in turn would contribute to the decaying monsoon in the other hemisphere. Secondly, the tropical eastern Pacific-America-Atlantic sector is a region of weak upper westerly winds or the "westerly duct" (e.g., Dickinson 1971; Webster and Holton 1982). Thus, planetary waves triggered by monsoon diabatic heating anomalies, for example over the SAM region, could propagate across the Equator and influence atmospheric circulation over the NAM (e.g., Gedney and Valdes 2000). Finally, coupled ocean-atmospheric model simulations suggest that reduced monsoon diabatic heating, for example over the SAM region, could influence sea-surface temperature anomalies (SSTA) over the tropical eastern Pacific and Atlantic (e.g., Richter and Xie 2008; Nobre et al. 2009), which in turn could influence the NAM (e.g., Carleton et al. 1990; Higgins and Shi 2001; Liebmann and Marengo 2001; Marengo 2004; McCabe et al. 2004; Kushnir et al. 2010; Nigam et al. 2011).

Although the above processes may be favored by geographic and atmospheric dynamic configurations over the American continents and adjacent oceans, it is virtually unknown whether any of them provides a significant connection between the NAM and SAM, and, if so, what is the role of such a connection in determining climate variability of the American monsoons, especially in a changing climate. This chapter reviews the observed relationships between the NAM and SAM, the potential underlying physical mechanisms, and their importance in determining the variability of these American monsoons. It suggests challenges and a possible path forward to advance our understanding of this subject.

9.2 Is There Evidence Suggesting a Connection Between the American Monsoons?

Monsoons are commonly defined as the regions where the annual range of rainfall exceeds 2 mm/day and 70 % of the annual mean (e.g., Wang and Ding 2011), although there are many other similar criteria used for regional monsoon studies. The NAM encompasses the intense rainfall emanating from the eastern Pacific Inter-Tropical Convergence Zone (ITCZ), extending northward over Mexico to the southwestern United States (SW US), northeastward over the Gulf of Mexico, and southward to the Central American isthmus and northernmost South America. As the NAM expands northward, the upper tropospheric monsoon anticyclonic center shifts from southwestern to northwestern Mexico along the Sierra Madre Occidental, and finally to the SW US. Moisture is transported to the NAM region by a broad-scale southeastern flow in the lower and middle troposphere from the Gulf of Mexico and low-level jets (LLJs) over the Gulf of California and east of the Rockies. The latter, along with synoptic disturbances from the north, control the active and break phases of the NAM.

The SAM includes the Amazon and adjacent Atlantic ITCZ to the north and northeast, the South Atlantic Convergence Zone (SACZ) to the southeast, and central Brazil and Bolivia to the southwest. Its anticyclonic circulation (the Bolivian High) is centered close to the Altiplano Plateau. Moisture is transported by the northeasterly trade winds from the Atlantic Ocean to the Amazon, where it rains out and is recycled, and then is transported to the SACZ and southern Brazil by the South American LLJs (SALLJs). Trenberth et al. (2000), Vera et al. (2006), Mechoso (2011), Liebmann and Mechoso (2011), and Wang and Ding (2011) have provided concise and excellent descriptions of the structure of the NAM, SAM, and global monsoons and the mechanisms that control them. Chapters 6 and 7 of this book provide a more comprehensive discussion of the NAM and SAM.

Once a monsoon is established, it tends to reinforce itself through moisture convergence in the atmospheric boundary layer (ABL) driven by the monsoon diabatic heating. This stabilization of the monsoon makes it less prone to external influences exerted by other monsoon systems. In contrast, the circulations during the transition periods of monsoon onset and demise are unstable and so likely more prone to external influences, including those from other monsoons. Thus, we focus on the inter-monsoon connections during the period of monsoon onset and demise.

9.2.1 Is There a Cross-Hemispheric Relationship Between the Onset and Ending of American Monsoons?

Could the onset of the NAM influence the demise of the SAM, or vice versa? Under the concept of a regional monsoon, the onset and demise of a monsoon system are determined by the surface heating contrast between the local land and adjacent

oceanic regions. Influence from other monsoon systems is generally not considered. However, under the concept of a global monsoon, the transition from the NAM to the SAM, or vice versa, is part of the seasonal transition of the large-scale tropical overturning circulation (e.g., Trenberth et al. 2000; Wang and Ding 2011), with its rising branch controlled by the monsoon onset in the hemisphere of spring and its compensational sinking branch located over the decaying monsoon in the hemisphere of fall (Trenberth et al. 2000). Thus, the onset of NAM could, in principle, influence the demise of the SAM or vice versa. However, whether such a hypothetical link exists in reality is unclear.

The seasonal evolution of the onset and demise of the NAM and SAM (Fig. 9.1) is summarized as follows: Beginning in early boreal spring (February and March), the Western Hemispheric Warm Pool of SST (≥27.5 °C; Wang and Enfield 2001) first begins expanding northward into the northeastern tropical Pacific (Fig. 9.1a), then over the Caribbean Sea and western Atlantic (Fig. 9.1b). Subsequently, the rainy area (rain rate ≥ 7 mm/day) moves from the southern Amazon to the northernmost area of the South American continent and then to the Central American isthmus during April–June. By early- to mid-June, the rainy season expands to southwestern Mexico and then advances to northwestern Mexico, and

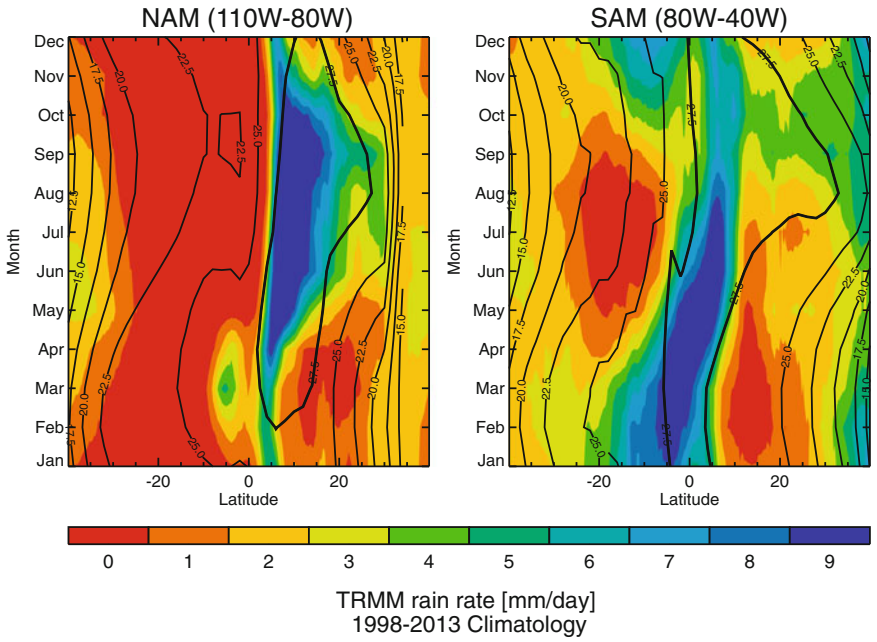

Fig. 9.1 Seasonal-latitudinal evolution of rain rate (shown by *shades*) and sea surface temperature (shown by *contours*) over the NAM (80°–110°W) and the SAM (40°–80°W) sectors suggesting a close temporal relationship between the onset of the NAM and demise of the SAM and vice versa. The Tropical Rainfall Measurement Mission (TRMM) rain rate and NOAA interpolated SST data are used for the period of 1998–2013 in units of mm/day and °C, respectively

the southwestern U.S. in July and August, when surface sensible heat flux over the Sierra Madre peaks (e.g., Douglas et al. 1993; Higgins et al. 1997; Barlow et al. 1998). At the same time, the dry season reaches its peak over the SAM region.

In August, the northern edge of the warm pool in the eastern Pacific and western Atlantic begins to retreat southward. However, rainfall in the NAM region continues to expand until reaching its northernmost location in September. From late September to early October, the dry-to-wet transition season, as indicated by increasing rainfall, begins over the Southern Amazon (5°–15°S, Fig. 9.1b). Rather than gradually moving southward across the Equator as a mirror image of the NAM onset, another rainy center forms in the southern Amazon in October. The northward and southward spread of the center is associated with the onset of the SAM (Kousky 1988; Horel et al. 1989; Liebmann and Marengo 2001). The NAM, remaining over southern Mexico, ends abruptly after the onset of SAM (Fig. 9.1a).

The temporal relationship shown in Fig. 9.1 provides some evidence that the onset of the NAM contributes to the demise of the SAM or vice versa. Alternatively, these correspondences could solely result from the seasonal migration of surface solar heating and SSTs. Wang and Fu (2002) show that during the monsoon transitions in the equinox seasons, rainfall change over South America leads that of the cross-equatorial flow, whereas during the peak of the monsoons in solstice seasons, variations in the cross-equatorial flow lead that of rainfall. These relationships suggest that the reversal of the cross-equatorial flow may be driven by rainfall change during the onset and demise of the SAM, and its variability contributes to rainfall variability once the monsoon is established; however, such analysis of the rainfall is limited to the South American continent. Consequently, the link between the dry-to-wet transition of the NAM, the southerly reversal of the trade wind over the Gulf of Mexico, and the cross-equatorial flow is not clear.

Does the reversal of the cross-equatorial flow influence the NAM onset during the boreal spring (March–May)? Apparently it does not. Higgins et al. (1997), Adams and Comrie (1997), and Higgins and Shi (2001) suggest that the moisture supply to western Mexico, i.e., the NAM core region, is dominated by the LLJs over the Gulf of California. Extra-tropical synoptic systems and intensification of the LLJs largely control the active and break phases of this monsoon rainfall.

Conversely, could the onset of NAM contribute to the reversal of the cross-equatorial flow over the American-Atlantic sector? To our knowledge, this question has not been addressed in the literature, but the following provides some evidence for such a connection. We look at the lead-lag regression between the anomalous near surface wind (925 hPa) over the eastern Pacific-American western Atlantic sector and the anomalous NAM V-index during April-June, the period of the NAM onset and SAM demise (Fig. 9.2a, b). Seasonal change has been removed in both fields. The SAM and NAM V-indices are defined, by the meridional wind at 925 hPa averaged over western Amazonia (5°S–5°N, 65°–75°W), and that over northern Mexico and the southwestern U.S. (17.5°–35°N, 120°W–100°W), respectively. These domains are chosen because the robust seasonal reversal of their meridional winds, including the cross-equatorial flow, meets the criterion of a global monsoon index (Lu and Chan 1999; Wang and Fu 2002; Li and Zeng 2002).

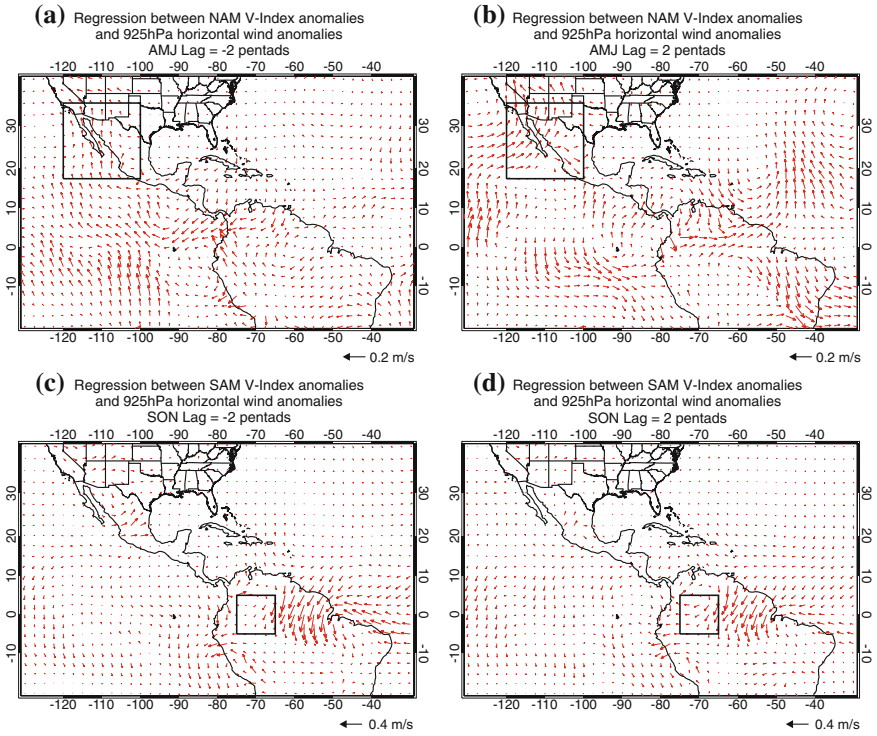

Fig. 9.2 The near surface wind anomalies (925 hPa) lagging the NAM and SAM V-indices anomalies, respectively, suggest an influence of the NAM onsets on the SAM demise during boreal spring and that of the SAM onset on the NAM demise in austral spring. **a** The 925 hPa wind anomalies lagging the NAM V-index anomalies by 2 pentads based on linear regression during the period of NAM onset and SAM demise (April–June) for 1979–2013. The lagged southerly meridional wind anomalies within the SAM region after the southerly NAM V-index suggest that the onset/intensification of the NAM could contribute to the demise/weakening of the SAM during boreal spring. **b** As in (**a**), but for the 925 hPa wind anomalies leading the NAM V-index anomalies by 2 pentads. The lack of southerly anomalies over the SAM region suggests that the southerly 925 hPa wind anomalies over the SAM region shown in (**a**) are not due to the correlation of the winds on seasonal scale. **c** As in (**a**), but for the 925 hPa wind anomalies lagging the SAM V-index anomalies by 2 pentads during the period of SAM onset and NAM demise (September–November). These northerly meridional wind anomalies over the NAM region lagging the northerly SAM V-index suggest that the onset/intensification of the SAM could contribute to the demise/weakening of the NAM during austral spring. **d** As (**c**), but for the 925 hPa wind anomalies leading the SAM V-index anomalies by 2 pentads. The lack of northerly anomalies over the NAM region suggests that the northerly 925 hPa wind anomalies over the NAM region shown in (**c**) are not due to the correlation of the winds on a seasonal scale. The regions of NAM and SAM V-indices are shown by black boxes in each panel. The scale of the wind vector and unit are indicated below the lower-right corner of each panel. NCEP-NCAR reanalysis is used

As evidenced for an influence of NAM onset on SAM demise, Fig. 9.2a shows southeasterly and easterly wind anomalies over western Amazonia and anticyclonic anomalies over southeastern Brazil, lagging the southerly NAM V-index by 2 pentads. The former indicates a weakening of moisture transport to Amazonia and SACZ, and both would weaken the SAM rainfall, whereas the latter indicates a strengthening of the NAM. Similar wind patterns persist for phases lagging the southern NAM-V index anomalies by 1–4 pentads (not shown), and are accompanied by southerly meridional wind anomalies over the eastern Pacific and anomalous anticyclonic circulation over the Central American isthmus and adjacent eastern Pacific and Caribbean Sea.

To evaluate whether the regression pattern shown in Fig. 9.2a is a result of auto-correlation of the wind anomalies, we compare it to the anomalous wind pattern that leads the NAM V-index by two pentads (Fig. 9.2b). The anomalous southeasterly wind over western Amazonia and anticyclonic circulation over southeast Brazil shown in Fig. 9.2a are replaced by the anomalous westerly wind over the equatorial Amazonia, strong northerly over the northeastern Brazil and cyclonic anomalous over southeast Brazil in Fig. 9.2b. The anomalous wind over the southeast Pacific is dominated by northerly or northwesterly leading the NAM V-index (Fig. 9.2b) instead of the southerly winds that lag the NAM V-index. These distinctively different anomalous wind patterns before and after the anomalous southerly NAM V-index suggests that the intensification of the NAM could weaken the SAM during April–June.

How can the intensified NAM weaken the SAM? Rodwell and Hoskins (2001) have shown that the rising motion driven by monsoon diabatic heating can induce poleward flow into the monsoon region, as required by Sverdrup vorticity balance. This mechanism presumably explains the northerly flow over western Mexico, the southwestern and central U.S., and eastern Pacific shown in Fig. 9.2a. How these changes would physically influence southeasterly wind anomalies over the equatorial western Amazonia is not clear; however, their statistical relationship, as shown in Fig. 9.2a, b, highlights the need to investigate their underlying physical mechanisms.

During austral spring (September–November), the onset of SAM is primarily driven by an increase of surface solar radiation and the resultant increase of surface fluxes, and thus the humidity in the ABL increases over the Amazon (e.g., Fu et al. 1999; Li and Fu 2004). The latter increases the moisture transport to the SACZ, and thus its rainfall intensity during the cyclonic phase of the Pacific-to-South America (PSA) wave train over the SACZ region (e.g., Mechoso et al. 2005; Li and Fu 2006; Ma and Mechoso 2007). Liebmann et al. (1999) have shown an anomalous northerly cross-equatorial flow two days after the intensification of the SACZ, suggesting that the increase of convective diabatic heating associated with the intensified SACZ could further drive the northerly SAM V-index and intensify moisture transport to the SAM region. The positive feedback between the SAM rainfall and northerly cross-equatorial flow and moisture transport eventually lead to the SAM onset.

Could this SAM onset influence the NAM demise during austral spring? Fig. 9.2c, d appear to suggest so. Figure 9.2c shows anomalous northerly and northwesterly winds over the NAM region lagging the northerly SAM V-index by two pentads (Fig. 9.2c). The former is associated with the weakening of the NAM over northwest Mexico, whereas the latter is associated with the intensification of the SAM over Amazonia. In contrast, Fig. 9.2d shows nearly zero or southwesterly wind anomalies over the NAM region prior to the northerly SAM V-index, suggesting stronger moisture transport to eastern Mexico. Thus, the distinctive weakening of the NAM following the strengthening of the SAM (Fig. 9.2c) indicates the possibility of the latter impacting the former.

Over the equatorial and southeastern tropical Pacific, eastern equatorial South America, and tropical western Atlantic, northerly meridional wind anomalies are correlated both leading and lagging the SAM V-index with some change in magnitudes. This weak dependence on the SAM V-index suggests that these northerly wind anomalies are probably connected to large-scale seasonal changes of the SSTs and wind fields.

Although the observed relationships shown in Figs. 9.1 and 9.2 are only suggestive, and the supporting evidence available in the literature is indirect, together they point toward a possible influence of the onset monsoon on the demising monsoon over the American continents during the equinox seasons, as illustrated schematically in Fig. 9.3—namely, as discussed above, the onsets of the NAM and SAM are primarily driven by the seasonal change of SSTs over the adjacent oceans, regional land surface heating, and associated meso-scale and regional circulation change, rather than by any remote influence through inter-monsoon connection. However, such connections seem possible for the monsoon demise. Its variability appears to be related to the variability of the reversal of the large-scale cross-equatorial flow as primarily driven by the onset monsoon on the opposite side of the equator. The importance of such an influence relative to that of the seasonal migration of the SST in the eastern tropical Pacific and western tropical Atlantic for the reversal of the cross-equatorial flow over the American sector is not clear, and needs to be investigated.

9.2.2 *Is the Monsoon Variability Connected on the Intra-seasonal to Multi-decadal Scales?*

Significant correlation between the variability of the NAM and SAM has been found on intra-seasonal, inter-annual, and decadal scales (Wang and Fu 2002; Arias et al. 2015). However, the NAM and SAM systems share the same tropical sources of variability at different time scales, such as the Madden-Julian Oscillation (MJO), El Niño-Southern Oscillation (ENSO), Atlantic Multi-decadal Oscillation (AMO), and Pacific Decadal Variability (PDV—e.g., Carleton et al. 1990; Higgins and Shi 2001; Liebmann and Marengo 2001; Marengo 2004; Lorenz and Hartmann 2006;

(a) The onset of the NAM contributes to the southerly reversal of the V-index of SAM, (the cross-equatorial flow over South America) and so contributes to its demise during April-June

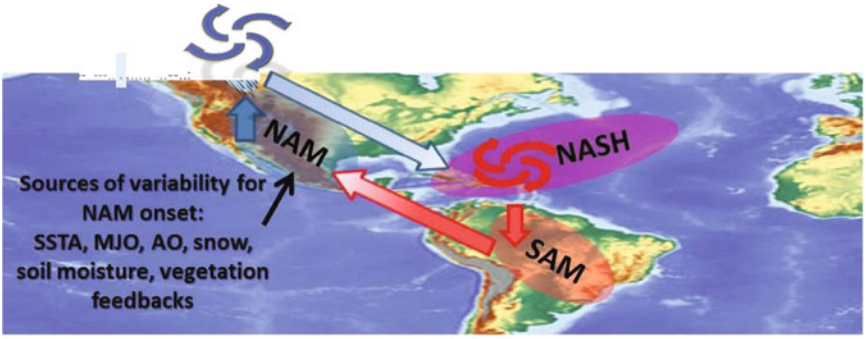

(b) The onset of the SAM contributes to the northerly reversal of the the V-index of NAM and so contributes to its demise during September-October

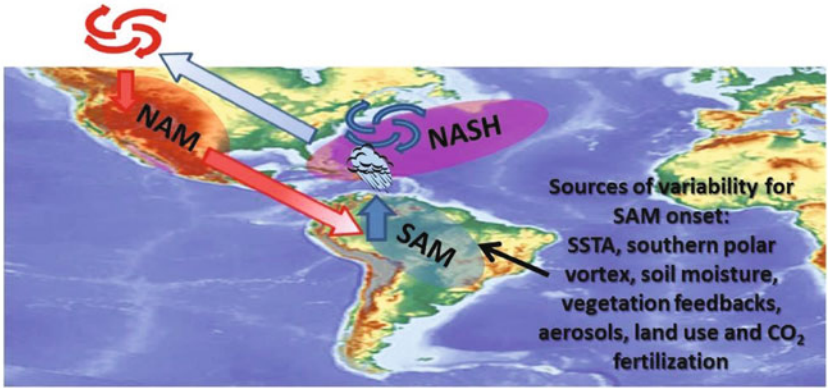

Fig. 9.3 Schematic illustration of how **a** The NAM onset influences the seasonal reversal of the large-scale overturning circulation along the western edge of the NASH, contributing to the demise of the SAM during April–June. The sources of NAM onset variability are listed in the text box; **b** As in (**a**), but for the influence of the SAM onset on the demise of the NAM during September–November

Casarin and Kousky 1986; Kiladis and Weickmann 1992; Nogues-Paegle and Mo 1997; Paegle et al. 2000; Carvalho et al. 2004; Grantz et al. 2007; Zhu et al. 2007; Hu and Feng 2008; Arias et al. 2012). This shared forcing can result in correlated rainfall variability between these two monsoon systems, posing a challenge for observational diagnosis of any direct physical linkage between them.

Whether or not there is such a linkage between intra-seasonal and multi-decadal climate variability of the NAM and SAM is virtually unknown. To illustrate the need for investigating this potential linkage, we show the co-variability between NAM and SAM in Figs. 9.4 and 9.5 for the austral spring season. The co-variations of NAM and SAM rainfall anomalies on the intra-seasonal time scale can be represented by the two leading modes of the singular value decomposition (SVD) of the 30–70 day band-pass filtered pentad precipitation anomalies (seasonality is removed) in the NAM and SAM regions for 1979–2010. The two modes are characterized by an in-phase relationship and an out-of-phase relationship, respectively, between the intra-seasonal precipitation anomalies in the two monsoon regions. The first mode shows in-phase correlations of rainfall between Central America and South America between 10°N and 20°S (Fig. 9.4a, b). Such simultaneous increase or decrease of rainfall over both regions is correlated with an anticyclonic low-level flow centered over Mexico and an enhanced easterly wind over the eastern Pacific ITCZ area. The second mode shows an out-of-phase correlation between rainfall over Central America and that over the western Amazon and the land part of the SACZ (Fig. 9.4c, d), suggesting an intra-seasonal increase of rainfall in Central America and an anomalous anticyclonic circulation over the Gulf of Mexico and western Caribbean Sea in association with a decrease of rainfall over the SAM. The associations of anomalous NAM and SAM precipitation with the anomalous V-indices on the intra-seasonal time scale can be seen from the lead and lag correlations between the corresponding SVD time series and the V-indices in Fig. 9.5.

The SAM V-index anomalies (Fig. 9.5a) are negatively correlated with the leading first SVD mode of SAM rainfall anomalies, suggesting that an increase of SAM rainfall may drive the northerly cross-equatorial flow over South America, i.e., the SAM V-index. The SAM V-index is also positively correlated with the leading second SVD mode of the SAM rainfall, suggesting that an intensification of SACZ and decrease of rainfall over the Amazon may give rise to an anomalous southerly cross-equatorial flow over South America. The SAM V-index is only marginally correlated with the in-phase and leading first SVD principal component of the NAM rainfall.

Surprisingly, the NAM V-index (Fig. 9.5b) anomalies are correlated with the in-phase and lagged first SVD of the NAM and SAM precipitation anomalies. The physical implication of such a relationship is unclear, but it may represent the influence of MJO on the eastern Pacific ITCZ and the resultant intra-seasonal variations of both the NAM and SAM rainfall variability, as has been suggested by many previous studies (Higgins and Shi 2001; Lorenz and Hartmann 2006; Casarin and Kousky 1986; Kiladis and Weickmann 1992; NoguesPaegle and Mo 1997; Paegle et al. 2000; Carvalho et al. 2004).

The inter-annual relationships between monthly anomalies of the NAM and SAM can be different from their counterparts on the intra-seasonal time scale. For example, during austral spring, the two leading SVD modes are both dominated by a seesaw relationship between the NAM and the SAM precipitation anomalies. The pattern of the first mode shows that an increase of rainfall over the SACZ is

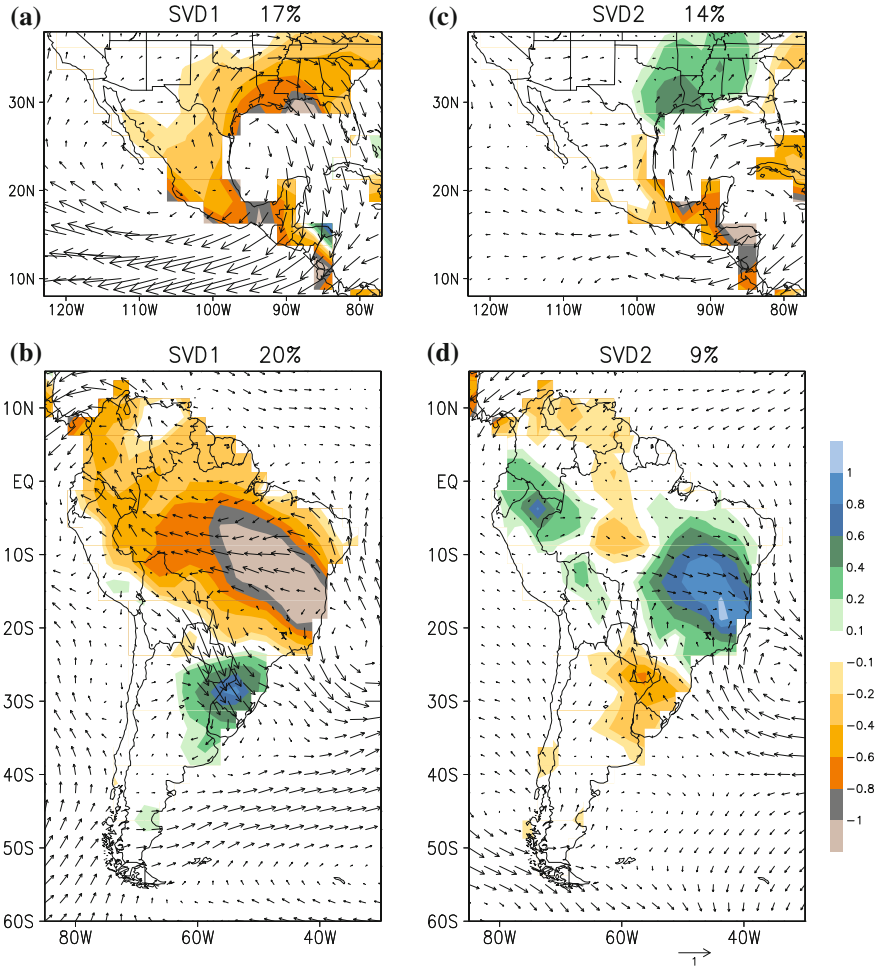

Fig. 9.4 The pentad rainfall anomalies (*shades*, mm/day) and near surface wind anomalies (925 hPa, vectors, *unit* m s^{-1}), respectively, projected onto (**a**), (**b**) the first and (**c**), (**d**) second SVD modes of intra-seasonal variation of the precipitation over the NAM and SAM regions, respectively, during austral spring. The intra-seasonal rainfall anomalies are obtained by a 30–70 day band-pass filtered for 1979–2010. The percentage of the total intra-seasonal precipitation variance explained by each mode is given at the top right of each panel. The precipitation data are the NOAA CMAP pentad data and the 925 hPa pentad winds are derived from the NCEP/NCAR reanalysis daily data

correlated with a decrease of rainfall over the Central American isthmus (Fig. 9.6a, b), and an anomalous anticyclonic flow over the Gulf of Mexico and western Caribbean Sea. Both the anomalous rainfall and associated wind patterns resemble the second SVD mode of the intra-seasonal rainfall anomalies between NAM and SAM regions (Fig. 9.4c, d). The second SVD mode shows that an increase in

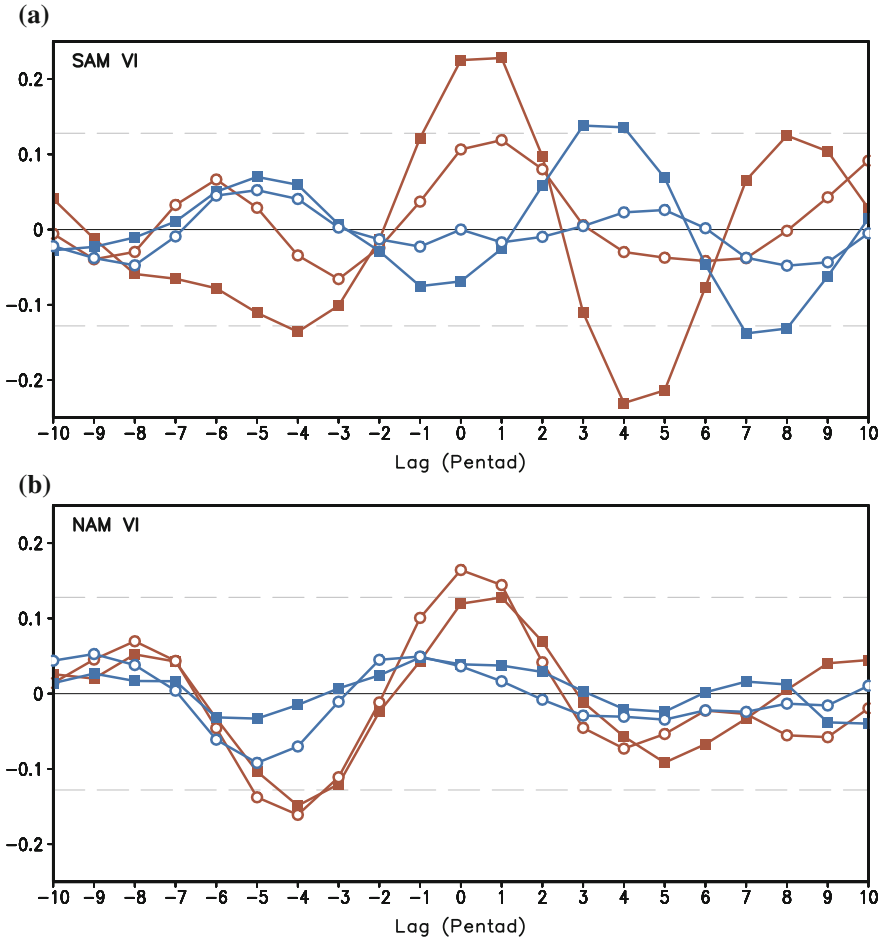

Fig. 9.5 Lead and lag correlations between **a** The anomalous pentad SAM V-index (NCEP/NCAR reanalysis data) and the time series of the first (*red*) and second (*blue*) SVD modes of the 30–70 day band-pass filtered precipitation anomalies over the SAM region (*closed square*) and the NAM region (*open circle*) during austral spring for 1979–2010. and **b** Similar lead and lag correlations, but with the NAM V-index. Negative lag means the V-index leading precipitation. *Gray dash lines* denote the 99 % significance level; the number of effective samples is determined based on Chen (1981)

rainfall over the equatorial and northernmost South America is correlated with an increase in rainfall over southern Mexico and a decrease in rainfall over an area extending from southeastern Texas to eastern Georgia (Fig. 9.6c, d). The associated anomalous low-level wind pattern in Fig. 9.6c resembles that of the first SVD mode of intra-seasonal rainfall over the NAM region (Fig. 9.4a), but not over the SAM region (cf. Fig. 9.6d, b).

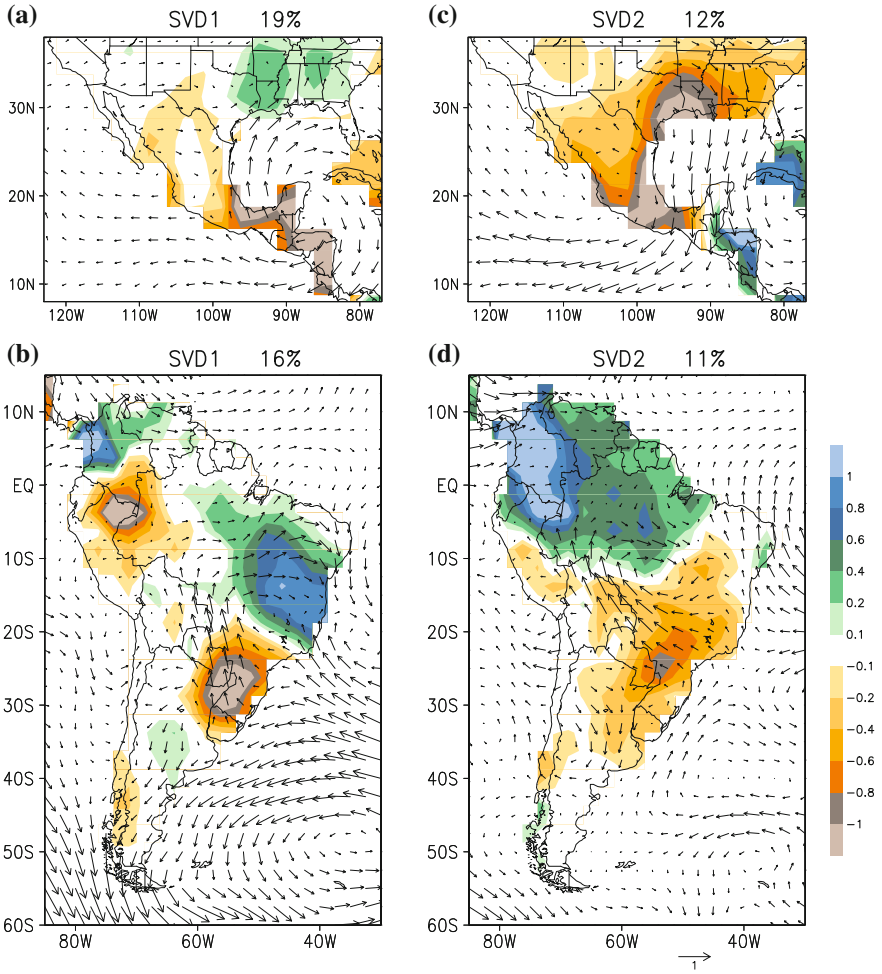

Fig. 9.6 As in Fig. 9.4, but for the monthly mean rainfall anomalies (*shading*, mm/day) and 925 hPa wind anomalies (vector, *unit* m s^{-1}) projected onto (**a**), (**b**) the first and (**c**), (**d**) the second SVD modes of monthly precipitation anomalies over the two monsoon regions for austral spring

The differences of spatial correlation patterns between intra-seasonal and inter-annual rainfall variability are expected because the former is largely controlled by the atmospheric internal variability and wave response to diabatic heating anomalies, whereas the latter is dominated by the patterns of SSTA associated with major modes of the coupled ocean-atmospheric variability. These modes could easily overwhelm any signal of inter-hemispheric monsoon connection, where such a signal exists.

On a decadal scale, Lee et al. (2014) have shown the connection among the climate variability of the northern hemispheric monsoons (i.e., Asian, African, and

North American) to be a result of changing El Niño types. In particular, from 1994 to 2009 these northern hemispheric monsoons intensified during the summer and weakened during the winter, and their inter-annual variability became weaker than during 1979–1993. By contrast, the variability of southern hemispheric monsoons has not changed. Consequently, no connection between the variations of NAM and the SAM intensity is found in their study. However, Arias et al. (2015) have observed a statistically significant correlation between an early demise of the NAM and a late onset of the SAM on inter-annual and decadal scales (Fig. 9.7). Such an early demise of the NAM and late onset of the SAM is also correlated with an increase of rainfall and moisture convergence over the tropical eastern Pacific and the Central American isthmus, leading to moisture divergence from the NAM and SAM regions. The early ending of the NAM is also influenced by a westward displacement of the NASH, which enhances moisture divergence from the NAM region (Arias et al. 2012). On an inter-annual scale, the increase of rainfall over the northeastern tropical Pacific and Central American isthmus appears to be connected to the warmer SST anomalies over the central and eastern Pacific, and the westward expansion of the NASH appears to be linked to the variability of the Asian monsoon (Chen et al. 2001; Kelly and Mapes 2011) and surface temperature changes over Africa (Miyasaka and Nakamura 2005; Li et al. 2012). On a decadal scale, the earlier demise of NAM and the late onset of SAM appear to be related to the global SST warming and positive AMO modes. The influence of one monsoon on the other cannot be isolated from the above oceanic variability modes.

In short, the observed relationships between the inter-annual and decadal variability of the NAM and SAM onset and demise appear to be primarily forced by the tropical Pacific and Atlantic SST variability, and possibly a global warming mode (Arias et al. 2012, 2015). Whether an inter-monsoon connection plays any significant role in determining these observed correlations cannot be established.

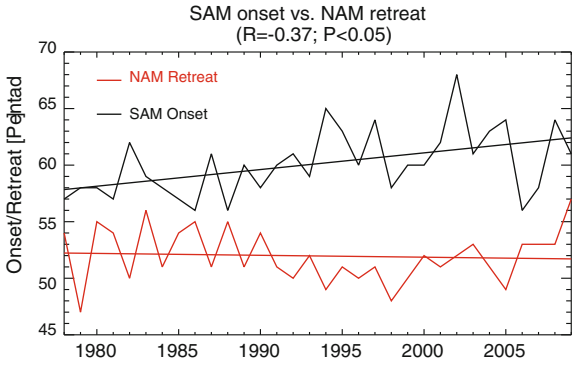

Fig. 9.7 The time series of the NAM demise date (*red*) and SAM onset date (*black*) show an increasing time gap between the NAM demise and SAM onset between 1978 and 2009. The early NAM retreats and late SAM onset dates are also statistically correlated at $P < 0.05$. Correlation is computed for the de-trended time series

9.2.3 *Could Inter-monsoon Connections Influence Monsoon Variability Induced by Climate Change and Land Use?*

Liu et al. (2009) have used climate model simulations to explore connections between the variability of monsoons globally, using a coupled ocean-atmospheric model. Their study suggests that without external forcing, the individual monsoons' variabilities are not interdependent. However, when they are forced by external factors, such as changes of atmospheric greenhouse gases, aerosols, and Earth's orbit, connection appears, e.g., the global monsoons are intensified during the Medieval Warming Period and weakened during the Little Ice Age. Such correlated change is due to the greater land surface temperature changes than those of the ocean, leading to a greater land-ocean surface temperature contrast in a warmer climate and a weaker land-ocean surface temperature contrast in a cooler climate. A similar mechanism appears to be responsible for the projected intensification of Northern Hemispheric global monsoons by the climate models that participated in the Fifth Report of the Intergovernmental Panel on Climate Change (e.g., Lee and Wang 2014).

Could land surface processes and land use influence not only the SAM but also the NAM, or vice versa, through inter-monsoon connections? Both numerical model experiments and observations suggest that conversion of the rainforests to pasture and produce would reduce ET in the dry season and increase runoff in the wet season (Dickinson and Henderson-Sellers 1988; Gash and Nobre 1997; Davidson et al. 2012; Harper et al. 2014). The former would reduce the dry season rainfall and delay the SAM, since ET is the main source of rainfall during those seasons (Li and Fu 2004; Fu and Li 2004). Such an effect could be further exacerbated by fire-generated aerosols, produced as part of land use over the Amazon (e.g., Zhang et al. 2008; Bevan et al. 2009; Zhang et al. 2009). The latter would increase annual peak river flow over the SAM region. In addition, the improved vegetation water use efficiency in an elevated atmospheric CO_2 environment would also reduce ET and possibly rainfall in the dry season, and increase runoff in the wet season (Sellers et al. 1996; Gedney et al. 2006; Doutriaux-Boucher et al. 2009; Coe et al. 2011; Pu and Dickinson 2014). Whether such a vegetation response to the elevated atmospheric CO_2 with changing land use over the SAM will influence the NAM has not been directly addressed in the literature, yet such a possibility exists for several reasons:

Firstly, Nobre et al. (2009) showed that in a coupled ocean-atmospheric system, rainfall reduction due to large-scale removal of the rainforests over the Amazon could induce an El Niño-like SSTA pattern, which in turn would exacerbate rainfall reduction over the SAM region. We suggest that such an El Niño-like SSTA pattern could also potentially weaken the NAM due to an equatorward shift of the eastern Pacific ITCZ (e.g., Higgins and Shi 2001). Secondly, Gedney and Valdes (2000) have suggested that a Rossby wave train induced by rainfall reduction due to deforestation over the Amazon would increase rainfall over the southern U.S. and

Mexico during the boreal winter season. Such an atmospheric wave response to deforestation over the Amazon could in principle influence the NAM during the boreal spring and fall (e.g., Dickinson 1971), but has not been investigated. Finally, observations have shown a statistically significant intensification of hurricanes as they pass the Amazon and Orinoco river plumes (Field 2007). Thus, an increase of runoff and river flow due to large-scale deforestation could potentially increase the intensity of hurricanes in the Caribbean Sea. The hurricanes that make landfall over Mexico can significantly influence the NAM rainfall. Whether these mechanisms suggested by numerical model experiments and past observations will influence long-term and future climate variability of the NAM and SAM in a changing climate needs to be clarified.

9.3 Outstanding Questions, Challenges and a Path Forward

Few studies on the connection between the NAM and SAM are found in the literature, but the available evidence discussed in this chapter points toward a possible link between these two monsoon systems that deserves further investigation. Such a link could be provided by the influence of the monsoon onset on cross-equatorial flow, atmospheric wave responses, and oceanic feedback to the monsoon heating anomalies, and through these processes an influence on the decaying monsoon. With such inter-monsoon links, the climate variability of the NAM could be influenced by that of the SAM, or vice versa, in addition to the variability of the regional land surface and adjacent ocean climate conditions. Although the variability of both the NAM and SAM in today's climate is mainly forced by tropical oceanic and atmospheric variability, such as ENSO, AMO, and MJO, an inter-monsoon link may be more important for understanding the variability of American monsoons in the future, when the anthropogenic forced change becomes dominant, especially over the SAM region. For example, were the above-discussed inter-monsoon links to exist, the reduced ET due to CO_2 fertilization of the rainforest and large-scale land use over the Amazon would not only delay the onset of the SAM, but also impact the demise of the NAM. Likewise, a future earlier onset of the NAM could influence the demise of the SAM. Thus, a clarification of inter-monsoon connections would provide a key to addressing this future variability of the American monsoons.

Without concrete evidence, the inter-monsoon links over the Americas, as well as globally, remains speculative. As a first step, it is critical for future investigations to address these outstanding questions:

a. What is the relative importance of inter-monsoon links versus the variability of the regional land surface and adjacent oceans in determining monsoon climate variability, especially in the future?

b. What are the key dynamic mechanisms that provide the inter-monsoon links over the Americas, and globally?
c. How would the response of the Amazonian rainforests, the world's largest biome, to elevated CO_2 and global climate change, influence the NAM? How would a change of NAM influence the demise of the SAM?

Because the NAM and SAM systems share mostly the same sources of tropical oceanic and atmospheric variability, one of the main challenges is to isolate the inter-monsoon links from the correlated variability forced by these common sources of the tropical variability. Understanding the atmospheric dynamic responses on synoptic to intra-seasonal scales through observational analysis, numerical model experiments of various levels of complexity, and clarification of the role of inter-monsoon connection in improving seasonal prediction and future climate projections, would be particularly useful.

Acknowledgments We thank Drs. Robert Dickinson and Bing Pu for their constructive comments and help in improving the manuscript. This work was supported by the National Science Foundation grant (AGS-0937400) and the National Oceanic and Atmospheric Administration Modeling, Analysis, Predictions and Projections Program grant (NA10OAR4310157). Paola A. Arias was supported by "Comisión Nacional de Investigación Científica y Tecnológica de Chile" grant FONDECYT #3140570 and the Programme "Estrategia de Sostenbilidad 2015-2016" at Universidad de Antioquia, Colombia.

References

Adams DK, Comrie AC (1997) The North American monsoon. B Am Meteorol Soc 78(10):2197–2213

Arias PA, Fu R, Mo KC (2012) Decadal variation of rainfall seasonality in the north american monsoon region and its potential causes. J Clim 25(12):4258–4274

Arias PA, Fu R, Vera CS, Rojas M (2015) A correlated shortening of the North and South American monsoon seasons in the past few decades. Clim Dynam 1–22. doi: 10.1007/s00382-015-2533-1

Barlow M, Nigam S, Berbery EH (1998) Evolution of the North American monsoon system. J Clim 11(9):2238–2257

Bevan SL, North PRJ, Grey WMF, Los SO, Plummer SE (2009) Impact of atmospheric aerosol from biomass burning on Amazon dry-season drought. J Geophys Res-Atmos 114

Carleton AM, Carpenter DA, Weser PJ (1990) Mechanisms of interannual variability of the Southwest United-States summer rainfall maximum. J Clim 3(9):999–1015

Carvalho LMV, Jones C, Liebmann B (2004) The South Atlantic convergence zone: Intensity, form, persistence, and relationships with intraseasonal to interannual activity and extreme rainfall. J Clim 17(1):88–108

Casarin DP, Kousky VE (1986) Anomalias de precipitacão no sul do Brasil e variacões na circulacão atmosférica. Rev Bras Meteorol 1:83–90

Chen WY (1981) Fluctuations in Northern Hemisphere 700 mb height field associated with the Southern Oscillation. Mon Wea Rev 110:808–823

Chen P, Hoerling MP, Dole RM (2001) The origin of the subtropical anticyclones. J Atmos Sci 58 (13):1827–1835

Coe MT, Latrubesse EM, Ferreira ME, Amsler ML (2011) The effects of deforestation and climate variability on the streamflow of the Araguaia River, Brazil. Biogeochemistry 105(1–3): 119–131

Davidson EA, de Araujo AC, Artaxo P, Balch JK, Brown IF, Bustamante MMC, Coe MT, DeFries RS, Keller M, Longo M, Munger JW, Schroeder W, Soares BS, Souza CM, Wofsy SC (2012) The Amazon basin in transition. Nature 481(7381):321–328

Dickinson RE (1971) Cross-equatorial eddy momentum fluxes as evidence of tropical planettary wave sources. Q J Roy Meteor Soc 97(414):554

Dickinson RE, Henderson-Sellers A (1988) Modeling tropical deforestation—a study of Gcm land surface parametrizations. Q J Roy Meteor Soc 114(480):439–462

Douglas MW, Maddox RA, Howard K, Reyes S (1993) The Mexican Monsoon. J Clim 6 (8):1665–1677

Doutriaux-Boucher M, Webb MJ, Gregory JM, Boucher O (2009) Carbon dioxide induced stomatal closure increases radiative forcing via a rapid reduction in low cloud. Geophys Res Lett 36

Ffield A (2007) Amazon and Orinoco River plumes and NBC rings: Bystanders or participants in hurricane events? J Clim 20(2):316–333

Fu WR (2004) Transition of the large-scale atmospheric and land surface conditions from the dry to the wet season over Amazonia as diagnosed by the ECMWF reanalysis. J Clim 17 (13):2637–2651

Fu R, Li WH (2004) Influence of land surface on transition from dry to wet season over the Amazon. J Theor Appl Clim 78(123):97–110

Fu R, Zhu B, Dickinson RE (1999) How do atmosphere and land surface influence seasonal changes of convection in the tropical amazon? J Clim 12(5):1306–1321

Gash JHC, Nobre CA (1997) Climatic effects of Amazonian deforestation: Some results from ABRACOS. B Am Meteorol Soc 78(5):823–830

Gedney N, Valdes PJ (2000) The effect of Amazonian deforestation on the northern hemisphere circulation and climate. Geophys Res Lett 27(19):3053–3056

Gedney N, Cox PM, Betts RA, Boucher O, Huntingford C, Stott PA (2006) Detection of a direct carbon dioxide effect in continental river runoff records. Nature 439(7078):835–838

Grantz K, Rajagopalan B, Clark M, Zagona E (2007) Seasonal shifts in the North American monsoon. J Clim 20(9):1923–1935

Harper A, Baker IT, Denning AS, Randall DA, Dazlich D, Branson M (2014) Impact of Evapotranspiration on Dry Season Climate in the Amazon Forest. J Clim 27(2):574–591

Higgins RW, Shi W (2001) Intercomparison of the principal modes of interannual and intraseasonal variability of the North American Monsoon System. J Clim 14(3):403–417

Higgins RW, Yao Y, Wang XL (1997) Influence of the North American monsoon system on the US summer precipitation regime. J Climate 10(10):2600–2622

Horel JD, Hahmann AN, Geisler JE (1989) An Investigation of the Annual cycle of convective activity over the tropical Americas. J Clim 2(11):1388–1403

Hu Q, Feng S (2008) Variation of the North American summer monsoon regimes and the Atlantic multidecadal oscillation. J Clim 21(11):2371–2383

Kelly P, Mapes B (2011) Zonal mean wind, the Indian monsoon, and July drying in the western Atlantic subtropics. J Geophys Res-Atmos 116

Kiladis GN, Weickmann KM (1992) Circulation anomalies associated with tropical convection during northern winter. Mon Weather Rev 120(9):1900–1923

Kousky VE (1988) Pentad outgoing long wave radiation climatology for the South American sector. Rev Bras Meteorol 3:217–231

Kushnir Y, Seager R, Ting MF, Naik N, Nakamura J (2010) Mechanisms of Tropical Atlantic SST Influence on North American Precipitation Variability. J Clim 23(21):5610–5628

Lee JY, Wang B (2014) Future change of global monsoon in the CMIP5. Clim Dynam 42(1–2):101–119

Lee E-J, Ha K-J, Jhun J-G (2014) Interdecadal changes in interannual variability of the global monsoon precipitation and interrelationships among its subcomponents. Clim Dynam 42(9–10):2585–2601. doi:10.1007/s00382-013-1762-4

Li JP, Zeng QC (2002) A unified monsoon index. Geophys Res Lett 29(8):1274. doi:10.1029/2001GL013874Li

Li W, Fu R (2006) Influence of cold air intrusions on the wet season onset over Amazonia. J Clim 19(2):257–275

Li W, Ting M Li L, Liu Y (2012) Intensification of Northern Hemisphere subtropical highs in a warming climate. Nat Geosci 5:830–834

Liebmann B, Marengo JA (2001) Interannual variability of the rainy season and rainfall in the Brazilian Amazon basin. J Clim 14(22):4308–4318

Liebmann B, Kiladis GN, Marengo JA, Ambrizzi T, Glick JD (1999) Submonthly convective variability over South America and the South Atlantic convergence zone. J Clim 12(7):1877–1891

Liebmann B, Mechoso CR (2011) The South American Monsoon System. Research and Forecast 9

Liu J, Wang B, Ding QH, Kuang XY, Soon WL, Zorita E (2009) Centennial variations of the global monsoon precipitation in the last millennium: results from ECHO-G Model. J Clim 22 (9):2356–2371

Lorenz DJ, Hartmann DL (2006) The effect of the MJO on the North American monsoon. J Clim 19(3):333–343

Lu E, Chan JCL (1999) A unified monsoon index for south China. J Clim 12(8):2375–2385

Ma HY, Mechoso CR (2007) Submonthly variability in the South American Monsoon System. J Meteorol Soc Jpn 85A:385–401

Marengo JA (2004) Interdecadal variability and trends of rainfall across the Amazon basin. Theor Appl Climatol 78(1–3):79–96

McCabe GJ, Palecki MA, Betancourt JL (2004) Pacific and Atlantic Ocean influences on multidecadal drought frequency in the United States. P Natl Acad Sci USA 101(12):4136–4141

Mechoso CR, Robertson AW, Ropelewski CF, Grimm AM (2005) The American monsoon systems: An introduction. In: Chang C-Pea (ed) the global monsoon system: research and forecast. WMO/TD No. 1266 (TMRP Report No. 70), pp 197–206

Mechoso CR (2011) The south American monsoon systems. The Global Monsoon System: Research and Forecast 5:137

Miyasaka T, Nakamura H (2005) Structure and formation mechanisms of the northern hemisphere summertime subtropical highs. J. Clim 18:5046–5065. doi:10.1175/JCLI3599.1

Nigam S, Guan B, Ruiz-Barradas A (2011) Key role of the atlantic multidecadal oscillation in 20th century drought and wet periods over the Great Plains. Geophys Res Lett 38

Nobre P, Malagutti M, Urbano DF, de Almeida RAF, Giarolla E (2009) Amazon deforestation and climate change in a coupled model simulation. J Clim 22(21):5686–5697. doi:10.1175/2009JCLI2757.1

Nogues-Paegle J, Mo KC (1997) Alternating wet and dry conditions over South America during summer. Mon Weather Rev 125(2):279–291

Paegle JN, Byerle LA, Mo KC (2000) Intraseasonal modulation of South American summer precipitation. Mon Weather Rev 128(3):837–850

Pu B, Dickinson RE (2014) Hydrological changes in the climate system from leaf responses to increasing CO_2. Clim Dynam 42(7–8):1905–1923

Richter I, Xie SP (2008) On the origin of equatorial Atlantic biases in coupled general circulation models. Clim Dynam 31(5):587–598

Rodwell M, Hoskins B (2001) Subtropical anticyclones and summer monsoons. J Clim 14:3192–3211

Sellers PJ, Bounoua L, Collatz GJ, Randall DA, Dazlich DA, Los SO, Berry JA, Fung I, Tucker CJ, Field CB, Jensen TG (1996) Comparison of radiative and physiological effects of doubled atmospheric CO_2 on climate. Science 271(5254):1402–1406

Trenberth KE, Stepaniak DP, Caron JM (2000) The global monsoon as seen through the divergent atmospheric circulation. J Clim 13(22):3969–3993

Vera C et al. (2006) Toward a unified view of the American monsoon systems. J Clim 19 (20):4977–5000

Wang B, Ding QH (2011) Concept of global monsoon In: Chang C-P, Ding YH, Lau G, Johnson RH, Wang B, Yasunari T (eds) The global monsoon system: research and forecast, 2nd Edn, vol 5. World Scientific Series on Asia-Pacific Weather and Climate. World Scientific Publication Company, p 608

Wang CZ, Enfield DB (2001) The tropical western hemisphere warm pool. Geophys Res Lett 28 (8):1635–1638

Wang H, Fu R (2002) Cross-equatorial flow and seasonal cycle of precipitation over South America. J Clim 15(13):1591–1608

Webster PJ, Holton JR (1982) Cross-Equatorial response to middle-latitude forcing in a zonally varying basic state. J Atmos Sci 39(4):722–733

Zhang Y, Fu R, Yu HB, Dickinson RE, Juarez RN, Chin M, Wang H (2008) A regional climate model study of how biomass burning aerosol impacts land-atmosphere interactions over the Amazon. J Geophys Res-Atmos 113(D14)

Zhang Y, Fu R, Yu HB, Qian Y, Dickinson R, Dias MAFS, Dias PLD, Fernandes K (2009) Impact of biomass burning aerosol on the monsoon circulation transition over Amazonia. Geophys Res Lett 36

Zhu CM, Cavazos T, Lettenmaier DP (2007) Role of antecedent land surface conditions in warm season precipitation over northwestern Mexico. J Clim 20(9):1774–1791

Chapter 10
The Madden–Julian Oscillation and the Monsoons

Charles Jones

Abstract The Madden–Julian Oscillation (MJO) is the most important type of tropical intra-seasonal variations in the Earth System and has an influential role on the monsoons. This influence is manifested in many ways, especially on the precipitation variability of the monsoons in Asia, India, Australia–Indonesia, Africa, and the Americas. The MJO shows substantial variations on seasonal and inter-annual time scales. In addition, observational and modeling studies indicate that the activity of the MJO on decadal and longer time scales may be sensitive to the warming of the planet, especially over the tropical Indian and Pacific Oceans. This chapter reviews the influence of the MJO on monsoon systems and discusses several studies that investigated future projections of climate change and potential changes in the MJO.

Keywords Madden–Julian Oscillation · MJO · Monsoons · Climate change · CMIP5 · Tropical intra-seasonal oscillations

10.1 The Madden–Julian Oscillation

The Madden–Julian Oscillation (MJO) was discovered in the early 1970s (Madden and Julian 1971, 1972, 1994; Zhang 2005; Lau and Waliser 2012). Madden and Julian carried out spectral and cross-spectral analyses using meteorological time series from a few surface and radiosonde stations sparsely distributed over the tropics, most of which had less than 10 years' worth of data. Nevertheless, they were able to show, with rigorous statistical confidence, that the tropical atmosphere has a large-scale eastward propagating oscillation with intra-seasonal time scales

C. Jones (✉)
Department of Geography, University of California Santa Barbara, Santa Barbara, CA, USA
e-mail: cjones@eri.ucsb.edu

C. Jones
Earth Research Institute, University of California Santa Barbara, Santa Barbara, CA, USA

© Springer International Publishing Switzerland 2016

L.M.V. de Carvalho and C. Jones (eds.), *The Monsoons and Climate Change*,
Springer Climate, DOI 10.1007/978-3-319-21650-8_10

typically in the range of 40–50 days. Additional observational studies revealed that the range of time variations is broader (30–60 days) than originally proposed (Weickmann et al. 1985; Knutson and Weickmann 1987; Madden and Julian 1994; Zhang 2005; Lau and Waliser 2012). Interestingly, the MJO intensity and duration vary from event to event and the oscillation can occur as a single isolated event or in series of successive episodes, when one event begins directly after a preceding event (Matthews 2008; Jones 2009; Jones and Carvalho 2011b).

The oscillation is mainly confined to a latitudinal band between 20°S and 20°N, and spreads eastward across all longitudes with phase speeds on the order of 5–10 m s^{-1}. The horizontal structure is dominated by wavenumbers one and two in the zonal direction, and its anomalous vertical structure is baroclinic (Hendon and Salby 1994; Madden and Julian 1994). Interaction between anomalies in convective activity and the large-scale circulation is strongest in the Indian and western Pacific Oceans, where the oscillation reaches its maximum amplitude. The oscillation manifests itself throughout the tropical troposphere with significant variations in mesoscale convective systems, tropical cyclones, clouds, precipitation, humidity, temperature, pressure and other variables (Hendon and Liebmann 1994; Hendon 1995; Hendon and Salby 1996; Maloney and Hartmann 2000; Zhu et al. 2003; Ziemke and Chandra 2003; Jones et al. 2004b; Kiladis et al. 2005; Aiyyer and Molinari 2008; Camargo et al. 2009; Chand and Walsh 2010; Barnes and Houze 2013; Zhang 2013; Guy and Jorgensen 2014; Peatman et al. 2014; Tsuboi and Takemi 2014; Virts and Wallace 2014) and even in the lower stratosphere (Weare 2010a, b; Weare et al. 2012).

In addition to its tropospheric signal, the MJO manifestation is also found in near-surface variables, and upper- and deep-ocean variability (Krishnamurti et al. 1988; Jones and Weare 1996; Zhang 1996; Hendon et al. 1998; Jones et al. 1998; Hendon 2000; McPhaden 2002; Matthews and Meredith 2004; Matthews and Li 2005; Waliser et al. 2005; Isoguchi and Kawamura 2006; Krishnamurti et al. 2007; Matthews et al. 2007; Jin et al. 2013). The influential nature of the MJO has also been identified on interactions with El Niño/Southern Oscillation (ENSO) and it has been hypothesized that the MJO may act as a triggering mechanism for some ENSO events via an oceanic Kelvin wave forcing in the tropical Pacific (Lau and Chan 1988; Hendon et al. 1998; McPhaden 1999; Moore and Kleeman 1999a, b; Fasullo and Webster 2000; Zavala-Garay et al. 2003, 2005; McPhaden 2004; Lau 2005; Feng et al. 2014).

The MJO involves intense tropical convective heating anomalies (Hendon and Salby 1994, 1996; Kiladis et al. 2005; Morita et al. 2006) that induce significant tropical-extratropical interactions during its life cycle (Matthews and Kiladis 1999; Matthews et al. 2004; Seo and Son 2012; Gloeckler and Roundy 2013). Consequently, the MJO significantly influences the variability of precipitation and temperature over the globe (Jones and Carvalho; Higgins and Mo 1997; Mo and Higgins 1998; Higgins et al. 2000; Jones 2000; Jones et al. 2004b; Zhang 2005; Lin and Brunet 2009; Lin et al. 2010; Becker et al. 2011; Jones and Carvalho 2011a, 2014; Ralph et al. 2011; Yoo et al. 2012a, b; Schreck et al. 2013; Zhang 2013) as well as forecast skill in the medium-extended ranges (Ferranti et al. 1990; Lau and

Chang 1992; Hendon et al. 2000; Jones and Schemm 2000; Jones et al. 2000, 2004a, b, 2011a, b; Gottschalk et al. 2010; Vitart and Molteni 2010; Matsueda and Endo 2011; Vitart 2014).

Over the years, significant efforts have been devoted to understanding the mechanisms that are involved in the MJO initiation and propagation characteristics, including its representation in global climate models (Hayashi and Golder 1986, 1988, 1993; Hendon and Salby 1994, 1996; Jones and Weare 1996; Slingo et al. 1996; Waliser et al. 1999, 2003; Hendon 2000; Zhang 2005, 2013; Lin et al. 2006; Zhang et al. 2006; Lau and Waliser 2012). Comprehensive discussions of the existing theories of the MJO can be found elsewhere (Wang 2005; Zhang 2005; Lau and Waliser 2012).

Given the influential nature of the MJO on weather and climate variability, including the monsoon systems, there is significant interest in determining how global climate change will impact the MJO. In the following sections, we review the influence of the MJO on monsoon systems and discuss several studies that investigated future projections of climate change and potential changes in the MJO.

10.2 The MJO and Monsoons

Before beginning, it is worth noting some differences in terminology found in the MJO literature. Some authors use "MJO" in reference to only boreal winter activity because the oscillation shows clear equatorial eastward propagation; "boreal summer intra-seasonal oscillation" (BSIO and variations of it) refers to the summer activity of the tropical intra-seasonal oscillation, when meridional propagation is frequently observed over the Indian Ocean and Indonesia (Wang and Rui 1990; Madden and Julian 1994; Wang and Xie 1997; Lawrence and Webster 2002; Jones et al. 2004c). In this chapter, for simplicity, MJO refers to the large-scale tropical intra-seasonal oscillation that occurs year-round, including BSIO.

The influence of the MJO on monsoon systems has been demonstrated in many previous studies (Madden and Julian 1994; Webster et al. 1998; Jones et al. 2004b, c; Lau and Waliser 2012; Zhang 2013). This influence has been detected in the monsoons over Southeast Asia (Lau and Chan 1986; Fu and Wang 2004; Wang 2006), India (Wang and Rui 1990; Kripalani et al. 1995, 2004; Krishnamurthy and Shukla 2000; Goswami and Mohan 2001), Australia (Hendon and Liebmann 1990; Kawamura et al. 2002; Hung and Yanai 2004), North America (Rasmusson and Arkin 1993; Mo et al. 1997; Higgins and Shi 2000; Cavazos et al. 2002; Cavazos and Rivas 2004; Johnson et al. 2007), South America (Nogues-Paegle and Mo 1997, 2002; Jones and Schemm 2000; Nogues-Paegle et al. 2000; Carvalho et al. 2002a, b, 2004a ; Jones and Carvalho 2002; Jones et al. 2004b; De Souza and Ambrizzi 2006; Silva and Carvalho 2007; Muza et al. 2009) and Africa (Matthews 2004; Mounier and Janicot 2004; Pohl et al. 2005; 2007; Rao and Sikka 2007; Mohino et al. 2012; Hart et al. 2013; Berhane and Zaitchik 2014). As the MJO propagates eastward with characteristic time scales of between 30 and 60 days, the oscillation induces

intra-seasonal variability in precipitation and atmospheric circulation over the monsoon areas. These changes are especially expressed as "active" and "break" periods in the activity of the monsoons.

10.3 Climate Change and the MJO

In this section, we begin by discussing the seasonal, inter-annual and multi-year variations in the MJO in the present climate. As mentioned in the introduction, a significant challenge to further understanding how global warming will impact the MJO is the inability of current global climate models to realistically simulate all of the observed characteristics of the MJO.

The MJO has a relatively well-defined seasonality in its behavior, which can be explained by the latitudinal position of tropical heat sources, such that the greatest amplifications occur in the spring equinox when maximum sea surface temperatures (SSTs) are near the Equator (Salby et al. 1994). Another interesting characteristic of the MJO is its variability from year to year (Wang and Rui 1990; Gutzler 1991; Weickmann 1991; Jones et al. 2004c). A causal relationship for this inter-annual behavior, especially its association with ENSO (Lau 2005), is not fully understood. Observational studies indicate that before the onset of warm ENSO episodes, as SST anomalies in the central Pacific become sufficiently positive, MJO events tend to spread farther east into the equatorial Pacific (Weickmann 1991; McPhaden 1999; Kessler and Kleeman 2000; Kessler 2001; Jones et al. 2004c; Zhang 2005). Because both the MJO and ENSO occur irregularly in time, with differing amplitudes and spatiotemporal characteristics, clear and statistically robust relationships between both phenomena have been difficult to identify. Although previous studies have found that indexes of MJO activity in the boreal winter are uncorrelated with SST anomalies associated with ENSO (Hendon et al. 1999; Slingo et al. 1999), warm ENSO episodes can affect the inter-annual variability of boreal summer northwestward spreading MJO events in the western North Pacific. Moreover, warm ENSO phases can strengthen MJO events occurring in May–July, possibly indicating a seasonal dependency on the MJO–ENSO relationship (Teng and Wang 2003). More recently, Bellenger and Duvel (2012) found that warm ENSO episodes impact the eastward extension of boreal winter MJO events into the central Pacific as well as an increase (decrease) in the MJO perturbation over the western Pacific (eastern Indian Ocean).

10.3.1 The MJO in the Present Climate

The behavior of the MJO in the present climate, on time scales longer than inter-annual, has been difficult to assess, given that the first generation of re-analyses extend back only to the 1940s–1950s (Kalnay et al. 1996; Simmons and

Gibson 2000). In addition, temporal changes in the number of available observations (e.g., radiosondes, satellites, etc.) impose some challenges in differentiating real climate shifts from spurious changes based on artifacts.

Despite these challenges, changes in MJO behavior in recent decades have been investigated. Slingo et al. (1999), for instance, used an MJO index derived from NCEP/NCAR reanalysis (Kalnay et al. 1996), and found a clear trend in tropical intra-seasonal activity with low amplitudes between 1958 and 1976 and high amplitudes between 1977 and 1996, coinciding with the 1970s climate shift (Graham 1994). Additionally, numerical simulations with a global atmospheric model forced with observed SSTs from 1949 to 1993 reproduced the positive trend in intra-seasonal activity since the mid-1970s, suggesting that the trend in intra-seasonal activity could be real. Slingo et al. (1999) further speculated that the MJO may become more active as tropical oceans experience prolonged warming.

Jones and Carvalho (2006) also used NCEP/NCAR reanalysis to investigate the long-term behavior of the MJO and found statistically significant positive linear trends in upper- and lower-tropospheric zonal winds during the summer and winter seasons. They also developed a methodology based on the number of events to characterize low-frequency changes in MJO activity and suggested that the MJO appears to exhibit regime changes with intervals of between 5 and 15 years; a Fourier analysis indicated that summer MJO regimes show a variability of about 18.5 years. Likewise, Pohl and Matthews (2007) found that the mean amplitude of the MJO was 16 % greater from 1976 to 2005, compared to the 1950–1975 period.

The variability of the MJO in the present climate was further investigated by Jones (2009), who developed an empirical model of the MJO. The temporal variability of the MJO is represented with a homogeneous nine-state first-order Markov chain in which state 0 represents quiescent days, and states 1–8 are phases of the MJO when it is active. Transition probabilities are estimated based on the historical record of MJO events. The model is called "homogeneous" because the transition probabilities do not vary in time. Once the model simulates time series of phase transitions, composites of convective and circulation anomalies determine the spatial structure of the events. In the homogeneous model, the amplitudes of the MJOs are stochastically generated with a Gaussian frequency distribution and events occur irregularly in time and can appear as single isolated events or sequences of successive MJOs. The MJO in the model can have different eastward propagations and the zonal scale is consistent with the observations.

Jones and Carvalho (2011b) extended Jones's (2009) results and developed a non-homogeneous stochastic model of the MJO in which the transition probabilities vary as a function of low-frequency variations in SSTs in the tropical Indian and western Pacific Oceans. The model driven by observed SST anomalies is capable of reproducing the activity of the MJO during the reanalysis period, indicating a regime of near-normal activity in 1948–1972 (3.4 events a year^{-1}), and two regimes of high activity in 1973–1989 (3.9 events a year^{-1}) and 1990–2008 (4.6 events a year^{-1}). The model was also applied to the pre-reanalysis period and suggested decadal shifts in the MJO with near-normal levels between 1880 and 1895 (3.4 events a year^{-1}), low activity from 1896 to 1917 (2.6 events a year^{-1}), and a return

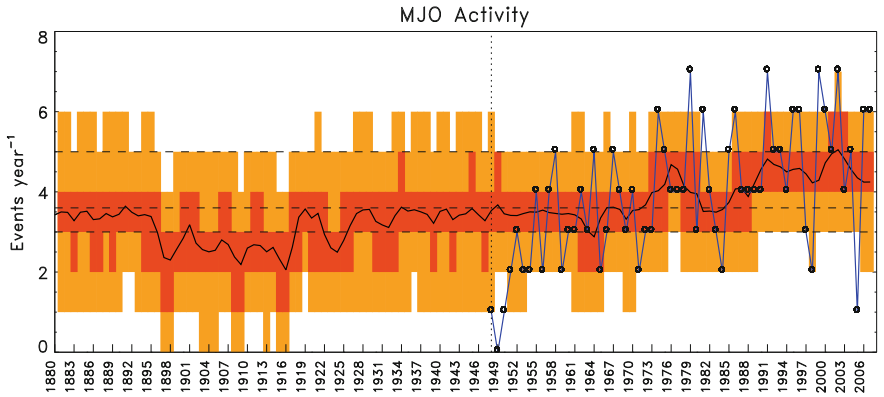

Fig. 10.1 MJO activity from 1880 to 2008. *Black solid curve* shows ensemble mean number of events per year^{-1} obtained with non-homogeneous stochastic model simulations (1,000 members). *Red* and *orange shading* indicate inter-quartile and 5th–95th quartile spreads. Observed number of MJO events per year^{-1} is shown by *blue curve* with *circles*. *Vertical dotted line* indicates the beginning of reanalysis data. *Horizontal lines* indicate inter-quartile (3–5 events per year^{-1}) and ensemble mean number of events per year^{-1} (3.6 events per year^{-1}) obtained with a homogeneous stochastic model (Jones and Carvalho 2011b)

to near-normal levels from 1918 to 1947 (3.3 events a year^{-1}) (Fig. 10.1). To date, the only other attempt to understand the activity of the MJO in the historical record was completed by Oliver and Thompson (2012), who developed an empirical model to reconstruct the variability of the oscillation from 1905 until 2008, using the Wheeler and Hendon (2004) method and the twentieth century reanalysis (Compo et al. 2006). Next, we review several studies that have investigated projections of potential changes in the MJO in future climates.

10.3.2 Climate Change and the MJO

Observational and theoretical evidence points to the undeniable fact that the Earth's climate is changing rapidly, and anthropogenic activities are playing a vital role (Solomon et al. 2007; Field et al. 2012). Assessing how the continuing warming of the planet will modify the MJO is important, given its influence in weather and climate variability. However, significant challenges are met when investigating this problem. As previously mentioned, current global climate models are not able to realistically simulate all of the observed characteristics of the MJO (Zhang 2005; Zhang et al. 2006). Lin et al. (2006) and Hung et al. (2013) provide detailed discussions of the representation of the MJO in current global climate models and recent improvements in simulation.

Jones and Carvalho (2011c) developed the first attempt to infer potential changes in the MJO in a future climate change scenario. They used the non-homogeneous stochastic model of Jones and Carvalho (2011b), in which the probabilities of MJO

initiation and propagation are empirically derived from observed low-frequency variations in SST in the tropical Indian and western Pacific Oceans. They focused on potential changes in MJO activity, defined as the number of events occurring within a selected period of time. Probabilistic projections of changes in the activity of the MJO were investigated using projections of SST from five coupled climate models for the 2010–2099 period in the A1B global warming scenario (IPCC 2007). The SST projections were used to drive the non-homogeneous stochastic model of the MJO.

Figure 10.2 shows decadal shifts in the projected mean number of MJO events and suggests progressive increases from the current mean of 4.6 events year^{-1} to about 5.7 events year^{-1} by 2094–2099. Furthermore, although the 95th percentile of the distributions remains virtually unchanged in the projections, the 5th percentile increases from three (2010–2027) to four events by 2038–2049. They further hypothesized that the positive trends in MJO activity are related to warming of the tropical Indian Ocean and western Pacific and increases in the background CAPE (convectively available potential energy) necessary for triggering MJO events. It is important to note, however, that the MJO initiation and propagation in the stochastic model is parameterized as a function of low-frequency SSTs in the Indian and western Pacific Warm Pool but does not account for changes in tropical mean SSTs, which can be relevant for MJO variability (Maloney and Xie 2013).

Since Jones and Carvalho's findings (2011b), numerous studies investigating MJO variability in future climate scenarios have been carried out. Takahashi et al.

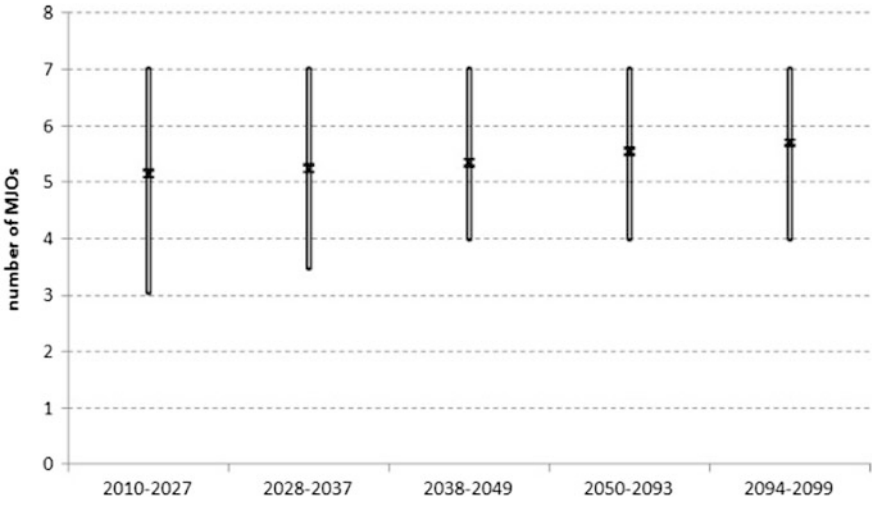

Fig. 10.2 Projected changes in MJO activity from 2010 to 2099. Each *bar* summarizes statistics obtained with stochastic simulations: mean number of events per year^{-1} (*circles*), 95 % confidence level (*horizontal ticks*), and 5th and 95th percentiles (tips of the *bars*). Changes between adjacent time periods indicated on the *bottom* axis are significant at the 5 % level (Jones and Carvalho 2011c)

(2011) analyzed simulations from 12 Coupled Model Intercomparison Project (CMIP3) models to investigate possible changes in the MJO and extratropical influences in East Asia. Changes in the convective signal associated with the MJO were mixed, with seven models indicating increases and five suggesting decreased activity. Some of the models predict an intensification of the extratropical circulation response to the MJO and increased low-level moisture transport over East Asia. Their results highlight the difficulty in obtaining consistent projections of changes in the MJO from global climate models, given their differing skills in realistically simulating the oscillation.

Liu (2013) performed aqua-planet simulations with the National Center for Atmospheric Research (NCAR) CAM2 model, using uniform surface warming of 2 and 4 K. The large-scale structure (zonal wave numbers 1–4) of the MJO in the model remained unaltered in the 4 K simulations, but increases in intra-seasonal variance and the number of intense MJO events were found. Additionally, these

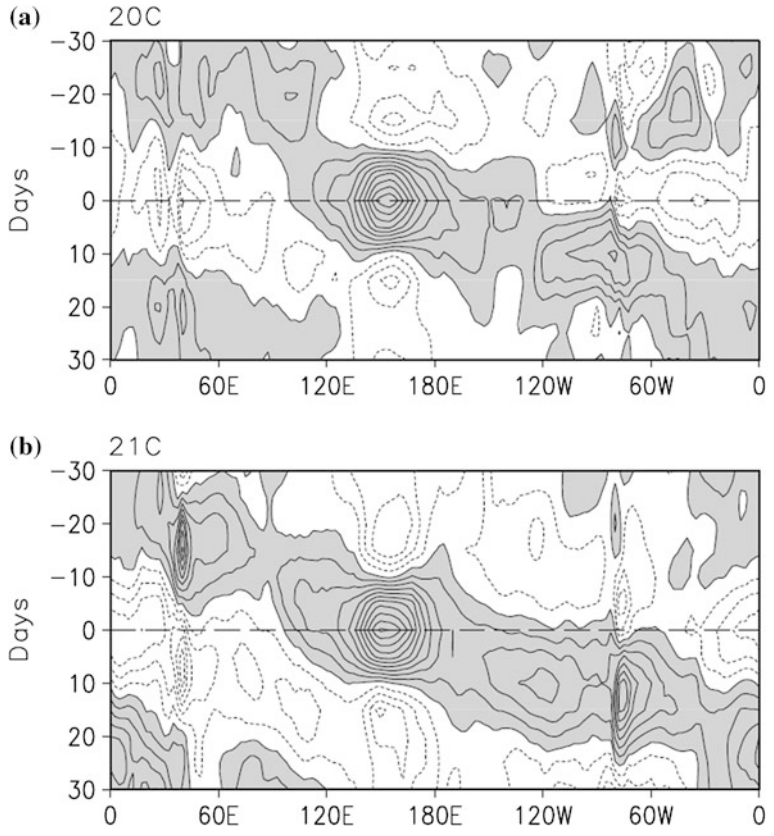

Fig. 10.3 Lag correlation of 20–100 days filtered 850-hPa zonal wind (reference point at 155°E, 0°N) averaged in the 20 DJFM seasons for **a** the twentieth century, and **b** the A1B_21C experiments. Contour interval is 0.1 and values ≥0 are shaded (Liu et al. 2013)

idealized simulations indicated that the intra-seasonal variance in the 20–30-day range is more sensitive than the 30–60-day range.

Liu et al. (2013) used the Max Planck Institute ECHAM5 atmospheric global climate model to further investigate changes in the MJO in the A1B global warming scenario of the IPCC (2007). The coupled version of this model (ECHAM5/MPI-OM) was reported as one of two models that most realistically represented the MJO in the CMIP3 simulations (Lin et al. 2006). The MJO, in uncoupled simulations forced with SSTs, had reasonable eastward propagation and zonal structure, but the intra-seasonal power was substantially reduced compared to observations. The control simulation for the twentieth century was compared with the run for the A1B scenario with a projected 3 K surface warming in the tropics. The simulations indicated enhanced background precipitation variance rather than preferential increases in specific frequency bands. Moreover, the results indicated strengthening (weakening) of the zonal winds associated with the MJO in the lower (upper) troposphere (Fig. 10.3).

Maloney and Xie (2013) also carried out aqua-planet simulations with the NCAR CAM3 climate model, using three idealized SST warming patterns: end of the twenty-first century, zonally symmetric, and globally uniform warming. Model intra-seasonal variability was found to decrease for zonally symmetric warming and significantly increase in the globally uniform warming simulation. Their results highlight the fact that potential changes in the MJO are sensitive to the spatial pattern of tropical surface warming.

Schubert et al. (2013) examined millennium-long simulations with the Max Planck Institute for Meteorology Earth System Model (MPI-ESM) and found that the model MJO shows significant inter-annual (2–6 years) to inter-decadal

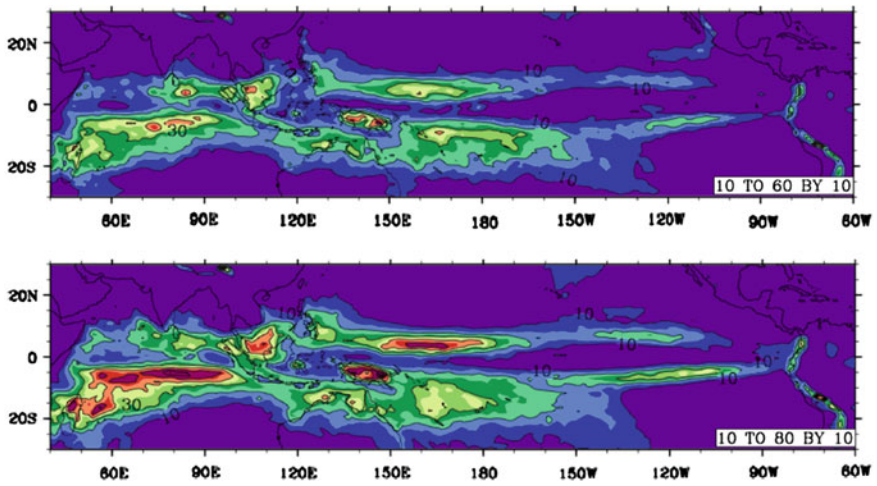

Fig. 10.4 Percentage variance of intra-seasonal precipitation in the twentieth century (*top*) and twenty-first century (*bottom*) run. The contours are drawn for every 10 % increase in variance explained by the intra-seasonal precipitation (Subramanian et al. 2014)

(10–20 years) internal variability. Sensitivity experiments suggest that solar variability may contribute to 11 and 22 years' variability, and volcanic forcing tends to enhance decadal variations of the MJO. In contrast, they did not find any significant influence of anthropogenic land use change in the twentieth century on the MJO. The sensitivity experiments, however, did identify increases in the strength of the MJO associated with increases in CO_2 concentrations (1 % per year since 1850), suggesting that the oscillation might intensify as a result of global warming.

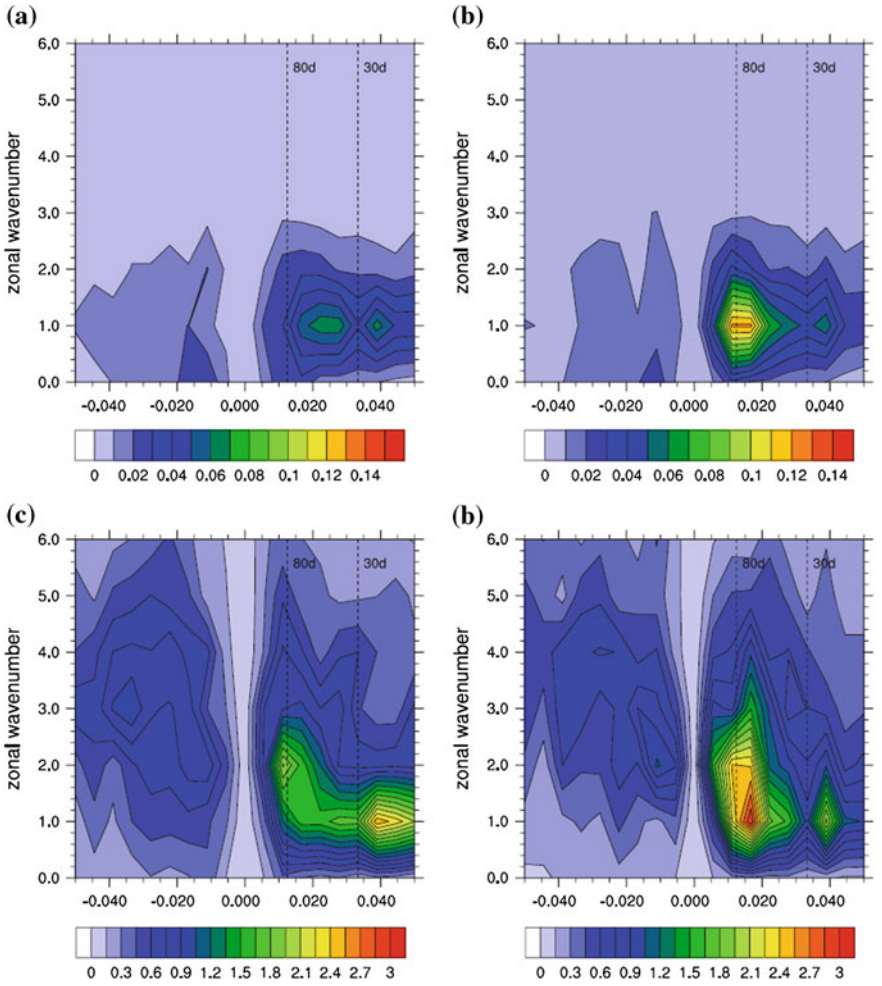

Fig. 10.5 Wavenumber-frequency power spectra (m^2/s^2) for 850 hPa zonal winds averaged in the boreal winter seasons over 10°S–10°N for **a** the 20th forcing, and **b** the twenty-first century forcing. Wavenumber-frequency power spectra (W^2/m^4) for Outgoing Longwave Radiation averaged in the boreal winter seasons over 10°S–10°N for **c** the twentieth century forcing, and **d** the twenty-first century forcing (Subramanian et al. 2014)

Lastly, Subramanian et al. (2014) analyzed simulations of the NCAR community climate system model version 4 (CCSM4) and compared the variability of the MJO in the twentieth century against the scenario for representative concentration pathway 8.5 (RCP8.5) at the end of the twenty-first century (IPCC 2013). They found that the MJO in the RCP8.5 scenario shows increased intra-seasonal variance in precipitation (Fig. 10.4) and increased intensity of MJO events (Fig. 10.5). Additionally, they observed the frequency of weak MJO events to decrease in the RCP8.5 scenario.

The influence of the MJO on the monsoons is significant and has been extensively investigated over the years. Understanding the long-term behavior of the MJO in the past may yield important clues about future changes in the oscillation. However, given its characteristic intra-seasonal time scale, paleoclimatic records do not provide enough information to understand the variability of the MJO prior to the twentieth century. Gridded products, such as re-analyses, can provide valuable information on the spatiotemporal characteristics of the MJO, but uncertainties of variations on decadal and longer time scales are great, especially in the pre-satellite data record. Global climate models are an interesting alternative for studying changes in the MJO. However, current models still need to improve significantly in order to be capable of simulating all of the observed properties of the MJO. Given the limitations, few studies have attempted to investigate future changes in the MJO, either empirically or with climate models, and although their conclusions are highly model-dependent, the results suggest a possible scenario: the MJO may strengthen and become more active in a warmer climate. Exactly how the continued warming of the planet will modify the MJO and, consequently, its role in the variability of the monsoons, is still an open question.

Acknowledgments The author would like to thank the Climate and Large-scale Scale Dynamics Program of the National Science Foundation (AGS-1053294 and AGS 1116105), the NOAA Climate Program Office (NA10OAR4310170), the CGIAR Research Program on Climate Change, Agriculture and Food Security (CCAFS), and the International Potato Center in Lima, Peru (SB120184) for their support.

References

Aiyyer A, Molinari J (2008) MJO and tropical cyclogenesis in the Gulf of Mexico and eastern Pacific: case study and idealized numerical modeling. J Atmos Sci 65:2691–2704

Barnes HC, Houze RA (2013) The precipitating cloud population of the Madden–Julian Oscillation over the Indian and west Pacific Oceans. J Geophys Res-Atmos 118:6996–7023

Becker EJ, Berbery EH, Higgins RW (2011) Modulation of cold-season U.S. daily precipitation by the Madden–Julian Oscillation. J Clim 24:5157–5166

Bellenger H, Duvel JP (2012) The event-to-event variability of the boreal winter MJO. Geophys Res Lett 39

Berhane F, Zaitchik B (2014) Modulation of daily precipitation over East Africa by the Madden–Julian Oscillation. J Clim 27:6016–6034

Camargo SJ, Wheeler MC, Sobel AH (2009) Diagnosis of the MJO modulation of tropical cyclogenesis using an empirical index. J Atmos Sci 66:3061–3074
Carvalho LMV, Jones C, Liebmann B (2002a) Extreme precipitation events in southeastern South America and large-scale convective patterns in the South Atlantic convergence zone. J Clim 15:2377–2394
Carvalho LMV, Jones C, Silva Dias MAF (2002b) Intraseasonal large-scale circulations and mesoscale convective activity in tropical South America during the TRMM-LBA campaign. J Geophys Res Atmos 107. doi:10.1029/2001JD000745
Carvalho LMV, Jones C, Liebmann B (2004) The South Atlantic convergence zone: intensity, form, persistence, and relationships with intraseasonal to interannual activity and extreme rainfall. J Clim 17:88–108
Cavazos T, Rivas D (2004) Variability of extreme precipitation events in Tijuana, Mexico. Clim Res 25:229–242
Cavazos T, Comrie AC, Liverman DM (2002) Intraseasonal variability associated with wet monsoons in southeast Arizona. J Clim 15:2477–2490
Chand SS, Walsh KJE (2010) The influence of the Madden–Julian Oscillation on tropical cyclone activity in the Fiji region. J Clim 23:868–886
Compo GP, Whitaker JS, Sardeshmukh PD (2006) Feasibility of a 100-year reanalysis using only 373 surface pressure data. Bull Am Meteorol Soc 87:175–190
De Souza EB, Ambrizzi T (2006) Modulation of the intraseasonal rainfall over tropical Brazil by the Madden–Julian Oscillation. Int J Climatol 26:1759–1776
Fasullo J, Webster PJ (2000) Atmospheric and surface variations during westerly wind bursts in the tropical western Pacific. Q J R Meteorol Soc 126:899–924
Feng J, Liu P, Chen W, Wang X (2014) Contrasting Madden–Julian Oscillation activity during various stages of EP and CP El Niños. Atmos Sci Lett n/a–n/a
Ferranti L, Palmer TN, Molteni F, Klinker K (1990) Tropical-extratropical interaction associated with the 30-60 day oscillation and its impact on medium and extended range prediction. J Atmos Sci 47:2177–2199
Field CB et al (2012) Managing the risks of extreme events and disasters to advance climate change adaptation. A special report of Working Groups I and II of the intergovernmental panel on climate change. Cambridge University Press, Cambridge, UK, and New York, NY, USA, 582 pp
Fu XH, Wang B (2004) The boreal-summer intraseasonal oscillations simulated in a hybrid coupled atmosphere-ocean model. Mon Weather Rev 132:2628–2649
Gloeckler LC, Roundy PE (2013) Modulation of the extratropical circulation by combined activity of the Madden–Julian Oscillation and equatorial Rossby waves during boreal winter. Mon Weather Rev 141:1347–1357
Goswami BN, Mohan RSA (2001) Intraseasonal oscillations and interannual variability of the Indian summer monsoon. J Clim 14:1180–1198
Gottschalck J et al (2010) A framework for assessing operational Madden–Julian Oscillation forecasts a Clivar MJO working group project. Bull Am Meteorol Soc 91:1247–1258
Graham NE (1994) Decadal-scale climate variability in the tropical and North Pacific during the 1970s and 1980s—observations and model results. Clim Dyn 10:135–162
Gutzler DS (1991) Interannual fluctuations of intraseasonal variance of near-equatorial zonal winds. J Geophys Res Oceans 96:3173–3185
Guy N, Jorgensen DP (2014) Kinematic and precipitation characteristics of convective systems observed by airborne doppler radar during the life cycle of a Madden–Julian Oscillation in the Indian ocean. Mon Weather Rev 142:1385–1402
Hart NCG, Reason CJC, Fauchereau N (2013) Cloud bands over southern Africa: seasonality, contribution to rainfall variability and modulation by the MJO. Clim Dyn 41:1199–1212
Hastenrath S, Polzin D, Mutai CC (2007) Diagnosing the 2005 drought in equatorial East Africa. J Clim 20:4628–4637

Hayashi Y, Golder DG (1986) Tropical intraseasonal oscillations appearing in a GFDL general-circulation model and FGGE data. 1. Phase propagation. J Atmos Sci 43:3058–3067
Hayashi Y, Golder DG (1988) Tropical intraseasonal oscillations appearing in a Gfdl general-circulation model and Fgge data. 2. Structure. J Atmos Sci 45:3017–3033
Hayashi Y, Golder DG (1993) Tropical 40-50-day and 25-30-day oscillations appearing in realistic and idealized Gfdl climate models and the Ecmwf dataset. J Atmos Sci 50:464–494
Hendon HH (1995) Length of day changes associated with the Madden–Julian Oscillation. J Atmos Sci 52:2373–2383
Hendon HH (2000) Impact of air-sea coupling on the Madden–Julian Oscillation in a general circulation model. J Atmos Sci 57:3939–3952
Hendon HH, Liebmann B (1990) The intraseasonal (30-50 day) oscillation of the Australian summer monsoon. J Atmos Sci 47:2909–2923
Hendon HH, Salby ML (1994) The life-cycle of the Madden–Julian Oscillation. J Atmos Sci 51:2225–2237
Hendon HH, Liebmann B (1994) Organization of convection within the Madden–Julian Oscillation. J Geophys Res Atmos 99:8073–8083
Hendon HH, Salby ML (1996) Planetary-scale circulations forced by intraseasonal variations of observed convection. J Atmos Sci 53:1751–1758
Hendon HH, Liebmann B, Glick JD (1998) Oceanic Kelvin waves and the Madden–Julian Oscillation. J Atmos Sci 55:88–101
Hendon HH, Zhang CD, Glick JD (1999) Interannual variation of the Madden–Julian Oscillation during austral summer. J Clim 12:2538–2550
Hendon HH, Liebmann B, Newman M, Glick JD, Schemm JE (2000) Medium-range forecast errors associated with active episodes of the Madden–Julian Oscillation. Mon Weather Rev 128:69–86
Higgins RW, Mo KC (1997) Persistent North Pacific circulation anomalies and the tropical intraseasonal oscillation. J Clim 10:223–244
Higgins RW, Shi W (2000) Dominant factors responsible for interannual variability of the summer monsoon in the Southwestern United States. J Clim 13:759–776
Higgins RW, Schemm JKE, Shi W, Leetmaa A (2000) Extreme precipitation events in the western United States related to tropical forcing. J Clim 13:793–820
Hung CW, Yanai M (2004) Factors contributing to the onset of the Australian summer monsoon. Q J R Meteorol Soc 130:739–758
Hung MP, Lin JL, Wang WQ, Kim D, Shinoda T, Weaver SJ (2013) MJO and convectively coupled equatorial waves simulated by CMIP5 climate models. J Clim 26:6185–6214
Indeje M, Semazzi FH, Ogallo LJ (2000) ENSO signals in East African rainfall seasons. Int J Climatol 20:19–46
IPCC (2007) Climate change 2007: the physical science basis. Contribution of Working Group I to the fourth assessment report of the intergovernmental panel on climate change, 996 pp
IPCC (2013) The physical science basis. In: Stocker TF, Qin D, Plattner G-K, Tignor M, Allen SK, Boschung J, Nauels A, Xia Y, Bex V, Midgley PM (eds) Contributions of Working Group I to the fifth assessment report of the intergovernmental panel on climate change. Cambridge University Press, Cambridge, United Kingdom and New York, NY, USA, 1535 pp
Isoguchi O, Kawamura H (2006) MJO-related summer cooling and phytoplankton blooms in the South China Sea in recent years. Geophys Res Lett 33
Jin D, Waliser DE, Jones C, Murtugudde R (2013) Modulation of tropical ocean surface chlorophyll by the Madden–Julian Oscillation. Clim Dyn 40:39–58
Johnson RH, Ciesielski PE, McNoldy BD, Rogers PJ, Taft RK (2007) Multiscale variability of the flow during the North American monsoon experiment. J Clim 20:1628–1648
Jones C (2000) Occurrence of extreme precipitation events in California and relationships with the Madden–Julian Oscillation. J Clim 13:3576–3587
Jones C (2009) A homogeneous stochastic model of the Madden–Julian Oscillation. J Clim 22:3270–3288

Jones C, Carvalho LMV (2014) Sensitivity to Madden–Julian Oscillation variations on heavy precipitation over the contiguous United States. Atmos Res 147–148, 10–26
Jones C, Weare BC (1996) The role of low-level moisture convergence and ocean latent heat fluxes in the Madden and Julian Oscillation: an observational analysis using ISCCB data and ECMWF analyses. J Clim 9:3086–3104
Jones C, Schemm J-KE (2000) The influence of intraseasonal variations on medium-range weather forecasts over South America. Mon Weather Rev 128:486–494
Jones C, Carvalho LMV (2002) Active and break phases in the South American monsoon system. J Clim 15:905–914
Jones C, Carvalho LMV (2006) Changes in the activity of the Madden–Julian Oscillation during 1958-2004. J Clim 19:6353–6370
Jones C, Carvalho LMV (2011a) Spatial-intensity variations in extreme precipitation in the contiguous United States and the Madden–Julian Oscillation. J Clim (in press)
Jones C, Carvalho LMV (2011b) Stochastic simulations of the Madden–Julian Oscillation activity. Clim Dyn 36:229–246. doi:10.1007/s00382-00009-00660-00382
Jones C, Carvalho LMV (2011c) Will global warming modify the activity of the Madden–Julian Oscillation? Q J R Meteorol Soc 137:544–552. doi:10.1002/qj.1765
Jones C, Carvalho LMV (2014b) Sensitivity to Madden–Julian Oscillation variations on heavy precipitation over the contiguous United States. Atmos Res 147–148:10–26
Jones C, Waliser DE, Gautier C (1998) The influence of the Madden–Julian Oscillation on ocean surface heat fluxes and sea surface temperature. J Clim 11:1057–1072
Jones C, Waliser DE, Schemm JKE, Lau WKM (2000) Prediction skill of the Madden and Julian Oscillation in dynamical extended range forecasts. Clim Dyn 16:273–289
Jones C, Waliser DE, Lau KM, Stern W (2004a) The Madden–Julian Oscillation and its impact on Northern Hemisphere weather predictability. Mon Weather Rev 132:1462–1471
Jones C, Waliser DE, Lau KM, Stern W (2004b) Global occurrences of extreme precipitation and the Madden–Julian Oscillation: observations and predictability. J Clim 17:4575–4589
Jones C, Gottschalck J, Carvalho LMV, Higgins WR (2011a) Influence of the Madden–Julian Oscillation on forecasts of extreme precipitation in the contiguous United States. Mon Weather Rev 139:332–350
Jones C, Carvalho LMV, Gottschalck J, Higgins WR (2011b) The Madden–Julian Oscillation and the relative value of deterministic forecasts of extreme precipitation in the contiguous United States. J Clim 24:2421–2428
Jones C, Carvalho LMV, Higgins RW, Waliser DE, Schemm JKE (2004c) Climatology of tropical intraseasonal convective anomalies: 1979-2002. J Clim 17:523–539
Kalnay E et al (1996) The NCEP/NCAR 40-year reanalysis project. Bull Am Meteorol Soc 77:437–471
Kawamura R, Fukuta Y, Ueda H, Matsuura T, Iizuka S (2002) A mechanism of the onset of the Australian summer monsoon. J Geophys Res Atmos 107
Kessler WS (2001) EOF representations of the Madden–Julian Oscillation and its connection with ENSO. J Clim 14:3055–3061
Kessler WS, Kleeman R (2000) Rectification of the Madden–Julian Oscillation into the ENSO cycle. J Clim 13:3560–3575
Kiladis GN, Straub KH, Haertel PT (2005) Zonal and vertical structure of the Madden–Julian Oscillation. J Atmos Sci 62:2790–2809
Knutson TR, Weickmann KM (1987) 30-60 day atmospheric oscillations: composite life cycles of convection and circulation anomalies. Mon Weather Rev 115:1407–1436
Kripalani RH, Singh SV, Panchawagh N (1995) Variability of the summer monsoon rainfall over Thailand—comparison with features over India. Int J Climatol 15:657–672
Kripalani RH, Kulkarni A, Sabade SS, Revadekar JV, Patwardhan SK, Kulkarni JR (2004) Intra-seasonal oscillations during monsoon 2002 and 2003. Curr Sci 87:325–331
Krishnamurthy V, Shukla J (2000) Intraseasonal and interannual variability of rainfall over India. J Clim 13:4366–4377

Krishnamurti TN, Oosterhof DK, Mehta AV (1988) Air sea interaction on the time scale of 30 to 50 days. J Atmos Sci 45:1304–1322
Krishnamurti TN, Chakraborty A, Krishnamurti R, Dewar WK, Clayson CA (2007) Passage of intraseasonal waves in the subsurface oceans. Geophys Res Lett 34
Lau KM, Chan PH (1988) Intraseasonal and interannual variations of tropical convection—a possible link between the 40-50 day oscillation and Enso. J Atmos Sci 45:506–521
Lau WKM (2005) El Nino southern oscillation connection. In: Lau WKM, Waliser DE (eds) Intraseasonal variability in the atmosphere-ocean climate system. Springer, Chichester, 436 pp
Lau WKM, Chan PH (1986) Aspects of the 40-50 day oscillation during the northern summer as inferred from outgoing longwave radiation aspects of the 40-50 day oscillation during the northern summer as inferred from outgoing longwave radiation. Mon Weather Rev 114: 1354–1367
Lau WKM, Chang FC (1992) Tropical intraseasonal oscillation and its prediction by the Nmc operational model. J Clim 5:1365–1378
Lau WKM, Waliser DE (2012) Intraseasonal variability in the atmosphere-ocean climate system, 2nd edn. Springer, Chichester 613 pp
Lawrence DM, Webster PJ (2002) The boreal summer intraseasonal oscillation: relationship between northward and eastward movement of convection. J Atmos Sci 59:1593–1606
Lin H, Brunet G (2009) The influence of the Madden–Julian Oscillation on Canadian wintertime surface air temperature. Mon Weather Rev 137:2250–2262
Lin H, Brunet G, Mo R (2010) Impact of the Madden–Julian Oscillation on wintertime precipitation in Canada. Mon Weather Rev 138:3822–3839
Lin JL et al (2006) Tropical intraseasonal variability in 14 IPCC AR4 climate models. Part I: Convective signals. J Clim 19:2665–2690
Liu P (2013) Changes in a modeled MJO with idealized global warming. Clim Dyn 40:761–773
Liu P et al (2013) MJO change with A1B global warming estimated by the 40-km ECHAM5. Clim Dyn 41:1009–1023
Madden RA, Julian PR (1971) Detection of a 40-50 day oscillation in the zonal wind in the tropical Pacific. J Atmos Sci 28:702–708
Madden RA, Julian PR (1972) Description of global-scale circulation cells in the tropics with a 40-50 day period. J Atmos Sci 29:1109–1123
Madden RA, Julian PR (1994) Observations of the 40-50-day tropical oscillation-a review. Mon Weather Rev 122:814–837
Maloney ED, Hartmann DL (2000) Modulation of eastern North Pacific hurricanes by the Madden–Julian Oscillation. J Clim 13:1451–1460
Maloney ED, Xie S-P (2013) Sensitivity of tropical intraseasonal variability to the pattern of climate warming. J Adv Model Earth Syst 5:32–47
Matsueda M, Endo H (2011) Verification of medium-range MJO forecasts with TIGGE. Geophys Res Lett 38
Matthews AJ (2004) Intraseasonal variability over tropical Africa during northern summer. J Clim 17:2427–2440
Matthews AJ (2008) Primary and successive events in the Madden–Julian Oscillation. Q J R Meteorol Soc. doi:10.1002/qj.1224
Matthews AJ, Kiladis GN (1999) The tropical-extratropical interaction between high-frequency transients and the Madden–Julian Oscillation. Mon Weather Rev 127:661–677
Matthews AJ, Meredith MP (2004) Variability of Antarctic circumpolar transport and the Southern Annular Mode associated with the Madden–Julian Oscillation. Geophys Res Lett 31. doi:10.1029/2004GL021666
Matthews AJ, Li HYY (2005) Modulation of station rainfall over the western Pacific by the Madden–Julian Oscillation. Geophys Res Lett 32
Matthews AJ, Hoskins BJ, Masutani M (2004) The global response to tropical heating in the Madden–Julian Oscillation during the northern winter. Q J R Meteorol Soc 130:1991–2011

Matthews AJ, Singhruck P, Heywood KJ (2007) Deep ocean impact of a Madden–Julian Oscillation observed by Argo floats. Science 318:1765–1769
McPhaden MJ (1999) Genesis and evolution of the 1997-98 El Nino. Science 283:950–954
McPhaden MJ (2002) Mixed layer temperature balance on intraseasonal timescales in the equatorial Pacific Ocean. J Clim 15:2632–2647
McPhaden MJ (2004) Evolution of the 2002/03 El Nino. Bull Am Meteorol Soc 85:677–695
Mo KC, Higgins RW (1998) Tropical influences on California precipitation. J Clim 11:412–430
Mo KC, Paegle JN, Higgins RW (1997) Atmospheric processes associated with summer floods and droughts in the central United States. J Clim 10:3028–3046
Mohino E, Janicot S, Douville H, Li LZX (2012) Impact of the Indian part of the summer MJO on West Africa using nudged climate simulations. Clim Dyn 38:2319–2334
Moore AM, Kleeman R (1999a) The nonnormal nature of El Nino and intraseasonal variability. J Clim 12:2965–2982
Moore AM, Kleeman R (1999b) Stochastic forcing of ENSO by the intraseasonal oscillation. J Clim 12:1199–1220
Morita J, Takayabu YN, Shige S, Kodama Y (2006) Analysis of rainfall characteristics of the Madden–Julian Oscillation using TRMM satellite data. Dyn Atmos Oceans 42:107–126
Mounier F, Janicot S (2004) Evidence of two independent modes of convection at intraseasonal timescale in the West African summer monsoon. Geophys Res Lett 31
Muza MN, Carvalho LMV, Jones C, Liebmann B (2009) Intraseasonal and interannual variability of extreme dry and wet events over Southeastern South America and subtropical Atlantic during the austral summer. J Clim 22:1682–1699
Nogues-Paegle J, Mo KC (1997) Alternating wet and dry conditions over South America during Summer. Mon Weather Rev 125:279–291
Nogues-Paegle J, Mo KC (2002) Linkages between summer rainfall variability over South America and sea surface temperature anomalies. J Clim 15:1389–1407
Nogues-Paegle J, Byerle LA, Mo KC (2000) Intraseasonal modulation of South American summer precipitation. Mon Weather Rev 128:837–850
Oliver ECJ, Thompson KR (2012) A reconstruction of Madden–Julian Oscillation variability from 1905 to 2008. J Clim 25:1996–2019
Peatman SC, Matthews AJ, Stevens DP (2014) Propagation of the Madden–Julian Oscillation through the maritime continent and scale interaction with the diurnal cycle of precipitation. Q J R Meteorol Soc 140:814–825
Pohl B, Matthews AJ (2007) Observed changes in the lifetime and amplitude of the Madden–Julian Oscillation associated with interannual ENSO sea surface temperature anomalies. J Clim 20:2659–2674
Pohl B, Camberlin P, Roucou P (2005) Typology of pentad circulation anomalies over the Eastern Africa-Western Indian Ocean region, and their relationship with rainfall. Clim Res 29:111–127
Pohl B, Richard Y, Fauchereau N (2007) Influence of the Madden–Julian Oscillation on southern African summer rainfall. J Clim 20:4227–4242
Ralph FM, Neiman PJ, Kiladis GN, Weickmann K, Reynolds DW (2011) A multiscale observational case study of a Pacific atmospheric river exhibiting tropical-extratropical connections and a mesoscale frontal wave. Mon Weather Rev 139:1169–1189
Rao PS, Sikka DR (2007) Interactive aspects of the Indian and the African summer monsoon systems. Pure appl Geophys 164:1699–1716
Rasmusson EM, Arkin PA (1993) A global view of large-scale precipitation variability. J Clim 6:1495–1522
Salby ML, Garcia RR, Hendon HH (1994) Planetary-scale circulations in the presence of climatological and wave-induced heating. J Atmos Sci 51:2344–2367
Schreck CJ, Cordeira JM, Margolin D (2013) Which MJO events affect North American temperatures? Mon Weather Rev 141:3840–3850
Schubert JJ, Stevens B, Crueger T (2013) Madden–Julian Oscillation as simulated by the MPI earth system model: over the last and into the next millennium. J Adv Model Earth Syst 5: 71–84

Seo KH, Son SW (2012) The global atmospheric circulation response to tropical diabatic heating associated with the Madden–Julian Oscillation during northern winter. J Atmos Sci 69:79–96
Silva AE, Carvalho LMV (2007) Large-scale index for South America Monsoon (LISAM). Atmos Sci Lett 8:51–57
Simmons AJ, Gibson JK (2000) The ERA-40 Project Plan, ERA-40 Project Report Series No. 1 ECMWF, Shinfield Park, Reading, UK, 63 pp
Slingo JM, Rowell DP, Sperber KR, Nortley E (1999) On the predictability of the interannual behaviour of the Madden–Julian Oscillation and its relationship with El Nino. Q J R Meteorol Soc 125:583–609
Slingo JM et al (1996) Intraseasonal oscillations in 15 atmospheric general circulation models: results from an AMIP diagnostic subproject. Clim Dyn 12:325–357
Solomon S, Qin D, Manning M, Marquis M, Averyt KB, Tignor M, Miller HL Jr (2007) Climate change 2007: the physical science basis. Cambridge University Press, Cambridge, 996 pp
Subramanian A, Jochum M, Miller AJ, Neale R, Seo H, Waliser D, Murtugudde R (2014) The MJO and global warming: a study in CCSM4. Clim Dyn 42:2019–2031
Takahashi C, Sato N, Seiki A, Yoneyama K, Shirooka R (2011) Projected future change of MJO and its extratropical teleconnection in east Asia during the northern winter simulated in IPCC AR4 models. Sola 7:201–204
Teng HY, Wang B (2003) Interannual variations of the boreal summer intraseasonal oscillation in the Asian-Pacific region. J Clim 16:3572–3584
Tsuboi A, Takemi T (2014) The interannual relationship between MJO activity and tropical cyclone genesis in the Indian Ocean. Geosci Lett 1:9
Virts KS, Wallace JM (2014) Observations of temperature, wind, cirrus, and trace gases in the tropical tropopause transition layer during the MJO*. J Atmos Sci 71:1143–1157
Vitart F (2014) Evolution of ECMWF sub-seasonal forecast skill scores. Q J R Meteorol Soc 140:1889–1899
Vitart F, Molteni F (2010) Simulation of the Madden–Julian Oscillation and its teleconnections in the ECMWF forecast system. Q J R Meteorol Soc 136:842–855
Waliser DE, Lau KM, Kim JH (1999) The influence of coupled sea surface temperatures on the Madden–Julian Oscillation: a model perturbation experiment. J Atmos Sci 56:333–358
Waliser DE, Murtugudde R, Strutton P, Li JL (2005) Subseasonal organization of ocean chlorophyll: prospects for prediction based on the Madden–Julian Oscillation. Geophys Res Lett 32:L23602. doi:10.1029/2005GL024300
Waliser DE et al (2003) AGCM simulations of intraseasonal variability associated with the Asian summer monsoon. Clim Dyn 21:423–446
Walker GT (1923) Correlation in seasonal variations of weather, VIII: a preliminary study of world weather. Memoirs of the Indian Meteorological Department, Indian Meteorological Department
Wang B (2005) Theory. In: Lau WKM, Waliser DE (eds) Intraseasonal variability in the atmosphere-ocean climate system. Springer, Chichester, 436 pp
Wang B (2006) The Asian monsoon. Springer, Chischester 787 pp
Wang B, Rui H (1990) Synoptic climatology of transient tropical intraseasonal convection anomalies—1975-1985. Meteorol Atmos Phys 44:43–61
Wang B, Xie XS (1997) A model for the boreal summer intraseasonal oscillation. J Atmos Sci 54:72–86
Weare BC (2010a) Extended Eliassen-Palm fluxes associated with the Madden–Julian Oscillation in the stratosphere. J Geophys Res Atmos 115
Weare BC (2010b) Madden–Julian Oscillation in the tropical stratosphere. J Geophys Res Atmos 115
Weare BC, Cagnazzo C, Fogli PG, Manzini E, Navarra A (2012) Madden–Julian Oscillation in a climate model with a well-resolved stratosphere. J Geophys Res Atmos 117
Webster PJ, Magana VO, Palmer TN, Shukla J, Tomas RA, Yanai M, Yasunari T (1998) Monsoons: processes, predictability, and the prospects for prediction. J Geophys Res Oceans 103:14451–14510

Weickmann KM (1991) El-Nino Southern oscillation and Madden–Julian (30-60 Day) oscillations during 1981-1982. J Geophys Res Oceans 96:3187–3195

Weickmann KM, Lussky GR, Kutzbach JE (1985) Intraseasonal (30–60 Day) fluctuations of outgoing longwave radiation and 250 mb streamfunction during northern winter. Mon Weather Rev 113:941–961

Wheeler MC, Hendon HH (2004) An all-season real-time multivariate MJO index: development of an index for monitoring and prediction. Mon Weather Rev 132:1917–1932

Yoo C, Lee S, Feldstein S (2012a) The impact of the Madden–Julian Oscillation trend on the Antarctic warming during the 1979-2008 austral winter. Atmos Sci Lett 13:194–199

Yoo C, Lee S, Feldstein SB (2012b) Mechanisms of Arctic surface air temperature change in response to the Madden–Julian Oscillation. J Clim 25:5777–5790

Zavala-Garay J, Moore AM, Perez CL, Kleeman R (2003) The response of a coupled model of ENSO to observed estimates of stochastic forcing. J Clim 16:2827–2842

Zavala-Garay J, Zhang C, Moore AM, Kleeman R (2005) The linear response of ENSO to the Madden–Julian Oscillation. J Clim 18:2441–2459

Zhang C (2013) Madden–Julian Oscillation: bridging weather and climate. Bull Am Meteorol Soc 94:1849–1870

Zhang CD (1996) Atmospheric intraseasonal variability at the surface in the tropical western Pacific Ocean. J Atmos Sci 53:739–758

Zhang CD (2005) Madden–Julian Oscillation. Rev Geophys 43:1–36

Zhang CD et al (2006) Simulations of the Madden–Julian Oscillation in four pairs of coupled and uncoupled global models. Clim Dyn 27:573–592

Zhu CW, Nakazawa T, Li JP (2003) Modulation of twin tropical cyclogenesis by the MJO westerly wind burst during the onset period of 1997/98 ENSO. Adv Atmos Sci 20:882–898

Ziemke JR, Chandra S (2003) A Madden–Julian Oscillation in tropospheric ozone. Geophys Res Lett 30

Chapter 11
Glaciers and Monsoon Systems

Bodo Bookhagen

Abstract This chapter will analyze the impact of monsoon systems on glaciers. Most of the tropical glaciers in the Andes and Himalayas vary greatly in time and space, and are heavily influenced by their corresponding monsoon systems. This chapter will review climatic boundary conditions and provide a regional assessment of glacial changes in monsoonal systems with focuses on the central Andes and Himalayas.

Keywords Andes · Himalayas · High Mountain Asia · Atmospheric lapse rate · Snow water equivalent · Runoff · Glacial contribution

11.1 Glaciers and Global Monsoon Systems

Glaciers around the world are rapidly shrinking, especially in low-latitude regions (Baraer et al. 2012; Bolch et al. 2011, 2012; Bradley et al. 2006; Hanshaw and Bookhagen 2014; Huss 2012; Kaser et al. 2006; Oerlemans 2005; Price and Weingartner 2012; Vaughan et al. 2013; Vuille et al. 2008). Glaciers are an important source of clean water and provide a significant portion of the annual hydrologic budget in some regions (Archer and Fowler 2004; Huss et al. 2008; Kaser et al. 2010; Radic and Hock 2011; Vaughan et al. 2013; Viviroli and Weingartner 2004). Especially in the tropical Andes, glacial-melt contribution is important (Kaser et al. 2010; Vuille et al. 2008); other tropical and low-latitude regions with mountain ranges obtain their runoff from transiently stored waters in the form of snow and ice (Barnett et al. 2005; Bookhagen and Burbank 2010; Kaser et al. 2010; Viviroli and Weingartner 2004). However, the contribution of glacial runoff is difficult to determine and varies from year to year. Remote-sensing studies

B. Bookhagen (✉)
Institute of Earth and Environmental Science, University of Potsdam,
Karl-Liebknecht-Str. 24/25, 14467 Potsdam-Golm, Germany
e-mail: Bodo.Bookhagen@uni-potsdam.de

© Springer International Publishing Switzerland 2016

L.M.V. de Carvalho and C. Jones (eds.), *The Monsoons and Climate Change*,
Springer Climate, DOI 10.1007/978-3-319-21650-8_11

can help to assess general trends in glacial areas, elevation changes, and velocities, but in situ field work adds crucially important measurements unavailable at the scale of the most remotely sensed datasets (Finger et al. 2012; Hanshaw and Bookhagen 2014; Huggel et al. 2002; Paul et al. 2004; Quincey et al. 2007; Scherler et al. 2011a, b).

From a geographic perspective, glaciers in the tropics and low-latitude regions are limited to high-elevation regions where temperatures are low enough to maintain year-round ice. The areas that this chapter will focus on are the Andes of South America and the Himalayas in eastern Asia (Fig. 11.1); both areas are glacierized to different degrees because of their varying topographic and climatic boundary conditions.

Here, we loosely define global monsoon regions as the areas where the grid-cell summer-minus-winter precipitation rate exceeds 2.5 mm/day and the local summer precipitation exceeds 55 % of the annual total (Wang and Fan 1999) (Fig. 11.1).

While glaciers are important for water resources in some tropical regions, the seasonal snow cover may provide an equally important contribution to annual runoff (Bookhagen and Burbank 2010; Viviroli and Weingartner 2004). For example, river systems in the western and northwestern Himalayas, such as the Indus, derive more than 50 % of their annual runoff from snow-melt waters (Archer and Fowler 2004; Bookhagen and Burbank 2010; Immerzeel et al. 2009), but only a small percentage of runoff is derived from glacial-melt waters (Jeelani et al. 2012). There is no significant snow cover in the central Andes, but south of 30°S, the Andes have a persistent seasonal snow cover (Figs. 11.2 and 11.4), but this is

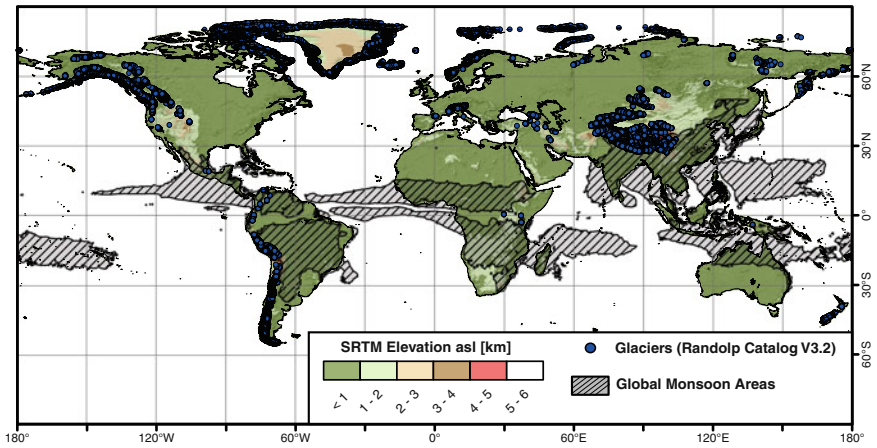

Fig. 11.1 Global distribution of glaciers using the Randolph Catalog (V3.2—*blue dots*) (Arendt et al. 2012), shaded-relief topography (SRTM) (Farr et al. 2007), and TRMM 3B42V7-based monsoonal areas (*gray-hatched areas*) (Huffman et al. 2007). Global monsoon domains are approximated by the approach of B. Wang and Fan (1999), where the grid-cell summer-minus-winter precipitation rate exceeds 2.5 mm/day and the local summer precipitation exceeds 55 % of the annual total

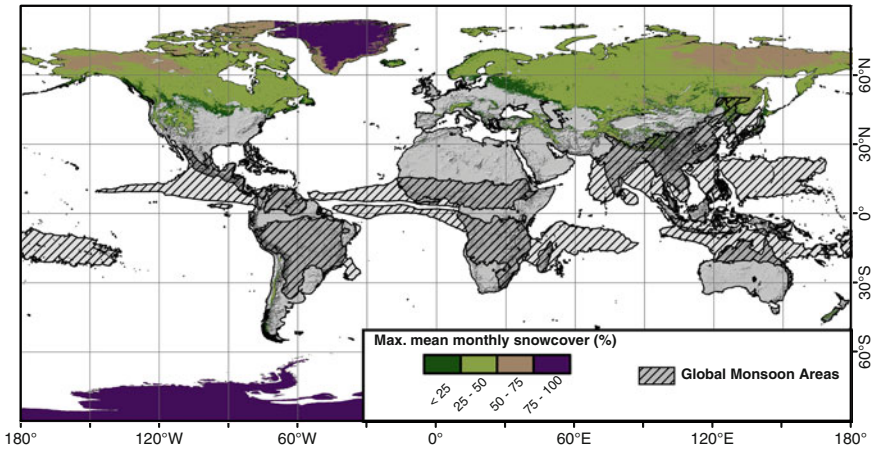

Fig. 11.2 Maximum annual snow cover extent based on MODIS product MOD10C1.005 (Hall et al. 2006) from February 2000 until April 2014. *Hatched areas* indicate global-monsoon areas (cf. Fig. 11.1). Note the low snow cover for most monsoonal areas, except in the Himalayas

outside the South American Monsoon domain. The Himalayas have a seasonal snow cover, especially in their west and northwest, at elevations above 4 or 5 km (Fig. 11.2).

Snow-cover measurements based on satellite imagery only indicate areal extent, but not snow volume or snow amount. For example, a thin, persistent snow cover may have the same signal as a thick, seasonal cover, but their water equivalents differ significantly. Hence, snow water equivalent (SWE) measurements give a better estimate for the amount of water stored in high elevation areas. However, remote-sensing measurements of SWE do not have high spatial resolution and are hampered by technical difficulties (Pulliainen and Hallikainen 2001; Tait 1998; Tedesco et al. 2004b). A compilation of annual SWE for ~10 years—from 2002 to 2011—shows high SWE amounts for the global monsoonal domain only in the Himalayas (Fig. 11.3). The southern Andes show significant seasonally stored SWE as well, but are not part of the global monsoon domain.

The IPCC's Fourth Assessment identifies snowmelt as a key component of the hydrology and climate for High Mountain Asia (HMA)—roughly defined as the area from the Tien Shan in the north, down to the Himalayas in the south, and from the Pamir in the west to the edge of the Tibetan Plateau in the east (Jacob et al. 2012; Lemke et al. 2007). The time lag between seasonal snowfall and snowmelt sustains runoff during the drier summer months. A warmer climate could change the timing of melt and the volume of the snowpack, and would have significant consequences for water resources and power generation, particularly in year-round water provisioning. Among the world's snow-dominated regions, the western Himalayas and central Asia are particularly susceptible to changes in the timing of snowmelt, as reservoir capacity is currently not sufficient to buffer large seasonal shifts in the hydrograph (Barnett et al. 2005). Similarly, the IPCC's Fifth Assessment report

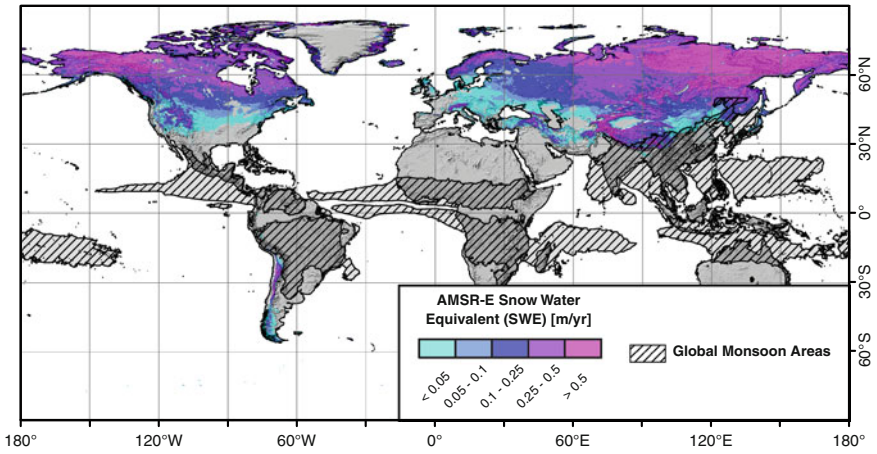

Fig. 11.3 Annual snow water equivalent (SWE) based on passive microwave data (AMSR-E) (Tedesco et al. 2004a) from June 2002 to Oct 2011. SWE is generally low in monsoon-dominated areas (cf. Fig. 11.1), except in High Mountain Asia (HMA)

released in the fall of 2013 makes clear regional distinction in societal impacts due to transiently stored moisture in the form of snow, ice, and permafrost (IPCC 2013).

Taken together, many large cities and densely populated areas in the Andes and Himalayas are located above 2,000 m elevation and depend almost entirely on high altitude water stored in snowpack and glaciers to complement scarce rainfall during the dry season. The increase in glacial melting leads to higher glacial melt water fluxes, but much of the water loss is no longer seasonally restored. The long-term consequences of this are that dry-season runoff will be significantly reduced over the coming decades. While wet season runoff may be higher for the first few decades—due to increased melting—it will decline when the glaciers start to adjust to their new equilibriums. Importantly, mean annual runoff may not change very much, but when water is most needed during the dry season to support agriculture and hydropower generation, water availability will be significantly reduced.

In the tropical areas influenced by the monsoon, temperature remains nearly constant throughout the year, but the hydrological cycle typically has pronounced wet and dry phases. For that reason, the mass and surface energy balance of tropical glaciers are very different than mid- or high-latitude glaciers (Kaser 2001; Vuille et al. 2008; Wagnon et al. 1999). At mid- or high latitudes, winter is the accumulation and summer the ablation season, but ablation and accumulation occur year-round on tropical glaciers. Because of the relatively stable year-round temperature regime, melting occurs mainly in the ablation zone below the snow line altitude, and accumulation is mostly restricted to regions above the snow-rain line, which often remains at a constant altitude throughout the year (Vuille et al. 2008). Field studies and field measurements are rare throughout the tropical regions due to the high altitude of the glaciers, but the few existing studies reveal that the largest mass loss and gain occurs during wet seasons (Francou et al. 2003). In the South

American Monsoon domain, inter-annual glacial variations are also controlled by the El Niño-Southern Oscillation (ENSO) phenomenon, which dictates moisture transport and controls regional temperature. Positive ENSO cycles often result in strongly negative glacial mass balances (melting) due to reduced moisture transport into the central Andes (Bookhagen and Strecker 2010). In contrast, moisture transport during negative ENSO cycles is often increased and results in balanced or slightly positive mass balances in glaciers in the north-central and central Andes (Francou et al. 2003; Vuille et al. 2008; Wagnon et al. 2001).

This section summarizes some of the recent findings in cryospheric sciences, regional retreat rates, climatic trends, and their impact on the downstream society. In a second step, I will link global glacial distributions to monsoon domains and will focus on the South American Andes and the Himalayas in eastern Asia.

11.2 Datasets and Methods

The analysis and synthesis presented in this chapter relies on several field and remote-sensing datasets. I rely on high-spatial resolution remote sensing data, because most climatic reanalysis datasets do not have the spatial resolution necessary to capture the steep climatic and topographic gradients of large mountain ranges.

Glacial extents were derived from the Randolph Glacier Inventory (RGI), a community-based dataset of global glacier outlines (Version 3.2) (Arendt et al. 2012) (Fig. 11.1). These data are referred to as RGI V3.2. Additional glacial outlines were taken from Hanshaw and Bookhagen (2014) for the central Andes.

Rainfall data were based on the Tropical Rainfall Measurement Mission (TRMM) product 3B42 (Boers et al. 2013; Bookhagen 2010; Bookhagen and Strecker 2010; Huffman et al. 2007). This product has a 3-h temporal resolution (data were aggregated to daily time steps) and a spatial resolution of 0.25° × 0.25° (about 25 × 25 km^2) with an observational range from 1998 to 2014. In addition, high-spatial resolution TRMM 2B31 data were used to decipher orographic rainfall barriers. These data are based on the raw orbital observations that have been interpolated to regularly-spaced 90-m grids (Bookhagen and Burbank 2006, 2010; Bookhagen and Strecker 2008, 2012). A study comparing TRMM 3B42 with various other precipitation datasets for South America indicates good agreement between station and remotely sensed data at large spatial scales (Carvalho et al. 2012). A comparison of station data and gridded rainfall data for the Himalayas indicates that TRMM 3B42 and TRMM 2B31 perform reasonably well (Andermann et al. 2011).

Snow cover data were derived from the MODIS (Moderate Resolution Imaging Spectroradiometer) product MOD10C1 daily dataset with 0.05° × 0.05° ($\sim 5 \times 5\,km^2$) spatial resolution (Hall et al. 2006). Data were aggregated to monthly or seasonal time steps where needed. Data ranged between March 2001 and April 2014.

Land Surface Temperature data were derived from the MODIS product MOD11C1 daily dataset with 0.05° × 0.05° spatial resolution (Wan 2008; Wan and Dozier 1996). Here, we rely on the nighttime data because they provide more accurate surface-temperature measurements (Bookhagen and Burbank 2010; Wang et al. 2008). Data were aggregated to monthly values where needed.

Snow water equivalent (SWE) is based on passive microwave measurements onboard the AMSR-E (Advanced Microwave Scanning Radiometer—EOS) platform (Pulliainen and Hallikainen 2001; Tait 1998; Tedesco et al. 2004b). Daily data with a spatial resolution of 0.25° × 0.25° were generated between May 2002 and Oct 2011.

I have used the centroids of glacial outline polygons from RGI V3.2 for display purposes (e.g., Figs. 11.1 and 11.4), and has used the polygon extents to calculate topographic and climatic statistics from various datasets (e.g., Figs. 11.5 and 11.10).

Along-latitude (Fig. 11.5) and along-longitude (Figs. 11.6 and 11.10), profiles were generated for each row or column of data, respectively—that is, the along-latitude profile for the Andes was generated by first projecting all data to an equal-area grid with the same spatial resolution using bilinear resampling. Secondly, row-wise statistical measurements (average, minimum, maximum) were generated for elevations >500 m asl, which correspond to the mountainous Andes and exclude low-lying areas. Finally, these data were smoothed with a 5-km running-average filter along the profile direction.

11.3 Glaciers in the Andes and the South American Monsoon System (SAMS)

11.3.1 Climatic Background

The South American Monsoon System (SAMS) is an important feature of the global monsoon domain (e.g., Kitoh et al. 2013) and is characterized by highly seasonal features. For an in-depth review, refer to Carvalho et al. (2011b); Marengo et al. (2012); Vera et al. (2006). A comprehensive description of the SAMS is found in Chap. 6 of this book.

In short, low-level moisture transport from the tropical Atlantic onto the South American continent is driven by trade winds initiated near the Intertropical Convergence Zone (ITCZ), in combination with differential heating between ocean and land during the monsoon season (December–January–February, DJF) (Marengo et al. 2012; Vera et al. 2006). An integral part, and the most distinctive feature of the SAMS, is the South Atlantic Convergence Zone (SACZ), which is characterized by a convective band of precipitation extending southeastward from the central Amazon Basin (Carvalho et al. 2002; Jones and Carvalho 2002). The SACZ exhibits a dipole-like pattern with strengthened precipitation in the SACZ when precipitation in southeast South America (SESA) is reduced, and vice versa

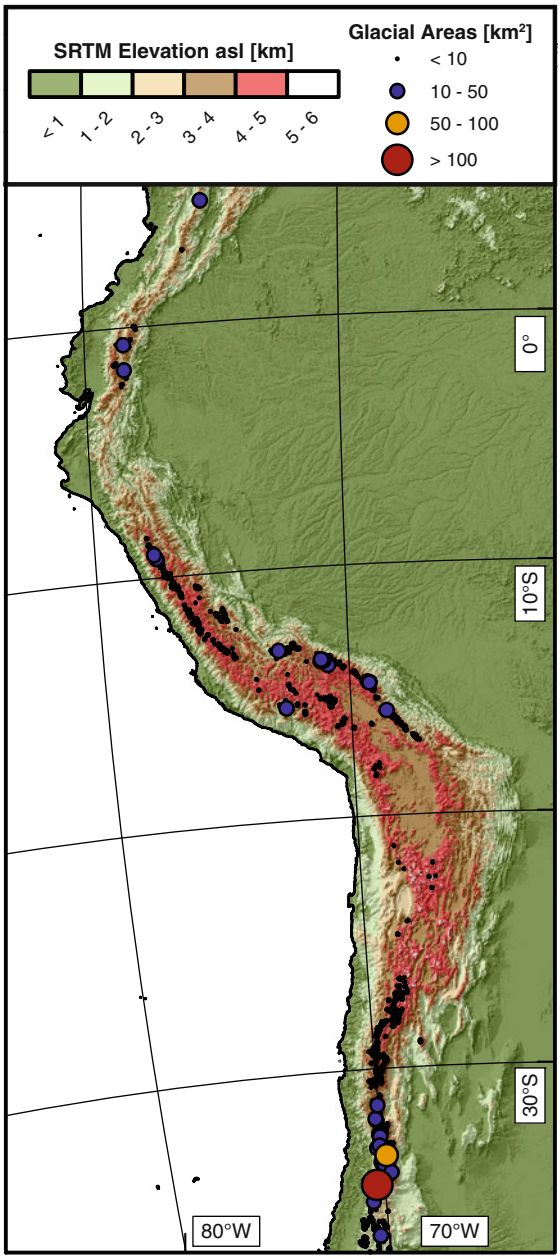

Fig. 11.4 Topography and glacial sizes based on RGIV3.2 (Arendt et al. 2012) for South America. The large majority of glaciers in the northern and central Andes are <10 km^2 (cf. glacial sizes for the Himalayas in Fig. 11.8). Outside the monsoon-influenced region south of 30°S, larger glaciers exist due to higher moisture influx

(e.g., Carvalho et al. 2004; Marengo et al. 2012; Vera et al. 2006). The low-level flow from the Amazon basin westward in the form of the South American Low-Level Jet (SALLJ) is deflected southward by the Andes (Marengo et al. 2012). When the moisture-laden clouds are orographically lifted, they result in a prominent

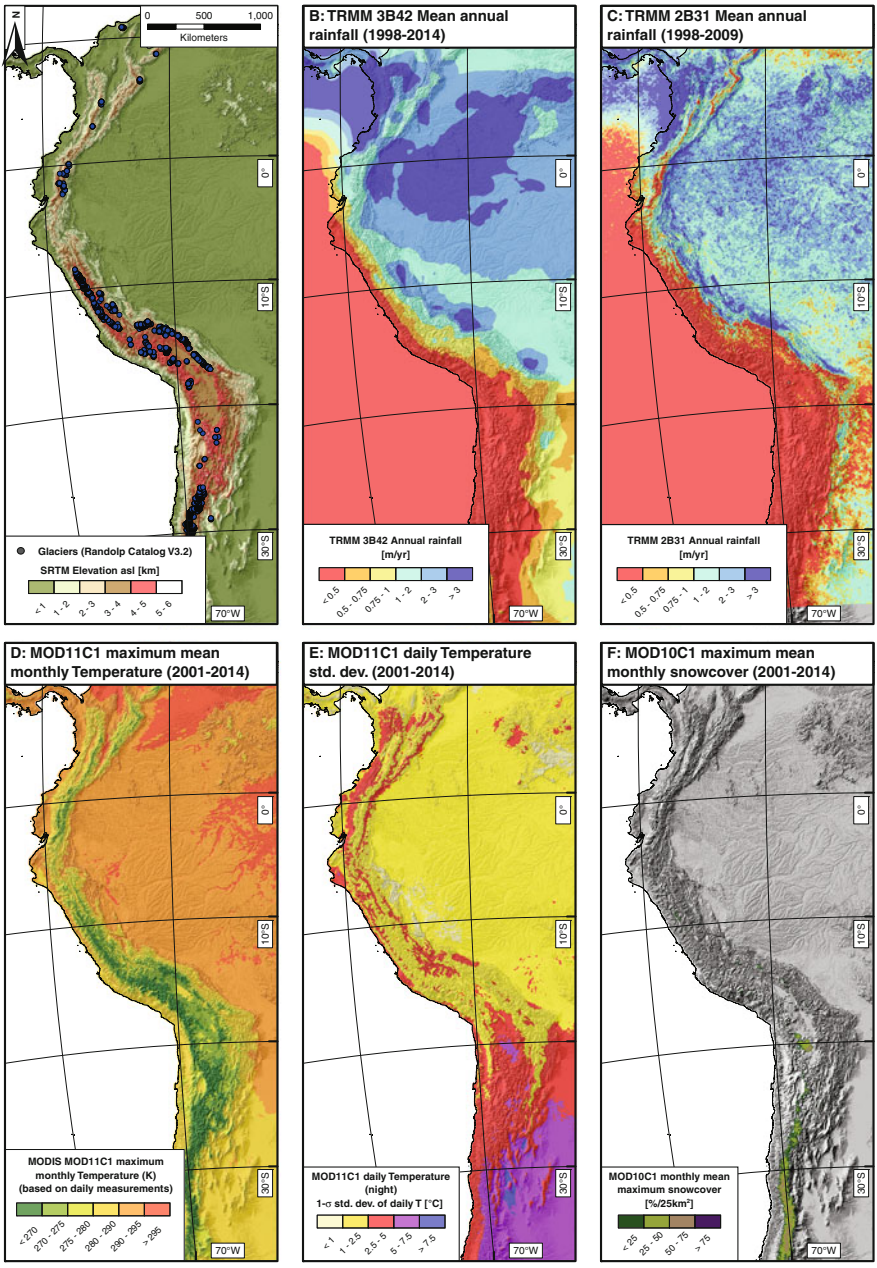
N
0 500 1,000
Kilometers
0°
10°S
30°S
70°W
Glaciers (Randolp Catalog V3.2)
SRTM Elevation asl [km]
< 1
1 - 2
2 - 3
3 - 4
4 - 5
5 - 6
B: TRMM 3B42 Mean annual rainfall (1998-2014)
TRMM 3B42 Annual rainfall [m/yr]
< 0.5
0.5 - 0.75
0.75 - 1
1 - 2
2 - 3
> 3
C: TRMM 2B31 Mean annual rainfall (1998-2009)
TRMM 2B31 Annual rainfall [m/yr]
< 0.5
0.5 - 0.75
0.75 - 1
1 - 2
2 - 3
> 3
D: MOD11C1 maximum mean monthly Temperature (2001-2014)
MODIS MOD11C1 maximum monthly Temperature (K) (based on daily measurements)
< 270
270 - 275
275 - 280
280 - 285
285 - 290
> 295
E: MOD11C1 daily Temperature std. dev. (2001-2014)
MOD11C1 daily Temperature (night)
1-σ std. dev. of daily T [°C]
< 1
1 - 2.5
2.5 - 5
5 - 7.5
> 7.5
F: MOD10C1 maximum mean monthly snowcover (2001-2014)
MOD10C1 monthly mean maximum snowcover [%/25km²]
< 25
25 - 50
50 - 75
> 75

◀ **Fig. 11.5** **a** Dataset compilation for South America. *Top left panel* shows topography and glacier location based on RGI V3.2 (Arendt et al. 2012). **b** Mean annual TRMM 3B42 rainfall (spatial resolution: ~25 × 25 km^2 and 3-h temporal resolution) (Boers et al. 2013; Bookhagen and Strecker 2010; Huffman et al. 2007). **c** Mean annual rainfall based on high-spatial resolution TRMM 2B31 data (Bookhagen and Burbank 2006, 2010; Bookhagen and Strecker 2008). Note the overall similarity between TRMM 3B42 and 2B31, but the generally more pronounced orographic rainfall peak along the eastern Andes due to the higher spatial resolution of product 2B31. **d** MODIS MOD11C1 maximum mean monthly temperature based on daily data from March 2001 to April 2014 collected during nighttime conditions (Wan 2008). Note the temperature gradient between the high-elevation Andes and the low-elevation Amazon plains. **e** 1-sigma standard deviation of daily temperatures from March 2001 to April 2014. Note the low variability in the tropical regions, including the tropical Andes. However, in the subtropical regions at ~27°S, nighttime temperature variability exceeds 7.5 and 10 °C. **f** MODIS MOD10C1 maximum mean monthly snow cover based on daily data from March 2001 to April 2014 (Hall et al. 2006). There is no significant snow cover in the central Andes in the tropical regions, but in the subtropical southern Andes, snow cover becomes more dominant

orographic rainfall peak along the eastern Andean mountain front (Bookhagen and Strecker 2008) (Fig. 11.4c). Rainfall peaks at the mountain front at elevations of ~1 km; rainfall at higher elevations, for example above 3 km, is greatly reduced (Boers et al. 2013; Bookhagen and Strecker 2008, 2012). The steep topographic gradient results in a significant climatic gradient from east to west across the eastern Andes: the frontal areas are moist, tropical climates with mean annual rainfall >4 m/year (Bookhagen and Strecker 2008) and dense vegetation cover. The higher elevation areas—only 100 km westwards—are semi-arid to arid (<0.5 m/year), with little to no vegetation cover. It is this steep climatic gradient that defines mountain climate and makes this region very vulnerable to climate shifts (Baraer et al. 2012; Barnett et al. 2005; Bradley et al. 2006).

The tropical Andes contain more than 99 % of the world's tropical glaciers: Peru 71 %, Bolivia 20 %, Ecuador 4 %, and Colombia-Venezuela 4 % (Kaser 1999) (Fig. 11.4). In most north-central Andean regions, glaciers cover the highest peaks, which are often volcanoes in the northern Andes (Figs. 11.1 and 11.5). Several mountain peaks in the central and south-central Andes are presently too dry to maintain glaciers, but extensive evidence suggests past glaciation on these peaks (Abbott et al. 2003; Haselton et al. 2002; Thompson et al. 2003). The runoff generated from some of these tropical glaciers are an integral part of the hydrologic cycle in the northern and north-central Andes, especially in Peru (e.g., Kaser et al. 2010). Furthermore, melt waters from these glaciers provide resources not only for drinking water and hydropower generation, but also for agriculture and recreation (Buytaert et al. 2006, 2011; Buytaert and De Bievre 2012).

11.3.2 Glacial Retreat Rates and Trends

Glacial retreat in the tropical Andes over the last three decades is unprecedented since the maximum extension of the Little Ice Age (LIA, mid-seventeenth to early eighteenth centuries) (Rabatel et al. 2013). Venezuela has the northernmost tropical

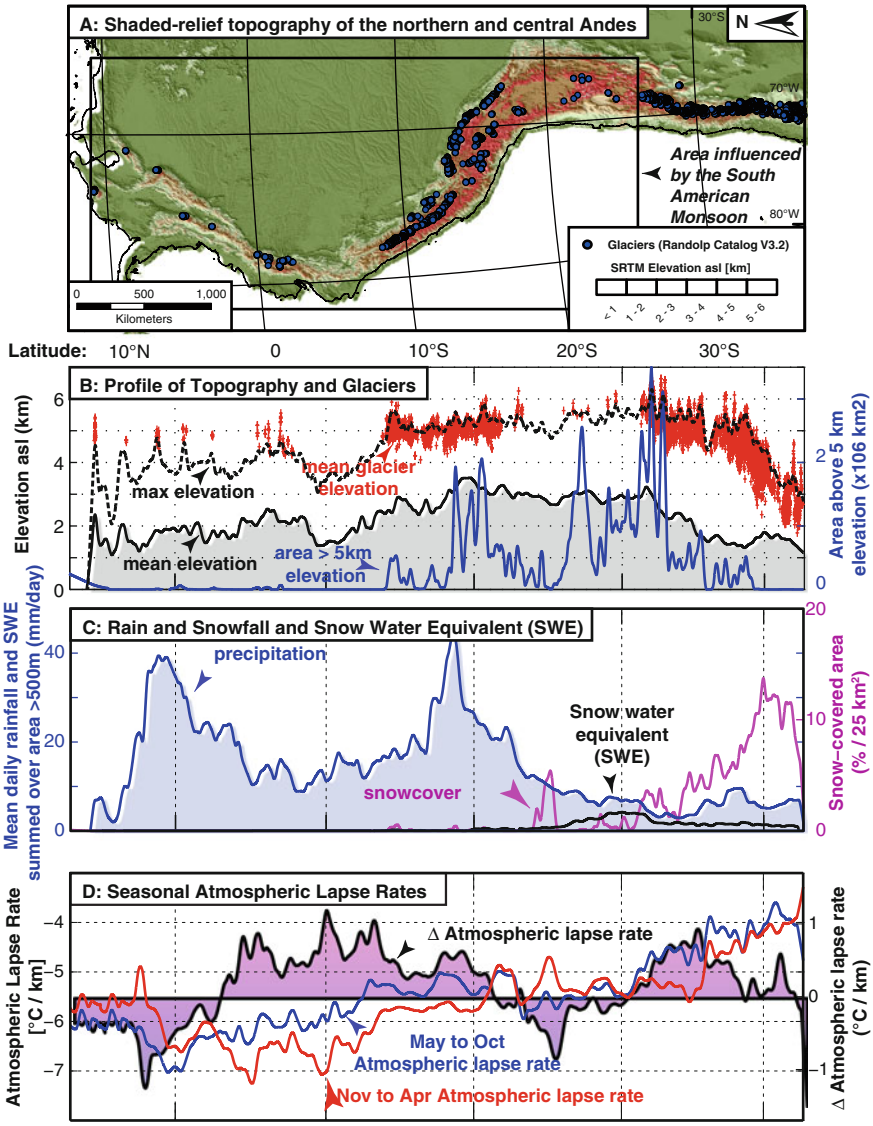
A: Shaded-relief topography of the northern and central Andes
30°S
N
70°W
80°W
Area influenced by the South American Monsoon
Glaciers (Randolp Catalog V3.2)
SRTM Elevation asl [km]
< 1
1 - 2
2 - 3
3 - 4
4 - 5
5 - 6
0
500
1,000
Kilometers
Latitude: 10°N 0 10°S 20°S 30°S
B: Profile of Topography and Glaciers
Elevation asl (km)
max elevation
mean glacier elevation
mean elevation
area > 5km elevation
Area above 5 km elevation (x106 km2)
C: Rain and Snowfall and Snow Water Equivalent (SWE)
Mean daily rainfall and SWE summed over area >500m (mm/day)
precipitation
Snow water equivalent (SWE)
snowcover
Snow-covered area (% / 25 km²)
D: Seasonal Atmospheric Lapse Rates
Atmospheric Lapse Rate [°C / km]
Δ Atmospheric lapse rate
May to Oct Atmospheric lapse rate
Nov to Apr Atmospheric lapse rate
Δ Atmospheric lapse rate (°C / km)

◀ **Fig. 11.6** Topographic, climatic, and glacial distribution through South America. **a** Shaded-relief topography of the northern and central Andes shows glacier locations (Arendt et al. 2012). *Black box* outlines the area influenced by the South American Monsoon System (cf. *hashed areas* in Fig. 11.1). **b** Shows topographic profile from North to South along the Andes orogen for elevations above 500 m asl (i.e., grid cells from the Amazon Basin and other low-elevation areas are excluded). The maximum elevation (*dashed line*) denotes peaks. Most of the peaks near the Equator are volcanoes that are covered by small glaciers. Note that the heavily glacierized areas in the southern Andes are not part of the monsoon domain (south of ~28°S). **c** The heavily glaciated Cordillera Oriental in Peru (~10°S) is characterized by high monsoonal precipitation, but low snow cover. Throughout the tropical Andes, there is no persistent snow cover and only very little snow-water equivalent (SWE) amounts. Only at the southern end of the monsoon domain, widespread snow cover and SWE become more dominant. SWE and precipitation are scaled similarly and show the daily water amount for the area above 500 m elevation. This can be converted to annual amounts by multiplying with 365. **d** Atmospheric lapse rate (°C/km) for the austral summer (November–April) and winter (May–October) is between −7 and −5 °C/km for the northern and central Andes, but increases to >−5 °C/km to the south of the monsoon domain. Note that seasonal lapse rate differences in the central Andes can exceed 1 °C/km

glacier (Figs. 11.1 and 11.4), but has lost more than 95 % of its glacier-covered area since the 1950s (Vuille et al. 2008). Peru contains the largest amount of all tropical glaciers in the low latitudes, and most of these glaciers are located in the monsoon-dominated Cordillera Occidental and Oriental (Figs. 11.1 and 11.4) (Arendt et al. 2012; Rabatel et al. 2013; Vuille et al. 2008). Similarly, glaciers in the Cordillera Vilcanota and the Quelccaya Ice Cap area in the northern central Andes in Peru have retreated with rates of 3.99 ± 1.15 km^2 year^{-1} (Cordillera Vilcanota) and 0.57 ± 0.19 km^2 year^{-1} (Quelccaya Ice Cap) (Hanshaw and Bookhagen 2014). Importantly, glacial retreat has accelerated between the decades of 1988–1999 and 2000–2010 by 13 % (Hanshaw and Bookhagen 2014). The late 1970s have been identified as a break point in the trend of glacial declines: mean mass balances per year were −0.2 m water equivalent (w.e.) between 1964 and 1975, and increased to −0.76 m w.e. between 1976 and 2010 (Rabatel et al. 2013). This timing coincides with a shift of the SAMS (Carvalho et al. 2011a, b).

It has been argued that monthly mass balance measurements on glaciers in Bolivia, Ecuador, and Colombia are controlled by the variability of sea surface temperatures of the Pacific Ocean at decadal time scales (Rabatel et al. 2013), but other climatic phenomena such as ENSO cycles or the Madden Julian Oscillation (MJO) (e.g., Carvalho et al. 2004) may have similar impacts. No clear precipitation trend has been identified in the tropical Andes, but temperature increased at a rate of 0.10 °C/decade during the last 70 years. It has been argued that more ENSO events with changing spatiotemporal patterns and a warming troposphere over the tropical Andes may explain much of the recent glacial shrinkage (Bradley et al. 2009, 2006; Hardy et al. 2003; Rabatel et al. 2013).

Glaciers in the northern central Andes span a wide range of elevations (Fig. 11.6), and the glacial retreat rate is dependent on glacial median elevation: glaciers with lower median elevation are declining at faster rates than those with higher median elevations. Specifically, glaciers with median elevations around 5.2 km asl are retreating at a rate of ~1 m year^{-1} faster than glaciers with median

elevations around 5.4 km asl (Hanshaw and Bookhagen 2014). To the south of the Peruvian Cordillera, glaciers in the Bolivian Cordillera Real have lost between 60 and 80 % of their mass since the mid-seventeenth to early eighteenth centuries, with most of the mass loss occuring during the past 50 years (Rabatel et al. 2013). The southernmost glaciers influenced by the monsoon are near 24°S (Fig. 11.4); the ubiquitous glaciers to the south are fed not only by the South American Monsoon System, but by the westerly wind systems and are not taken into account in this chapter.

Glacial retreat or advance is controlled by several factors, including precipitation, temperature, ice rheology, and surface-energy budgets. In tropical locations, temperature stays surprisingly similar throughout the year (Kaser 1999; Vuille et al. 2008) (cf. Fig. 11.5e), but overall temperature gradients vary (Fig. 11.6d). Daily temperatures throughout the year are fairly constant across 30° of latitude from north of the Equator to the south-central Andes (Fig. 11.5d, e). However, in the extra-tropical regions south of ~30°S, temperatures have a seasonal component and vary by more than 7.5 °C (Fig. 11.5e). The atmospheric lapse rate that describes the temperature change with elevation has a slightly negative trend from north to south but is generally constant along the tropical central Andes (Fig. 11.6d). Austral summer lapse rates (November to April) in the tropical Andes are between −6 and −7 °C/km, but increase to higher rates (~−4.5 °C/km) to the south in the extra-tropical regions. The austral winter atmospheric overall lapse rate is slightly higher, but shows similar spatial patterns to the austral summer lapse rate. The lapse rates at the latitudes of the central Andean plateau (Altiplano and Puna de Atacama) is higher than in the northern central Andes, because of a decrease of the temperature gradient between foreland and plateau region: the high-elevation Altiplano and Puna de Atacama orogenic plateaus heat up and reduce the temperature gradient (Fig. 11.6d). This phenomenon also has been observed in the Tibetan Plateau area (cf. Fig. 11.10c). The decrease in the atmospheric lapse rate in the central Andean plateau region leads to higher temperatures at higher elevations as compared to northern regions. This reduces the area that can be glacierized, and hence glacial areas in this region are smaller because of a decrease in moisture supply and higher temperatures.

Average daily temperatures and annual temperature variation have a strong topographic control: Intermontane basins that are lower than surrounding mountain ridges, for example, basins of 10–10,000 km^2 on the Altiplano-Puna de Atacama Plateau or in the south-central Andes, show larger annual temperature variation than the eastern slopes of the Andes (Fig. 11.5d, e). These intermontane basins influence local climate, lapse rates, and precipitation processes (Bookhagen and Strecker 2008; Rohrmann et al. 2014; Romatschke and Houze 2013).

The occurrence of glaciers is controlled by moisture supply and temperature, and both factors are controlled by topography and the monsoon. Only the highest peaks are covered by glaciers (Fig. 11.5b) and only in regions with sufficient moisture supply and steep atmospheric lapse rates. The heavily glacierized eastern Cordillera in Peru receives large amounts of rainfall (Fig. 11.5b, c). But to the south of this area, present-day rainfall decreases and fewer current glaciers exist. During

previous pluvial periods in the Late Pleistocene, these areas received more moisture in conjunction with a possible temperature decrease, and mountain peaks were glaciated (Abbott et al. 2003; Haselton et al. 2002). Thus, the central Andes centering around 20°S have large areas of more than 5 km elevation and can be glacierized, if atmospheric conditions allow.

11.4 Glaciers in the Himalayas and the Indian Monsoon System (IMS)

11.4.1 Climatic Background

Two principal climate regimes dominate High Mountain Asia (HMA): the Indian Summer Monsoon and the Winter Western Disturbances (WWD). During the summer months, the monsoon is driven by a temperature differential between ocean and land, and upon encountering the orographic barrier of the Himalayas, monsoonal winds bring heavy precipitation to the region (see Chaps. 3 and 4). In the western part of the HMA, monsoonal precipitation is significantly less than in the east and central Himalayas, principally because of the increasing distance from the Bay of Bengal—the main source of water vapor for the monsoon (Bookhagen and Burbank 2006, 2010; Wulf et al. 2010.

During the winter, the pressure gradient that drives the monsoon reverses, resulting in WWD—westerly upper tropospheric synoptic-scale waves (Wulf et al. 2010). In contrast to the monsoons, WD travel at higher tropospheric altitudes and are therefore susceptible to orographic capture and intensification at high elevations (Cannon et al. 2014; Lang and Barros 2004; Wulf et al. 2010). The WD are responsible for much of the winter precipitation in western HMA, especially at large-scale topographic features such as the Karakoram (Wulf et al. 2010). As a result, the western half of HMA receives more snowfall than the central or eastern Himalayas, demonstrated by the significantly greater snow-covered area (SCA) (Immerzeel et al. 2009; Wulf et al. 2010) (Fig. 11.9b). Consequently, snowmelt contributions to annual river runoff in western HMA are considerably greater in comparison to the eastern and central Himalayas, where monsoonal rainfall is the dominant source of river runoff (Immerzeel et al. 2009; Jeelani et al. 2012; Wulf et al. 2010) (Fig. 11.7).

In addition to the WD, the Tien Shan also experiences winter storms originating from the Siberian steppes (Aizen et al. 1995). The interaction between the WWD and the North Atlantic oscillation, as well as the Siberian anticyclonic circulation, determines the quantity of winter precipitation for the region, and this can vary along the entire mountain range (Aizen et al. 1997). Importantly, similar to the Himalayas, the northern Tien Shan experience a precipitation and mean temperature gradient that runs from the northwest to the southeast (Sorg et al. 2012).

Seasonal snow in HMA also plays an important role in the regional climate (Bookhagen and Burbank, 2010; Immerzeel et al. 2009; Wang et al. 2014) (Fig. 11.7). Upper tropospheric air temperatures over the Tibetan Plateau are

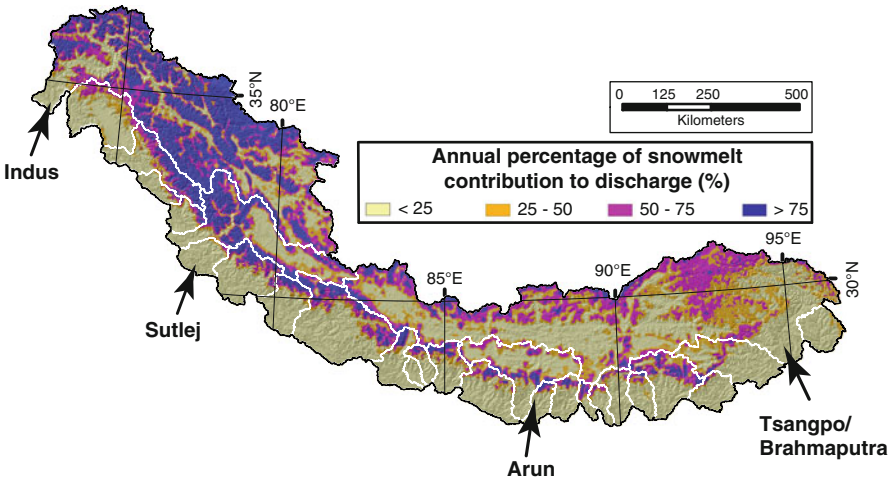

Fig. 11.7 The spatial pattern of snowmelt contribution to river discharge in the Himalayas derived from calibrated and validated satellite products and degree-day runoff modeling (modified according to Bookhagen and Burbank 2010). Note the high snowmelt contribution in the western Himalayas (e.g., the Indus and Sutlej catchments). Crucially, the areas with significant annual snowmelt contribution to river runoff are located at high elevations in remote regions with few to no monitoring stations

substantially warmer than air temperatures above the Indian Ocean. This tropospheric temperature gradient is thought to drive the Indian monsoon (Fu and Fletcher 1985). It has been hypothesized that larger amounts of seasonal snow cover over the Tibetan Plateau could reduce the magnitude of the Indian monsoon by reducing land surface temperatures, thereby reducing the tropospheric temperature gradient (Barnett et al. 1989; Blanford 1884). However, some recent studies indicate a weak positive correlation between Eurasian snow cover and monsoon rainfall (Robock et al. 2003). While reductions in seasonal snow in western HMA may or may not affect monsoon rainfall, such reductions would seriously decrease water resource availability for river basins in the west.

The WD are responsible for much of the seasonal snow accumulation in HMA (Dimri 2005; Wulf et al. 2010) (Fig. 11.7). Still, the Indian summer monsoon can contribute high elevation seasonal snow to the central and eastern Himalayas and the Tibetan Plateau (Bookhagen and Burbank 2006; Bookhagen et al. 2005; Putkonen 2004; Wulf et al. 2010). However, SCA is more extensive and persistent in the western Himalayas than in the central and eastern Himalayas (Bookhagen and Burbank 2010), and also peaks much later in the western Himalayas (Immerzeel et al. 2009). Furthermore, snowlines are lower in the western Himalayas (Scherler et al. 2011a). These findings are consistent with the higher topography of the western Himalayas and the storm tracks of the WD. In general, snow cover has trended downward throughout HMA, but in some cases SCA has increased, for example in the Karakoram (Immerzeel et al. 2009; Tahir et al. 2011). This finding is

consistent with the Karakoram glacier anomaly—a region of positive mass balance, either as a result of increased wintertime precipitation or decreased summer temperature (Bolch et al. 2012). Either way, it is important to note that in both Immerzeel et al. (2009) and Tahir et al. (2011), trends were not significant at the 0.05 confidence interval and the study time periods were relatively short, i.e., <10 years. In the Tien Shan and Hindu Kush, there is less information on the spatial and temporal extent of SCA. However, in the Tien Shan, snow cover thickness and duration have been found to be steadily decreasing since the 1940s (Aizen et al. 1997; Sorg et al. 2012).

11.4.2 Glacial Retreat Rates and Trends

The release of glacial melt reaches its crest in the summer and early autumn and can be critical for both agricultural activities and natural ecosystems (Alford and Armstrong 2010; Bolch et al. 2012; Ficke et al. 2007; Menon et al. 2013; Sorg et al. 2012; Sultana et al. 2009; Valentin et al. 2008; Wulf et al. 2010). As a result, changes in the melt water regime due to climate warming could have consequences for food security and ecosystem services, particularly for the western HMA. Melting glaciers can also increase the risk of ice/snow avalanches and glacial lake outburst floods (Quincey et al. 2007; Richardson and Reynolds 2000). However, it is unlikely that significant changes in annual runoff will occur soon, although shrinkage outside the Karakoram will increase the seasonality of runoff with impact on agriculture and hydropower generation. Glaciers in the western Himalayas are larger than in the central or eastern Himalayas, and thus will have a slower response time to climatic shifts (Fig. 11.8).

Most Himalayan glaciers are losing mass at rates similar to glaciers around the globe, except for the Karakoram area (Bolch et al. 2012; Gardelle et al. 2012; Kaab et al. 2012; Scherler et al. 2011b). Despite recent efforts, the climatic and cryospheric processes in the high-elevation Himalayas are still poorly understood. This is partly due to the difficultly inherent in accessing this region, but also due to the size and topographic complexity of glaciers in the region (Hewitt 2014). In western HMA, glaciers are in general receding, but not responding uniformly to climate warming (Hewitt 2014; Scherler et al. 2011b). Regional patterns have been detected, but even these have inconsistencies as a result of local variations in climate. Mayewski and Jeschke (1979) compiled the first observations of glacier advance and retreat in HMA. The study's database was spatially limited, but the "big picture" indicated that most glaciers were in retreat or standing still since about 1850. Current observations suggest that this trend is continuing in the central and eastern Himalayas and the outer Tien Shan (Bolch et al. 2012; Gardelle et al. 2012; Kaab et al. 2012; Scherler et al. 2011b; Sorg et al. 2012). However, the Karakoram has remained a regional anomaly (Bolch et al. 2012; Gardelle et al. 2013; Hewitt 2005); Karakoram glaciers have oscillated or surged over the past century, indicating a positive mass balance. Recently, Gardelle et al. (2012) speculated that

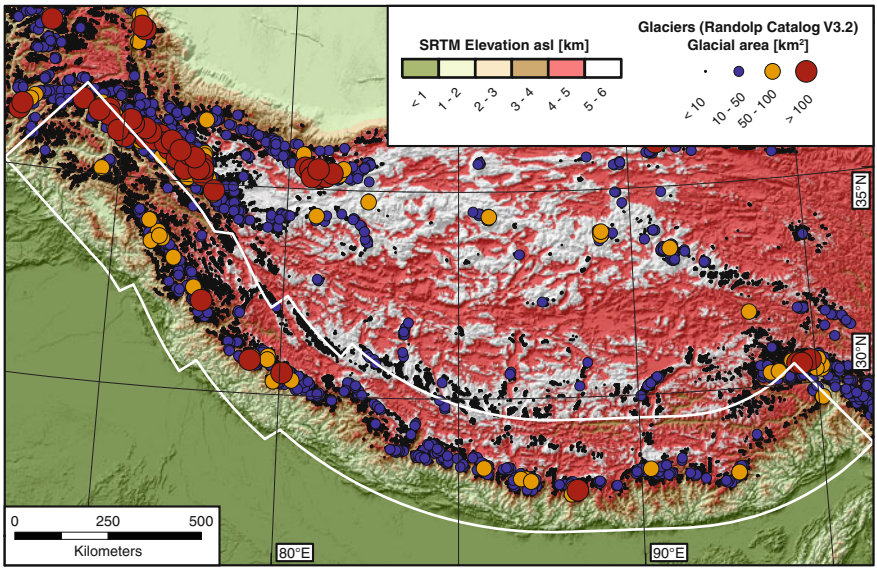

Fig. 11.8 SRTM topography and glacial sizes following the Randolph Catalog V3.2 (Arendt et al. 2012). The *white delineated area* following the main Himalayan arc indicates the area of the longitudinal profile shown in Fig. 11.10. Note the large glacial sizes in the western and northwestern Himalayas

increased winter precipitation and/or cooler summers might be responsible for glacier stability or expansion in the Karakoram.

The depletion of many Himalayan glaciers has garnered media attention in recent years, because of concern over the future of regional water resources. However, while glacial melt may constitute most of the summer discharge in headwater basins, glacial melt over bigger watersheds comprises only a small amount of the annual river runoff (Bookhagen and Burbank 2010; Jeelani et al. 2012; Pal et al. 2013). For example, in the Liddar watershed (a tributary of the Indus), glacial melt contributes 2 % to the annual total, whereas snowmelt comprises 60 % of the annual runoff (Jeelani et al. 2012).

The glacial size distribution in the Himalayas shows a clear climatic and topographic signal (Fig. 11.9): glaciers in the western Himalayas receive significant precipitation in the form of snow during WD, resulting in significant snowcover (Fig. 11.9b) and snow-water amounts (Fig. 11.10b). In addition, the potential area that can be glaciated—for example, delineated by the area above 5 km elevation—is much larger in the western Himalayas than in the eastern (Fig. 11.10a). Mean annual temperatures in the western Himalayas are lower and also show a larger variability, based on daily temperature data collected during nighttime conditions from March 2001 until April 2014 (MODIS product MOD11C1 Wan 2008) (Fig. 11.9e, f). Rainfall in the Himalayan foreland shows a clear east-to-west

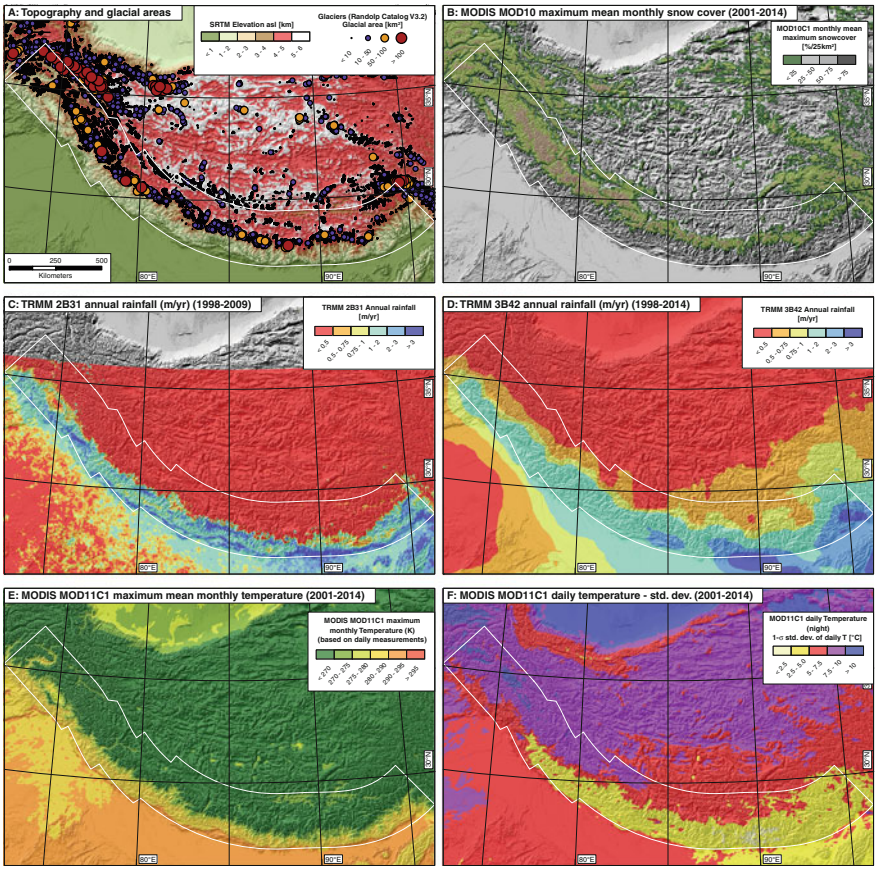

Fig. 11.9 Dataset compilation for the Himalayas. **a** Shows SRTM topography and glacier locations based on RGI V3.2 (Arendt et al. 2012). **b** MODIS MOD10C1 maximum mean monthly snowcover based on daily data from March 2001 to April 2014 (Hall et al. 2006). There is a steep east-to-west snow cover gradient with high snowcover amounts in the western Himalayas due to heavy snowfall during westerly disturbances. **c** Mean annual rainfall based on high-spatial resolution TRMM 2B31 data (Bookhagen and Burbank 2006, 2010; Bookhagen and Strecker 2008). There is a band of nearly continuous, high orographic rainfall at the first topographic rise of the Himalayas—separating the Ganges Plain from the mountainous Himalayas. **d** Mean annual TRMM3B42 rainfall (spatial resolution: $\sim 25 \times 25$ km^2 and 3-h temporal resolution) (Boers et al. 2013; Bookhagen and Strecker 2010; Huffman et al. 2007). Note the overall similarity between TRMM3B42 and 2B31 rainfall patterns, but only the TRMM 2B31 data depict the orographic rainfall band. **e** MODIS MOD11C1 maximum mean monthly temperature based on daily data from March 2001 to April 2014 collected during nighttime conditions (Wan 2008). **f** 1-sigma standard deviation of daily temperature (nighttime conditions) from March 2001 to April 2014. Note the low-to-moderate variability in the eastern and central Himalayas, but the high variability in the western Himalayas and in the southern Tibetan Plateau

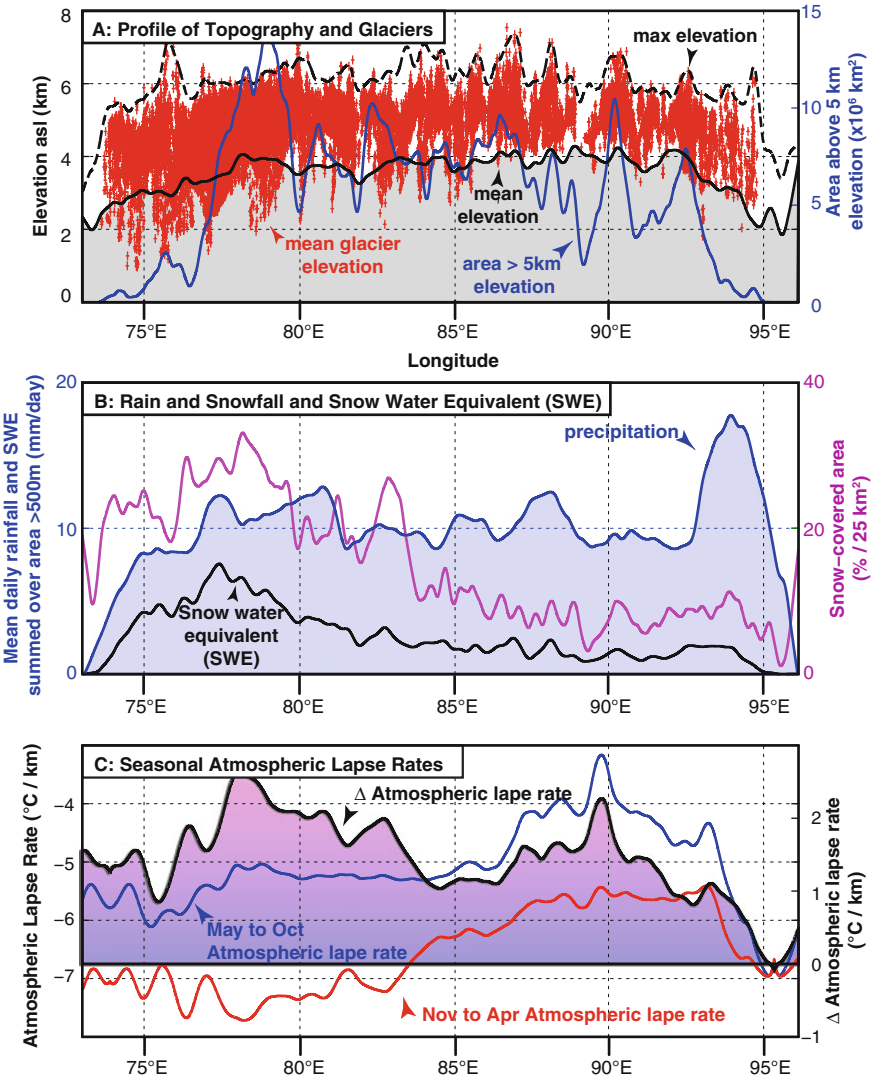

Fig. 11.10 West-to-east profiles showing topography, climatic variables, and atmospheric lapse rates. Values have been averaged from north to south within the *white delineated area* shown in Figs. 11.8 and 11.9. **a** Maximum (*black*, *dashed line*) and mean elevation (*solid line*) and area above 5-km elevation. Note the different Y-axis scales as compared to Fig. 11.6. *Red crosses* denote mean glacier elevation. **b** TRMM 3B42-derived precipitation is shown in *blue* and snow-water equivalent (SWE) in *black* (both datasets are shown with the same Y-axis scale). The *magenta line* denotes a snow-covered area. Note the west-to-east gradient with high snow cover in the western areas due to the influence of winter westerly disturbance. **c** Summer atmospheric lapse rates (*blue line*) are higher than during the winter (*red line*). Lapse rates in the central and eastern Himalayas are higher in the summertime (i.e., higher temperatures at higher elevations) because of the heating of the Tibetan Plateau and a reduction of the temperature gradient

gradient with more rainfall in the eastern regions closer to the moisture source of the Bay of Bengal (Bookhagen and Burbank 2010) (Fig. 11.9c, d). However, rainfall in the mountainous Himalayas is more evenly distributed and doesn't show a strong gradient, although rainfall to the west of the Shillong Plateau at 90E is higher than elsewhere in the Himalayas (Figs. 11.9c, d and 11.10b) (Bookhagen and Burbank 2010; Bookhagen et al. 2005).

In order to decipher the large-scale climatic and topographic gradients and their impact on glaciers, a west-to-east profile was constructed that averages values along the Himalayan arc in a north–south direction (Fig. 11.10). I focus on the areas above 500 m elevations and exclude low-elevation areas such as the Ganges foreland and Indus plain. In other words, the focus is on data close to the main Himalayan arc and does not include the Tibetan plateau. The area is outlined by a white polygon in Figs. 11.9 and 11.10. This analysis reveals that the maximum elevations along the Himalayan arc remain roughly similar and vary between 6 and 8 km (Fig. 11.10a), but the area above 5 km varies widely and hence modifies conditions for cryospheric processes. These data are an approximation of the hypsometric differences between the eastern and western Himalayas. A clear west-to-east gradient exists for snow-covered areas and snow-water equivalent with large amounts of both in the west. There, about half of the annual precipitation falls as snow (Fig. 11.10b). The summer atmospheric lapse rate is between 5–6 °C/km in the western and central Himalayas, but decreases to 3.5–4.5 °C/km in the eastern Himalayas due to a stronger heating of the Tibetan Plateau (Fig. 11.10c); this is significant because higher elevations in the eastern Himalayas tend to be warmer than in the western. The winter atmospheric lapse rate shows a weaker west-to-east gradient because of reduced impacts of the high-elevation Tibetan Plateau.

11.5 Conclusions

Two areas of the global monsoonal domain are characterized by significant glaciation: the northern and central Andes and the Himalayas (cf. Fig. 11.1). This chapter elucidates the differences in climatic and topographic boundary conditions between the two. The tropical northern and central Andes have no seasonal snow cover, and glaciers of small to moderate size are limited to high-elevation areas. In contrast, the western Himalayas have a significant winter snow cover due to the influence of "Winter Western Disturbances," and this area hosts some of the largest glaciers outside of the polar regions and Greenland (Fig. 11.8). While precipitation and seasonal moisture distribution is important for glacier occurrence, hypsometry (or "area vs. elevation") can have significant impacts as well. The central Himalayas and the Cordillera Blanca in Peru do not provide large accumulation areas at high elevations and hence glaciers are limited to the relatively small areas at which year-round temperatures are low and moisture supply is sufficient. The western Himalayas have large areas above 5 and 6 km elevation (Fig. 11.10c). At decadal or longer time scales, the atmospheric lapse rate or temperature changes with elevation

influence glacial behavior. It is important to note that an annual lapse rate may not be representative of the relevant conditions influencing glacial formation, and instead, seasonal lapse rates are more useful for deciphering temperature changes with elevation (Figs. 11.6c and 11.10c).

References

Abbott MB, Wolfe BB, Wolfe AP, Seltzer GO, Aravena R, Mark BG, Polissar PJ, Rodbell DT, Rowe HD, Vuille M (2003) Holocene paleohydrology and glacial history of the central Andes using multiproxy lake sediment studies. Palaeogeogr Palaeoclimatol Palaeoecol 194(1–3):123–138. doi:10.1016/s0031-0182(03)00274-8

Aizen VB, Aizen EM, Melack JM (1995) Climate, snow cover, glaciers, and runoff in the Tien-Shan, Central-Asia. Water Resour Bull 31(6):1113–1129

Aizen VB, Aizen EM, Melack JM, Dozier J (1997) Climatic and hydrologic changes in the Tien Shan, Central Asia. J Clim 10(6):1393–1404. doi:10.1175/1520-0442(1997)010<1393:cahcit>2.0.co;2

Alford D, Armstrong R (2010) The role of glaciers in stream flow from the Nepal Himalaya. Cryosphere Discuss 4(2):469–494. doi:10.5194/tcd-4-469-2010

Andermann C, Bonnet S, Gloaguen R (2011) Evaluation of precipitation data sets along the Himalayan front, *Geochemistry Geophysics Geosystems*, *12*, doi:10.1029/2011gc003513

Archer DR, Fowler HJ (2004) Spatial and temporal variations in precipitation in the Upper Indus Basin, global teleconnections and hydrological implications. Hydrol Earth Syst Sci 8(1):47–61

Arendt A et al (2012) Randolph glacier inventory—a dataset of global glacier outlines: Version 3.2, edited, Global Land Ice Measurements from Space, Boulder, Colorado, USA. Digital Media

Baraer M, Mark BG, McKenzie JM, Condom T, Bury J, Huh KI, Portocarrero C, Gomez J, Rathay S (2012) Glacier recession and water resources in Peru's Cordillera Blanca. J Glaciol 58(207):134–150. doi:10.3189/2012JoG11J186

Barnett TP, Adam JC, Lettenmaier DP (2005) Potential impacts of a warming climate on water availability in snow-dominated regions. Nature 438(7066):303–309. doi:10.1038/nature04141

Barnett TP, Dümenil L, Schlese U, Roeckner E, Latif M (1989) The effect of Eurasian snow cover on regional and global climate variations. J Atmos Sci 46(5):661–686. doi:10.1175/1520-0469(1989)046<0661:TEOESC>2.0.CO;2

Blanford HF (1884) On the connexion of the Himalaya snowfall with dry winds and seasons of drought in India. Proc R Soc London 37:1–23

Boers N, Bookhagen B, Marwan N, Kurths J, Marengo J (2013) Complex networks identify spatial patterns of extreme rainfall events of the South American Monsoon System. Geophys Res Lett 40(16):4386–4392. doi:10.1002/grl.50681

Bolch T et al (2012) The state and fate of Himalayan glaciers. Science 336(6079):310–314. doi:10.1126/science.1215828

Bolch T, Pieczonka T, Benn DI (2011) Multi-decadal mass loss of glaciers in the Everest area (Nepal Himalaya) derived from stereo imagery. Cryosphere 5(2):349–358. doi:10.5194/tc-5-349-2011

Bookhagen B (2010) Appearance of extreme monsoonal rainfall events and their impact on erosion in the Himalaya. Geomat Nat Hazards Risk 1(1):37–50. doi:10.1080/19475701003625737

Bookhagen B, Burbank DW (2006) Topography, relief, and TRMM-derived rainfall variations along the Himalaya. Geophys Res Lett 33(8). doi:10.1029/2006gl026037

Bookhagen B, Burbank DW (2010) Toward a complete Himalayan hydrological budget: spatiotemporal distribution of snowmelt and rainfall and their impact on river discharge. J Geophys Res Earth Surf 115. doi:10.1029/2009jf001426

Bookhagen B, Strecker MR (2008) Orographic barriers, high-resolution TRMM rainfall, and relief variations along the eastern Andes. Geophys Res Lett 35(6). doi:10.1029/2007gl032011

Bookhagen B, Strecker MR (2010) Modern Andean rainfall variation during ENSO cycles and its impact on the Amazon Basin. In: Hoorn HVC, Wesselingh F (eds) Neogene history of Western Amazonia and its significance for modern diversity. Blackwell Publishing, Oxford

Bookhagen B, Strecker MR (2012) Spatiotemporal trends in erosion rates across a pronounced rainfall gradient: Examples from the southern Central Andes. Earth Planet Sci Lett 327:97–110. doi:10.1016/j.epsl.2012.02.005

Bookhagen B, Thiede RC, Strecker MR (2005) Abnormal monsoon years and their control on erosion and sediment flux in the high, and northwest Himalaya. Earth Planet Sci Lett 231(1–2):131–146. doi:10.1016/j.epsl.2004.11.014

Bradley RS, Keimig FT, Diaz HF, Hardy DR (2009) Recent changes in freezing level heights in the Tropics with implications for the deglacierization of high mountain regions. Geophys Res Lett 36. doi:10.1029/2009gl037712

Bradley RS, Vuille M, Diaz HF, Vergara W (2006) Threats to water supplies in the tropical Andes. Science 312(5781):1755–1756. doi:10.1126/science.1128087

Buytaert W, Celleri R, De Bievre B, Cisneros F, Wyseure G, Deckers J, Hofstede R (2006) Human impact on the hydrology of the Andean paramos. Earth Sci Rev 79(1–2):53–72. doi:10.1016/j.earscirev.2006.06.002

Buytaert W, Cuesta-Camacho F, Tobon C (2011) Potential impacts of climate change on the environmental services of humid tropical alpine regions. Glob Ecol Biogeogr 20(1):19–33. doi:10.1111/j.1466-8238.2010.00585.x

Buytaert W, De Bievre B (2012) Water for cities: the impact of climate change and demographic growth in the tropical Andes. Water Resour Res 48. doi:10.1029/2011wr011755

Cannon F, Carvalho LMV, Jones C, Bookhagen B (2014) Multi-annual variations in winter westerly disturbance activity affecting the Himalaya. Clim Dyn. doi: 10.1007/s00382-014-2248-8

Carvalho LMV, Jones C, Liebmann B (2002) Extreme precipitation events in southeastern South America and large-scale convective patterns in the South Atlantic convergence zone. J Clim 15 (17):2377–2394. doi:10.1175/1520-0442(2002)015<2377:epeiss>2.0.co;2

Carvalho LMV, Jones C, Liebmann B (2004) The South Atlantic convergence zone: Intensity, form, persistence, and relationships with intraseasonal to interannual activity and extreme rainfall. J Clim 17(1):88–108. doi:10.1175/1520-0442(2004)017<0088:tsaczi>2.0.co;2

Carvalho LMV, Jones C, Posadas AND, Quiroz R, Bookhagen B, Liebmann B (2012) Precipitation characteristics of the South American Monsoon System derived from multiple datasets. J Clim 25(13):4600–4620. doi:10.1175/jcli-d-11-00335.1

Carvalho LMV, Jones C, Silva AE, Liebmann B, Dias PLS (2011a) The South American Monsoon System and the 1970s climate transition. Int J Climatol 31(8):1248–1256. doi:10.1002/joc.2147

Carvalho LMV, Silva AE, Jones C, Liebmann B, Dias PLS, Rocha HR (2011b) Moisture transport and intraseasonal variability in the South America monsoon system. Clim Dyn 36(9–10):1865–1880. doi:10.1007/s00382-010-0806-2

Dimri AP (2005) The contrasting features of winter circulation during surplus and deficient precipitation over Western Himalayas. Pure appl Geophys 162(11):2215–2237. doi:10.1007/s00024-006-0092-4

Farr TG et al (2007) The shuttle radar topography mission. Rev of Geophys 45(2). doi:10.1029/2005rg000183

Ficke AD, Myrick CA, Hansen LJ (2007) Potential impacts of global climate change on freshwater fisheries. Rev Fish Biol Fish 17(4):581–613. doi:10.1007/s11160-007-9059-5

Finger D, Heinrich G, Gobiet A, Bauder A (2012) Projections of future water resources and their uncertainty in a glacierized catchment in the Swiss Alps and the subsequent effects on

hydropower production during the 21st century. Water Resour Res 48, W02521. doi:10.1029/2011wr010733
Francou B, Vuille M, Wagnon P, Mendoza J, Sicart JE (2003) Tropical climate change recorded by a glacier in the central Andes during the last decades of the twentieth century: Chacaltaya, Bolivia, 16 degrees S. J Geophys Res Atmos 108(D5). doi:10.1029/2002jd002959
Fu C, Fletcher JO (1985) The relationship between Tibet-tropical ocean thermal contrast and interannual variability of Indian monsoon rainfall. J Climate Appl Meteorol 24(8):841–847. doi:10.1175/1520-0450(1985)024<0841:TRBTTO>2.0.CO;2
Gardelle J, Berthier E, Arnaud Y (2012) Slight mass gain of Karakoram glaciers in the early twenty-first century. Nat Geosci 5(5):322–325. doi:10.1038/ngeo1450
Gardelle J, Berthier E, Arnaud Y, Kaab A (2013) Region-wide glacier mass balances over the Pamir-Karakoram-Himalaya during 1999-2011. Cryosphere 7(4):1263–1286. doi:10.5194/tc-7-1263-2013
Hall DK, Riggs GA, Salomonson VV (2006) MODIS/Terra snow cover daily L3 global 0.05 deg CMG V005, MOD10C1, Digital Media, edited, National Snow and Ice Data Center, Boulder, Colorado USA
Hanshaw MN, Bookhagen B (2014) Glacial areas, lake areas, and snow lines from 1975 to 2012: status of the Cordillera Vilcanota, including the Quelccaya Ice Cap, northern central Andes, Peru. The Cryosphere 8(2):359–376. doi:10.5194/tc-8-359-2014
Hardy DR, Vuille M, Bradley RS (2003) Variability of snow accumulation and isotopic composition on Nevado Sajama, Bolivia. J Geophys Res Atmos 108(D22). doi:10.1029/2003jd003623
Haselton K, Hilley G, Strecker MR (2002) Average Pleistocene climatic patterns in the southern central Andes: controls on mountain glaciation and paleoclimate implications. J Geol 110 (2):211–226. doi:10.1086/338414
Hewitt K (2005) The Karakoram anomaly? Glacier expansion and the 'elevation effect', Karakoram Himalaya. Mt Res Dev 25(4):332–340. doi:10.1659/0276-4741(2005)025[0332:tkagea]2.0.co;2
Hewitt K (2014) Glaciers of the Karakoram Himalaya. Springer, Dordrecht
Huffman GJ, Adler RF, Bolvin DT, Gu GJ, Nelkin EJ, Bowman KP, Hong Y, Stocker EF, Wolff DB (2007) The TRMM multisatellite precipitation analysis (TMPA): quasi-global, multiyear, combined-sensor precipitation estimates at fine scales. J Hydrometeorol 8(1):38–55. doi:10.1175/jhm560.1
Huggel C, Kaab A, Haeberli W, Teysseire P, Paul F (2002) Remote sensing based assessment of hazards from glacier lake outbursts: a case study in the Swiss Alps. Can Geotech J 39(2):316–330. doi:10.1139/t01-099
Huss M (2012) Extrapolating glacier mass balance to the mountain range scale: the European Alps 1900-2100. Cryosphere Discuss 6(1117–1156)
Huss M, Farinotti D, Bauder A, Funk M (2008) Modelling runoff from highly glacierized alpine drainage basins in a changing climate. Hydrol Process 22(19):3888–3902. doi:10.1002/hyp.7055
Immerzeel WW, Droogers P, de Jong SM, Bierkens MFP (2009) Large-scale monitoring of snow cover and runoff simulation in Himalayan river basins using remote sensing. Remote Sens Environ 113(1):40–49. doi:10.1016/j.rse.2008.08.010
IPCC (2013) Climate change 2013: the physical science basis. Contribution of Working Group I to the fifth assessment report of the intergovernmental panel on climate change. Cambridge University Press, Cambridge, United Kingdom and New York, NY, USA, 1535 pp
Jacob T, Wahr J, Pfeffer WT, Swenson S (2012) Recent contributions of glaciers and ice caps to sea level rise. Nature 482(7386):514–518. doi:10.1038/nature10847
Jeelani G, Feddema JJ, van der Veen CJ, Stearns L (2012) Role of snow and glacier melt in controlling river hydrology in Liddar watershed (western Himalaya) under current and future climate. Water Resour Res 48. doi:10.1029/2011wr011590
Jones C, Carvalho LMV (2002) Active and break phases in the South American Monsoon System. J Clim 15(8):905–914. doi:10.1175/1520-0442(2002)015<0905:aabpit>2.0.co;2

Kaab A, Berthier E, Nuth C, Gardelle J, Arnaud Y (2012) Contrasting patterns of early twenty-first-century glacier mass change in the Himalayas. Nature 488(7412):495–498. doi:10.1038/nature11324

Kaser G (1999) A review of the modern fluctuations of tropical glaciers. Global Planet Change 22 (1–4):93–103. doi:10.1016/s0921-8181(99)00028-4

Kaser G (2001) Glacier-climate interaction at low latitudes. J Glaciol 47(157):195–204. doi:10.3189/172756501781832296

Kaser G, Cogley JG, Dyurgerov MB, Meier MF, Ohmura A (2006) Mass balance of glaciers and ice caps: consensus estimates for 1961-2004. Geophys Res Lett 33(19). doi:10.1029/2006gl027511

Kaser G, Grosshauser M, Marzeion B (2010) Contribution potential of glaciers to water availability in different climate regimes. Proc Natl Acad Sci USA 107(47):20223–20227. doi:10.1073/pnas.1008162107

Kitoh A, Endo H, Krishna Kumar K, Cavalcanti IFA, Goswami P, Zhou T (2013) Monsoons in a changing world: a regional perspective in a global context. J Geophys Res Atmos n/a–n/a. doi:10.1002/jgrd.50258

Lang TJ, Barros AP (2004) Winter storms in the central Himalayas. J Meteorol Soc Jpn 82(3):829–844. doi:10.2151/jmsj.2004.829

Lemke P et al (2007) Observations: changes in snow, ice and frozen ground, in climate change 2007: the physical science basis. In: Solomon S, Qin D, Manning M, Chen Z, Marquis M, Averyt KB, Tignor M, Miller HL (eds) Contribution of Working Group I to the fourth assessment report of the intergovernmental panel on climate change. Cambridge University Press, Cambridge, UK, pp 337–383

Marengo JA et al (2012) Recent developments on the South American Monsoon System. Int J Climatol 32(1):1–21. doi:10.1002/joc.2254

Mayewski PA, Jeschke PA (1979) Himalayan and Trans-Himalayan glacier fluctuations since AD 1812. Arct Alpine Res 267–287

Menon A, Levermann A, Schewe J (2013) Enhanced future variability during India's rainy season. Geophys Res Lett 40(12):3242–3247. doi:10.1002/grl.50583

Oerlemans J (2005) Extracting a climate signal from 169 Glacier records. Science 308(5722):675–677. doi:10.1126/science.1107046

Pal I, Lall U, Robertson AW, Cane MA, Bansal R (2013) Predictability of Western Himalayan river flow: melt seasonal inflow into Bhakra Reservoir in northern India. Hydrol Earth Syst Sci 17(6):2131–2146. doi:10.5194/hess-17-2131-2013

Paul F, Kaab A, Maisch M, Kellenberger T, Haeberli W (2004) Rapid disintegration of Alpine glaciers observed with satellite data. Geophys Res Lett 31(21). doi:10.1029/2004gl020816

Price MF, Weingartner R (2012) Global change and the world's mountains. Mt Res Dev 32(S1): S3–S6

Pulliainen J, Hallikainen M (2001) Retrieval of regional snow water equivalent from space-borne passive microwave observations. Remote Sens Environ 75(1):76–85. doi:10.1016/s0034-4257(00)00157-7

Putkonen JK (2004) Continuous snow and rain data at 500 to 4400 m altitude near Annapurna, Nepal, 1999-2001. Arct Antarct Alp Res 36(2):244–248. doi:10.1657/1523-0430(2004)036[0244:CSARDA]2.0.CO;2

Quincey DJ, Richardson SD, Luckman A, Lucas RM, Reynolds JM, Hambrey MJ, Glasser NF (2007) Early recognition of glacial lake hazards in the Himalaya using remote sensing datasets. Global Planet Change 56(1–2):137–152. doi:10.1016/j.gloplacha.2006.07.013

Rabatel A et al (2013) Current state of glaciers in the tropical Andes: a multi-century perspective on glacier evolution and climate change. Cryosphere 7(1):81–102. doi:10.5194/tc-7-81-2013

Radic V, Hock R (2011) Regionally differentiated contribution of mountain glaciers and ice caps to future sea-level rise. Nat Geosci 4(2):91–94. doi:http://www.nature.com/ngeo/journal/v4/n2/abs/ngeo1052.html-supplementary-information

Richardson SD, Reynolds JM (2000) An overview of glacial hazards in the Himalayas. Quatern Int 65:31–47

Robock A, Mu M, Vinnikov K, Robinson D (2003) Land surface conditions over Eurasia and Indian summer monsoon rainfall. J Geophys Res 108(D4):4131. doi:10.1029/2002JD002286

Rohrmann A, Strecker MR, Bookhagen B, Mulch A, Sachse D, Pingel H, Alonso RN, Schildgen TF, Montero C (2014) Can stable isotopes ride out the storms? The role of convection for water isotopes in models, records, and paleoaltimetry studies in the central Andes. Earth Planet Sci Lett 407:187–195. doi:10.1016/j.epsl.2014.09.021

Romatschke U, Houze RA (2013) Characteristics of precipitating convective systems accounting for the summer rainfall of tropical and subtropical South America. J Hydrometeorol 14(1):25–46. doi:10.1175/jhm-d-12-060.1

Scherler D, Bookhagen B, Strecker MR (2011a) Hillslope-glacier coupling: the interplay of topography and glacial dynamics in High Asia. J Geophys Res Earth Surf 116. doi:10.1029/2010jf001751

Scherler D, Bookhagen B, Strecker MR (2011b) Spatially variable response of Himalayan glaciers to climate change affected by debris cover. Nat Geosci 4(3):156–159. doi:10.1038/ngeo1068

Sorg A, Bolch T, Stoffel M, Solomina O, Beniston M (2012) Climate change impacts on glaciers and runoff in Tien Shan (Central Asia). Nat Clim Change 2(10):725–731. doi:10.1038/NCLIMATE1592

Sultana H, Ali N, Iqbal MM, Khan AM (2009) Vulnerability and adaptability of wheat production in different climatic zones of Pakistan under climate change scenarios. Clim Change 94(1–2):123–142. doi:10.1007/s10584-009-9559-5

Tahir A, Chevallier P, Arnaud Y, Ahmad B (2011) Snow cover dynamics and hydrological regime of the Hunza River basin, Karakoram Range, Northern Pakistan. Hydrol Earth Syst Sci Discuss 8(2):2821–2860. doi:10.5194/hess-15-2275-2011

Tait AB (1998) Estimation of snow water equivalent using passive microwave radiation data. Remote Sens Environ 64(3):286–291. doi:10.1016/s0034-4257(98)00005-4

Tedesco M, Kelly R, Foster JL, Chang ATC (2004a) AMSR-E/Aqua Daily L3 global snow water equivalent EASE-grids. Version 2. [indicate subset used], edited, NASA DAAC at the National Snow and Ice Data Center, Boulder, Colorado USA

Tedesco M, Pulliainen J, Takala M, Hallikainen M, Pampaloni P (2004b) Artificial neural network-based techniques for the retrieval of SWE and snow depth from SSM/I data. Remote Sens Environ 90(1):76–85. doi:10.1016/j.rse.2003.12.002

Thompson LG, Mosley-Thompson E, Davis ME, Lin PN, Henderson K, Mashiotta TA (2003) Tropical glacier and ice core evidence of climate change on annual to millennial time scales. Clim Change 59(1–2):137–155. doi:10.1023/a:1024472313775

Valentin C et al (2008) Runoff and sediment losses from 27 upland catchments in Southeast Asia: Impact of rapid land use changes and conservation practices. Agric Ecosyst Environ 128(4):225–238. doi:10.1016/j.agee.2008.06.004

Vaughan DG et al (2013) Observations: cryosphere. In: Climate change 2013: the physical science basis. Contribution of Working Group I to the fifth assessment report of the intergovernmental panel on climate change. Cambridge University Press, Cambridge, United Kingdom and New York, NY, USA

Vera C et al (2006) Toward a unified view of the American monsoon systems. J Clim 19(20):4977–5000. doi:10.1175/jcli3896.1

Viviroli D, Weingartner R (2004) The hydrological significance of mountains: from regional to global scale. Hydrol Earth Syst Sci 8(6):1016–1029

Vuille M, Francou B, Wagnon P, Juen I, Kaser G, Mark BG, Bradley RS (2008) Climate change and tropical Andean glaciers: past, present and future. Earth Sci Rev 89(3–4):79–96. doi:10.1016/j.earscirev.2008.04.002

Wagnon P, Ribstein P, Francou B, Sicart JE (2001) Anomalous heat and mass budget of Glaciar Zongo, Bolivia, during the 1997/98 El Nino year. J Glaciol 47(156):21–28. doi:10.3189/172756501781832593

Wagnon P, Ribstein P, Kaser G, Berton P (1999) Energy balance and runoff seasonality of a Bolivian glacier. Global Planet Change 22(1–4):49–58. doi:10.1016/s0921-8181(99)00025-9

Wan ZM (2008) New refinements and validation of the MODIS land-surface temperature/emissivity products. Remote Sens Environ 112(1):59–74. doi:10.1016/j.rse.2006.06.026

Wan ZM, Dozier J (1996) A generalized split-window algorithm for retrieving land-surface temperature from space. IEEE Trans Geosci Remote Sens 34(4):892–905

Wang B, Fan Z (1999) Choice of south Asian summer monsoon indices. Bull Am Meteorol Soc 80 (4):629–638. doi:10.1175/1520-0477(1999)080<0629:cosasm>2.0.co;2

Wang SJ, Zhang MJ, Pepin NC, Li ZQ, Sun MP, Huang XY, Wang Q (2014) Recent changes in freezing level heights in High Asia and their impact on glacier changes. J Geophys Res Atmos 119(4):1753–1765. doi:10.1002/2013jd020490

Wang W, Liang S, Meyers T (2008) Validating MODIS land surface temperature products using long-term nighttime ground measurements. Remote Sens Environ 112(3):623–635. doi:10.1016/j.rse.2007.05.024

Wulf H, Bookhagen B, Scherler D (2010) Seasonal precipitation gradients and their impact on fluvial sediment flux in the Northwest Himalaya. Geomorphology 118(1–2):13–21. doi:10.1016/j.geomorph.2009.12.003

Index

© Springer International Publishing Switzerland 2016

L.M.V. de Carvalho and C. Jones (eds.), *The Monsoons and Climate Change*,
Springer Climate, DOI 10.1007/978-3-319-21650-8